SYNTHESIS OF FUNCTIONAL HYDROGELS

EDITED BY: Weifeng Zhao, Qiang Wei and Baolin Guo

frontiers Research Topics

About Frontiers

Frontiers is more than just an open-access publisher of scholarly articles: it is a pioneering approach to the world of academia, radically improving the way scholarly research is managed. The grand vision of Frontiers is a world where all people have an equal opportunity to seek, share and generate knowledge. Frontiers provides immediate and permanent online open access to all its publications, but this alone is not enough to realize our grand goals.

Frontiers Journal Series

The Frontiers Journal Series is a multi-tier and interdisciplinary set of open-access, online journals, promising a paradigm shift from the current review, selection and dissemination processes in academic publishing. All Frontiers journals are driven by researchers for researchers; therefore, they constitute a service to the scholarly community. At the same time, the Frontiers Journal Series operates on a revolutionary invention, the tiered publishing system, initially addressing specific communities of scholars, and gradually climbing up to broader public understanding, thus serving the interests of the lay society, too.

Dedication to Quality

Each Frontiers article is a landmark of the highest quality, thanks to genuinely collaborative interactions between authors and review editors, who include some of the world's best academicians. Research must be certified by peers before entering a stream of knowledge that may eventually reach the public - and shape society; therefore, Frontiers only applies the most rigorous and unbiased reviews.
Frontiers revolutionizes research publishing by freely delivering the most outstanding research, evaluated with no bias from both the academic and social point of view. By applying the most advanced information technologies, Frontiers is catapulting scholarly publishing into a new generation.

What are Frontiers Research Topics?

Frontiers Research Topics are very popular trademarks of the Frontiers Journals Series: they are collections of at least ten articles, all centered on a particular subject. With their unique mix of varied contributions from Original Research to Review Articles, Frontiers Research Topics unify the most influential researchers, the latest key findings and historical advances in a hot research area! Find out more on how to host your own Frontiers Research Topic or contribute to one as an author by contacting the Frontiers Editorial Office: researchtopics@frontiersin.org

SYNTHESIS OF FUNCTIONAL HYDROGELS

Topic Editors:
Weifeng Zhao, Sichuan University, China
Qiang Wei, Sichuan University, China
Baolin Guo, Xi'an Jiaotong University, China

Table of Contents

Synthesis and Characterization of Photoresponsive Macromolecule for Biomedical Application

Juan Pang, Ziyu Gao, Long Zhang, Huiming Wang and Xiaohong Hu*

School of Material Engineering, Jinling Institute of Technology, Nanjing, China

Azobenzene, a photo switcher, has attracted increasing interest due to its structural response to photo stimulus in the field of information science and chemical sensing in the recent decades. However, limited water solubility and cytotoxicity restrained their applications in the biomedical field. In research, HA-AZO has been designed as a water soluble photo switcher in biomedical application. Synthesized HA-AZO had good water-solubility and a stable π-π^* transition absorbance peak trans-isomer. With exposure to UV, transformation from trans-isomer to cis-isomer of HA-AZO could be realized according to UV spectra. Reversely, trans-isomer could be gradually recovered from cis-isomer in the dark. Simultaneously, quick response and slow recovery could be detected in the process of structural change. Moreover, repeated illumination was further used to detect the antifatigue property of HA-AZO, which showed no sign of fatigue during 20 circles. The influence of pH value on UV spectrum for HA-AZO was investigated in the work. Importantly, in acid solution, HA-AZO no longer showed any photoresponsive property. Additionally, the status of HA-AZO under the effect of UV light was investigated by DLS results and TEM image. Finally, in vitro cytotoxicity evaluations were performed to show the effects of photoresponsive macromolecule on cells.

Keywords: azobenzene, photo switcher, photoresponsive macromolecule, biomedical application, hyaluronic acid

INTRODUCTION

Photoresponsive molecules, which cause reversible changes, i.e., their chemical and physical properties changes due to structural change with a light stimulus, have attracted increasing interest in the field of information science and chemical sensing in the recent decades (Sun et al., 2012; Li et al., 2014; Yuan et al., 2014; Kim et al., 2015). Among photo molecular switches, azobenzenes have been intensively investigated due to the precise spatiotemporal control (Li et al., 2014; Kim et al., 2015). Upon exposure to UV light, azobenzenes can isomerize from the trans-form to the cis-form (Henzl et al., 2006; Kumar and Suresh, 2009; Schmidt et al., 2010). However, the cis-form is unstable and liable to reversely isomerize to trans-form under the action of visible light or slight heat (Henzl et al., 2006; Kumar and Suresh, 2009; Schmidt et al., 2010). Given the fact that cis- and trans-isomers of azobenzenes have a different spatial arrangement of the aromatic moieties, physical and chemical properties of azobenzenes varied a lot, some examples being π-π stack interaction among molecules, dipole moments, and surface wettability (Li et al., 2014; Yuan et al., 2014; Lin et al., 2016, 2017). Consequently, azobenzenes became particularly popular as photoresponsive chromophores in a number of research fields including biomedical fields (Deka et al., 2015; Liu et al., 2015; Bian et al., 2016a,b). Recently, on account of photo-controlled reversible supermolecular interaction between

azobenzenes and cyclodextrins, hydrogels as well as films with controllable pores or passages crosslinked by the supermolecular interaction have been designed and synthesized to respond to photo-stimuli from external environment (Chen et al., 2009; Chiang and Chu, 2015; Wang et al., 2015). In addition to these reports, visible light driven azobenzene-based photo-switching molecules have been theoretically designed by different substitute groups (Pang et al., 2014, 2016; Ye et al., 2015).

On account of aqueous physiological environments, chemicals in the application of biomedicine-related fields should have aqueous dissolvability (Gao et al., 2016; Wang et al., 2016; Gu et al., 2017; Ha et al., 2018). From this point, the application of azobenzene in the biomedicine-related field is restricted not only due to its low aqueous dissolvablity but also due to cytotoxicity in water. In order to solve this problem, a water-soluble photo switch was designed. From previous research, some natural polysaccharides such as hyaluronic acid (HA), chitosan, chondroitin sulfate (CS) and the like is proven to be water soluble and have good biocompatibility especially for HA, which plays an important role in the organization and stabilization of ECM, cell proliferation, and differentiation (Hu et al., 2011; Hu and Gong, 2016). Moreover, HA can lubricate joints, adjust permeability of vessel walls, improve transport of protein and ions, and accelerate wound healing (Yue et al., 2017; Andreasen et al., 2018). Hence, HA is assumed to be an ideal macromolecule or material in biomedical application. In view of these facts, a photoresponsive macromolecule was designed using HA as a backbone and AZO as a side chain in this work.

In consideration of reactivity and carboxyl groups on HA molecules, p-aminoazobenzene was grafted onto the main chain of HA to obtain a photoresponsive macromolecule. In order to clarify the properties of the photosensitive macromolecules, molecular responsive properties as a function of irradiation time, pH value, and recovered time as well as fatigue resistance of the responsive property was characterized in the research. As a macromolecule, its molecular aggregation in water is also important to evaluate the interaction between molecules and provide potential material for biomedical application. Therefore, the macromolecule with different responsive status in water was tracked by dynamic light scattering (DLS) and molecular aggregation in water was also confirmed by transmission electron microscope (TEM) images. Finally, cell viability and apoptosis profile was used to evaluate the cytotoxicity of photoresponsive macromolecule.

Although azobenzenes have been intensively investigated, work still needs to be done to obtain a biocompatible photoresponsive macromolecule for biomedical application, characterize their structure and assess their properties including cytotoxicity properties.

EXPERIMENTAL SECTION

Materials
1-Ethyl-3-(3-dimethylaminopropyl) carbodiimide hydrochloride (EDC), N-hydroxysuccinimide (NHS), 2-morpholinoethane sulfonic acid (MES), and p-aminoazobenzene (AZO) was purchased from Aladdin. Hyaluronate acid (HA, M_w = 1,000 kDa) was obtained from Shandong Furuida Co., China. Trypsin,

Dulbecco's modified Eagle's medium (DMEM), fluorescein diacetate (FDA), and 3-(4, 5-dimethyl) thiazol-2,5-dimethyl tetrazolium bromide (MTT) were obtained from Sigma. Fetal bovine serum (FBS) was purchased from Sijiqing biotech. Co., China. All other reagents and solvents were of analytical grade and used as received.

Synthesis of HA-AZO
HA-AZO was synthesized by amidation between HA and aminoazobenzene (AZO). Briefly, 500 mg of EDC and 200 mg of NHS were successively added to 10 mL of 2% HA solution with magnetic stirring. Meanwhile, 10 mg of AZO was dissolved in 10 mL DMF. After 30 min, 100 mg of MES was further added to HA solution. HA solution and AZO solution were subsequently mixed together and the reaction was maintained for 5 h at room temperature. Then, the final solution was dialyzed with a dialysis bag of 10 kDa cut-off molecular weight for 3 days to remove unreacted chemicals and byproduct of small molecular weight. Finally, HA-AZO was obtained by freeze drying at −60°C at a pressure of 7–8 Pa.

Characterization of HA-AZO
HA-AZO was characterized by $_1$H nuclear magnetic resonance ($_1$H NMR, Bruker, AV500) using D_2O as solvent. HA-AZO water solution, AZO water solution, and AZO DMSO solution was characterized by UV spectroscopy (Cary 50). UV lamp (10 W) was used as photosource to induce tran-to-cis transition of AZO domain. In order to track the structural change of molecules, real-time UV spectra as a function of irradiation time and recovery time was recorded. Repeated irradiation and recovery method were applied to demonstrate the fatigue resistance of molecules. Macromolecule status in water solution was characterized by dynamic light scattering (DLS, nano ZS) and transmission electron microscope (TEM, Philips, Tecnai 12).

Cytotoxicity Evaluation of HA-AZO
HUVEC cells were incubated in a humidified atmosphere of 95% air and 5% CO_2 at 37°C. The used cells were detached using 0.25% trypsin in PBS for the experiment. Simultaneously, HA-AZO and AZO were dissolved in DMEM with certain concentration separately with the same molar ratio. Then, 100 μL of above-mentioned solution was added into each well of 96-well culture plate, and into which the 100 μL cell suspension containing 5,000 cells was subsequently added. Cells were characterized as a function of cultural time. MTT assay was used to characterize cytoviability. Briefly, 20 μL MTT was supplemented into wells of the culture plate, which were then put back to continually culture cells for another 4 h. Two hundred microliters DMSO was added to dissolve the formed formazan pigment. The absorbance of above solution at 490 nm was recorded by a microplate reader (Infinite M200 PRO).

Besides MTT assay, apoptosis profile of cells was characterized by PI/FITC double staining (Annexin V). Briefly, 1 mL of above-mentioned HA-AZO solution or AZO solution was added into each well of 12-well culture plate, into which 1 mL cell suspension containing 200,000 cells was subsequently added. Cells of each well were detached using 0.25% trypsin without EDTA after culturing for 24 h separately. Detached cells were washed with

1×binding buffer, resuspended in 500 μL 1×binding buffer, and subsequently ordinal stained by PI solution and FITC solution for 15 min. The stained cells detected by flow cytometry (FCM, BD, C6) within 1 h in dark.

Statistical Analysis

Data were analyzed using the t-test for differences. Results were reported as means ± standard deviation. The significant level was set at $p < 0.05$.

RESULT AND DISCUSSION

Synthesis of HA-AZO

Synthesized HA-AZO was characterized by $_1$H NMR as shown in **Figure 1**. The details of chemical shift are listed as follows: the chemical shift at 1.9 ppm is attributed to the protons of CH_3-O at 1 position, the chemical shifts from 3.1 to 4.0 ppm are attributed to the protons of pyranose ring, and the chemical shift at 7.9 ppm is attributed to the protons of benzene ring of AZO at 2 position. The chemical shift at 2 position confirmed successful grafting of AZO onto HA main chain. Besides qualitative analysis, $_1$H-NMR provided quantitative information since areas of resonance peaks are proportional to number of protons. According to areas in **Figure 1** at 1 and 2 positions, the degree of substituent (DS) could be calculated using the average proton intensity ratio of the protons of benzene ring/CH_3-O, which is 2.2% (per two pyranose ring).

Characterization of HA-AZO

It was found that HA-AZO had good water-solubility. Hence, HA-AZO water solution was used for the following characterization. Firstly, UV spectra of HA-AZO water solution

as a function of irradiation time and recovery time were shown in **Figures 2A,B**. In one aspect, the peak at 360 nm belonging to π-π* transition for trans-isomer decreased significantly and the peak at 420 nm belonging to n-π* transition for cis-isomer increased a little with irradiation time until 60 s, which was an obvious sign to indicate that the trans-form had been transferred to the cis-form (**Figure 2A**). In another aspect, without irradiation, the peaks at 360 and 420 nm were gradually recovered to their original state within 10 min, which indicated that the recovery of trans-form for AZO domain of HA-AZO was realized (**Figure 2B**). Structural change upon photo guaranteed the molecular responsive property for HA-AZO. Moreover, rapid transfer from trans to cis upon photo exhibited quick responsive time for the macromolecule, and simultaneously gradual recovering process indicated enough controllable time. Effective structural change, rapid responsive time, and enough operation time are all desirable properties for a macromolecule photo switch. As a contrast, UV spectra of AZO water solution showed no change after irradiation without any change of isomer (Figure s1), although AZO DMF solution showed some photo-responsive properties (Figure s2). Secondly, fatigue resistance of molecular switch was essential for its actual application, which was evaluated by repeated irradiation and recovery and characterized by UV spectrum as shown in **Figures 2C,D**. It was found that the minimum absorbance at 346 nm for HA water solution after irradiation was stabilized at 0.7–0.8 regardless of circle time, and simultaneously maximum absorbance at 360 nm either initial or after recovery was stabilized at 1.5–1.7 regardless of circle time (**Figure 2C**). The results showed that cis-form could be stable and exist after irradiation, whereas the trans-form could be recovered after removal of irradiation. Furthermore, the response time
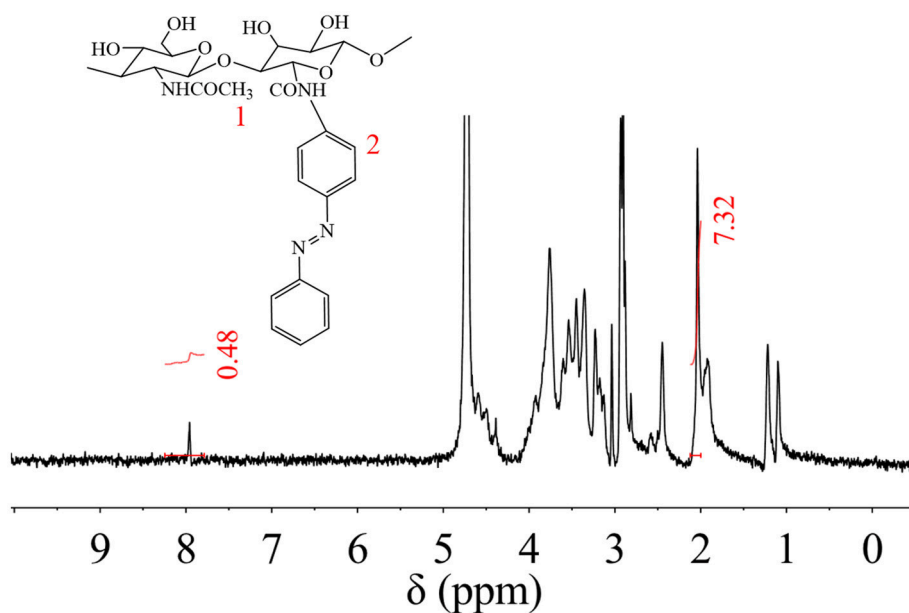
FIGURE 1 | $_1$H NMR spectrum of HA-AZO.
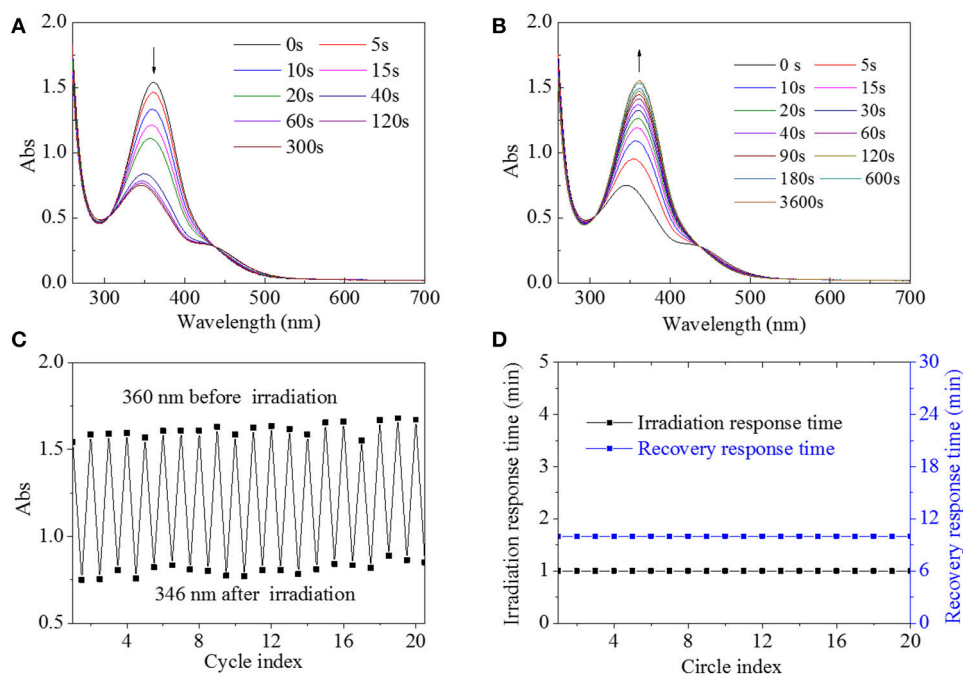
FIGURE 2 | UV spectra of HA-AZO water solution as a function of irradiation time (A) and recovery time (B). (C) Absorbance at 360/346 nm of HA-AZO water solution as a function of circle index. (D) Irradiation response time and recovery response time in dark as a function of circle index.
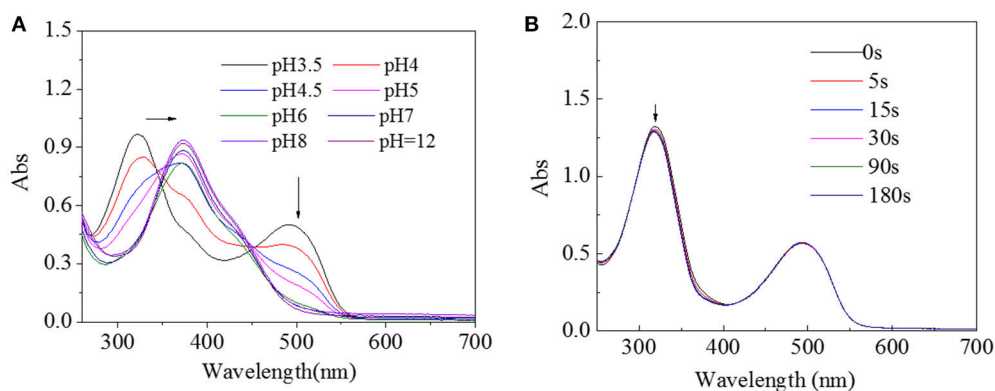
FIGURE 3 | (A) UV spectra of HA-AZO water solution as a function of pH value. (B) UV spectra of HA-AZO water solution as a function of irradiation time in pH = 3.5 medium.

with irradiation was stable at 1 min, and the recovery time was stable at 10 min regardless of circle time (**Figure 2D**). From these results, it is inferred that HA-AZO has no sign of fatigue or phenomenon of photobleaching. As a contrast, even in DMF, the photoresponsive property weakened as a function of circle time (Figure s3A), and furthermore, the response time and recovery time shortened with increase of circle time (Figure s3B), which was unfavorable for its application as a photo switch. By contrast, HA-AZO had obvious superiority to AZO molecule as a photo switch, especially in water solution.

Since pH value is also an important factor in physiological environment, UV spectra of HA-AZO solution with different pH value was tracked as shown in **Figure 3A**. With decreasing pH value, the peak at 360 nm shifted to 320 nm and a new peak at 500 nm gradually increased when pH value was lower than 6. The blue shift from 360 to 320 nm was estimated to protonation effect of benzene ring for π-π* transition and emerging peak at 500 nm was estimated to n-π* transition in effects of protonation. In addition, in order to inspect the influence of irradiation on structure of HA-AZO, UV spectra of acid HA-AZO solution as a function of irradiation
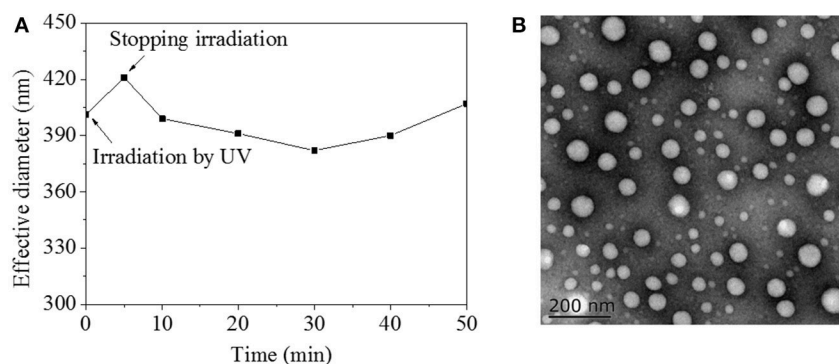
FIGURE 4 | (A) Effective diameter of HA-AZO water solution a function of time by influence of UV irradiation; **(B)** TEM images of HA-AZO dropped by HA-AZO water solution and dried naturally.

time was detected as shown in **Figure 3B**. It was found that the macromolecule has no responsive property in acid environment since UV irradiation had no influence on its UV spectra, which indicated that HA-AZO exhibited pH-dependent photoresponsive property. Theoretically, no visible trans-to-cis transition in acid environment might be the case, for two reasons. One is unstability of cis-form structure with very short existing time beyond characterization. The other one is protonation of AZO induces cis-form structure (from n-π* transition) that coexists with trans-form structure in natural state, which indicates that trans-to-cis transition is induced in acid environment. However, no defined deduction has been verified by sufficient proof. Furthermore, since AZO molecule in water exhibited no trans-to-cis transition due to aggregation of molecules according to Figure S1, AZO molecule in water could not have pH-dependent photo responsive property.

On account of π-π stacking interaction between AZO domains, HA-AZO macromolecule might be in aggregation state, which was characterized by DLS and TEM as shown in **Figure 4**. Before irradiation, the effective diameter of HA-AZO solution was 405 nm (**Figure 4A**). The effective diameter increased after irradiation and then decreased gradually along with time until 30 min (**Figure 4A**). According to previous research, π-π stacking interaction between AZO molecules could be disaggregated when the trans-form transferred to cis-form, which made the interaction within aggregations weakened. The weaker interaction could lead aggregations to swell and dismiss at the end. However, since chain movement of macromolecule need time, recovery process of cis to trans came to procedure before aggregations dismissed completely. In recovery procedure, dismissed aggregations gradually reassembled again along with time. In further step, HA-AZO aggregations were observed by TEM as shown in **Figure 4B**. Spherical aggregations with diameter of 20–100 nm were homogeneously distributed in the TEM image. Because HA-AZO aggregations in water were in swollen state,

diameter detected by DLS was much larger than that detected by TEM.

Cytotoxicity of HA-AZO

Since biocompatibility of the macromolecule was an essential factor for its biomedical application, preliminarily cytotoxicity assessment was performed by *in vitro* culture of HUVEC cells. In this method, cells were cocultured with HA-AZO on TCPs, and simultaneously, cytoviability and cell apoptosis profiles were used to evaluate the biocompatibility of HA-AZO. As shown in **Figure 5**, the viability of cells decreased with HA-AZO concentration regardless of culture time. On the first day, OD of cells with HA-AZO showed no obvious decline, estimated 80% of that on TCPs even when HA-AZO concentration was as high as 5 mg/mL, which indicated that HA-AZO had no obvious acute cytotoxicity. However, cells with HA-AZO showed much lower OD than cells without HA-AZO after cells were cultured for some time. Moreover, OD of cells increased with cultured time, which indicated that cells proliferated along with time. However, it was inferred from OD statistic data that cells with HA-AZO showed slower proliferation rate than that of control (without HA-AZO), and the proliferation rate decreased along with HA-AZO concentration. These results indicated that proliferation of cells might be inhibited by HA-AZO. As a contrast, equivalent AZO exhibited great acute cytotoxicity and complete proliferation inhibition (Figure s4).

In the cell apoptosis profile, live cells on TCPs without HA-AZO were approaching 78% and the dead cells were estimated to be 18% after cells were cultured for 3 days (**Figure 6A**). Further live cells on TCPs decreased with the increase of HA-AZO concentration (**Figure 6B–D**). Even when HA-AZO concentration was 5 mg/mL, live cells had been estimated 60%. The results were consistent with their viability as shown in **Figure 5**. As a contrast, equivalent AZO exhibited great cytotoxicity with less live cells and more dead cells in Figure s5.
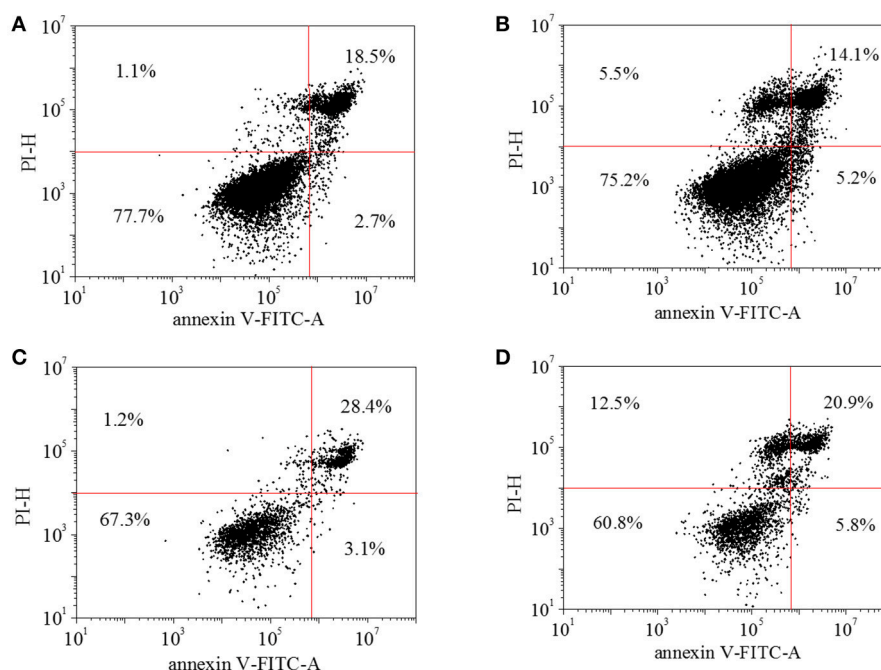
FIGURE 6 | HUVEC cell apoptosis profile of with **(A)** 0 mg/mL HA-AZO, **(B)** 1 mg/mL HA-AZO, **(C)** 5 mg/mL HA-AZO, **(D)** 10 mg/mL HA-AZO. Cells was stained by FITC/PI.
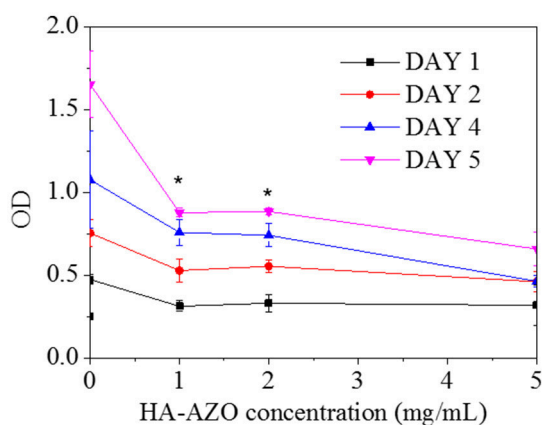
FIGURE 5 | Optical density of HUVEC cells after cultured different time as a function of HA-AZO concentration. Cells was incubated with MTT.

CONCLUSION

HA-AZO was successfully synthesized with DS of 2.2%. Synthesized HA-AZO had good water-solubility and a stable π-π* transition absorbance peak trans-isomer. Upon UV for 5 min, transformation from trans-isomer to cis-isomer of HA-AZO could be realized according to UV spectra. Reversely, trans-isomer could be gradually recovered from cis-isomer in 1 h in dark. This characteristics revealed the reversible photo-responsive property of HA-AZO molecule with quick response

and slow recovery. Moreover, antifatigue property of HA-AZO was confirmed by repeated illumination. The blue shift from 360 to 320 nm and emerging peak at 500 nm were found in low pH value solution. In acid solution, HA-AZO no longer showed any photo responsive property. HA-AZO was in small aggregation and its size was influenced by irradiation and varied with recovery time. Finally, *in vitro* evaluation showed little acute cytotoxicity, but the cell growth could be inhibited by HA-AZO. These properties indicated that HA-AZO was an optimal photo responsive macromolecule for biomedical application. The toxicity of AZO has been verified not only by our results but also by other researchers. Hence, their application in biomedical field is rarely reported. While the AZO grafting product HA-AZO exhibits little acute cytotoxicity from the result of both cell viability and cell apoptosis profile after 1 d, acute cytotoxicity is evaluated with 24 h before cell division. Theoretically, cell viability should multiply and increase with cultured days, since cells divide in every 24 h. Actually, cell growth viability showed little increase with cultured days. However, the increased rate is much lower than both that of TCPs control and theoretical calculation. These results showed that HA-AZO influenced cell proliferation and cell division, which indicated that the grafting product might have some genetic toxicity.

AUTHOR CONTRIBUTIONS

JP designed the macromolecule and predicted its property. ZG synthesized the macromolecule. LZ and HW investigated the

properties of the macromolecule. XH was responsible for the whole manuscript.

SUPPLEMENTARY MATERIAL

The Supplementary Material for this article can be found online at: https://www.frontiersin.org/articles/10.3389/fchem.2018.00217/full#supplementary-material

REFERENCES

Andreasen, C. M., Ding, M., Andersen, T. L., and Overgaard, S. (2018). Effects of substitute coated with hyaluronic acid or poly-lactic acid on implant fixation: Experimental study in ovariectomized and glucocorticoid-treated sheep. *J. Tissue Eng. Regener. Med.* 12, e1122–e1130. doi: 10.1002/term.2447

Bian, Q., Wang, W., Han, G., Chen, Y., Wang, S., and Wang, G. (2016a). Photoswitched cell adhesion on azobenzene-containing self-assembled films. *Chemphyschem* 17, 2503–2508. doi: 10.1002/cphc.201600362

Bian, Q., Wang, W., Wang, S., and Wang, G. (2016b). Light-triggered specific cancer cell release from cyclodextrin/azobenzene and aptamer-modified substrate. *ACS Appl. Mater. Interfaces* 8, 27360–27367. doi: 10.1021/acsami.6b09734

Chen, X., Hong, L., You, X., Wang, Y., Zou, G., Su, W., et al. (2009). Photo-controlled molecular recognition of α-cyclodextrin with azobenzene containing polydiacetylene vesicles. *Chem. Commun.* 1356–1358. doi: 10.1039/b820894h

Chiang, C. Y., and Chu, C. C. (2015). Synthesis of photoresponsive hybrid alginate hydrogel with photo-controlled release behavior. *Carbohydr. Polym.* 119, 18–25. doi: 10.1016/j.carbpol.2014.11.043

Deka, S. R., Yadav, S., Mahato, M., and Sharma, A. K. (2015). Azobenzene-aminoglycoside: self-assembled smart amphiphilic nanostructures for drug delivery. *Colloids Surf. B Biointerfaces* 135, 150–157. doi: 10.1016/j.colsurfb.2015.07.026

Gao, A., Wu, Q., Wang, D., Ha, Y., Chen, Z., and Yang, P. (2016). A superhydrophobic surface templated by protein self-assembly and emerging application toward protein crystallization. *Adv. Mater.* 28, 579–587. doi: 10.1002/adma.201504769

Gu, J., Su, Y., Liu, P., Li, P., and Yang, P. (2017). An environmentally benign antimicrobial coating based on a protein supramolecular assembly. *ACS Appl. Mater. Interfaces* 9, 198–210. doi: 10.1021/acsami.6b13552

Ha, Y., Yang, J., Tao, F., Wu, Q., Song, Y. J., Wang, H., et al. (2018). Phase-transited lysozyme as a universal route to bioactive hydroxyapatite crystalline film. *Adv. Funct. Mater.* 28:1704476. doi: 10.1002/adfm.201704476

Henzl, J., Mehlhorn, M., Gawronski, H., Rieder, K. H., and Morgenstern, K. (2006). Reversible cis-trans isomerization of a single azobenzene molecule. *Angew. Chem.* 45, 603–606. doi: 10.1002/anie.200502229

Hu, X., and Gong, X. (2016). A new route to fabricate biocompatible hydrogels with controlled drug delivery behavior. *J. Colloid Interface Sci.* 470, 62–70. doi: 10.1016/j.jcis.2016.02.037

Hu, X., Li, D., Zhou, F., and Gao, C. (2011). Biological hydrogel synthesized from hyaluronic acid, gelatin and chondroitin sulfate by click chemistry. *Acta Biomater.* 7,1618–1626. doi: 10.1016/j.actbio.2010.12.005

Kim, D. Y., Lee, S. A., Park, M., Choi, Y. J., Kang, S. W., and Jeong, K. U. (2015). Multi-responsible chameleon molecule with chiral naphthyl and azobenzene moieties. *Soft Matter* 11, 2924–2933. doi: 10.1039/C5SM00073D

Kumar, B., and Suresh, K. A. (2009). Kinetics of trans-cis isomerization in azobenzene dimers at an air-water interface. *Phys. Rev. E Stat. Nonlinear Soft Matter Phys.* 80:021601. doi: 10.1103/PhysRevE.80.021601

Li, Z., Wang, P., Liu, B., Wang, Y., Zhang, J., Yan, Y., et al. (2014). Unusual, photo-induced self-assembly of azobenzene-containing amphiphiles. *Soft Matter* 10, 8758–8764. doi: 10.1039/C4SM01395F

Lin, L. R., Tang, H. H., Wang, Y. G., Wang, X., Fang, X. M., and Ma, L. H. (2017). Functionalized Lanthanide(III) complexes constructed from azobenzene derivative and beta-diketone ligands: luminescent, magnetic, and reversible trans-to-cis photoisomerization properties. *Inorg. Chem.* 56, 3889–3900. doi: 10.1021/acs.inorgchem.6b02819

Lin, L. R., Wang, X., Wei, G. N., Tang, H. H., Zhang, H., and Ma, L. H. (2016). Azobenzene-derived tris-beta-diketonate lanthanide complexes: reversible trans-to-cis photoisomerization in solution and solid state. *Dalton Trans.* 45, 14954–14964. doi: 10.1039/C6DT01310D

Liu, G. F., Ji, W., Wang, W. L., and Feng, C. L. (2015). Multiresponsive hydrogel coassembled from phenylalanine and azobenzene derivatives as 3D scaffolds for photoguiding cell adhesion and release. *ACS Appl. Mater. Interfaces* 7, 301–307. doi: 10.1021/am506202s

Pang, J., Tian, Z. Q., and Mab, J. (2014). Theoretical design of visible light driven azobenzene-basedphoto-switching molecules. *Chem. Phys. Lett.* 613, 110–114. doi: 10.1016/j.cplett.2014.07.048

Pang, J., Ye, Y. F., Tian, Z. Q., Pang, X. Y., and Wu, C. Y. (2016). Theoretical insight into azobis-(benzo-18-crown-6) ether combined with the alkaline earth metal cations. *Comput. Theor. Chem.* 1076, 17–22. doi: 10.1016/j.comptc.2015.04.012

Schmidt, R., Hagen, S., Brete, D., Carley, R., Gahl, C., Dokic, J., et al. (2010). On the electronic and geometrical structure of the trans- and cis-isomer of tetra-tert-butyl-azobenzene on Au(111). *Phys. Chem. Chem. Phys.* 12, 4488–4497. doi: 10.1039/b924409c

Sun, Y., Yu, C., Liu, Z., Huang, C., Hao, Q., and Xu, L. (2012). Synthesis, structure, photo-responsive properties of 4-(2-fluorobenzylideneamino)antipyrine: a combined experimental and theoretical study. *Spectrochim. Acta A Mol. Biomol. Spectrosc.* 97, 1013–1022. doi: 10.1016/j.saa.2012.07.117

Wang, D., Ha, Y., Gu, J., Li, Q., Zhang, L., and Yang, P. (2016). 2D protein supramolecular nanofilm with exceptionally large area and emergent functions. *Adv. Mater.* 28, 7414–7423. doi: 10.1002/adma.201506476

Wang, D., Wagner, M., Butt, H. J., and Wu, S. (2015). Supramolecular hydrogels constructed by red-light-responsive host-guest interactions for photo-controlled protein release in deep tissue. *Soft Matter* 11, 7656–7662. doi: 10.1039/C5SM01888A

Ye, Y. F., Pang, J., Zhou, X. J., and Huang, J. W. (2015). Understanding the torsion effects on optical properties of azobenzene derivatives. *Comput. Theor. Chem.* 1066, 28–33. doi: 10.1016/j.comptc.2015.11.022

Yuan, K., Guo, Y. J., and Zhao, X. (2014). A novel photo-responsive azobenzene-containing nanoring host for fullerene-guest facile encapsulation and release. *Phys. Chem. Chem. Phys.* 16, 27053–27064. doi: 10.1039/C4CP03687E

Yue, C., Sun, H., Liu, W. J., Guan, B., Deng, X., Zhang, X., et al. (2017). Environmentally benign, rapid, and selective extraction of gold from ores and waste electronic materials. *Angew. Chem.* 56, 9331–9335. doi: 10.1002/anie.201703412

TiO₂ as Photosensitizer and Photoinitiator for Synthesis of Photoactive TiO₂-PEGDA Hydrogel Without Organic Photoinitiator

Sarah Glass, Betsy Trinklein, Bernd Abel and Agnes Schulze*

Leibniz Institute of Surface Engineering (IOM), Leipzig, Germany

The replacement of potentially toxic photoinitiators is of increasing interest regarding the synthesis of biomaterials by photopolymerization. Therefore, we present a new method for the preparation of UV polymerized hydrogels with TiO_2 as a photoinitiator. Titania is known to be an excellent photoactive compound which is non-toxic, inert, and cheap. The so-formed hydrogels possess excellent mechanical properties, a high swelling ratio, and high thermal stability. Furthermore, no TiO_2 is released from the hydrogels. Thus, the material is highly suitable for medical applications. Additionally, the present TiO_2 in the hydrogels remains photoactive as demonstrated by degradation of methylene blue. This enables the application of TiO_2-hydrogels in photodynamic therapy.

Keywords: hydrogels, titania, biomaterial, photopolymerization, photodynamic therapy

INTRODUCTION

Hydrogels are three-dimensional polymeric networks made out of highly hydrophilic monomers (Wichterle, 1960; Hoare and Kohane, 2008). They can be produced from natural materials like chitosan, dextran, and gelatin (Cabral et al., 2014; Wisotzki et al., 2014; Chan et al., 2015), or from artificial monomers [e.g., poly(ethylene glycol), polyamides, and several more] (Fujishige and Ando, 1989; Lin and Anseth, 2009). Mixtures of both are also possible (Jiang et al., 1999). Of course, the choice of material influences its properties (Ahmed, 2015) and therefore its application. Typical applications for hydrogels are artificial tissues (Lee and Mooney, 2001), wound dressings (Frykberg and Banks, 2015), contact lenses, drug delivery systems (Hoare and Kohane, 2008) and several other biomedical applications (Peppas et al., 2000; Ahmed, 2015; Caló and Khutoryanskiy, 2015; Chai et al., 2017).

Hydrogels are very often synthesized by photopolymerization (Peppas and Khare, 1993; Fairbanks et al., 2009). Herein a photoinitiator is used which produces reactive species, such as radicals, when irradiated with light. These radicals can initiate polymerization reactions for hydrogel synthesis. In general, a non-cytotoxic and biocompatible material is required for biomedical applications. Nevertheless, some photoinitiators are known to be cytotoxic (Williams et al., 2005; Mironi-Harpaz et al., 2012; Xu et al., 2015). The toxicity of photoinitiators is usually dependent on the concentration and exposed tissue (Sabnis et al., 2009). Consequently, crosslinking efficiency and cytotoxicity have to be considered (Mironi-Harpaz et al., 2012). Therefore, an alternative biocompatible photoinitiator is preferable. A promising photoinitiator candidate could be TiO_2 (titania), which has been used as an inorganic photoinitiator for materials synthesis in previous studies (Wan et al., 2006; Liao et al., 2014; Lobry et al., 2016).

Titania is a well-studied photoactive compound with excellent mechanical, optical, and physical properties (Kazuhito et al., 2005; Chen and Mao, 2007; Gupta and Tripathi, 2011). Furthermore, TiO$_2$ possesses high chemical stability, superhydrophilicity (Gan et al., 2007), biocompatibility (López-Huerta et al., 2014), reusability, and can be produced at low cost (Kumar and Bansal, 2013). Therefore, it has been investigated regarding several applications such as water purification (Kumar and Bansal, 2013), antifogging (Gan et al., 2007), disinfectant (Kumar and Bansal, 2013), and anticancer therapy (Lee et al., 2010) in the last centuries (Kazuhito et al., 2005).

TiO$_2$ is a semiconductor and has a band gap of 3.2 eV ($\lambda < 390$ nm). It exists in an amorphous phase that is non-photoactive (Henderson, 2011). Furthermore, there are three natural crystalline modifications: anatase, rutile, and brookite (Gupta and Tripathi, 2011). Rutile and anatase have been especially investigated since the 1950s (Kazuhito et al., 2005). Anatase was found to be more photoactive than rutile and brookite (Auguliaro et al., 1990; Zhang et al., 2014). Therefore, anatase is favored in photocatalytic applications. The composition of titania is dependent on various conditions during the preparation such as temperature (Gupta and Tripathi, 2011), pressure, and others (Fischer et al., 2017). A well-known, commercially available TiO$_2$ composite to be mentioned here is Degussa P25. Here, the anatase to rutile ratio is 70:30.

Given the fact that TiO$_2$ has such outstanding properties, it is widely used in various (hybrid) materials. Typical examples are concretes (Qin et al., 2015), ceramics (Bianchi et al., 2017), and also polymeric materials like membranes (Fischer et al., 2017) and hydrogels (Zhang et al., 2013). Such polymeric materials may also be used for photocatalytic or photomedical applications like photodynamic therapy (PDT). In PDT, so called photosensitizers (either organic dyes or photoactive pigments) are employed. A photosensitizer can produce singlet oxygen or other reactive oxygen species like hydroxyl radicals when irradiated with light (Raab, 1900). For several years this mechanism has been used very effectively in photomedicine (Rehman et al., 2016) because these reactive oxygen species are highly toxic against cancer cells (Dolmans et al., 2003). Moreover, photosensitizers have been used for the treatment of bacteria, viruses and fungi for some years (Juzeniene et al., 2007). Consequently, they are used in non-oncologic applications like infected or badly healing wounds.

As a result, TiO$_2$ is an ideal candidate as a photoinitiator and photoactive compound in polymeric hybrid materials. In the present study, TiO$_2$ was used with two functions at the same time as shown in **Figure 1**:

(1) photoinitiator: initiation of the photopolymerization to prepare the biocompatible hydrogel
(2) photosensitizer: formation of singlet oxygen/reactive oxygen species as a possible application in photodynamic therapy.

A hydrogel prepared with TiO$_2$ remains photoactive, and because no organic photoinitiator is used it is non-cytotoxic. Because of the mechanical properties of the hydrogel it can also be applied as a wound dressing or bandage. Furthermore, this new method enables, in general, the synthesis of materials for biomedical applications.

MATERIAL AND METHODS

Materials

Poly(ethylene glycol)diacrylate with an average mass of 700 g mol^{-1} (PEGDA), titanium isopropoxide (97% in isopropanol, TTIP), 37 wt% hydrochloric acid, nutrient solution, fetal bovine serum and phosphate buffer saline (PBS) were purchased from Sigma-Aldrich (St. Louis, USA). A stock solution of 50 wt% PEGDA in water was used to prepare the formulations. 1-[4-(2-hydroxyethoxy)-phenyl]-2-hydroxy-2-methyl-1 propane 1-one (α-HAP) was bought from IGM Resins B.V. (Waalwijk, Netherlands). Resazurin solution (Alamar blue) was purchased from Thermo Fisher Scientific (Waltham, USA).

A Merck ultrapure water system was used to purify water. All chemicals were used without further purification.

Preparation of Crystalline TiO$_2$-Nanoparticles

The TiO$_2$ nanoparticle synthesis follows the method recently employed for polymer membranes (Fischer et al., 2017). In that process, 8.1 ml TTIP was slowly added to 80 ml of 0.1 M hydrochloric acid. The mixture was transferred to a temperature- and pressure-safe Teflon beaker and was shaken at 300 rpm for 4 h. Afterwards, it was heated to 60°C for 20 h. Once cooled down, the clear liquid on top of the solution was removed and 22.5 ml of water were added. An opaque and white suspension was received. The amount of TiO$_2$ in the solution was determined gravimetrically to be 5 wt%. The solution was used within 2 days after preparation to avoid agglomeration.

XRD

The TiO$_2$ particles were dried at room temperature and crushed to a fine powder. X-ray diffractograms of these nanoparticles were recorded with a Rigaku Ultima IV X-ray diffraction spectrometer with Cu Kα radiation with the following parameters: 40 kV, 40 mA, scanning speed of 1.0° min^{-1}, and in increments of 0.02° in a 10–75° range.

The weight fractions (W) of anatase (A), brookite (B), and rutile (R) were calculated from the peak integrals by using the following equation, where A corresponds to the peak areas and k corresponds to the XRD response factors of the respective crystal phases:

$$W_{(A,R,B)} = \frac{k_{(A,R,B)} \cdot A_{(A,R,B)}}{k_A \cdot A_A + k_R \cdot A_R + k_B \cdot A_B} \tag{1}$$

The response factors were set to ($k_A = 0.886$, $k_R = 1$ and $k_B = 2.721$) (Liu et al., 2016).

Hydrogel Synthesis

All hydrogels were prepared with 30 wt% PEGDA, PBS, and a photoinitiator. The formulations were sonicated for 15 min and afterwards irradiated with a medium pressure mercury lamp (UV Technik Meyer GmbH, Germany) on a conveyor. The light dose corresponded to 7,000 mJ cm^{-2} and 2,500 mJ cm^{-2} for the TiO$_2$

FIGURE 1 | Schematic graphic of the usage of TiO$_2$ nanoparticles as (1) photoinitiator and (2) photosensitizer.

FIGURE 2 | XRD pattern of crystallite TiO$_2$ nanoparticles. The main reflexes were marked with A (anatase), B (brookite) and R (rutile).
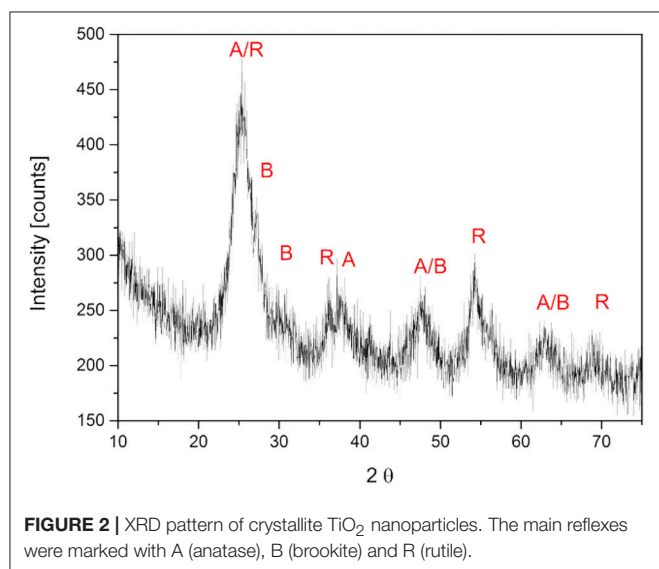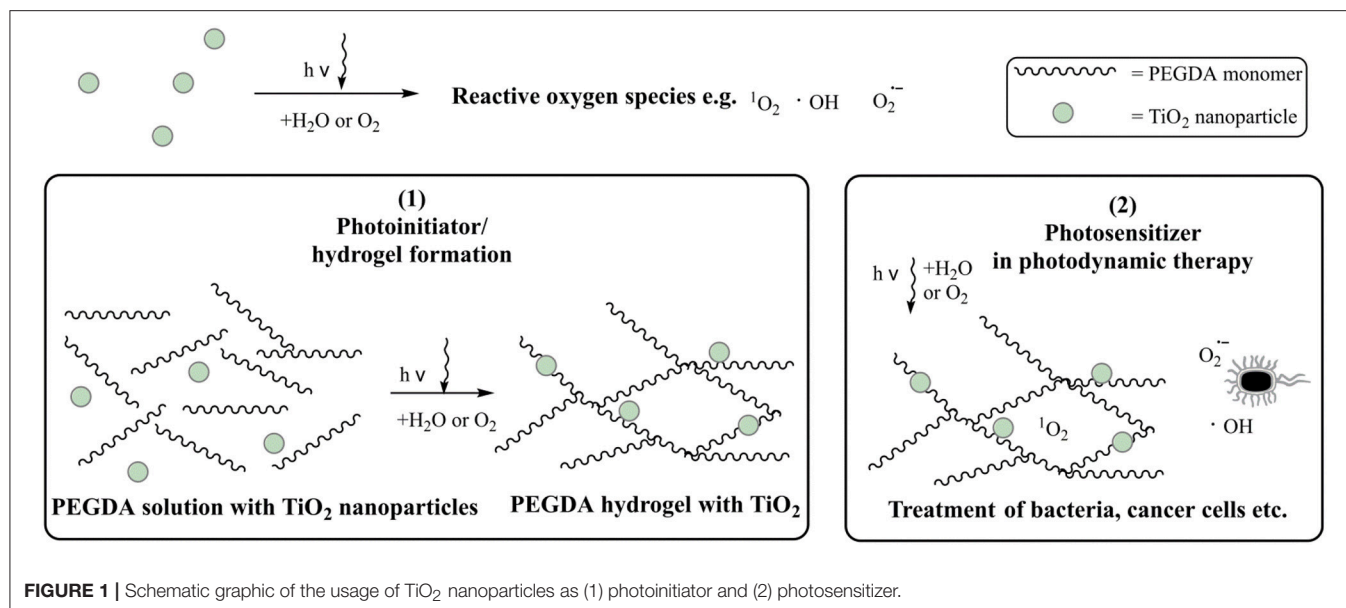
gels and the α-HAP gels, respectively. Afterwards, the gels were washed with PBS for 24 h and then shaken in water for 2 h at 200 rpm. Finally, the gels were dried at 40°C for 24 h in a N$_2$ atmosphere. The hydrogels were synthesized either with 1 wt% crystalline TiO$_2$ or with 0.1 wt% of a commercial initiator (α-HAP) as a reference (Pelras et al., 2017). α-HAP was used because it is also known to be cytocompatible (Williams et al., 2005).

UV/VIS Spectroscopy

An UV-2101PC UV-Vis spectrometer from Shimadzu was used to record transmittance curves of the dried hydrogels. The studied range was 200–800 nm with 0.5 nm resolution. Samples had an average thickness of 1 mm.

Rheology

Rheological measurements of the dried hydrogels were performed on a MCR300 rheometer from Anton Paar (Graz, Austria). The rheometer was equipped with a planar 25 mm diameter head. The frequency was varied from 0.16 to 16 Hz. The probe head was pressed on the sample with a pressure of 10 N.

Swelling Ratio

The swelling ratio q was calculated as a ratio of the mass of the wet hydrogel directly after preparation and washing (m_{wet}), to the mass of the dry hydrogel (m_{dry}) as shown in equation (2). Swelling ratios are given in percent.

$$q = \frac{m_{wet}}{m_{dry}} \qquad (2)$$

Scanning Electron Microscopy

The freshly dried hydrogels were sputtered with a 30 nm chromium layer using a Leybold Z400 sputter system. Afterwards, scanning electron microscopy (SEM) was performed using an Ultra-55 microscope equipped with a Gemini Detector both from Zeiss (Jena, Germany) at a pressure of 2×10^{-5} mbar and 5 kV voltages. The top, bottom, and cross-section of all gels were analyzed.

Release Study

The dried hydrogels were immersed in 10 mL PBS buffer at 37°C. The TiO$_2$ particles were allowed to release for 24 h. Afterwards the PBS buffer was changed completely. The process was repeated twice. The solutions after 24, 48, and 72 h were analyzed photometrical with an infinite M200 reader from Tecan (Maennedorf, Switzerland). The absorbance of TiO$_2$ at 300 nm was detected. Furthermore, the amount of TiO$_2$ lost to the solution was observed with inductively coupled plasma atomic emission spectroscopy (ICP-OES) with a Ciros vision spectrometer from spectro (Kleve, Deutschland).
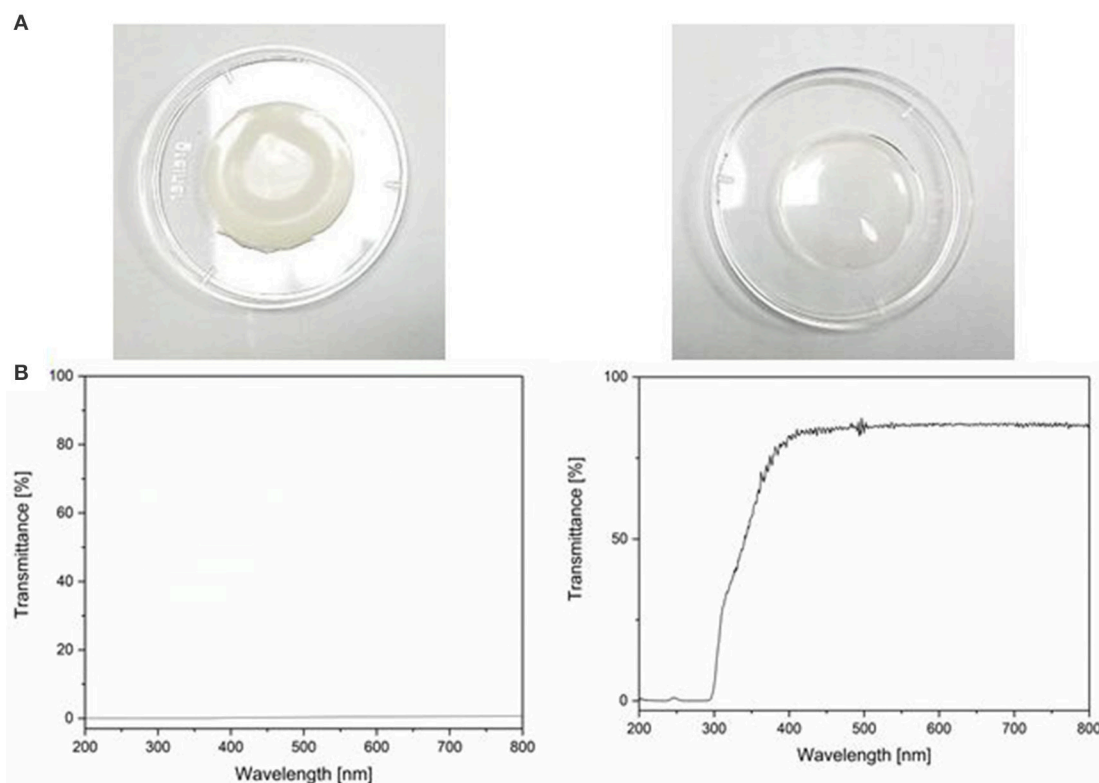
FIGURE 3 | (A) Photo of hydrogels prepared with TiO_2 nanoparticles as photoinitiator (left) and with the commercial photoinitiator α-HAP (right). **(B)** UV/VIS transmittance spectra of the aforementioned.

Determination of the Photoactivity

Photoactivity was measured by monitoring the decomposition of methylene blue as reported before (Fischer et al., 2014). Therefore, the gel was immersed in a 20 μM methylene blue PBS solution for 24 h in the dark to make sure the dye uptake of the gel was complete and equilibrium was established. A circle of a diameter of 1 cm was cut in the gels. Afterwards the gels were placed in 8 ml of a 20 μM solution of methylene blue and irradiated with a sunlamp (Heraus Original Hanau Suncare tanning tube 21/25 slim) for 2 h in total. For the first 40 min the concentrations were detected every 10 min, afterwards every 20 min. The concentrations were recorded with an infinite M200 reader from Tecan (Maennedorf, Switzerland).

Thermal Degradation

The thermal stability of the produced dried hydrogels was observed by thermos gravimetric analysis. A Pyris 1 TGA from Perkin Elmer was used to perform this measurement. Air was used as purge gas. The temperature range was 20–800°C with a heat rate of 10°C min^{-1}.

Cytotoxicity

Hydrogels were sterilized by autoclaving. Afterwards they were extracted in RPMI-1640 medium. A 1 ml solution was used per 3 cm² hydrogel surface. The cell concentration was set to 6.7×10^4 cells ml^{-1}. Afterwards, 20 μl fetal bovine serum and

TABLE 1 | Mechanical properties of the hydrogels. Rheological data were recorded at 1 Hz.

	PEGDA hydrogel with TiO_2	PEGDA hydrogel with α-HAP
G*	55.2 kPa	131.3 kPa
G′	3.1 kPa	3.6 kPa
G″	55.2 kPa	131.3 kPa
tan(δ)	0.057	0.029
q	392%	342%

20 μl Alamar Blue were added to 180 μl of the cell suspension. The cells (L929, mouse fibroblasts) were bred over night at 37°C in a 5% CO_2 atmosphere. After 24, 48, and 72 h the fluorescence of Alamar Blue at 590 nm was determined with an infinite M200 reader from Tecan (Maennedorf, Switzerland).

RESULTS AND DISCUSSION

Crystallinity of TiO_2 Nanoparticles

The prepared TiO_2 nanoparticle suspension was dried for 24 h at room temperature and crushed by mortar and pestle. The fine powder was analyzed by XRD to determine the crystal phases. The diffractogram is presented in **Figure 2**. The main reflexes were detected at 25.5°, 27.4°, 30.2°, 36.1°, 37.7°, 47.8°, 54.3°,
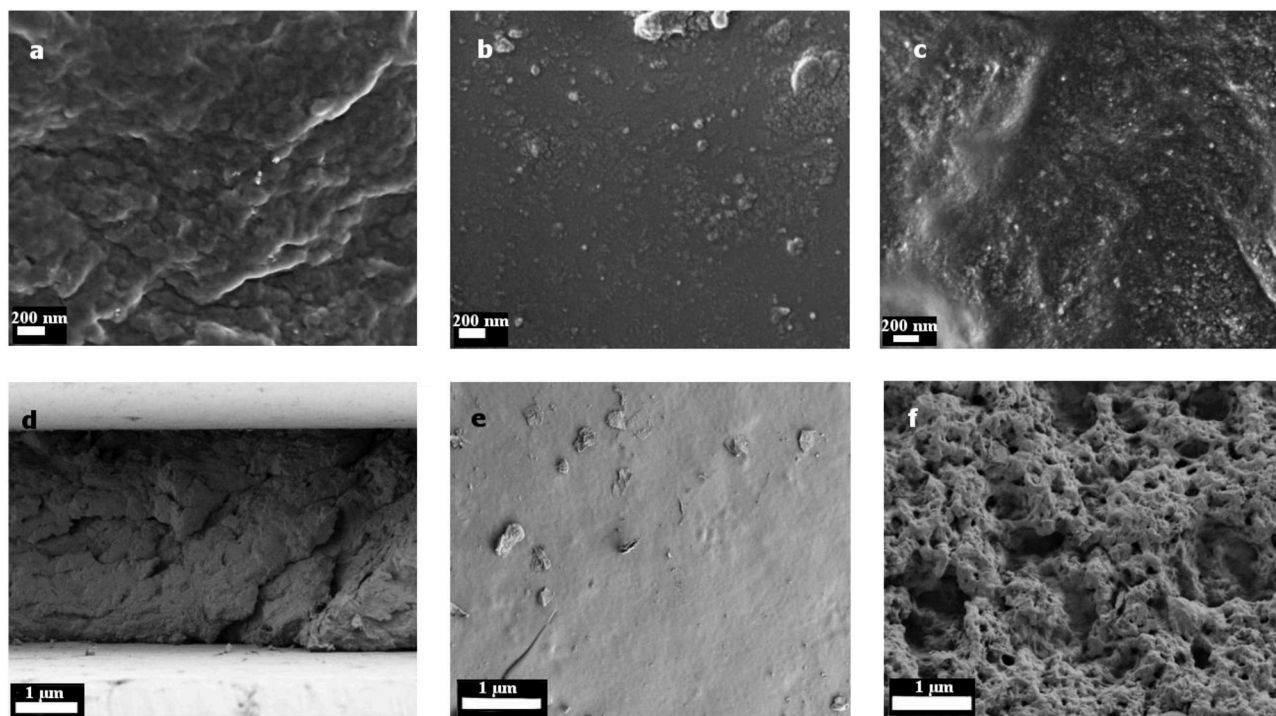
FIGURE 4 | SEM images of the hydrogels with TiO$_2$ as the photoinitiator. Pictures **(A)** and **(D)** show the cross section, **(B)** and **(E)** the top side and **(C)** and **(F)** the bottom side. In figures **(A)** to **(C)** the magnification is enlarged compared to figures **(D)** to **(F)**.
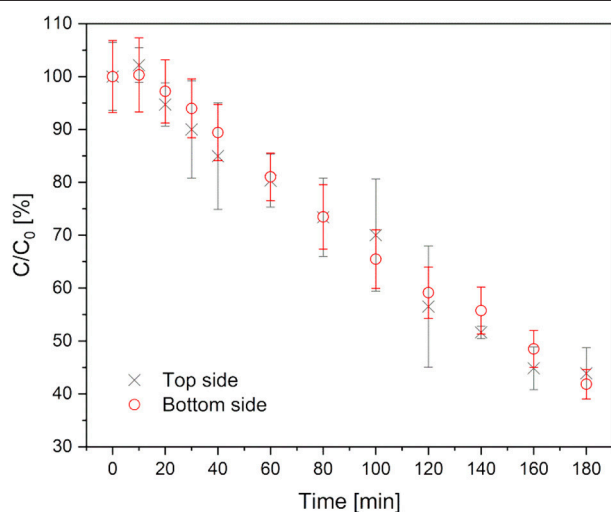
FIGURE 5 | Methylene blue degradation in hydrogels with TiO$_2$ as photoinitiator. Black crosses represent the degradation, when the top side is up, red circles when the bottom side is up.

63.5°, and 69.2°. They were related to the main crystal phases of titania [anatase (Horn et al., 1972), rutile (Swope et al., 1995), and brookite (Meagher and Lager, 1979)] in **Figure 2**. Moreover, the weight fractions were calculated with equation (1) to result in a ratio of anatase 61%, rutile 19%, and brookite 20%. A high

fraction of anatase like in this sample is reported to be favorable, because anatase is known to be the most photoactive crystal phase. (Zhang et al., 2014)

Hydrogel Appearance and Optical Properties

Figure 3A shows a picture of the dried hydrogels with TiO$_2$ (left) and α-HAP (right) after photopolymerization. The TiO$_2$ gels were about 1 mm thick and had a white, opaque, homogeneous, and shiny appearance. The diameter of the swollen gels was about 35 mm, while the dried gels had a diameter of 23 mm. The hydrogels prepared with the commercial photoinitiator α-HAP were transparent and had the same diameter and size like the hydrogels prepared with TiO$_2$ as the photoinitiator. The white color of the TiO$_2$-PEGDA-hydrogel was generated by the embedded TiO$_2$. Therefore it can be assumed that TiO$_2$ is homogeneously distributed in the gel.

The hydrogels synthesized with TiO$_2$ as the photoinitiator were white and absorbed light in the entire range of visible light. In **Figure 3B** the UV/VIS transmittance spectra of both hydrogels are displayed. The transmittance of the hydrogel matrix is about 70% starting from 350 nm. The overall transmittance was lower than 1% when TiO$_2$ was present in the hydrogel matrix.

Mechanical Properties

In **Table 1** the rheological data at a shear frequency of 1 Hz are shown. Dynamic modulus (G*), loss modulus (G'), storage modulus (G"), and loss factor [tan(δ)] were determined. The
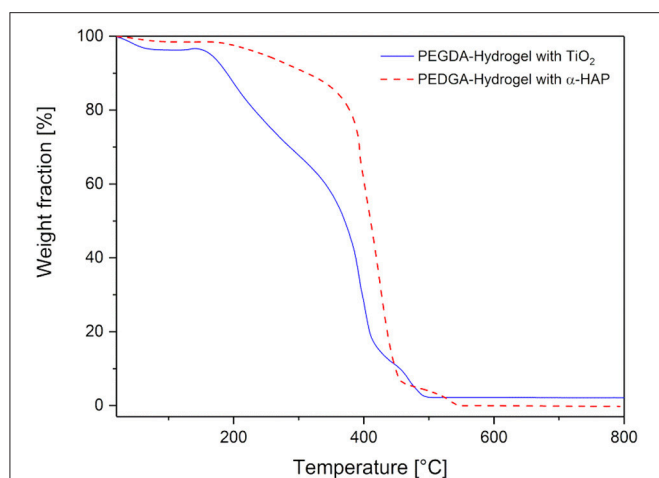
FIGURE 6 | Thermogravimetric analysis of the hydrogels prepared with commercial photoinitiator α-HAP (red, dotted line) compared to the ones with TiO$_2$ (blue, solid line).

TABLE 2 | Cell viability.

Time [h]	PEGDA hydrogel with TiO$_2$ (%)	PEGDA hydrogel with α-HAP (%)
24	98	99
48	97	97
72	97	99

complete graphs can be seen in **Supplementary Figure 1**. The moduli of the TiO$_2$-PEGDA hydrogels were much smaller compared to the PEGDA hydrogels with the commercial initiator. This means on the one hand that the gels with TiO$_2$ are much softer and less elastic (and therefore more viscous) than the gels with α-HAP. Higher softness could be beneficial for a medical application on tissue because the gels can adjust better with the tissue. On the other hand, an about three times smaller storage modulus (55.200 kPa compared to 131.333 kPa) corresponds to a larger mesh size (Lohmann et al., 2017) and a lower crosslinking density (Hajighasem and Kabiri, 2013). This influences the swelling ratio, too.

The swelling ratio of the TiO$_2$-hybrid-hydrogels was 392 ± 28%. This is significantly higher than the swelling ratio of the gels made with the commercial photoinitiator (342 ± 3%.). This indicates higher mesh sizes and therefore confirms the results of the rheological characterization. A further possible reason for the higher swelling ratio is the increased hydrophilicity of the hydrogel due to the presence of superhydrophilic TiO$_2$ nanoparticles (Wang et al., 1997, 1998; Gan et al., 2007). A higher swelling ratio is favorable for wound dressing applications because more wound exudate can be taken up and the dressing can be changed less often.

Morphology

In **Figure 4** the SEM images of the TiO$_2$ gels are shown. The top side was the side which was facing the lamp during

photopolymerization. This side of the gels (**Figures 4B,E**) was very smooth. The TiO$_2$ nanoparticles were displaced as small, white spots in and on the surface. They had a size of about 10 to 20 nm. On the top side only some few particles can be seen (see **Figure 4B**). The main part of the TiO$_2$ particles was finely distributed in the polymer matrix as it is demonstrated in **Figure 4A** and on the bottom side (**Figure 4C**). However, as can be seen in **Figure 4C**, there were some small aggregates found. The bottom side had a foam-like structure with several pores and holes. This can probably explain the higher swelling ratio compared to the smooth and dense gels with the commercial photoinitiator (**Supplementary Figure 1**), because those pores could encapsulate water. The hydrogels with α-HAP had a highly smooth top and bottom surface without any defects (**Supplementary Figure 2**).

TiO$_2$ Release and Photoactivity

In the release and photoactivity experiments only the hydrogels with TiO$_2$ as the photoinitiator/photosensitizer were investigated because the hydrogels with the commercial initiator α-HAP contained no photoactive substance.

The loss of TiO$_2$ nanoparticles is a main problem of many hybrid materials. If TiO$_2$ is released from the material the photoactivity decreases. Furthermore, nanoparticles are under suspicion to cause Alzheimer's disease (Maher et al., 2016). Therefore, a loss of TiO$_2$ in materials must be avoided for medical applications.

For this reason, a possible TiO$_2$ release was investigated as described in section Release Study after 24, 48, and 120 h by UV/VIS spectroscopy and by ICP-OES, respectively. Neither in UV/VIS analysis nor in ICP-OES measurements was TiO$_2$ detected. Consequently, the unwanted release of TiO$_2$ nanoparticles can be excluded; the particles were embedded permanently within the polymer network of the hydrogel.

The photoactivity was monitored by degradation of methylene blue over 180 min. As discussed in section Morphology of top/bottom side of the gel differs. Therefore, the top and bottom sides of the hydrogels with TiO$_2$ as the photoinitiator were investigated separately by turning each side up. The hydrogels were immersed in 20 μM methylene blue solution for 24 h in the dark.

The degradation of methylene blue is presented in **Figure 5**. In the first 10 min of irradiation a slight increase in the methylene blue concentration (about 5%) was detected. This can be explained by photodesorption as discussed for photochemical processes on TiO$_2$ (Becerril et al., 2013). Afterwards, the photodecomposition takes place. Approximately 20% methylene blue was degraded per hour. The degradation rate stayed nearly constant over the whole time of observation. This indicates a zeroth order reaction, which is typical for reactions on catalytic surfaces. After 180 min about 60% of the methylene blue had been degraded. Furthermore, the degradation profile of the top/bottom sides was comparable. Consequently, the different surface morphology does not affect the photoactivity of the hydrogel. However, it should be considered that the morphology that was detected by SEM showed dried samples,

while the hydrogels used in photocatalytic degradation tests were used in their swollen state. The recyclability of the hydrogels was not tested because they are meant for a one-time usage.

Thermal Stability

The thermogravimetric analysis of the dried hydrogels is presented in **Figure 6**. Both hydrogel types showed a small weight loss of 2 and 4%, respectively, at a temperature of 100°C. This corresponds to a loss of water, which was absorbed under atmospheric conditions. Here, it can be concluded again, that the hydrogels with TiO_2 have a slightly higher ability to absorb water (as already found for the swelling behavior in section Mechanical Properties). With increasing temperature, the weight of the hybrid gels stayed stable up to 150°C. This is very important to ensure a possible sterilization by autoclaving, which normally takes place at 121°C or 134°C. At higher temperatures thermal degradation was observed. First, there was a weight loss of about 35% up to a temperature of 330°C, followed by a degradation step of nearly 50% of the weight within the next 100°C. Above 450°C there was a forth weight loss of 5%. At 550°C the degradation was complete. There was a residual weight of about 2.2%, which corresponds to non-degradable TiO_2. The degradation of the hydrogel that was produced with the commercial initiator was almost the same, except the second weight loss was smaller (just 15% up to 400°C). This means the hydrogels produced with the commercial photoinitiator were more stable at higher temperatures than the ones produced with TiO_2. In all probability, the lower degradation temperature is induced by the lower crosslinking which was shown in section Mechanical Properties.

Cytotoxicity

For biomedical applications like bandages or photodynamic therapy, cytocompatibility is very important. To prove this, the cytotoxicity was studied by investigation of the viability of mouse fibroblasts. The viability of the cells in the hydrogel extracts is shown in **Table 2**. It was not possible to investigate the viability directly on the gels, because cells cannot adhere to the very smooth surface. For that reason the cytotoxicity of the extracts of the hydrogels was monitored. Nearly 100% of the cells survived up to 72 h in the extracts. We found no indication of toxicity of the material from the above experiments such that we assume non-toxicity of the gel as well. Further studies will shed more light into this. This may be of relevance for future medical applications.

CONCLUSION

In this study it was shown that nanosized crystalline TiO_2 can be used as a photoinitiator for polymeric PEGDA hydrogels. The TiO_2 used here consisted mainly of anatase. Using TiO_2 as a photoinitiator is beneficial for medical applications because commercial organic photoinitiators (or

their photocleavage products) are often toxic, while TiO_2 is known to be biocompatible. The synthesized hydrogels have a high dynamic modulus (55.2 kPa at 1 Hz) and are therefore decidedly mechanically stable while still elastic (tan(δ) ≈ 0.06). Additionally, they can be sterilized by autoclaving due to their sufficient thermal stability. We found no indication of toxicity of the hydrogel material. These outstanding properties make the hydrogels very promising candidates for medical applications such as usage as a wound patch. Furthermore, the TiO_2 was well distributed in the matrix and was still photoactive when irradiated with a sunlamp. Therefore, it can be used not only as a photoinitiator during polymerization of the hydrogels, but also as a photosensitizer in photodynamic therapy.

However, the photoactivity of the TiO_2 in the hydrogels must be improved in further studies. To do so, the transparency of the hydrogels shall be increased. This will enable the activation of TiO_2 below the polymer matrix and will allow the photosensitive material to be applied directly on a wound. Furthermore, additional biological tests like viability of further cell lines or antibacterial tests shall be done.

Nevertheless, TiO_2 may have great potential as a photoinitiator in hydrogel materials for medical applications, especially because of the photosensitizing effect of the hydrogels with TiO_2 which can be used in photodynamic therapy.

AUTHOR CONTRIBUTIONS

FUNDING

ACKNOWLEDGMENTS

SUPPLEMENTARY MATERIAL

The Supplementary Material for this article can be found online at: https://www.frontiersin.org/articles/10.3389/fchem.2018.00340/full#supplementary-material

REFERENCES

Ahmed, E. M. (2015). Hydrogel: preparation, characterization, and applications: a review. *J. Adv. Res.* 6, 105–121. doi: 10.1016/j.jare.2013.07.006

Auguliaro, V., Davì, E., Palmisano, L., Schiavello, M., and Sclafani, A. (1990). Influence of hydrogen peroxide on the kinetics of phenol photodegradation in aqueous titanium dioxide dispersion. *Appl. Catalysis* 65, 101–116. doi: 10.1016/S0166-9834(00)81591-2

Becerril, J. J., Arce, Z., and Hernandez, A. M. (2013). Methylene blue and 4-chlorophenol photodegradation using gamma-irradiated titanium oxide. *J. Chem. Soc. Pak.* 35, 23–26.

Bianchi, C. L., Sacchi, B., Capelli, S., Pirola, C., Cerrato, G., Morandi, S., et al. (2017). Micro-sized TiO2 as photoactive catalyst coated on industrial porcelain grès tiles to photodegrade drugs in water. *Environ. Sci. Pollut. Res. Int.* 25, 20348–20353. doi: 10.1007/s11356-017-9066-6

Cabral, J. D., Roxburgh, M., Shi, Z., Liu, L., Mcconnell, M., Williams, G., et al. (2014). Synthesis, physiochemical characterization, and biocompatibility of a chitosan/dextran-based hydrogel for postsurgical adhesion prevention. *J. Mater. Sci. Mater. Med.* 25, 2743–2756. doi: 10.1007/s10856-014-5292-3

Caló, E., and Khutoryanskiy, V. V. (2015). Biomedical applications of hydrogels: a review of patents and commercial products. *Eur. Polym. J.* 65, 252–267. doi: 10.1016/j.eurpolymj.2014.11.024

Chai, Q., Jiao, Y., and Yu, X. (2017). Hydrogels for biomedical applications: their characteristics and the mechanisms behind them. *Gels* 3:6. doi: 10.3390/gels3010006

Chan, M., Brooks, H. J., Moratti, S. C., Hanton, L. R., and Cabral, J. D. (2015). Reducing the oxidation level of dextran aldehyde in a chitosan/dextran-based surgical hydrogel increases biocompatibility and decreases antimicrobial efficacy. *Int. J. Mol. Sci.* 16, 13798–13814. doi: 10.3390/ijms160613798

Chen, X., and Mao, S. S. (2007). Titanium dioxide nanomaterials: synthesis, properties, modifications, and applications. *Chem. Rev.* 107, 2891–2959. doi: 10.1021/cr0500535

Dolmans, D. E. J. G. J., Fukumura, D., and Jain, R. K. (2003). Photodynamic therapy for cancer. *Nat. Rev. Cancer* 3, 380–387. doi: 10.1038/nrc1071

Fairbanks, B. D., Schwartz, M. P., Bowman, C. N., and Anseth, K. S. (2009). Photoinitiated polymerization of PEG-diacrylate with lithium phenyl-2,4,6-trimethylbenzoylphosphinate: polymerization rate and cytocompatibility. *Biomaterials* 30, 6702–6707. doi: 10.1016/j.biomaterials.2009.08.055

Fischer, K., Gawel, A., Rosen, D., Krause, M., Abdul Latif, A., Griebel, J., et al. (2017). Low-temperature synthesis of anatase/rutile/brookite tio2 nanoparticles on a polymer membrane for photocatalysis. *Catalysts* 7:209. doi: 10.3390/catal7070209

Fischer, K., Gläser, R., and Schulze, A. (2014). Nanoneedle and nanotubular titanium dioxide–PES mixed matrix membrane for photocatalysis. *Appl. Catalysis B Environ.* 160–161, 456–464. doi: 10.1016/j.apcatb.2014.05.054

Frykberg, R. G., and Banks, J. (2015). Challenges in the treatment of chronic wounds. *Adv. Wound Care* 4, 560–582. doi: 10.1089/wound.2015.0635

Fujishige, S. K., Ando, K. I. (1989). Phase transition of aqueous solutions of poly(n-isopropylacrylamide) and poly(n-isopropylmethacrylamide). *J. Phys. Chem.* 93, 3311–3313. doi: 10.1021/j100345a085

Gan, W. Y., Lam, S. W., Chiang, K., Amal, R., Zhao, H., and Brungs, M. P. (2007). Novel TiO2 thin film with non-UV activated superwetting and antifogging behaviours. *J. Mat. Chem.* 17, 952–954. doi: 10.1039/b618280a

Gupta, S. M., and Tripathi, M. (2011). A review of TiO2 nanoparticles. *Chin. Sci. Bull.* 56:1639. doi: 10.1007/s11434-011-4476-1

Hajighasem, A., and Kabiri, K. (2013). Cationic highly alcohol-swellable gels: synthesis and characterization. *J. Polymer Res.* 20:218. doi: 10.1007/s10965-013-0218-1

Henderson, M. A. (2011). A surface science perspective on TiO2 photocatalysis. *Surf. Sci. Rep.* 66, 185–297. doi: 10.1016/j.surfrep.2011.01.001

Hoare, T. R., and Kohane, D. S. (2008). Hydrogels in drug delivery: progress and challenges. *Polymer* 49, 1993–2007. doi: 10.1016/j.polymer.2008.01.027

Horn, M., Schwerdtfeger, C. F., and Meagher, E. P. (1972). Refinement of the structure of anatase at several temperatures. *Zeitschrift für Kristallographie* 136, 273–281.

Jiang, H., Su, W., Mather, P. T., and Bunning, T. J. (1999). Rheology of highly swollen chitosan/polyacrylate hydrogels. *Polymer* 40, 4593–4602. doi: 10.1016/S0032-3861(99)00070-1

Juzeniene, A., Peng, Q., and Moan, J. (2007). Milestones in the development of photodynamic therapy and fluorescence diagnosis. *Photochem. Photobiol. Sci.* 6, 1234–1245. doi: 10.1039/b705461k

Kazuhito, H., Hiroshi, I., and Akira, F. (2005). TiO$_2$ Photocatalysis: a historical overview and future prospects. *Jpn. J. Appl. Phys.* 44:8269. doi: 10.1143/JJAP.44.8269

Kumar, J., and Bansal, A. (2013). Photocatalysis by nanoparticles of titanium dioxide for drinking water purification: a conceptual and state-of-art review. *Mat. Sci. Forum* 764, 130–150. doi: 10.4028/www.scientific.net/MSF.764.130

Lee, C., Hong, C., Kim, H., Kang, J., and Zheng, H. M. (2010). TiO2 nanotubes as a therapeutic agent for cancer thermotherapy. *Photochem. Photobiol.* 86, 981–989. doi: 10.1111/j.1751-1097.2010.00731.x

Lee, K. Y., and Mooney, D. J. (2001). Hydrogels for tissue engineering. *Chem. Rev.* 101, 1869–1879. doi: 10.1021/cr000108x

Liao, C., Wu, Q., Su, T., Zhang, D., Wu, Q., and Wang, Q. (2014). Nanocomposite gels via *in situ* photoinitiation and disassembly of tio2–clay composites with polymers applied as uv protective films. *ACS Appl. Mater. Inter.* 6, 1356–1360. doi: 10.1021/am404515b

Lin, C. C., and Anseth, K. S. (2009). PEG hydrogels for the controlled release of biomolecules in regenerative medicine. *Pharm. Res.* 26, 631–643. doi: 10.1007/s11095-008-9801-2

Liu, C., Yu, T., and Tan, X. (2016). Characterization and photocatalytic activity of mixed nanocrystalline TiO2 powders prepared by xerogel-hydrothermal method in different acid solutions. *Transa. Tianjin Uni.* 22, 473–479. doi: 10.1007/s12209-016-2776-x

Lobry, E., Bt Bah, A. S., Vidal, L., Oliveros, E., Braun, A. M., Criqui, A., et al. (2016). Colloidal and supported TiO2: toward nonextractable and recyclable photocatalysts for radical polymerizations in aqueous dispersed media. *Macromole. Chem. Phys.* 217, 2321–2329. doi: 10.1002/macp.201600150

Lohmann, N., Schirmer, L., Atallah, P., Wandel, E., Ferrer, R. A., Werner, C., et al. (2017). Glycosaminoglycan-based hydrogels capture inflammatory chemokines and rescue defective wound healing in mice. *Sci. Translat. Med.* 9:eaai9044 doi: 10.1126/scitranslmed.aai9044

López-Huerta, F., Cervantes, B., González, O., Hernández-Torres, J., García-González, L., Vega, R., et al. (2014). Biocompatibility and surface properties of TiO2 thin films deposited by dc magnetron sputtering. *Materials* 7:4105. doi: 10.3390/ma7064105

Maher, B. A., Ahmed, I. A., Karloukovski, V., MacLaren, D. A., Foulds, P. G., Allsop, D., et al. (2016). Magnetite pollution nanoparticles in the human brain. *Proc. Nat. Acad. Sci. U.S.A.* 113, 10797–10801. doi: 10.1073/pnas.1605941113

Meagher, E. P., and Lager, G. A. (1979). Polyhedral thermal expansion in the TiO$_2$ polymorphs: refinement of the crystal structures of rutile and brookite at high temperature. *Can. Mineral.* 17, 77–85.

Mironi-Harpaz, I., Wang, D. Y., Venkatraman, S., and Seliktar, D. (2012). Photopolymerization of cell-encapsulating hydrogels: crosslinking efficiency versus cytotoxicity. *Acta Biomater.* 8, 1838–1848. doi: 10.1016/j.actbio.2011.12.034

Pelras, T., Glass, S., Scherzer, T., Elsner, C., Schulze, A., and Abel, B. (2017). Transparent low molecular weight poly(ethylene glycol) diacrylate-based hydrogels as film media for photoswitchable drugs. *Polymers* 9:639. doi: 10.3390/polym9120639

Peppas, N. A., Bures, P., Leobandung, W., and Ichikawa, H. (2000). Hydrogels in pharmaceutical formulations. *Eur. J. Pharm. Biopharm.* 50, 27–46. doi: 10.1016/S0939-6411(00)00090-4

Peppas, N. A., and Khare, A. R. (1993). Preparation, structure and diffusional behavior of hydrogels in controlled release. *Adv. Drug Deliv. Rev.* 11, 1–35. doi: 10.1016/0169-409X(93)90025-Y

Qin, Z. B., Zhang, W. T., Qian, G. P., Wu, X. L., and Li, Y. (2015). The effects of different ways of adding nano-TiO2 to concrete on the degradation performance of NO2. *Mat. Res. Innovat.* 19, S10-148–S110-154. doi: 10.1179/1432891715Z.0000000002127

Raab, O. (1900). Ueber die wirkung fluoreszierender stoffe auf infusorien. *Z. Biol.* 39, 524–546.

Rehman, F. U., Zhao, C., Jiang, H., and Wang, X. (2016). Biomedical applications of nano-titania in theranostics and photodynamic therapy. *Biomater. Sci.* 4, 40–54. doi: 10.1039/C5BM00332F

Sabnis, A., Rahimi, M., Chapman, C., and Nguyen, K. T. (2009). Cytocompatibility studies of an *in situ* photopolymerized thermoresponsive hydrogel nanoparticle system using human aortic smooth muscle cells. *J. Biomed. Mat. Res.* 91, 52–59. doi: 10.1002/jbm.a.32194

Swope, R. J., Smyth Joseph, R., and Larson Allen, C. (1995). H in rutile-type compounds: I. Single-crystal neutron and X-ray diffraction study of H in rutile. *Am. Mineralogist* 80, 448–453. doi: 10.2138/am-1995-5-604

Wan, T., Wang, Y. C., and Feng, F. (2006). Preparation of titanium dioxide/polyacrylate nanocomposites by sol–gel process in reverse micelles and *in situ* photopolymerization. *J. Appl. Polymer Sci.* 102, 5105–5112. doi: 10.1002/app.24166

Wang, R., Hashimoto, K., Fujishima, A., Chikuni, M., Kojima, E., Kitamura, A., et al. (1997). Light-induced amphiphilic surfaces. *Nature* 388, 431–432. doi: 10.1038/41233

Wang, R., Hashimoto, K., Fujishima, A., Chikuni, M., Kojima, E., Kitamura, A., et al. (1998). Photogeneration of highly amphiphilic tio2 surfaces. *Adv. Mat.* 10, 135–138. doi: 10.1002/(SICI)1521-4095(199801)10:2<135::AID-ADMA135>3.0.CO;2-M

Wichterle, O. L. D. (1960). Hydrophilic gels for biological use. *Nature* 185, 117–118. doi: 10.1038/185117a0

Williams, C. G., Malik, A. N., Kim, T. K., Manson, P. N., and Elisseeff, J. H. (2005). Variable cytocompatibility of six cell lines with photoinitiators used for polymerizing hydrogels and cell encapsulation. *Biomaterials* 26, 1211–1218. doi: 10.1016/j.biomaterials.2004.04.024

Wisotzki, E. I., Hennes, M., Schuldt, C., Engert, F., Knolle, W., Decker, U., et al. (2014). Tailoring the material properties of gelatin hydrogels by high energy electron irradiation. *J. Mater. Chem. B* 2, 4297–4309. doi: 10.1039/C4TB00429A

Xu, L., Sheybani, N., Yeudall, W. A., and Yang, H. (2015). The effect of photoinitiators on intracellular AKT signaling pathway in tissue engineering application. *Biomater. Sci.* 3, 250–255. doi: 10.1039/C4BM00245H

Zhang, H., Shi, R., Xie, A., Li, J., Chen, L., Chen, P., et al. (2013). Novel TiO2/PEGDA hybrid hydrogel prepared *in situ* on tumor cells for effective photodynamic therapy. *ACS Appl. Mater. Inter.* 5, 12317–12322. doi: 10.1021/am4025559

Zhang, J., Zhou, P., Liu, J., and Yu, J. (2014). New understanding of the difference of photocatalytic activity among anatase, rutile and brookite TiO2. *Phys. Chem. Chem. Phys.* 16, 20382–20386. doi: 10.1039/C4CP02201G

Multi-Layered Hydrogels for Biomedical Applications

Guiting Liu [1†], Zhangfan Ding [2†], Qijuan Yuan [1], Huixu Xie [2*] and Zhipeng Gu [1*]

[1] Key Laboratory of Sensing Technology and Biomedical Instrument of Guangdong Province, School of Biomedical Engineering, Sun Yat-sen University, Guangzhou, China, [2] State Key Laboratory of Oral Diseases, Department of Head and Neck Oncology, National Clinical Research Center for Oral Diseases, West China Hospital of Stomatology, Sichuan University, Chengdu, China

Multi-layered hydrogels with organization of various functional layers have been the materials of choice for biomedical applications. This review summarized the recent progress of multi-layered hydrogels according to their preparation methods: layer-by-layer self-assembly technology, step-wise technique, photo-polymerization technique and sequential electrospinning technique. In addition, their morphology and biomedical applications were also introduced. At the end of this review, we discussed the current challenges to the development of multi-layered hydrogels and pointed out that 3D printing may provide a new platform for the design of multi-layered hydrogels and expand their applications in the biomedical field.

Keywords: multi-layered hydrogel, layer-by-layer self-assembly, step-wise, photo-polymerization, sequential electrospinning, biomedical application

INTRODUCTION

Hydrogels are three-dimensional polymeric networks cross-linked by physical, chemical interactions or a combination of both. Due to the hydrophilicity of the polymer chains in network, hydrogels can absorb and retain large amounts of water while immersed in aqueous solutions (Ahmed, 2015). A key property of hydrogel matrices is that they have not only viscoelastic properties like many soft tissues but also permeability to different types of molecules, such as proteins, bioactive agents and growth factors (Pan et al., 2011; Gupta et al., 2014; Lau and Kiick, 2015). Therefore, hydrogels have been frequently utilized in the field of drug delivery and tissue engineering (Hoffman, 2001; Highley et al., 2016; Fundueanu et al., 2017). In most instances, hydrogels are used as homogeneous soft materials with uniform bulk properties (Elisseeff, 2008). To better mimic anisotropic and complex structure of body tissues, hierarchical hydrogels containing multiple layers with different biochemical cues and various mechanical properties play crucial role for biomedical applications (O'Leary et al., 2011; Hu and Chen, 2014; Martínezsanz et al., 2016). Further, multi-layered hydrogels, formulated by the combination of multiple cell types, drugs or some other exogenous factors, could realize the controlled release behavior or cell interactions. With the emergence of biomaterials and fabricated technologies, the multi-layered hydrogels have been widely design for achieving adequate perfusion in biomedical applications (Christensen et al., 2018; Wang et al., 2018).

In the past decade years, significant advances have been made in generating various multi-layered hydrogels. Most of these efforts so far have focused on engineering preparation of hydrogels with mimetic structure by different fabricating technologies. Since layer-by-layer (LBL) technology has attracted scientists to develop structure-controlled multi-layered hydrogels in the second half of the twentieth century, much important advancement has been brought in this field aim to ever

GRAPHICAL ABSTRACT | The preparation of multi-layered hydrogels and their biomedical applications.
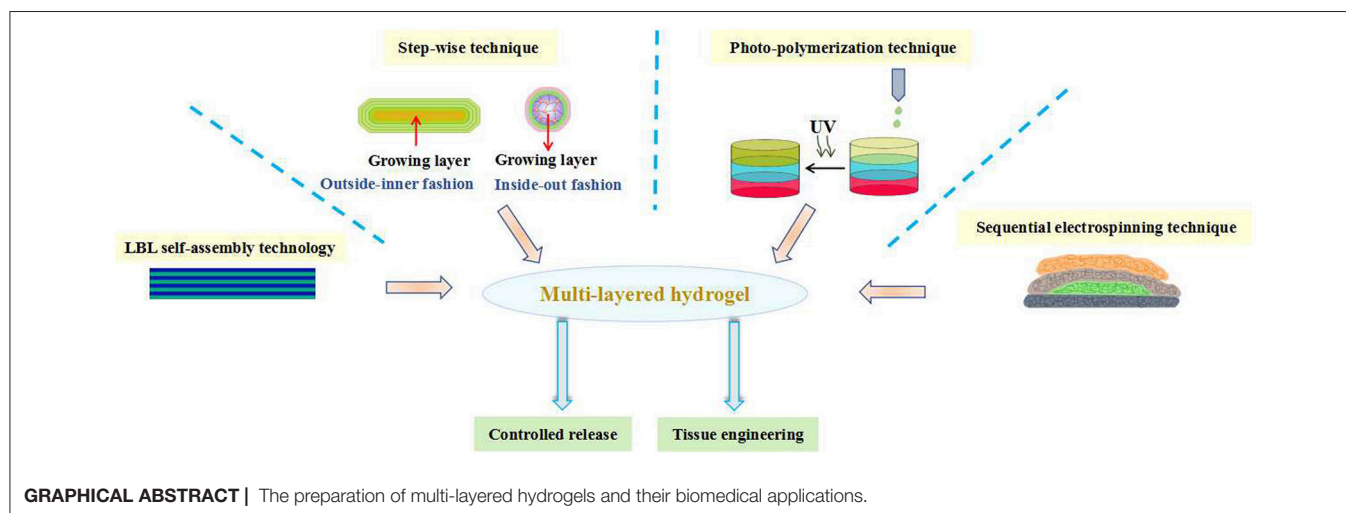
closer achieving structural functions. In recent years, in addition to the development of multi-layered hydrogels by LBL technique, an increasing number of scientists are also becoming involved in step-wise technique, photo-polymerization technique, sequential electrospinning technique and 3D printing technique ect. Owing to their simplicity, versatility and robustness, multi-layered hydrogels could be manufactured as promising biomaterials for clinical applications. Until now, however, the overview, challenges and outlook of the multi-layered hydrogels in the field of biomedical applications have not been systematically reported. Herein, this review aims to summarize the recent progress in the fabrication of multi-layered hydrogels and their applications in biomedical fields. Further, the development of multi-layered hydrogels will be reviewed according to their preparation methods from four aspects and their morphology and biomedical applications will also be introduced. At the end, current challenges and future perspectives of multi-layered hydrogels for biomedical applications are mainly discussed.

MULTI-LAYERED HYDROGEL BASED ON LAYER-BY-LAYER (LBL) SELF-ASSEMBLY TECHNOLOGY AND ITS BIOMEDICAL APPLICATIONS

At present, various technologies have emerged for the fabrication of multi-layered hydrogels. Among them, lay-by-layer (LBL) self-assembly technology has developed into the most commonly utilized method. In 1966, Iler et al. proposed the concept of LBL self-assembly for the first time. They used oppositely charged colloidal particles to alternately assemble on the glass substrate, and a film with controllable multi-layered structure was obtained (Iler, 1966). Since this pioneering work, LBL self-assembly technology has been extensively studied in the past few decades. The classic LBL self-assembly technology used the electrostatic interaction as a diving force to realize the process of assembly. With the deepening of study, a variety of

driving forces have been developed to achieve LBL self-assembly, such as hydrogen bonding, covalent bonding, supramolecular complexation, biospecific recognition, charge transfer complex, etc. (Hoshi et al., 2002; Stuart et al., 2010; Xue et al., 2017). The development of LBL self-assembly technology provides a versatile tool for the preparation of multi-layered hydrogels, which generally possess ultrathin and alternating layered structure.

Takeoka et al. prepared flexible, adhesive and robust polysaccharide nanosheet for surgical repair of tissue defects (Fujie et al., 2010). Alginate and chitosan, both of which are biocompatible and biodegradable, were selected as the building blocks to construct the nanosheet by spin-coating-assisted LBL method (**Figure 1**). The alternating layered structure of nanosheet was characterized by ellipsometric and IR spectroscopic test, which revealed that the thickness of one layer pair was about 2.9 nm, interfacial bonded by electrostatic interactions. The mechanical and physiological properties of the nanosheet could be easily modulated by the regulation of the concentration of polymers and the number of layers. The *in vivo* test showed that a nanosheet of 75 nm was suitable for the repairing of a visceral pleural defect in beagle dogs without any pleural adhesion. Such polysaccharide nanosheet has great potential as a novel tissue-defect repair material for various organs. In addition to the regulation of building blocks and the number of layers, the regulation of secondary structure could also contribute designable performance to the multi-layered hydrogels. For example, Hammond et al. prepared poly(ethylene oxide)-*block*-poly(ε-caprolactone) (PEO-*b*-PCL) micelles to carry the model drug triclosan. Then a multi-layered hydrogel film was fabricated by the alternating assembly of PEO-*b*-PCL micelles and poly(acrylic acid) (PAA) based on the hydrogen bond interactions in acidic solutions. Due to the weakness of hydrogen bonding, the multi-layered film disintegrated and released the PEO-*b*-PCL micelles under physiological conditions. Furthermore, the release period of triclosan could be extended by cross-linking the carboxylic acid groups of PAA layer (Kim et al., 2008). Li et al. prepared a

FIGURE 1 | Schematic representation of the SA/CS nanosheet used for tissue-defect repair. **(A)** Fabrication of a free-standing SA/CS nanosheet by LBL method. **(B)** Schematic explanation of tissue-defect by SA/CS nanosheet.
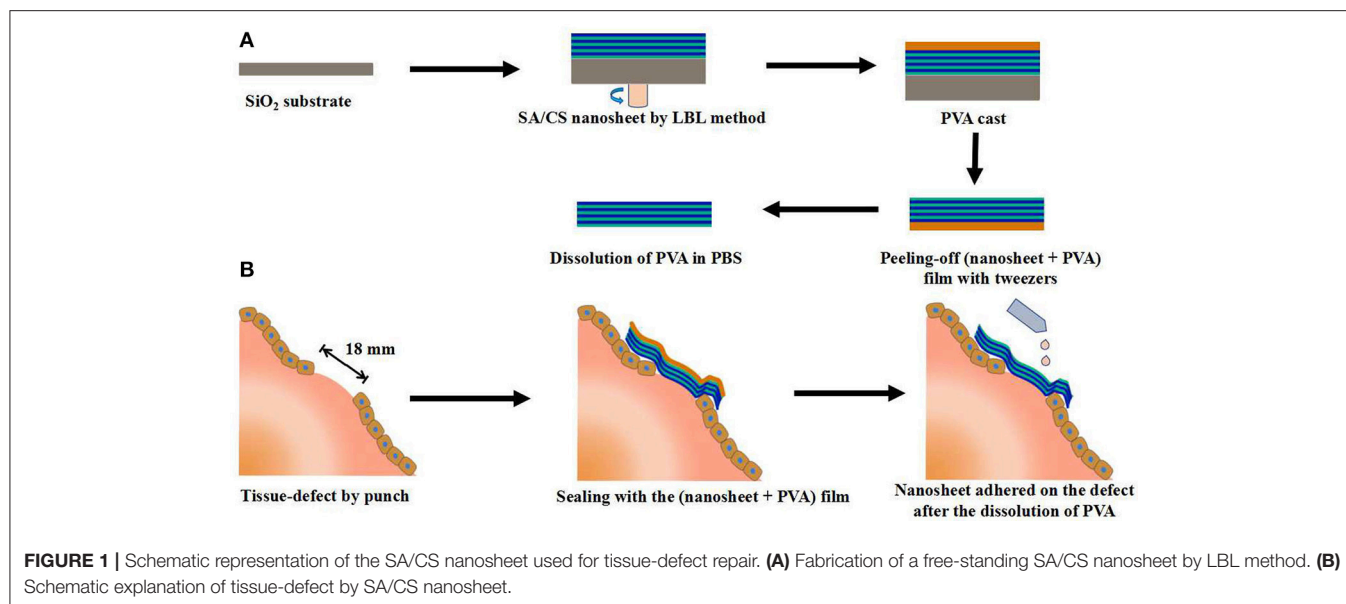
glucose-sensitive multi-layered hydrogel film based on glucose oxidase (GOD) and insulin as well as a 21-arm star polymer by LBL self-assembly technology, driving by electrostatic interaction (Chen et al., 2011). The *in vitro* study indicated that such multi-layered hydrogel film could act as a responsive system switch to glucose, due to the pH-sensitivity of star polymer. Furthermore, this kind of multi-layered film had the potential to realize the multiple controlled release of insulin by the further modify of star polymer.

In the past few decades, the application of implantable biomedical devices has achieved rapid development, such as artificial blood pump, intraocular lenses, artificial joint and cardiovascular stent (Moro et al., 2004; Mani et al., 2007; Guan et al., 2018). However, such applications face various problems, including metal hypersensitivity, infection and inflammation (Anderson, 2008; Lichter et al., 2016). In order to solve these problems, Ishihara's group did a lot of significantly work by the use of bioactive agents-loaded multi-layered hydrogel coatings on the implanted surface. For example, Ishihara et al. constructed a hydrogel coating with alternating six-layer structure on the surface of titanium alloy based on the synthesized phospholipid polymer (PMDV) and alginate by LBL technology, through the combination of electrostatic interaction and covalent bonding between PMDV and alginate (Choi et al., 2009b). Vascular endothelial growth factor (VEGF), a potent angiogenic signal transduction molecule, was selected as the model drug and loaded into the alginate layer by dispersing in alginate solutions in the process of self-assembly. The *in vitro* study showed that such multi-layered hydrogel coating achieved the sustained release of VEGF during one week. In another work, Ishihara et al. constructed a multi-layered hydrogel coating on titanium alloy surface based on another synthesized phospholipid polymer (PMBV) and poly(vinyl alcohol) (PVA) by LBL technology,

driving by the reversible covalent bonding between boronic acid groups of PMBV and hydroxyl groups of PVA (Choi et al., 2009a). Paclitaxel (PTX), a poorly water-soluble antineoplastic agent, was dispersed in PMBV aqueous solutions due to the amphiphilicity of PMBV. During the layer stacking process of LBL technology, the PTX-loaded PMBV layer could be located on the designated layer of the multi-layered hydrogel coating. And the content of PTX increased with the number of PTX-loaded PMBV layer. The additional layers of PMBV and PVA, without PTX, could work as diffusion-barrier. In this way, the multi-layered hydrogel coating could enable the controlled release of PTX depending on the location and number of PTX-loaded PMBV layer (**Figure 2**). In a further work, Ishihara et al. studied the regulation of cellular proliferation by the PTX-loaded PMBV/PVA multi-layered hydrogels (Choi et al., 2012). The cell culture experiments showed that the cell proliferation of human epidermal carcinoma A431 cell could be controlled by the amount of released PTX. A desirable cell proliferation could be achieved by the PMBV/PVA multi-layered hydrogel with PTX loaded on an appropriate layer. These works suggested that the multi-layered hydrogel coatings fabricated by the LBL technology have the huge potential applications for the loading and surface-mediated delivery of bioactive agents from implantable biomedical devices.

As bacterial infection, especially related to the biomedical implants, is a great threat to patients, significant efforts have recently been focused on the design and fabrication of antibacterial materials (Pavlukhina and Sukhishvili, 2011; Busscher et al., 2012). Among these researches, the study of antibacterial hydrogel coating fabricated by LBL technology has attracted extensively attentions (Moskowitz et al., 2010; Xu et al., 2017). For example, Zhu et al. constructed ultrathin multi-layered hydrogel films based on the two synthesized

FIGURE 2 | Schematic representation of PVA/PMBV multi-layered hydrogels with PTX incorporated in bottom and top layers.
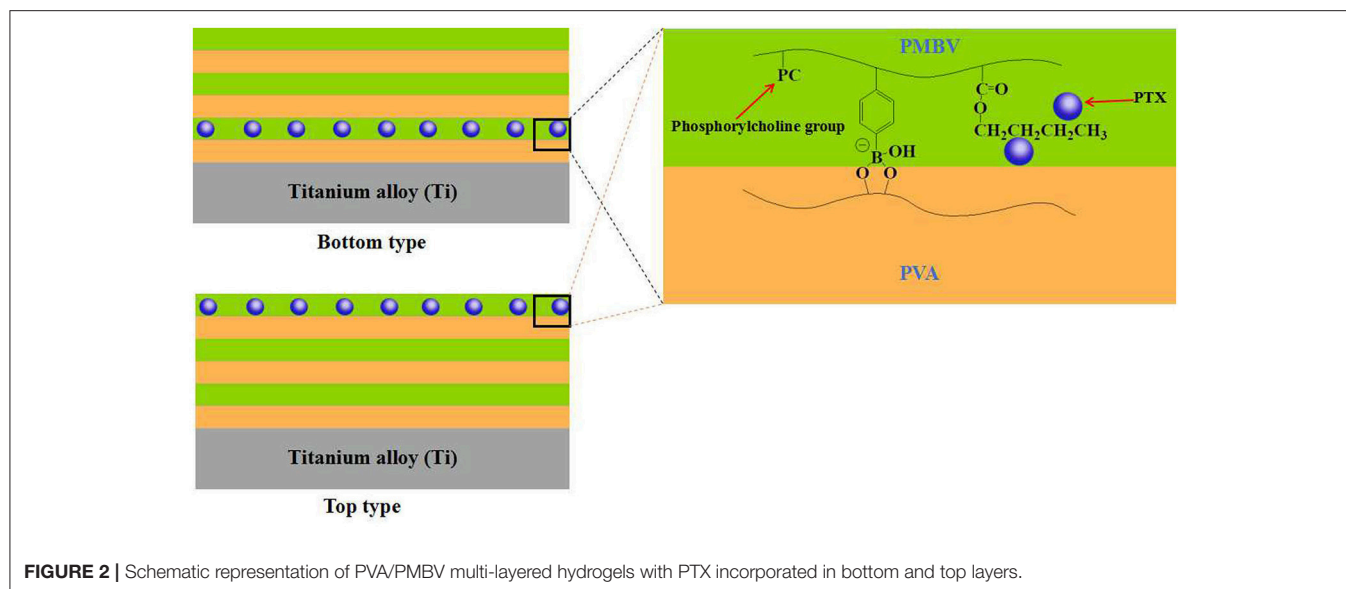
PEG-based polymers POEGDMAM containing multi-enes and POEGMS containing multi-thiols by LBL technology, driving by the thio-ene "click" reaction (Wang et al., 2014). Owing to the presence of quaternary ammonium groups in the POEGDMAM, such multi-layered films exhibited significant antibacterial activity against both gram-positive and gram-negative bacteria, and the more layers the better the effect. Werner et al. fabricated bio-hybrid hydrogel coating on the surface of thermoplastic polyurethane substrates based on amino functionalized star-shaped PEG and EDC-s-NHS activated heparin (Fischer et al., 2015). Then silver nanoparticles were encapsulated into the star-PEG/heparin hydrogel when immersed into $AgNO_3$ buffer solutions. Moreover, in order to regulate the release of silver ion, a silver-free star-PEG/heparin hydrogel was coated on the top of silver-loaded star-PEG/heparin hydrogel layer. The inhibition assay and blood incubation assay indicated that such multi-layered hydrogels could effectively combine antibacterial activity and hemocompatibility. In contrast to the traditional antibacterial hydrogel coating, Sukhishvili et al. fabricated bacteria-responsive hydrogel coatings without any antibacterial agents based on the self-defensive concept (Lu et al., 2015). They developed a family of polyanionic poly(2-alkylacrylic acids) (PaAAs) whose hydrophobicity could be modulated by their alkyl side chain length. Multi-layered hydrogels with varying hydrophobicity were constructed based on PaAAs and polyvinylpyrrolidone (PVPON) by LBL technology. The antibacterial activity assay indicated that when the medium turned acidic resulted from the bacterial proliferation, the PaAAs/PVPON hydrogels became more hydrophobic and dehydrated, and killed the bacterial contacted with the surface of hydrogel coatings. The more hydrophobic the PaAAs/PVPON hydrogels were, the better the killing efficiency was. Furthermore, the cell viability assays showed that such multi-layered hydrogel coatings exhibited no cytotoxicity to human osteoblasts.

MULTI-LAYERED HYDROGEL BASED ON STEP-WISE TECHNIQUE AND ITS BIOMEDICAL APPLICATIONS

Nature inspired materials have attracted increasing attentions in the biomedical field for the past decades (Zhao et al., 2014; Zhang et al., 2016). Like onion, spinal disc and egg, all of which having many different layers organized in a concentric fashion, inspired the fabrication of onion-like multi-layered hydrogels. These onion-like hydrogels have great potential application in biomedical fields, such as cell bioreactors, drug delivery, evaluation of cell-cell interactions and tissue engineering (Kunze et al., 2011; Baek et al., 2013). More recently, the step-wise technique has developed into the most commonly utilized method for the construction of hydrogels with onion-like architectures in an inside-out or outside-inner fashion.

Ladet et al. firstly reported the fabrication of onion-like hydrogels by controlling the kinetic gelation process of alginate or chitosan in an outside-inner fashion (Ladet et al., 2008). The precursor hydrogel could be easily prepared by evaporating water from the chitosan solution with water/1,2-propanediol mixed solvent. After the soaking of precursor hydrogel in NaOH and NaCl mixture solutions, the chitosan molecular chain was neutralized and physically cross-linked by hydrophobic interactions and hydrogen bonding due to the conversion of NH_3^+ to NH_2. By controlling the kinetics of neutralization, the first membrane of precursor hydrogel could be formed. After the multi-step interrupted gelation process, the multi-layered chitosan hydrogel with onion-like architecture was obtained (**Figure 3**). By the same method, the onion-like alginate hydrogel was also prepared by the neutralization of precursor hydrogel in $CaCl_2$ baths. In a further study, Ladet et al. investigated the bioactivity of the prepared onion-like chitosan hydrogel as chondrocytic cell bioreactors (Ladet et al., 2011). In this work,

FIGURE 3 | Schematic representation of chitosan multi-layered hydrogels prepared by step-wise technique.
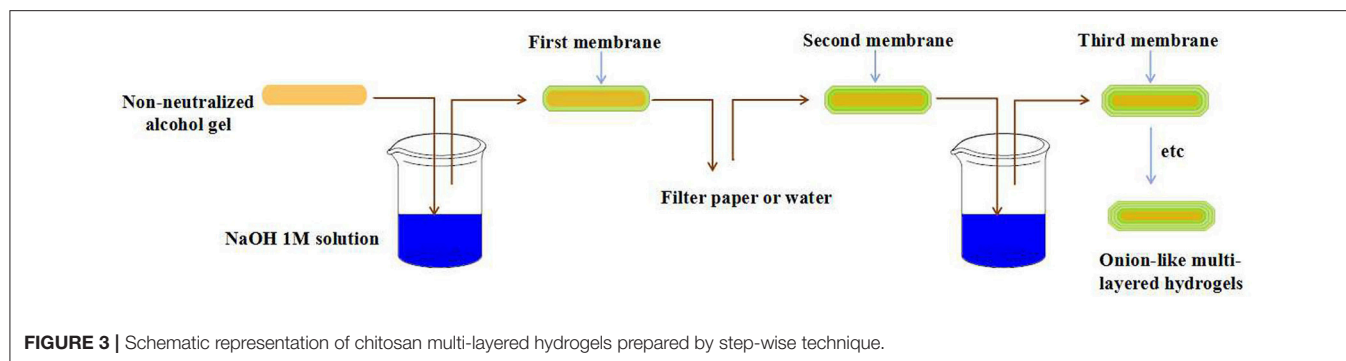
the articular rabbit chondrocytes were entrapped into the inter-membrane spaces of onion-like chitosan hydrogel and cultured for 45 days. This kind of multi-layered architecture had the ability to create the hypoxic physiological environment similar to the inter-vertebral disc tissues and cartilage. In addition, this multi-layered structure could prevent the cell penetration within the hydrogel matrix but allowed the protein diffusion throughout the hydrogel. The *in vitro* study revealed that chondrocytes not only formed cell aggregates and proliferated, but also produced numerous cartilage-type matrix proteins. Furthermore, no inflammatory markers were observed during the period of culture. Similarly, Hu et al. prepared multi-layer chitosan hydrogel by controlling the gelation process of chitosan solution, induced by acidic aqueous medium (Nie et al., 2015). Once the surface of chitosan solutions contacted with NaOH aqueous solutions, gelation started and the contact area transformed into a hydrogel layer instantly. Then the formed primary hydrogel acted as the medium between chitosan solutions and OH$^-$ source. As the OH$^-$ continued to diffuse, the onion-like chitosan hydrogel was formed with a layer-wise characteristic. By the utilization of such mechanism, multi-layered chitosan hydrogels with various architectures and shaped could be easily constructed in such an outside-inner fashion.

Besides the outside-inner fashion, the step-wise technique with an inside-out fashion, in which the precursor hydrogel core was constructed first and followed by the next different layers, was also commonly utilized to prepared multi-layer hydrogels with onion-like architecture. For example, Zhang et al. constructed onion-like cellulose hydrogel with high compressive strength and controllable architecture by a rapid contact of solid-liquid interface (He et al., 2014). Firstly, the agarose gel was prepared and worked as the precursor hydrogel core, and then soaked into acetic acid aqueous solutions. Subsequently, the agarose gel core with acetic acid was contacted with the cellulose solution with NaOH/urea mixture as solvent by a solid-liquid interface contact fashion. In this way, the first cellulose layer on the surface of agarose gel was formed, induced by the self-aggregation of cellulose chains resulted from the acid triggered destruction of cellulose inclusion complex in the NaOH/urea solutions. After the repeating of the above gelation process, the onion-like cellulose hydrogel was prepared. The architecture of the onion-like cellulose

hydrogel, such as layer thickness, inter-membrane space and size, could be regulated by controlling the morphology of precursor hydrogel core and the time of solid-liquid interface contact time, as well as cellulose concentrations. The *in vitro* study showed that such cellulose hydrogel exhibited excellent biocompatibility and the L929 cells could adhere and proliferate in the inter-membrane space. This kind of biocompatible multi-layered cellulose hydrogel with controlled architecture has bright application prospects in biomedical application. Zarket and Raghavan developed a novel strategy to constructed onion-like hydrogels in an inside-out fashion (Zarket and Raghavan, 2017). Normally, a precursor hydrogel core within water-soluble initiator was prepared first, and then was immersed into a solution containing a monomer (monomer A) and a cross-linker. With the diffusion of initiator into the surrounding solution, the polymerization of monomer A was trigged and the first layer on the surface of precursor hydrogel core was formed. By repeating such immersion process in another solution containing monomer B and a cross-linker, the second layer was formed. In this way, various layers with controlled compositions and properties could be systematically constructed around the precursor hydrogel core (**Figure 4**). As a result, the mechanical properties and architectures of the prepared onion-like hydrogels could be easily regulated. These multi-layered hydrogels prepared by such strategy have great potential applications in the field of multi-stimuli responsive drug delivery.

MULTI-LAYERED HYDROGEL BASED ON PHOTO-POLYMERIZATION TECHNIQUE AND ITS BIOMEDICAL APPLICATIONS

Photo-polymerization is a process that utilizes light to initiate a polymerization reaction to obtain a linear or cross-linked polymer structure (Shi et al., 2016). Photo-polymerization technique has been frequently utilized to construct hydrogels, which were generally formed *in situ* with a non-invasive manner (Sudhakar et al., 2015; Brown et al., 2018). Recently, the photo-polymerization technique has developed into a powerful tool to prepare multi-layered hydrogels with complex architectures, which were generally used for tissue engineering.

FIGURE 4 | Schematic representation of onion-like hydrogels based on an inside-out fashion.

FIGURE 5 | Schematic representation of three-layered hydrogels with spatially-varying mechanical properties by photo-polymerization technique.
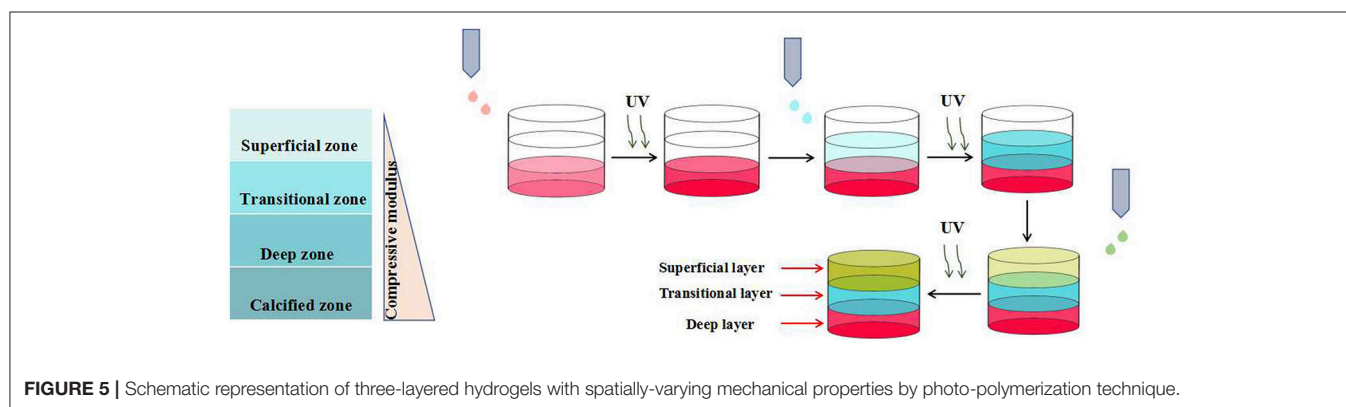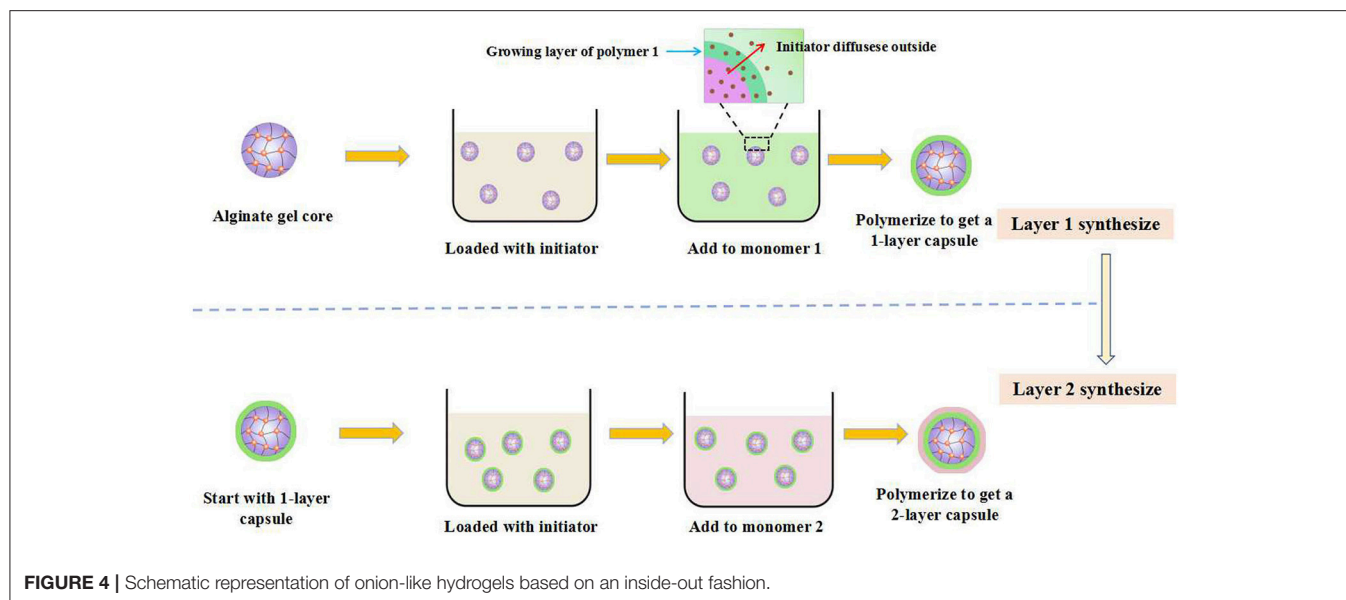
Roy et al. prepared a novel kind of multi-layered hydrogel with spatially-varying mechanical properties and composition by photo-polymerization technique (Nguyen et al., 2011). Articular cartilage with spatially-varying structure is comprised of four zones: the superficial, transitional, deep, and calcified zones. In order to mimic the architecture and function of native articular cartilage, the authors prepared a multi-layered hydrogels with three distinctive layers, corresponding to the superficial, transitional and deep zones, respectively. The pre-designed each layer of the hydrogel, possessing gradual biochemical and mechanical properties, was assembled in a layer-by-layer fashion (**Figure 5**). Such strategy could also be applied to mimic other complex tissues with spatially-varying properties, such as artificial skin, joints and blood vessels. Similarly, Bryant et al. constructed a poly(ethylene glycol)-based hydrogel with spatially-varying biochemical and mechanical properties for osteochondral tissue engineering by sequential photo-polymerization (Steinmetz et al., 2015). Such hydrogel with three distinctive layers was fabricated to mimic the cartilage, calcified cartilage and bone zones of osteochondral

tissues, respectively. The mechanical property of each layer was regulated by the concentration of macromer. And the biochemical property of each layer was modulated by varying the concentrations of chondroitin sulfate and RGD, both of which were selected as the extracellular matrix (ECM) molecules. Furthermore, the differentiation of human mesenchymal stem cells (hMSCs) within the multi-layered hydrogel matrix under intermittent dynamic compression was studied. The results indicated that dynamic mechanical stimulation could spatially guide hMSC differentiation efficiently. In another study, Bryant et al. constructed a multi-layered poly(ethylene glycol) (PEG) hydrogel with microchannels to promote the alignment of muscle cells (Hume et al., 2012). The inverse master mold with pre-designed width and depth was prepared by CLiPP polymerization first, then poly(ethylene glycol)diacrylate (PEGDA) solution was filled around the mold and irradiated by UV. After the removal of mold, PEG hydrogel with specific dimensions of macrochannels was formed. The *in vitro* study indicated that such three-dimensional long channels with width varying from 40 to 200 μm and depth varying from 100 to 200 μm promoted the muscle cell

alignment significantly, and the smaller the channel dimensions was, the better the improvement was.

MULTI-LAYERED HYDROGEL BASED ON SEQUENTIAL ELECTROSPINNING TECHNIQUE AND ITS BIOMEDICAL APPLICATIONS

Electrospun fibers have attracted numerous attentions due to their unique features, such as excellent mechanical properties, broad source of raw materials, high surface-area-to-volume ratio and designable morphology (Zucchelli et al., 2015; Wang and Windbergs, 2017). Sequential electrospinning technique, combining the advantages of electrospinning and multi-layering methodology, has also developed into a commonly used tool to construct multi-layered hydrogels for biomedical application (Kidoaki et al., 2005).

Kidoaki et al. constructed a dual drug loaded multi-layered hydrogel with time-programmed combination release behavior by sequential electrospinning technique (Okuda et al., 2010). Four function layers were sequential fabricated: first drug-loaded layer, barrier layer, second drug-loaded layer and basement layer (**Figure 6**). The model drug was dissolved in electrospinning solutions and loaded *in situ* during the electrospinning process. The *in vitro* experiments indicated that the release behavior of each drug could be controlled by the fiber diameter and the layer thickness. Thereby, the combination release of the dual drugs could be achieved by the pre-designed architecture of the multi-layered hydrogels. Such strategy has bright future in the fabrication of multi-layered hydrogels for combination therapy application. Cho et al. prepared polycaprolactone (PCL) nanofibers reinforced alginate (SA) hydrogels by sequential electrospinning technique (Jang et al., 2013). Briefly, PCL electrospun fibers were treated with ethanol, improving cohesion with SA hydrogel matrix, and evenly distributed on SA/CaCO$_3$ mixture solution, which was reapplied every five layers. With the repeating of such process, multi-layered SA hydrogels with various PCL nanofibers content were prepared. Compared with the pure SA hydrogels, the compressive strength and stiffness of PCL nanofibers reinforced SA hydrogels were improved by about 121 and 334%, respectively. In addition, the mechanical properties of such multi-layered composite hydrogels could be regulated by modulating the content of PCL nanofibers. Such mechanical property-enhanced hydrogels based on biocompatible polymer have great application as biomedical implants. Tuan et al. constructed a novel composite hydrogel scaffold based on fibrous poly-ε-caprolactone (PCL) and methacrylated gelatin (mGLT) for tendon tissue engineering by dual-electrospinning (Yang et al., 2016). After the co-electrospinning, composite scaffold could convert into composite hydrogel with uniform composition by photo-crosslinking retained mGLT. In this way, multi-layered composite hydrogels, mimicking native tendon tissues, could be fabricated by the photo-crosslinking of stacked scaffold sheets. Furthermore, cell seeding and photo-crosslinking could be performed simultaneously and the cell proliferation tests revealed that human ASCs impregnated into the multi-layered hydrogel still kept response to topographical cues and external tenogenic factors.

3D PRINTING TECHNIQUE

3D printing is a kind of rapid prototyping technology. It is a technology based on a digital model file and uses a powdery metal or plastic adhesive material to build an object by layer-by-layer printing (Rengier et al., 2010; Sun et al., 2013; Chia and Wu, 2015). Recently, numerous attentions have been attracted by the hydrogels prepared by 3D printing for biomedical applications. For example, Shang et al. used a conventional 3D printer to fabricate 3D calcium alginate hydrogels (Shang et al., 2017). Sodium alginate and CaCO$_3$ nanoparticles were premixed and filled into the syringe as 3D printing ink. Such mixture could be ejected onto a conductive substrate continuously by syringe nozzle and cross-linked by the Ca^{2+} released from the CaCO$_3$ particles after the applying of a DC voltage between the substrate and the nozzle. A hydrogel formation model can be established by the consideration of several parameters, such as deposition time and applied voltage. The cell viability test revealed that the encapsulated cells can maintain 99% survive rate after the gelation. In addition, 3D printing can fabricate calcium alginate hydrogels with controllable geometry, which expanded their biomedical applications (**Figure 7**). The layer-by-layer printing characteristics of 3D printing inspired us to construct multi-layered hydrogels by the alternating printing of various materials. Preparation of multi-layered hydrogels by 3D printing has many advantages, such as controllable hydrogel morphology,
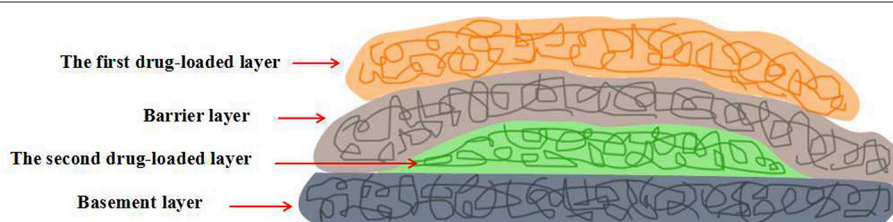
FIGURE 6 | Schematic representation of four-layered hydrogels with time-programmed combination release behavior by sequential electrospinning technique.
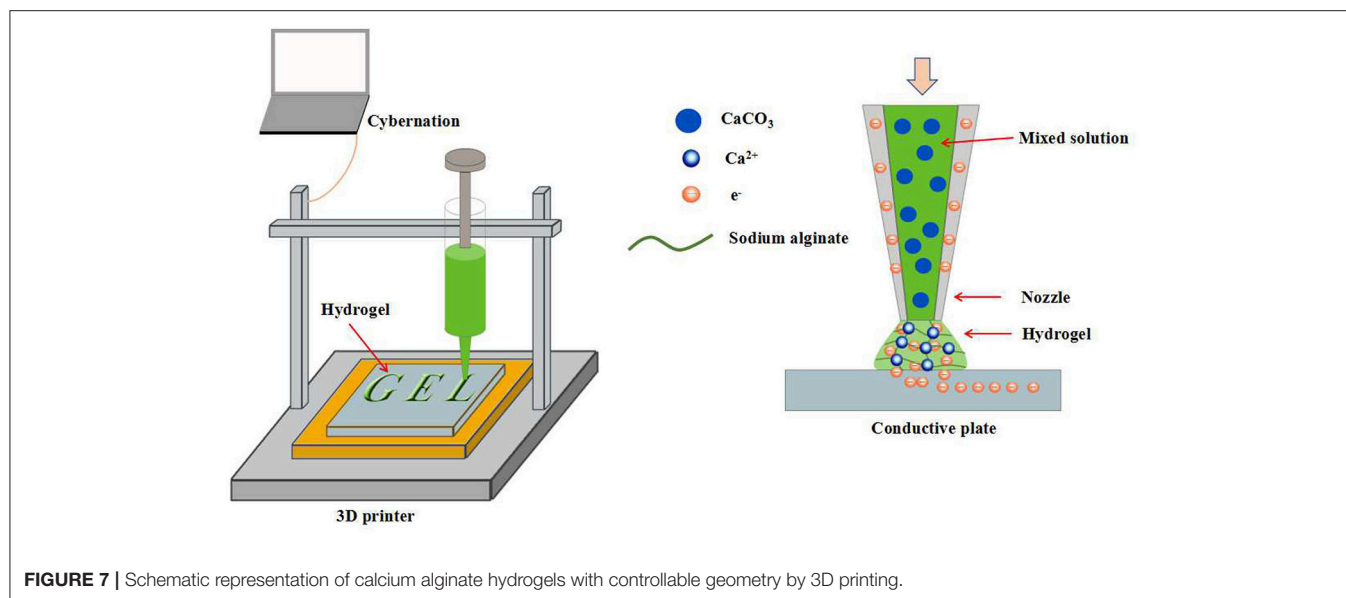
FIGURE 7 | Schematic representation of calcium alginate hydrogels with controllable geometry by 3D printing.

engineering preparation, etc. However, similar work is rarely reported. Maybe in the near future, multi-layered hydrogels prepared by 3D printing will emerge in the field of biomedical applications.

CONCLUSIONS AND OUTLOOK

In the past decades, multi-layered hydrogels with organization of various functional layers have been attracting extensive attentions, due to their ability to meet the diverse needs of biomedical applications. Although the preparation of multi-layered hydrogels has made great progress, some challenges still remained. For example, LBL self-assembly technology, the most commonly used methods for the preparation of multi-layered hydrogel, faces the following problems: (i) The construction process is carried out in a layer-by-layer fashion and the operation is cumbersome, which is not conducive to the construction of hydrogels with numerous layers and the engineering preparation of multi-layer hydrogels. (ii) The thickness of each layer within multi-layered hydrogels cannot be adjusted flexibly. (iii) The range of drugs suited to such operation is narrow and the efficiency of drug loading is low. For the other remaining preparation methods, they not only face the similar challenges as LBL self-assembly technique, but also cannot achieve the fine control of architecture structure of multi-layered hydrogels. These problems limit the performance regulation and engineering preparation of multi-layered hydrogels, which seriously restricts their application prospects in the biomedical field. Therefore, in order to overcome the shortcomings of the existing preparation techniques and further increase the application potential of multi-layered hydrogels, it is urgently needed to develop a

completely new methodology for the preparation of multi-layered hydrogels. More recently, 3D printing has developed into a versatile tool to create a three-dimensional object with almost any shape or geometry (Rengier et al., 2010; Ladd et al, 2013). Such process is rapid and intelligent, and is very suitable for the engineering preparation of objects with special structures. 3D printing was used to print metal powders in the early days, now it can print numerous polymer materials (Schubert et al., 2014; Ruminski et al., 2018; Tahayeri et al., 2018). Up to now, a large amount of literature has reported on the biomedical application of hydrogels generated by 3D printing (Bose et al., 2013; Gross et al., 2014; Muth et al., 2014). However, as far as we known, little literature reported the preparation of multi-layered hydrogels via 3D printing. Maybe in the near future, 3D printing can provide a new platform for the design of multi-layered hydrogels and expand their applications in the biomedical field.

AUTHOR CONTRIBUTIONS

GL, ZD, and QY prepared the manuscript and figures. ZG and HX revised and finalized the manuscript. All authors reviewed and approved the final paper.

ACKNOWLEDGMENTS

REFERENCES

Ahmed, E. M. (2015). Hydrogel: preparation, characterization, and applications: a review. *J. Adv. Res.* 6, 105–121. doi: 10.1016/j.jare.2013.07.006

Anderson, J. M. (2008). Foreign body reaction to biomaterials. *Semin. Immunol.* 20, 86–100. doi: 10.1016/j.smim.2007.11.004

Baek, K., Jeong, J. H., Shkumatov, A., Bashir, R., and Kong, H. (2013). *In situ* self-folding assembly of a multi-walled hydrogel tube for uniaxial sustained molecular release. *Adv. Mater.* 25, 5568–5573. doi: 10.1002/adma.201300951

Bose, S., Vahabzadeh, S., and Bandyopadhyay, A. (2013). Bone tissue engineering using 3D printing. *Mater. Today* 16, 496–504. doi: 10.1016/j.mattod.2013.11.017

Brown, T. E., Carberry, B. J., Worrel, B. T., Dudaryeva, O. Y., Mcbride, M. K., Bowman, C. N., et al. (2018). Photopolymerized dynamic hydrogels with tunable viscoelastic properties through thioester exchange. *Biomaterials* 178, 496–503 doi: 10.1016/j.biomaterials.2018.03.060

Busscher, H. J., van der Mei HC., Subbiahdoss, G., Jutte, P. C., van den Dungen, J. J., Zaat, S. A., et al. (2012). Biomaterial-associated infection: locating the finish line in the race for the surface. *Sci. Transl. Med.* 4:153rv110. doi: 10.1126/scitranslmed.3004528

Chen, X., Wu, W., Guo, Z., Xin, J., and Li, J. (2011). Controlled insulin release from glucose-sensitive self-assembled multilayer films based on 21-arm star polymer. *Biomaterials* 32, 1759–1766. doi: 10.1016/j.biomaterials.2010.11.002

Chia, H. N., and Wu, B. M. (2015). Recent advances in 3D printing of biomaterials. *J. Biol. Eng.* 9:4. doi: 10.1186/s13036-015-0001-4

Choi, J., Konno, T., Takai, M., and Ishihara, K. (2009a). Controlled drug release from multilayered phospholipid polymer hydrogel on titanium alloy surface. *Biomaterials* 30, 5201–5208. doi: 10.1016/j.biomaterials.2009.06.003

Choi, J., Konno, T., Takai, M., and Ishihara, K. (2009b). Smart controlled preparation of multilayered hydrogel for releasing bioactive molecules. *Curr. Appl. Phys.* 9, e259–e262. doi: 10.1016/j.cap.2009.06.054

Choi, J., Konno, T., Takai, M., and Ishihara, K. (2012). Regulation of cell proliferation by multi-layered phospholipid polymer hydrogel coatings through controlled release of paclitaxel. *Biomaterials* 33, 954–961. doi: 10.1016/j.biomaterials.2011.10.006

Christensen, K., Davis, B., Jin, Y., and Huang, Y. (2018). Effects of printing-induced interfaces on localized strain within 3D printed hydrogel structures. *Mater. Sci. Eng. C Mater. Biol. Appl.* 89, 65–74. doi: 10.1016/j.msec.2018.03.014

Elisseeff, J. (2008). Hydrogels: structure starts to gel. *Nat. Mater.* 7, 271–273. doi: 10.1038/nmat2147

Fischer, M., Vahdatzadeh, M., Konradi, R., Friedrichs, J., Maitz, M. F., Freudenberg, U., et al. (2015). Multilayer hydrogel coatings to combine hemocompatibility and antimicrobial activity. *Biomaterials* 56, 198–205. doi: 10.1016/j.biomaterials.2015.03.056

Fujie, T., Matsutani, N., Kinoshita, M., Okamura, Y., Saito, A., and Takeoka, S. (2010). Adhesive, flexible, and robust polysaccharide nanosheets integrated for tissue-defect repair. *Adv. Funct. Mater.* 19, 2560–2568. doi: 10.1002/adfm.200900103

Fundueanu, G., Constantin, M., Bucatariu, S., and Ascenzi, P. (2017). pH/thermo-responsive poly(N-isopropylacrylamide-co-maleic acid) hydrogel with a sensor and an actuator for biomedical applications. *Polymer* 110, 177–186. doi: 10.1016/j.polymer.2017.01.003

Gross, B. C., Erkal, J. L., Lockwood, S. Y., Chen, C., and Spence, D. M. (2014). Evaluation of 3D printing and its potential impact on biotechnology and the chemical sciences. *Anal. Chem.* 86, 3240–3253. doi: 10.1021/ac403397r

Guan, Q., Dai, Y., Yang, Y., Bi, X., Wen, Z., and Pan, Y. (2018). Near-infrared irradiation induced remote and efficient self-healable triboelectric nanogenerator for potential implantable electronics. *Nano Energy* 51, 333–339. doi: 10.1016/j.nanoen.2018.06.060

Gupta, M. K., Martin, J. R., Werfel, T. A., Shen, T., Page, J. M., and Duvall, C. L. (2014). Cell protective, ABC triblock polymer-based thermoresponsive hydrogels with ROS-triggered degradation and drug release. *J. Am. Chem. Soc.* 136, 14896–14902. doi: 10.1021/ja507626y

He, M., Zhao, Y., Duan, J., Wang, Z., Chen, Y., and Zhang, L. (2014). Fast contact of solid–liquid interface created high strength multi-layered cellulose hydrogels with controllable size. *ACS Appl. Mater. Interfaces* 6, 1872–1878. doi: 10.1021/am404855q

Highley, C. B., Prestwich, G. D., and Burdick, J. A. (2016). Recent advances in hyaluronic acid hydrogels for biomedical applications. *Curr. Opin. Biotechnol.* 40, 35–40. doi: 10.1016/j.copbio.2016.02.008

Hoffman, A. S. (2001). Hydrogels for biomedical applications. *Adv. Drug Deliv. Rev.* 944:62. doi: 10.1111/j.1749-6632.2001.tb03823.x

Hoshi, T., Sumiko Akase, A., and Anzai, J. (2002). Preparation of multilayer thin films containing avidin through sugar–lectin interactions and their binding properties. *Langmuir* 18, 7024–7028. doi: 10.1021/la0203685

Hu, Z., and Chen, G. (2014). Novel nanocomposite hydrogels consisting of layered double hydroxide with ultrahigh tensibility and hierarchical porous structure at low inorganic content. *Adv. Mater.* 26, 5950–5956. doi: 10.1002/adma.201400179

Hume, S. L., Hoyt, S. M., Walker, J. S., Sridhar, B. V., Ashley, J. F., Bowman, C. N., et al. (2012). Alignment of multi-layered muscle cells within three-dimensional hydrogel macrochannels. *Acta Biomater.* 8, 2193–2202. doi: 10.1016/j.actbio.2012.02.001

Iler, R. K. (1966). Multilayers of colloidal particles. *J. Colloid Interface Sci.* 21, 569–594. doi: 10.1016/0095-8522(66)90018-3

Jang, J., Lee, J., Seol, Y. J., Jeong, Y. H., and Cho, D. W. (2013). Improving mechanical properties of alginate hydrogel by reinforcement with ethanol treated polycaprolactone nanofibers. *Compos. Part B Eng.* 45, 1216–1221. doi: 10.1016/j.compositesb.2012.09.059

Kidoaki, S., Kwon, I. K., and Matsuda, T. (2005). Mesoscopic spatial designs of nano- and microfiber meshes for tissue-engineering matrix and scaffold based on newly devised multilayering and mixing electrospinning techniques. *Biomaterials* 26, 37–46. doi: 10.1016/j.biomaterials.2004.01.063

Kim, B. S., Park, S. W., and Hammond, P. T. (2008). Hydrogen-bonding layer-by-layer-assembled biodegradable polymeric micelles as drug delivery vehicles from surfaces. *ACS Nano* 2, 386–392. doi: 10.1021/nn700408z

Kunze, A., Giugliano, M., Valero, A., and Renaud, P. (2011). Micropatterning neural cell cultures in 3D with a multi-layered scaffold. *Biomaterials* 32, 2088–2098. doi: 10.1016/j.biomaterials.2010.11.047

Ladd, C., So, J. H., Muth, J., and Dickey, M. D. (2013). 3D printing of free standing liquid metal microstructures. *Adv. Mater.* 25, 5081–5085. doi: 10.1002/adma.201301400.

Ladet, S., David, L., and Domard, A. (2008). Multi-membrane hydrogels. *Nature* 452, 76–79. doi: 10.1038/nature06619

Ladet, S. G., Tahiri, K., Montembault, A. S., Domard, A. J., and Corvol, M. T. (2011). Multi-membrane chitosan hydrogels as chondrocytic cell bioreactors. *Biomaterials* 32, 5354–5364. doi: 10.1016/j.biomaterials.2011.04.012

Lau, H. K., and Kiick, K. L. (2015). Opportunities for multicomponent hybrid hydrogels in biomedical applications. *Biomacromolecules* 16, 28–42. doi: 10.1021/bm501361c

Lichter, J. A., Vliet, K. J. V., and Rubner, M. F. (2016). Design of antibacterial surfaces and interfaces: polyelectrolyte multilayers as a multifunctional platform. *Macromolecules* 42, 8573–8586. doi: 10.1021/ma901356s

Lu, Y., Wu, Y., Liang, J., Libera, M. R., and Sukhishvili, S. A. (2015). Self-defensive antibacterial layer-by-layer hydrogel coatings with pH-triggered hydrophobicity. *Biomaterials* 45, 64–71. doi: 10.1016/j.biomaterials.2014.12.048

Mani, G., Feldman, M. D., Patel, D., and Agrawal, C. M. (2007). Coronary stents: a materials perspective. *Biomaterials* 28, 1689–1710. doi: 10.1016/j.biomaterials.2006.11.042

Martínez-Sanz, M., Mikkelsen, D., Flanagan, B., Gidley, M. J., and Gilbert, E. P. (2016). Multi-scale model for the hierarchical architecture of native cellulose hydrogels. *Carbohydrate Polymers* 147, 542–555. doi: 10.1016/j.carbpol.2016.03.098

Moro, T., Takatori, Y., Ishihara, K., Konno, T., Takigawa, Y., Matsushita, T., et al (2004). Surface grafting of artificial joints with a biocompatible polymer for preventing periprosthetic osteolysis. *Nat. Mater.* 3, 829–836. doi: 10.1038/nmat1233

Moskowitz, J. S., Blaisse, M. R., Samuel, R. E., Hsu, H. P., Harris, M. B., Martin, S. D., et al. (2010). The effectiveness of the controlled release of

gentamicin from polyelectrolyte multilayers in the treatment of *Staphylococcus aureus* infection in a rabbit bone model. *Biomaterials* 31, 6019–6030. doi: 10.1016/j.biomaterials.2010.04.011

Muth, J. T., Vogt, D. M., Truby, R. L., and Mengüç, Y., et al. (2014). 3D printing: embedded 3D printing of strain sensors within highly stretchable elastomers. *Adv. Mater.* 26, 6307–6312. doi: 10.1002/adma.201400334

Nguyen, L. H., Kudva, A. K., Saxena, N. S., and Roy, K. (2011). Engineering articular cartilage with spatially-varying matrix composition and mechanical properties from a single stem cell population using a multi-layered hydrogel. *Biomaterials* 32, 6946–6952. doi: 10.1016/j.biomaterials.2011.06.014

Nie, J., Lu, W., Ma, J., Yang, L., Wang, Z., Qin, A., et al. (2015). Orientation in multi-layer chitosan hydrogel: morphology, mechanism, and design principle. *Sci. Rep.* 5:7635. doi: 10.1038/srep07635

Okuda, T., Tominaga, K., and Kidoaki, S. (2010). Time-programmed dual release formulation by multilayered drug-loaded nanofiber meshes. *J. Control. Release* 143, 258–264. doi: 10.1016/j.jconrel.2009.12.029

O'Leary, L. E., Fallas, J. A., Bakota, E. L., Kang, M. K., and Hartgerink, J. D. (2011). Multi-hierarchical self-assembly of a collagen mimetic peptide from triple helix to nanofibre and hydrogel. *Nat. Chem.* 3, 821–828. doi: 10.1038/nchem.1123

Pan, Y., Gao, Y., Shi, J., Wang, L., and Xu, B. (2011). A versatile supramolecular hydrogel of nitrilotriacetic acid (NTA) for binding metal ions and magnetorheological response. *J. Mater. Chem.* 21, 6804–6806. doi: 10.1039/c1jm10822k

Pavlukhina, S., and Sukhishvili, S. (2011). Polymer assemblies for controlled delivery of bioactive molecules from surfaces. *Adv. Drug Deliv. Rev.* 63, 822–836. doi: 10.1016/j.addr.2011.03.017

Rengier, F., Mehndiratta, A., von Tengg-Kobligk, H., Zechmann, C. M., Unterhinninghofen, R., Kauczor, H. U., et al. (2010). 3D printing based on imaging data: review of medical applications. *Int. J. Comput. Assist. Radiol. Surg.* 5, 335–341. doi: 10.1007/s11548-010-0476-x

Ruminski, S., Ostrowska, B., Jaroszewicz, J., Skirecki, T., Włodarski, K., Swieszkowski, W., et al. (2018). 3D printed PCL-based scaffolds provide an advantageous environment for osteogenic differentiation of human adipose-derived stem cells: ADSC osteogenesis in 3D scaffolds. *J. Tissue Eng. Regen. Med.* 12, e473–e485. doi: 10.1002/term.2310

Schubert, C., van Langeveld, M. C., and Donoso, L. A. (2014). Innovations in 3D printing: a 3D overview from optics to organs. *Br. J. Ophthalmol.* 98, 159–161. doi: 10.1136/bjophthalmol-2013-304446

Shang, W., Liu, Y., Wan, W., Hu, C., Liu, Z., Wong, C. T., et al. (2017). Hybrid 3D printing and electrodeposition approach for controllable 3D alginate hydrogel formation. *Biofabrication* 9:025032. doi: 10.1088/1758-5090/aa6ed8

Shi, S., Croutxé-Barghorn, C., and Allonas, X. (2016). Photoinitiating systems for cationic photopolymerization: ongoing push toward long wavelengths and low light intensities. *Prog. Polym. Sci.* 65, 1–41. doi: 10.1016/j.progpolymsci.2016.09.007

Steinmetz, N. J., Aisenbrey, E. A., Westbrook, K. K., Qi, H. J., and Bryant, S. J. (2015). Mechanical loading regulates human MSC differentiation in a multi-layer hydrogel for osteochondral tissue engineering. *Acta Biomater.* 21, 142–153. doi: 10.1016/j.actbio.2015.04.015

Stuart, M. A., Huck, W. T., Genzer, J., Müller, M., Ober, C., Stamm, M., et al. (2010). Emerging applications of stimuli-responsive polymer materials. *Nat. Mater.* 9, 101–113. doi: 10.1038/nmat2614

Sudhakar, C. K., Upadhyay, N., Jain, A., Verma, A., Charyulu, R. N., and Jain, S. (2015). Hydrogels–promising candidates for tissue engineering. *Nanotechnol. Appl. Tissue Eng.* 77–94. doi: 10.1016/B978-0-323-32889-0.00005-4

Sun, K., Wei, T. S., Ahn, B. Y., Seo, J. Y., Dillon, S. J., and Lewis, J. A. (2013). 3D printing of interdigitated Li-ion microbattery architectures. *Adv. Mater.* 25, 4539–4543. doi: 10.1002/adma.201301036

Tahayeri, A., Morgan, M., Fugolin, A. P., Bompolaki, D., Athirasala, A., Pfeifer, C. S., et al. (2018). 3D printed versus conventionally cured provisional crown and bridge dental materials. *Dental Mater.* 34, 192–200. doi: 10.1016/j.dental.2017.10.003

Wang J., and Windbergs, M. (2017). Functional electrospun fibers for the treatment of human skin wounds. *Eur. J. Pharm. Biopharm.* 119, 283–299. doi: 10.1016/j.ejpb.2017.07.001

Wang, H., Zha, G., Du, H., Gao, L., Li, X., Shen, Z., et al. (2014). Facile Fabrication of ultrathin antibacterial hydrogel films via layer-by-layer "click" chemistry. *Polym. Chem.* 5, 6489–6494. doi: 10.1039/c4py00900b

Wang, P., Li, Y., and Jiang, M. (2018). Effects of the multilayer structures on exenatide release and bioactivityinmicrosphere/thermosensitive hydrogel system. *Colloids Surf. B Biointerfaces* 171, 85–93. doi: 10.1016/j.colsurfb.2018.04.063

Xu, Q., Li, X., Jin, Y., Sun, L., Ding, X., Liang, L., et al. (2017). Bacterial self-defense antibiotics release from organic-inorganic hybrid multilayer films for long-term anti-adhesion and biofilm inhibition properties. *Nanoscale* 9, 19245–19254. doi: 10.1039/C7NR07106J

Xue, B., Wang, W., Qin, J. J., Nijampatnam, B., Murugesan, S., Kozlovskaya, V., et al. (2017). Highly efficient delivery of potent anticancer iminoquinone derivative by multilayer hydrogel cubes. *Acta Biomater.* 58, 386–398. doi: 10.1016/j.actbio.2017.06.004

Yang, G., Lin, H., Rothrauff, B. B., Yu, S., and Tuan, R. S. (2016). Multilayered polycaprolactone/gelatin fiber-hydrogel composite for tendon tissue engineering. *Acta Biomater.* 35, 68–76. doi: 10.1016/j.actbio.2016.03.004

Zarket, B. C., and Raghavan, S. R. (2017). Onion-like multilayered polymer capsules synthesized by a bioinspired inside-out technique. *Nat. Commun.* 8:193. doi: 10.1038/s41467-017-00077-7

Zhang, C., Mcadams, D. A., and Grunlan, J. C. (2016). Nano/micro-manufacturing of bioinspired materials: a review of methods to mimic natural structures. *Adv. Mater.* 28, 6292–6321. doi: 10.1002/adma.201505555

Zhao, N., Wang, Z., Cai, C., Shen, H., Liang, F., Wang, D., et al. (2014). Bioinspired materials: from low to high dimensional structure. *Adv. Mater.* 26, 6994–7017. doi: 10.1002/adma.201401718

Zucchelli, A., Focarete, M. L., Gualandi, C., and Ramakrishna, S. (2015). Electrospun nanofibers for enhancing structural performance of composite materials. *Polym. Adv. Technol.* 22, 339–349. doi: 10.1002/pat.1837

Conflict of Interest Statement: The authors declare that the research was conducted in the absence of any commercial or financial relationships that could be construed as a potential conflict of interest.

Preparation, Properties, and Applications of Graphene-Based Hydrogels

Guochao Liao[1], Junfeng Hu[2], Zhou Chen[2*], Ruiqian Zhang[3], Guanchun Wang[3] and Tairong Kuang[4]

[1] Joint Laboratory for Translational Cancer Research of Chinese Medicine of the Ministry of Education of the People's Republic of China, International Institute for Translational Chinese Medicine, University of Chinese Medicine, Guangzhou, China, [2] School of Mechanical and Power Engineering, Nanjing Tech University, Nanjing, China, [3] Science and Technology on Reactor Fuel and Materials Laboratory, Nuclear Power Institute of China, Chengdu, China, [4] Key Laboratory of Polymer Processing Engineering of Ministry of Education, South China University of Technology, Guangzhou, China

As a new carbon-based nanomaterial, graphene has exhibited unique advantages in significantly improving the combination properties of traditional polymer hydrogels. The specific properties of graphene, such as high electrical conductivity, high thermal conductivity and excellent mechanical properties, have made graphene not only a gelator to self-assemble into the graphene-based hydrogels (GBH) with extraordinary electromechanical performance, but also a filler to blend with small molecules and macromolecules for the preparation of multifunctional GBH. It fully exploits the practical applications of traditional hydrogels. This review summarizes the preparation methods, properties, and the applications of GBH. Further developments and challenges of GBH are also prospected.

Keywords: graphene, graphene oxide, hydrogels, applications, preparation

INTRODUCTION

Graphene is a new nanomaterial with strict two-dimensional layers structure (Geim, 2009; Shi et al., 2018). With excellent mechanical, high electrical and thermal properties, graphene is the ideal filler for polymer-based nanocomposites (Li and Kaner, 2008). Hydrogel is the moderate crosslinked and branched polymer with three dimensional network structures (Yuk et al., 2017). It is widely studied and applied because of the ability to absorb large quantities of water, swell quickly, soft, elastine, and biologic compatibility (Smith et al., 2010; Qiu and Park, 2012). Graphene has exhibited unique advantages in significantly improving the combination properties of traditional polymer hydrogels (Xu et al., 2010a; Kostarelos and Novoselov, 2014). Graphene in hydrogels plays two roles: the gelator to self-assemble into the hydrogels, and the filler to blend with small molecules and macromolecules for the preparation of multifunctional hydrogels, which are collectively called graphene-based hydrogels (GBH) (Wang et al., 2016; Zhao et al., 2017).

This review aims to demystify the preparation methods, performance aspects, and the applications of GBH. Further developments and challenges of GBH are also prospected.

PREPARATION METHODS AND PROPERTIES

Self-Assembly Method

Self-assembly method means that the basic structure of graphene oxide (GO) is spontaneously translated into a stable 3D graphene structure under the interaction of non-covalent π-π bond. It is considered an effective approach for fabricating GBH. Various self-assembly methods such as hydrothermal process (Liu et al., 2017), chemical reduction (Sheng et al., 2011), and metal ion induced process (Cong et al., 2012) have been developed for 3D GBH. They can obtain some unique structures and characteristics, such as porous network structure, ultra-low density, excellent thermal properties, and thermal stability (Kuang et al., 2015).

Self-assembled GBH was first prepared by one-step hydrothermal method from GO solution in 2010 (Xu et al., 2010a). The moisture content of the GBH reached up to 97.4 wt%, and it demonstrated high levels of strength. Furthermore, the electrical conductivity of the GBH was 5×10^{-3} S/cm, and the storage modulus (450-490 kPa) was greater several orders than the traditional hydrogels. The 3D multifunctional GBH, which was self-assembled by combining DNA and GO sheets, possessed good mechanical property, big dye-adsorption capacity, and excellent self-cure capability (Xu et al., 2010b). In order to further improve the reduction degree of graphene for better GBH, some chemical reducing agent, such as hydrazine hydrate (Zhang and Shi, 2011), oxalic acid (Zhang et al., 2012), ascorbic acid (Shi et al., 2014) et al., were added to GO solution.

Compared with traditional hydrogel, an increase in strength and excellent energy storage performance has been found from self-assembled GBH. However, the applications of pure self-assembled GBH are restricted by their relatively low mechanical properties. Therefore, graphene used as high quality nano-fillers for polymer composite hydrogels is the focus of nowadays researches.

Mixed Solution Method

It is a great challenge that single graphene sheets are easily caused agglomeration in the process of preparation and application, which leads to multilayer graphite. Compared with graphene, there are many oxygenous groups at the surface of GO, which can make GO perfect dispersion in polar solvents (water, ethanediol, DMF, and so on) (Paredes et al., 2008). The stable colloidal dispersion system usually occurs due to the strong hydrogen-bonds between GO and aqueous solution. In this case, mixed GO solution method is a very useful technology for fabricating GBH.

The graphene/gelatin hydrogel composite was fabricated by mixing graphene and gelatin solution (Tungkavet et al., 2015). The storage modulus response obviously enhanced with the graphene concentration increasing from 0 to 0.1%. The maximum of the highest storage modulus response and storage modulus sensitivity of graphene/gelatin hydrogel were 1.25×10^6 Pa and 3.52, respectively. The sulfonated graphene (SG)/poly(vinyl alcohol) (PVA) hydrogel, which was made by SG and PVA mixed solution, showed good mechanical property and intelligent adsorption property for cationic dyes compared to ordinary pure PVA hydrogel (Li et al., 2015). The tensile strength of the SG/PVA hydrogel increased with increasing SG, and the strength peak was as high as 37.34 kPa with 0.5wt% SG.

In-situ Polymerization

As a joint result of mixed GO, monomer-polymer, initiating agent, and other additives under certain conditions, in-situ polymerization of monomer-polymer occurs on the surface of GO, which leads to the final GO/polymer composite hydrogels. In-situ polymerization can be divided into two types based on the GO: the GO with and without treatment. The latter approach is grafting functional groups on the surface of GO, or stripping the nano-sheet layer from GO under ultrasonic and reacting with other monomers. GO also plays the role of cross-linking agent during the reaction. Such GO/polymer composite hydrogels possesses favorable dispersibility of GO, and uniform performance.

GO/polyacrylic acid (PAA) composite hydrogel was synthesized via cross-linking reaction of PAA at low temperature (Tai et al., 2013). The composite material displayed more excellent swelling characteristics and electrical response than the pure PAA hydrogel. GO/polyacrylamide (PAM) composite hydrogel was fabricated through in situ acrylonitrile polymerization in GO-water solution (Liu et al., 2012). The tensile strength of GO/PAM hydrogel was about 4.5 times higher than the pure PAM hydrogel, and the breaking elongation was 30 times exceeded than the PAM, but the content of GO was only 0.0079 wt%. GO/PAA hydrogel was prepared by in situ free radical polymerization triggered by graphene peroxide (Liu et al., 2013). It has the ability to self-heal when the fracture surfaces have maintained contact at low temperature or even room temperature for short periods. The recovery rate of the hydrogel can reach up to 88% at a prolonged healing time.

APPLICATIONS

The excellent performance of GBH is based on the inseparable synergy between hydrophobicity and π-conjugated structure in graphene sheets. GBH integrates mechanical strength, electrical conductivity, adsorption, hydroscopicity, water retention, controlled-release and biocompatibility together, and it will have broad application prospect in biomedical, supercapacitor, water treatment, dye absorption, catalyst carrier and intelligent response for microfluidic system (as shown in **Figure 1**).

Biomaterials in Biomedical Field

The water-rich GBH is similar to natural soft tissues, in addition to the high conductivity, good mechanical strength, favorable biocompatibility, and the non-covalent bonds between graphene/GO and some polymer (chitosan (CS), poly(N,N-dimethylacrylamide) (PDMAA), etc.), GBH are attracted much attention in tissue engineering. Jing et al. studied the mussel-inspired GO/CS composite hydrogel, which was prepared by incorporating protein polydopamine (PDA) (Jing et al., 2017). As the GO concentration increases to a suitable quantity, the electrical conductivity of the hydrogel could reach up to 1.22 mS/cm. Meanwhile the strength was 3 times higher than
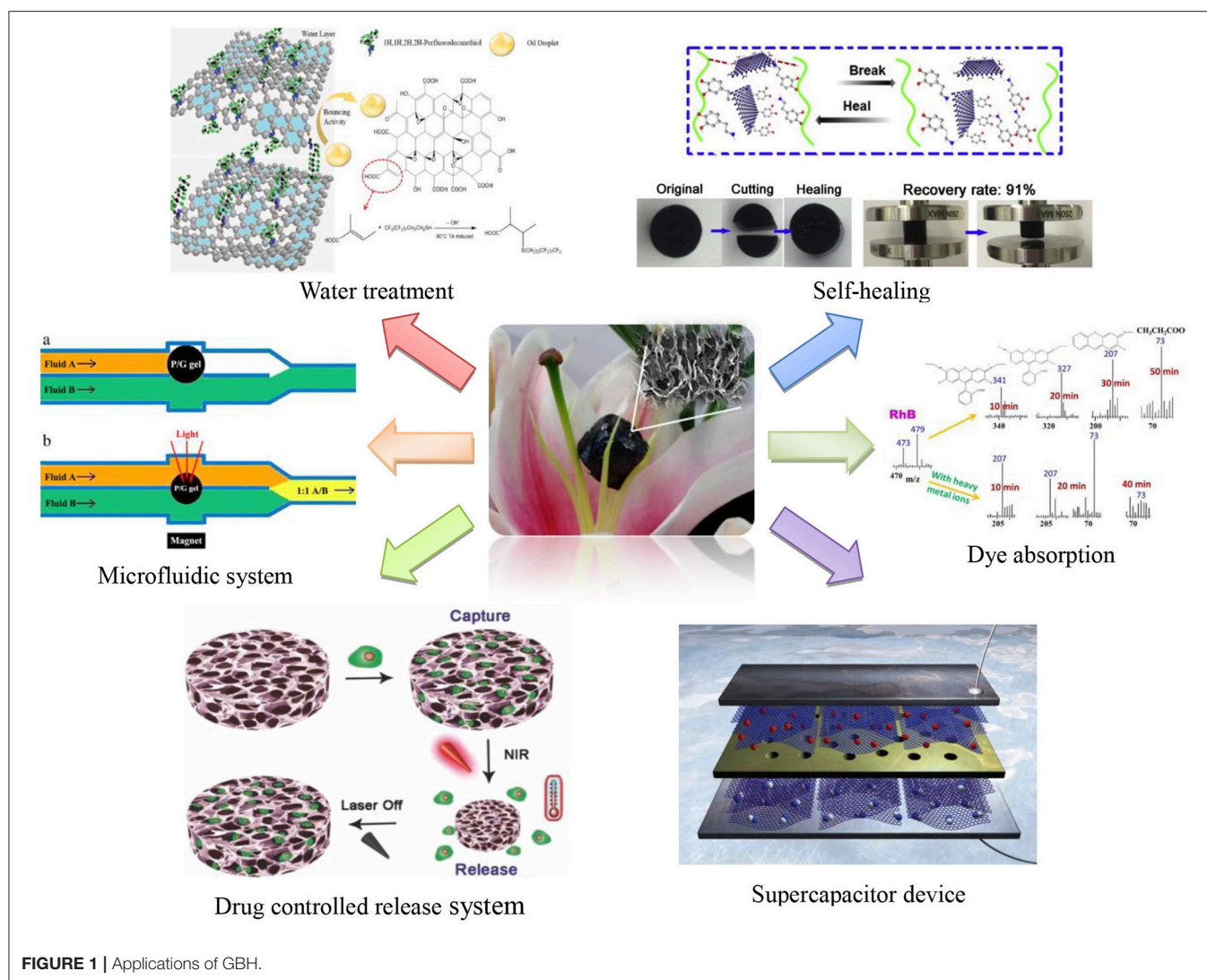
FIGURE 1 | Applications of GBH.

pure CS hydrogel. More importantly, GO/CS hydrogel could improve cellular activities and proliferation of human enhancer of filamentation 1 (HEF1) and cardiomyocytes (CMs).

Meanwhile intelligent GBH prepared by graphene/GO and stimuli-responsive polymer (PAA, PVA, Poly(N-isopropy-lacrylamide) (pNIPAAm), etc.) has shown attractive prospects in drug controlled release system on account of the huge specific area of GO or graphene. The graphene/Ag (mass ratio of 1:5) composite hydrogel, which was made through the cross-linking reaction of graphene with acrylic acid and methylene bisacrylamide, exhibited good biocompatibility, and high swelling ratio (Fan et al., 2014). It displayed a significant acceleration of healing with the hydrogel in the treatment of artificial wounds in rats. More importantly, the composite hydrogel was used to facilitate complete reconstruction in 15-day wound-healing. Bai et al. prepared GO/PVA composite hydrogel and applied it in selective drug release under physiological pH (Bai et al., 2010). They found that 84% vitamin B_{12} molecules can be diffused from the hydrogel into neutral PBS solution (pH

= 7.4) after 42 h. However, only 51% vitamin B_{12} molecules can be released in the acidic medium (pH = 1.7) at the same time. Li et al. successfully fabricated an NIR-responsive GBH as an active cell scaffold by pNIPAAm derivative solution and arginine-glycine-aspartic acid (RGD). The NIR-responsive GBH could efficiently capture cells, but also could release the cells on the stimulus of NIR light (Li et al., 2013).

Supercapacitor

As the major electrochemical components for energy storage and release, supercapacitor should possess high specific capacitance, big reversible capacity, and long cycle life. GBH can be used as innovative electrode materials for supercapacitor, because of their unique surface structures and excellent conductive properties.

Tan et al. researched the viscoelastic properties and electrical conductivity of self-assembly GBH. They found that the apparent electrical conductivity of the GBH can be controlled in a range from 0.01 to 6 S/cm, which is sufficient for many electrical applications (Tan et al., 2014). Wang et al. prepared

graphene/VO$_2$ nanobelt composite hydrogel by using V$_2$O$_5$ and GO as precursors. They found that the graphene/VO$_2$ hydrogel exhibited big specific capacitance (426 F/g), good cycling performance and high rate capability (Wang et al., 2013).

Water Treatment

The rapid development of petrochemical industry leads to a large number of industrial waste water, which contains significant amounts of acid, alkali salt, organic solvent, harmful dyes, or heavy metal ions. Hydrogel owns good hydrophilicity, at the same time it will not dissolve in water. The unique 3D crosslinked network structure makes hydrogel can be effective absorption and adsorption to high amounts of chemicals. The adsorptive abilities and adsorptive selectivity of hydrogel can be further improved by the huge specific surface area and electronegativity of graphene. Therefore hydrogel has shown a perfect foreground applied in sewage treatment and dye absorption.

LA/F/rGO hydrogel with good amphiphobicity was synthesized by hydrothermal process at low temperature with reduced GO, 1H,1H,2H,2H-perfluorodecanethiol (PF) and L-ascorbic acid (LA). The hydrogel possessed high selectivity to oil-water separating by pre-soaking (Hu et al., 2018). Dong et al. found that the Fe$_3$O$_4$/GO/polyacrylamide (PAM) hydrogel exhibited excellent mechanical property, high Photo-Fenton activity and big adsorption capacity. The hydrogel was achieved a 90% degradation of Rhodamine B (RhB, 20 mg/L) and a 72.7% degradation of chemical oxygen demand (COD, 2840 mg/L) in wastewater for 1 h under visible light (Dong et al., 2018). Organic pollutants and heavy metal ions could also be removed at the same time by the Fe$_3$O$_4$/GO/PAM hydrogel.

CONCLUSION

The specific properties of graphene, such as high electrical conductivity, high thermal conductivity, and excellent mechanical properties, have made graphene not only a gelator to self-assemble into the GBH with extraordinary electromechanical performance, but also a filler to blend with small molecules and macromolecules for the preparation of multifunctional GBH. It fully exploits the practical applications of traditional hydrogels. In view of the developing trend of hydrogel in recent years, theoretical researches are relatively high. Researchers are very interested in the application prospect of hydrogel for biomedical, tissue engineering, supercapacitor, water treatment, dye absorption, catalyst carrier, and intelligent response for microfluidic system. However compared to the practical applications, the actual operation research is very weak. The formation mechanism of graphene/GO hydrogel in the aqueous solution and the influencing function are not apparent yet. Design and fabrication of GBH with new structures and functions will be a significant challenge in the future.

REFERENCES

Bai, H., Li, C., Wang, X., and Shi, G. (2010). A pH-sensitive graphene oxide composite hydrogel. *Chem. Commun.* 46, 2376–2378. doi: 10.1039/c000051e

Cong, H. P., Ren, X. C., Wang, P., and Yu, S. H. (2012). Macroscopic multifunctional graphene-based hydrogels and aerogels by a metal ion induced self-assembly process. *ACS Nano* 6, 2693–2703. doi: 10.1021/nn300082k

Dong, C., Lu, J., Qiu, B., Shen, B., Xing, M., and Zhang, J. (2018). Developing stretchable and graphene-oxide-based hydrogel for the removal of organic pollutants and heavy metal ions. *Appl. Catalys. B Environ.* 222, 146–156. doi: 10.1016/j.apcatb.2017.10.011

Fan, Z., Liu, B., Wang, J., Zhang, S., Lin, Q., Gong, P., et al. (2014). A novel wound dressing based on Ag/Graphene polymer hydrogel: effectively kill bacteria and accelerate wound healing. *Adv. Funct. Mater.* 24, 3933–3943. doi: 10.1002/adfm.201304202

Geim, A. K. (2009). Science, graphene: status and prospects. *Science* 324, 1530–1534. doi: 10.1126/science.1158877

Hu, W., Zhang, P., Liu, X., Yan, B., Xiang, L., Zhang, J., et al. (2018). An amphiphobic graphene-based hydrogel as oil-water separator and oil fence material. *Chem. Eng. J.* 353, 708–716. doi: 10.1016/j.cej.2018.07.147

Jing, X., Mi, H. Y., Napiwocki, B. N., Peng, X. F., and Turng, L. S. (2017). Mussel-inspired electroactive chitosan/graphene oxide composite hydrogel with rapid self-healing and recovery behavior for tissue engineering. *Carbon N. Y.* 125, 557–570. doi: 10.1016/j.carbon.2017.09.071

Kostarelos, K., and Novoselov, K. S. (2014). Materials science. Exploring the interface of graphene and biology. *Science* 344, 261–263. doi: 10.1126/science.1246736

Kuang, T. R., Mi, H. Y., Fu, D. J., Jing, X., Chen, B., Mou, W. J., et al. (2015). Fabrication of poly(lactic acid)/graphene oxide foams with highly oriented and elongated cell structure via unidirectional foaming using supercritical carbon dioxide. *Ind. Eng. Chem. Res.* 54, 758–768. doi: 10.1021/ie503434q

Li, D., and Kaner, R. B. (2008). Materials science. Graphene-based materials. *Science* 320, 1170–1171. doi: 10.1126/science.1158180

Li, H., Fan, J., Shi, Z., Lian, M., Tian, M., and Yin, J. (2015). Preparation and characterization of sulfonated graphene-enhanced poly (vinyl alcohol) composite hydrogel and its application as dye absorbent. *Polymer (Guildf).* 60, 96–106. doi: 10.1016/j.polymer.2014.12.069

Li, W., Wang, J., Ren, J., and Qu, X. (2013). 3D graphene oxide–polymer hydrogel: near-infrared light-triggered active scaffold for reversible cell capture and on-demand release. *Adv. Mater.* 25, 6737–6743. doi: 10.1002/adma.201302810

Liu, J., Song, G., He, C., and Wang, H. (2013). Self-healing in tough graphene oxide composite hydrogels. *Macromol. Rapid Commun.* 34, 1002–1007. doi: 10.1002/marc.201300242

Liu, R., Liang, S., Tang, X. Z., Yan, D., Li, X., and Yu, Z. Z. (2012). Tough and highly stretchable graphene oxide/polyacrylamide nanocomposite hydrogels. *J. Mater. Chem.* 22, 14160–14167. doi: 10.1039/c2jm32541a

Liu, Y., Gao, T., Xiao, H., Guo, W., Sun, B., Pei, M., et al. (2017). One-pot synthesis of rice-like TiO 2 /graphene hydrogels as advanced electrodes for supercapacitors and the resulting aerogels as high-efficiency dye adsorbents. *Electrochim. Acta* 229, 239–252. doi: 10.1016/j.electacta.2017.01.142

Paredes J. I., Villar-Rodil, S., Martínez-Alonso, A., and Tascón, J. M. D. (2008). Graphene oxide dispersions in organic solvents. *Langmuir* 24,10560–10564. doi: 10.1021/la801744a

Qiu, Y., and Park, K. (2012). Environment-sensitive hydrogels for drug delivery. *Adv. Drug Deliv. Rev.* 64, 321–339. doi: 10.1016/j.addr.2012.09.024

Sheng, K. X., Yu-Xi, X. U., Chun, L. I., and Shi, G. Q. (2011). High-performance self-assembled graphene hydrogels prepared by chemical reduction of graphene oxide. *New Carbon Mater.* 26, 9–15. doi: 10.1016/S1872-5805(11)60062-0

Shi, J. L., Du, W. C., Yin, Y. X., Guo, Y. G., and Wan, L. J. (2014). Hydrothermal reduction of three-dimensional graphene oxide for binder-free flexible supercapacitors. *J. Mater. Chem. A* 2, 10830–10834. doi: 10.1039/c4ta01547a

Shi, X., Peng, X., Zhu, J., Lin, G., and Kuang, T. (2018). Synthesis of DOPO-HQ-functionalized graphene oxide as a novel and efficient flame retardant and its application on polylactic acid: thermal property, flame retardancy, and mechanical performance. *J. Colloid Interface Sci.* 524, 267–278. doi: 10.1016/j.jcis.2018.04.016

Smith, A. M., Williams, R. J., Tang, C., Coppo, P., Collins, R. F., Turner, M. L., et al. (2010). Fmoc-diphenylalanine self assembles to a hydrogel via a novel architecture based on π–π interlocked β-sheets. *Adv. Mater.* 20, 37–41. doi: 10.1002/adma.200701221

Tai, Z., Yang, J., Qi, Y., Yan, X., and Xue, Q. (2013). Synthesis of a graphene oxide-polyacrylic acid nanocomposite hydrogel and its swelling and electroresponsive properties. *RSC Adv.* 3, 12751–12757. doi: 10.1039/c3ra22335c

Tan, Z., Ohara, S., Abe, H., and Naito, M. (2014). Synthesis and processing of graphene hydrogels for electronics applications. *RSC Adv.* 4, 8874–8878. doi: 10.1039/c3ra46856a

Tungkavet, T., Seetapan, N., Pattavarakorn, D., and Sirivat, A. (2015). Graphene/gelatin hydrogel composites with high storage modulus sensitivity for using as electroactive actuator: effects of surface area and electric field strength. *Polymer (Guildf).* 70, 242–251. doi: 10.1016/j.polymer.2015.06.027

Wang, H., Yi, H., Chen, X., and Wang, X. (2013). One-step strategy to three-dimensional graphene/VO2 nanobelt composite hydrogels for high performance supercapacitors. *J. Mater. Chem. A* 2, 1165–1173. doi: 10.1039/C3TA13932H

Wang, R., Xu, C., and Lee, J. M. (2016). High performance asymmetric supercapacitors: new NiOOH nanosheet/graphene hydrogels and pure graphene hydrogels. *Nano Energy* 19, 210–221. doi: 10.1016/j.nanoen.2015.10.030

Xu, Y., Sheng, K., Li, C., and Shi, G. (2010a). Self-Assembled Graphene Hydrogel via a One-Step Hydrothermal Process. *ACS Nano* 4, 4324–4330. doi: 10.1021/nn101187z

Xu, Y., Wu, Q., Sun, Y., Bai, H., and Shi, G. (2010b). Three-dimensional self-assembly of graphene oxide and DNA into multifunctional hydrogels. *ACS Nano* 4, 7358–7362. doi: 10.1021/nn1027104

Yuk, H., Lin, S., Ma, C., Takaffoli, M., Fang, N. X., and Zhao, X. (2017). Hydraulic hydrogel actuators and robots optically and sonically camouflaged in water. *Nat. Commun.* 8:14230. doi: 10.1038/ncomms14230

Zhang, L., Chen, G., Hedhili, M. N., Zhang, H., and Wang, P. (2012). Three-dimensional assemblies of graphene prepared by a novel chemical reduction-induced self-assembly method. *Nanoscale* 4, 7038–7045. doi: 10.1039/c2nr32157b

Zhang, L., and Shi, G. (2011). Preparation of highly conductive graphene hydrogels for fabricating supercapacitors with high rate capability. *J. Phys. Chem. C* 115, 17206–17212. doi: 10.1021/jp204036a

Zhao, Y., Zhang, Y., Liu, A., Wei, Z., and Liu, S. (2017). Construction of three-dimensional hemin-functionalized graphene hydrogel with high mechanical stability and adsorption capacity for enhancing photodegradation of methylene blue. *ACS Appl. Mater. Interfaces* 9, 4006–4014. doi: 10.1021/acsami.6b10959

Synthesis and Biomedical Applications of Self-healing Hydrogels

Yi Liu[1] and Shan-hui Hsu[1,2]*

[1] *Institute of Polymer Science and Engineering, National Taiwan University, Taipei, Taiwan,* [2] *Institute of Cellular and System Medicine, National Health Research Institutes, Miaoli, Taiwan*

Hydrogels, which are crosslinked polymer networks with high water contents and rheological solid-like properties, are attractive materials for biomedical applications. Self-healing hydrogels are particularly interesting because of their abilities to repair the structural damages and recover the original functions, similar to the healing of organism tissues. In addition, self-healing hydrogels with shear-thinning properties can be potentially used as the vehicles for drug/cell delivery or the bioinks for 3D printing by reversible sol-gel transitions. Therefore, self-healing hydrogels as biomedical materials have received a rapidly growing attention in recent years. In this paper, synthesis methods and repair mechanisms of self-healing hydrogels are reviewed. The biomedical applications of self-healing hydrogels are also described, with a focus on the potential therapeutic applications verified through *in vivo* experiments. The trends indicate that self-healing hydrogels with automatically reversible crosslinks may be further designed and developed for more advanced biomedical applications in the future.

Keywords: self-healing hydrogel, synthesis mechanism, reversible crosslink, biomedical application, animal model

INTRODUCTION

Hydrogels are constructed by the crosslinked polymer networks as water-swollen gels. Hydrogels have received significant attention as the extracellular matrix mimics for biomedical applications because of their water-retention abilities, appropriate elasticities, and network structures (Wang and Heilshorn, 2015). The self-healing properties, originated from phenomena of wound healing in organisms, are used to describe materials with the ability to restore the morphology and mechanical properties after repeated damages. The microcapsule-laden hydrogels were developed that released healing agents at damage sites (White et al., 2001; Toohey et al., 2007). However, the irreversible healing process and potential interference of fillers limited their applications (Bergman and Wudl, 2008; Syrett et al., 2010). Besides, many dynamic hydrogels typically relied on external stimuli, such as high temperature, low pH, and light, to trigger dynamic crosslinks (Murphy and Wudl, 2010; Harada et al., 2014). The external stimuli would have adverse effects on the cells and living tissues. In this review, self-healing hydrogels are referred that automatically and reversibly repair the damages and recover the functions.

Self-healing hydrogels can be prepared through dynamic covalent bonds and non-covalent interactions. The dynamic equilibrium between dissociation and recombination of various interactions leads the hydrogel to heal damages and reform shapes. Commonly, dynamic covalent bonds exhibit stable and slow dynamic equilibriums, while non-covalent interactions show fragile and rapid dynamic equilibriums (Zou et al., 2017). With versatile mechanical properties,

self-healing hydrogels can be manufactured with robust, shear-thinning, or cell-adaptable properties for a broad range of applications, such as soft robots, 3D printing, and drug/cell delivery. In this review paper, we will take a detailed look at the current synthesis and biomedical applications of self-healing hydrogels. Firstly, various advanced strategies are introduced about the preparations and the mechanisms of self-healing hydrogels. Subsequently, biomedical applications of the self-healing hydrogels are described, especially, the ones that have been evaluated by animal models.

SELF-HEALING MECHANISMS

Self-healing hydrogels have been synthesized based on different chemistries and mechanisms as shown in **Figure 1**, including dynamic covalent bonds, non-covalent interactions, and multi-mechanism interactions. Each will be elaborated below.

Dynamic Covalent Bonding

Dynamic covalent chemistry, including imine formation, boronate ester complexation, catechol-iron coordination, Diels-Alder reaction, and disulfide exchange, is widely applied in the formation of self-healing hydrogel. Dynamic covalent bonds exhibit the stronger but slower dynamic equilibrium compared to non-covalent interactions.

The imine (or referred as Schiff base) is a compound with a carbon-nitrogen double bond formed by nucleophilic attack of amine to aldehyde or ketone. A number of self-healing hydrogels have been developed by aliphatic Schiff bases (Lü et al., 2015; Zhu, D. et al., 2017; Huang et al., 2018) or aromatic Schiff bases (Karimi and Khodadadi, 2016; Qu et al., 2017), in which aromatic Schiff bases show higher stability to maintain the mechanical properties compared to aliphatic Schiff bases (Zhang et al., 2011). Zhang et al. synthesized a dibenzaldehyde-terminated telechelic poly(ethylene glycol), namely difunctionalized PEG (DF-PEG), to form self-healing hydrogel through aromatic Schiff bases between benzaldehyde groups of DF-PEG and amino groups of chitosan (Zhang et al., 2011). The hydrogels were prepared rapidly under mild conditions at 20°C within 60 s, and they could be degraded by acidic pH, amino acids, vitamin B6 derivatives, and enzymes. The hydrogels were developed for 3D cell culture and cell delivery due to their cytocompatibility and injectability (Yang et al., 2012; Li et al., 2017; Zhang, Y. L. et al., 2017). Acylhydrazone and oxime are derivatives of imine with great stability, which have also been developed to synthesize the self-healing hydrogels (Deng et al., 2010; Grover et al., 2012; Lin et al., 2013; Mukherjee et al., 2015). For example, the self-healing hydrogel was prepared by adding oxidized sodium alginate into the mixture of N-carboxyethyl chitosan and adipic acid dihydrazide via dynamic imine and acylhydrazone bonds (Wei et al., 2015).

The reversible boronate ester bond is formed by complexation of boronic acid and diol, and its stability is dependent on pH-value and glucose concentration. Boronic acid and its derivatives, such as phenylboronic acid or phenylboronic acid-incorporated polymers, have been widely developed to prepare self-healing hydrogels. Yesilyurt et al. mixed phenylboronic acid and diol-modified poly(ethylene glycol) to form self-healing hydrogel that exhibited pH-responsive tunable mechanical properties, and glucose-responsive size-dependent release of proteins (Yesilyurt et al., 2016). The hydrogel was cytocompatible *in vitro*, and it showed a typical foreign body reaction *in vivo* without chronic inflammation. He et al. prepared self-healing hydrogel via complexation of a catechol-modified polymer and 1,3-benzenediboronic acid, which demonstrated high stability under alkaline conditions and low stability under acidic conditions (He et al., 2011). Another self-healing hydrogel was fabricated using the mixture of poly(ethylene glycol) diacrylate, dithiothreitol, and borax via permanent thiol-ene Michael addition and dynamic borax diol complexation in one-pot approach (He et al., 2015). The hydrogel can be injected with cells to form branched tubular channels for vascularization *in vitro* and easily removed by immersion in cell culture medium (Tseng et al., 2017).

The reversible coordinate bond between catechol and iron has been developed to prepare self-healing hydrogels. The reversibility of catechol-iron coordination bond can be controlled by adjusting pH conditions (Krogsgaard et al., 2013). When the environmental pH is raised from acidic to basic values, a rapidly self-healing hydrogel with high strength may form. Li et al. incorporated iron oxide (Fe_3O_4) nanoparticles with the catechol-modified polymers to form a self-healing hydrogel via reversible coordination bonds at the nanoparticle surface (Li et al., 2016). Self-healing hydrogel based on catechol-Fe_3O_4 nanoparticles structures exhibited magnetic properties and solid-like mechanics, in comparison with the fluid-like hydrogel by catechol-Fe(III) crosslinking.

The disulfide exchange provides dynamic covalent bonds to form self-healing hydrogels, which are sensitive to pH or redox potential (Wei, Z. et al., 2014). Recently, 1,2-dithiolane-functionalized polymers were synthesized to form self-healing hydrogels with rapid sol-gel transition via the disulfide exchange between the 1,2-dithiolane and dithiols (Barcan et al., 2015; Yu et al., 2017; Zhang and Waymouth, 2017). The disulfide exchange of 1,2-dithiolane can reform under neutral or weakly alkaline conditions, which can be further controlled by temperature.

Another important dynamic covalent chemistry in self-healing hydrogels is the thermally reversible Diels-Alder reaction (Liu and Chuo, 2013; Zhao et al., 2016; Shao et al., 2017). However, the biomedical applications of Diels-Alder reaction are limited because Diels-Alder bonds need a high temperature and a long duration to cleave and reform for self-healing properties. In recent reports, Diels-Alder chemistry was developed to form self-healing hydrogels combining with other reversible interactions, such as electrostatic interaction (Banerjee and Singha, 2017; Ghanian et al., 2018), coordination bond (Li et al., 2018a), imine bond (Li et al., 2018b), and acylhydrazone bond (Yu et al., 2015).

Non-covalent Interactions

Self-healing hydrogels can be produced through non-covalent interactions, such as hydrogen bond, electrostatic interaction, and hydrophobic interaction. The non-covalent interactions are less stable and more sensitive to environmental conditions (such as pH and temperature) compared to covalent interactions.

FIGURE 1 | Self-healing chemistries and mechanisms for various self-healing hydrogels, including dynamic covalent bonds, non-covalent interactions, and multi-mechanism interactions.
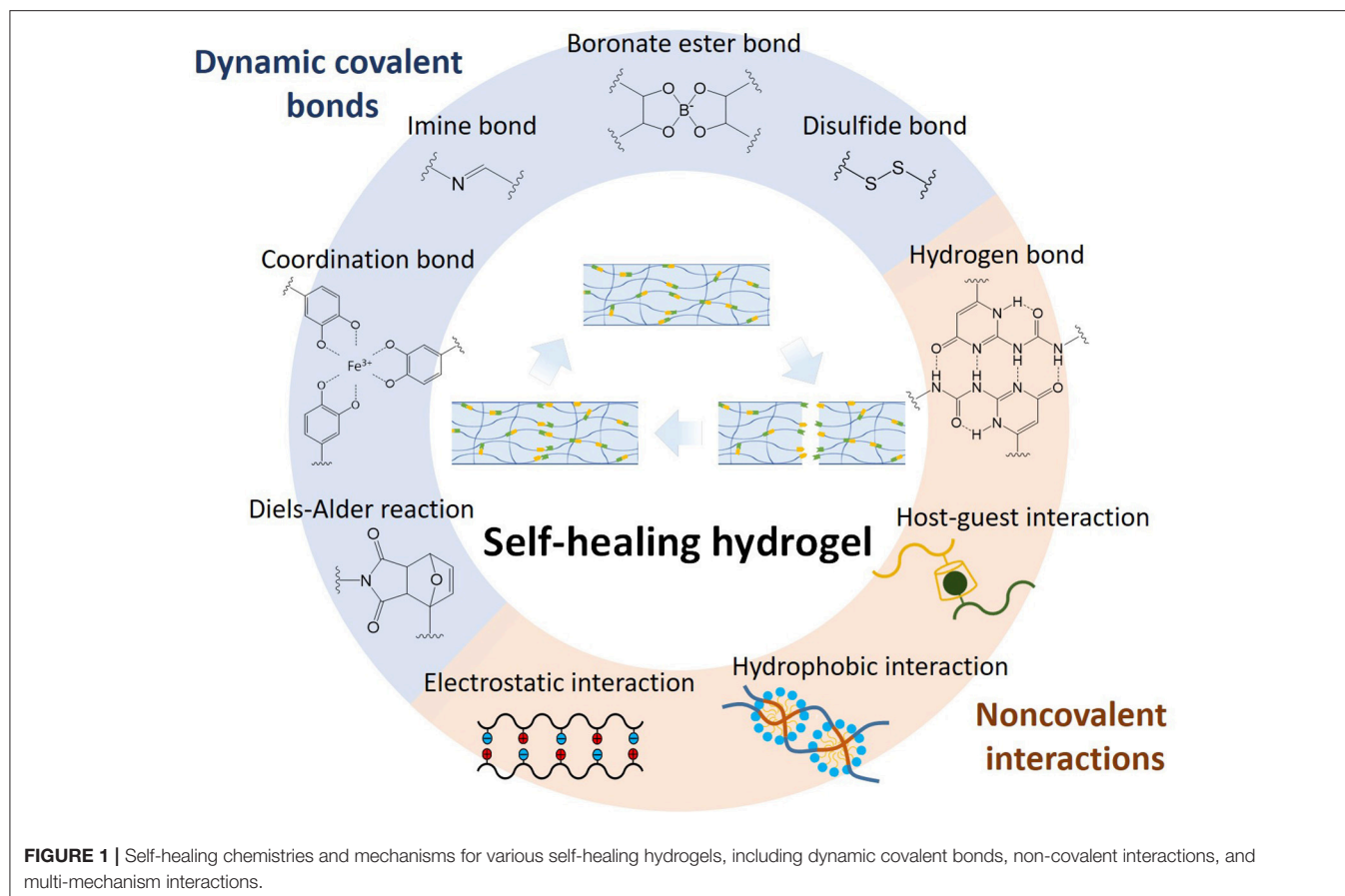
However, robust self-healing hydrogels can still form based on non-covalent interactions via special manufacturing procedures or nano- and micro-structures.

The hydrogen bonding is an attractive interaction between the hydrogen atoms and electronegative atoms, in which the hydrogen atom is bound to a high electronegative atom, such as nitrogen, oxygen, and fluorine. The polyvinyl alcohol-based self-healing hydrogels were developed using the freezing/thawing method via hydrogen bonding (Zhang et al., 2012; Zhang, Z. et al., 2017). Moreover, hydrogen bonding-based self-healing hydrogels were frequently reported with incorporations of various chemical moieties, such as 2-ureido-4-pyrimidone (UPy) moieties (Cui and del Campo, 2012; Dankers et al., 2012; Cui et al., 2013; Bastings et al., 2014; Chirila et al., 2014; Hou et al., 2015; Zhang et al., 2016), nucleobase moieties (Ye et al., 2017), deferoxamine moieties (Xu et al., 2017), and gallol moieties (Shin and Lee, 2017). In a recent work, the cytosine- and guanosine-modified hyaluronic acid (HA) formed self-healing hydrogel by Watson-Crick base pairing between the nucleobases through hydrogen bonding (Ye et al., 2017). The hydrogel exhibited pH-stimulated sol-gel transition where the hydrogel exhibited gel state in pH 6–8 and sol state in pH < 6 or > 8. In another example, Shin and Lee synthesized gallol-conjugated HA and added a gallol-rich crosslinker (i.e., oligo-epigallocatechin gallate) to form a

shear-thinning and self-healing hydrogel based on extensive hydrogen bonds of gallol-gallol and gallol-HA (Shin and Lee, 2017). The hydrogel was resistant to enzymatic degradation by protein (i.e., hyaluronidase) immobilization through non-covalent interactions between gallols and proteins.

Hydrophobic interactions occur as a consequence of aggregative hydrophobes in aqueous media. In many cases of self-healing hydrogels based on hydrophobic interactions, the surfactant micelles (Gulyuz and Okay, 2015; Liu, Y. et al., 2018) or liposomes (Rao et al., 2011; Hao et al., 2013) are employed as crosslinking points to construct the polymer chains comprising both hydrophilic and hydrophobic monomers. For example, the self-healing hydrogel could form via micellar copolymerization of hydrophobic monomer stearyl methacrylate and hydrophilic monomer acrylamide in the aqueous solution of sodium dodecyl sulfate (SDS) micelles (Tuncaboylu et al., 2011, 2012a,b). In these cases, the addition of salt into aqueous SDS solutions leads to micellar growth and solubilization of hydrophobes within SDS micelles. The hydrogel containing SDS micelles with the time-dependent dynamic moduli exhibited high elongation ratio and good self-healing ability, while after extraction of SDS, the hydrogel with time-independent dynamic moduli showed high mechanical strength and no self-healing ability. Self-healing hydrogel can also be prepared based on surfactant-free hydrophobic associations via solvent evaporation of an

aqueous polymer solution above a critical polymer concentration (Owusu-Nkwantabisah et al., 2017).

Self-healing hydrogels can form through reversible electrostatic interactions occurring in charged polymers and ions (Wei et al., 2013; Wei, H. et al., 2014), polyelectrolytes (Huang et al., 2014; Luo et al., 2015; Ren et al., 2016; Li, J. et al., 2017), polyampholytes (Ihsan et al., 2013; Sun et al., 2013), and zwitterionic fusions (Bai et al., 2014). For example, self-healing hydrogel was synthesized through reversible polyelectrolyte complexes of alginate and 2-hydroxypropyltrimethyl ammonium chloride chitosan (Ren et al., 2016). The two polymers were mixed to form self-healing hydrogel at charge neutrality followed by precipitation for 12 h. In addition to self-healing ability, the hydrogel exhibited shear-thinning property, high adhesive behavior, and cytocompatibility. Meanwhile, the polyampholytes can form self-healing hydrogels with tunable mechanical properties via electrostatic interactions between randomly dispersed cationic and anionic repeating groups in polymers (Sun et al., 2013). In analogy to double-network hydrogels, the tough polyampholyte hydrogels contained ionic strong bonds and weak bonds to maintain the shapes and enhance the shock absorbance and self-healing abilities, respectively. Besides, the more hydrophobic polyampholyte hydrogels exhibited the robust and poor self-healing properties, whereas the less hydrophobic polyampholyte hydrogels exhibited the soft and good self-healing properties (Sun et al., 2013).

Multi-mechanism Interactions

Supramolecular chemistry is widely applied to prepare self-healing hydrogels through various non-covalent interactions, such as host–guest interaction and protein–ligand recognition. In addition, hybrids of non-covalent interactions and/or permanent/dynamic covalent bonds were developed to prepare self-healing hydrogels for rapid recovery, long-term stability, high mechanical property, and/or multi-responsive behavior.

Host–guest interactions occur when two or more chemical species assemble via non-covalent interactions, such as van der Waals force, hydrogen bond, electrostatic interaction, and hydrophobic interaction. In host–guest chemistry, the macrocyclic host moiety is inserted inside the guest moiety to form a unique structure of the inclusion complexation. Host–guest interactions are used popularly to prepare the self-healing hydrogels, and many such hydrogels rely on external stimuli, such as temperature (Zheng et al., 2012), light (Yamaguchi et al., 2012), pH (Zheng et al., 2013), and redox potentials (Nakahata et al., 2011; Miyamae et al., 2015), to trigger the healing process. Meanwhile, host–guest hydrogels have also been developed to recover themselves without the need of external stimuli (Appel et al., 2012; Kakuta et al., 2013; Rodell et al., 2013; McKee et al., 2014). For example, the self-healing HA hydrogel was prepared based on the host–guest interactions of β-cyclodextrin-modified HA (host macromer) and adamantane-modified HA (guest macromer) (Rodell et al., 2013). The hydrogels exhibited shear-thinning property and rapid recovery at 25°C.

Catechol and gallol are polyphenolic moieties commonly distributed in organisms as important functional groups, which can form various covalent and non-covalent bonds, such

as Michael addition or Schiff base reaction with thiol and amine, coordination bonds with metals, hydrogen bonds, and aromatic interactions (Lee et al., 2007; Sileika et al., 2013). Li et al. developed a novel self-healing hydrogel by self-assembly of an ABA tri-block copolymer through the catechol-mediated hydrogen bonding and aromatic interaction, where the catechol-functionalized poly(N-isopropylacrylamide) (PNIPAM) and poly(ethylene oxide) (PEO) were each selected as A and B blocks for synthesis (Li et al., 2015). The hydrogel exhibited a thermo-responsive sol-gel transition and recovered its mechanical properties after repeated damages owing to PNIPAM moiety and catechol-mediated interaction, respectively. Moreover, Birkedal and coworkers prepared a self-healing and pH-responsive hydrogel using tannic acid (TA), metal ions, and polyallylamine (PAA) in one step (Krogsgaard et al., 2014a). Below pH 8, the hydrogel was crosslinked mostly by reversible hydrogen bonds, covalent crosslinks between TA and PAA, and coordination bonds between TA and iron ion; while above pH 8, irreversible bonds predominantly enhanced the gel modulus and hindered self-healing. Likewise, self-healing hydrogels were developed based on interactions between 3,4-dihydroxyphenylalanine-modified PAA (DOPA-PAA) and metal ions [such as Al(III), Ga(III), In(III), and Fe(III) ions; (Krogsgaard et al., 2014b)].

Dupin and coworkers reported for the first time the formation of self-healing hydrogels using gold(I) ions-crosslinked thiol-terminated PEG via metallophilic attractive forces (Casuso et al., 2014). The hydrogel exhibited cytocompatibility and mimicked the synovial fluid of the human joint in rheological properties under physiological conditions. Afterward, a series of self-healing hydrogels with tunable mechanical properties were prepared using $HAuCl_4$ (or $AgNO_3$) and 4-arm thiol-terminated polyethylene glycol $[(PEGSH)_4]$ in different ratios based on metal(I)-thiolate/disulfide exchange (Casuso et al., 2015). These hydrogels showed reversible mechanical properties and frequency-dependent stiffness/shock-absorbing properties at the physiological pH due to the metal(I)-thiolate/disulfide exchange. The potential of the hydrogel as an artificial nucleus pulposus for the intervertebral discs was demonstrated via a bovine *ex vivo* model using axial compression-tension cycles at different frequencies followed by creep experiments and μCT analysis (Pérez-San Vicente et al., 2017). Moreover, the hydrogels incorporating bioactive glass nanoparticles led to the stiffer properties for bone regeneration (Gantar et al., 2016). Meanwhile hydroxyapatite was formed after degradation of the nanoparticles.

On the basis of dynamic acylhydrazone and disulfide bonds, self-healing hydrogels with pH/redox dual responsive transitions have been developed (Deng et al., 2012). The hydrogel displayed self-healing properties in acidic and basic conditions based on the acylhydrazone and disulfide bonds, respectively. Additionally, acylhydrazone bonds were activated by the catalytic aniline in neutral conditions, and disulfide bonds were responsive to the redox conditions. Recently, the self-healing hydrogel was prepared from the mixture carboxyethyl cellulose-graft-dithiodipropionate dihydrazide and DF-PEG under 4-amino-DL-phenylalanine (4a-Phe) catalysis (Yang et al., 2017). The

gelation time of the hydrogel could be controlled by varying the total polymer content or the 4a-Phe concentration. The hydrogel was applied for controlled release of doxorubicin and 3D culture of L929 cells because of pH/redox responsiveness and cytocompatibility.

BIOMEDICAL APPLICATIONS OF SELF-HEALING HYDROGELS

Self-healing hydrogels have received increasing attentions in biomedical applications, such as wound healing (Gaharwar et al., 2014; Han et al., 2016; Zhao et al., 2017; Zhu, S. K. et al., 2017; Li et al., 2018; Liu, B. et al., 2018), drug delivery (Huebsch et al., 2014; Liu et al., 2016; Wang et al., 2016; Xing et al., 2016; Wang J. Y. et al., 2017; Xia et al., 2017; Yavvari et al., 2017; Zhu, C. et al., 2017; Hong et al., 2018), tissue engineering (Dankers et al., 2012; Bastings et al., 2014; Gaffey et al., 2015; Rodell et al., 2015a,b; Loebel et al., 2017), surface coating (Canadell et al., 2011; Yoon et al., 2011; Yang et al., 2015), 3D printing (Highley et al., 2015; Darabi et al., 2017; Loebel et al., 2017; Wang et al., 2018), and soft robot (Shi et al., 2015; Darabi et al., 2017; Han et al., 2017; Liu, B. et al., 2018; Liu et al., 2018). In these cases, dibenzaldehyde-based, UPy-based, catechol-based, and host–guest-based self-healing hydrogels are highlighted due to many evaluations of *in vivo* experiments. As summarized in **Table 1**, some animal models have been used to verify the biocompatibility and efficacy of self-healing hydrogels. Besides the biocompatibility, self-healing hydrogels require injectability and long-term stability for drug delivery, tissue engineering, and 3D printing; and toughness and conductivity for soft robot.

Drug Delivery

Self-healing hydrogel based on host–guest interactions between β-cyclodextrin-modified PEI and adamantane-modified PEG was developed for local siRNA release (Wang et al., 2018). The modified polymers assembled with siRNA to form polyplexes, which could improve the transfection efficiency and the viability of cells. When injected into the myocardium, the hydrogel with siRNA encapsulation enhanced the uptake of Cy5.5-siRNA and maintained the silencing of GFP for 1 week in a GFP-expressing rat.

Xing et al. reported an injectable and self-healing collagen-gold hybrid hydrogel with adjustable mechanical properties (Xing et al., 2016). This hydrogel was prepared through electrostatic interaction between positively charged collagen chains and negatively charged tetrachloroaurate ($[AuCl_4]^-$) ions, and further non-covalent interactions between subsequent biomineralized gold nanoparticles and collagen. The hydrogel was developed for localized delivery and sustained release of the photosensitive drug. By combinatorial photothermal and photodynamic therapies, the significantly enhanced antitumor efficacy was demonstrated through an *in vivo* antitumor test using the subcutaneous mouse model.

Self-healing hydrogels based on glycol chitosan and DF-PEG (GC-DP) have been developed for intratumor therapy *in vivo*. GC-DP hydrogel containing antitumor drug was injected into the disease position with a steady release *in situ* (Yang et al., 2017). Moreover, the ionic GC-DP hydrogel exhibited microwave susceptibility to produce high-temperature hyperthermia for tumor ablation (Wang J. Y. et al., 2017). A multi-antitumor system was developed based on GC-DP hydrogel containing doxorubicin/docetaxel-loaded poly(lactic-co-glycolic acid) (PLGA) nanoparticles and iron oxide for chemotherapy and magnetic hyperthermia (Xie et al., 2017). The system showed the greater *in vivo* antitumor efficacy under the alternative magnetic field compared to the hydrogel containing doxorubicin/docetaxel-loaded PLGA nanoparticles.

Tissue Engineering

Self-healing host–guest hydrogels have been developed to treat the myocardial infarction. The self-healing hydrogel, formed through host–guest interactions of adamantine- and β-cyclodextrin-modified HA, was injected into the ischemic myocardium encapsulating endothelial progenitor cells (EPCs) (Gaffey et al., 2015). A rodent model of acute myocardial infarction was employed to confirm that a significant increase in vasculogenesis was noted with the hydrogel encapsulating EPCs, compared to the treatment of EPCs alone or hydrogel alone. Moreover, the hydrogel was designed using adamantane/thiol-modified HA and cyclodextrin/methacrylate-modified HA through host–guest interaction and Michael addition (Rodell et al., 2015a). The reversible host–guest interaction and permanent Michael addition provided shear-thinning injection and high retention, respectively. Epicardial injection of the hydrogel in a rat myocardial infarction model showed significant improvement of the outcome compared to the untreated group and the hydrogel without Michael addition.

Self-healing hydrogels were designed as injectable carriers for growth factors using PEG end-functionalized with four-fold hydrogen-bonding ureidopyrimidinone (UPy) moieties. UPy-modified PEG hydrogel incorporated with antifibrotic growth factor was delivered in a pocket introduced under the kidney capsule of rats (Dankers et al., 2012). The kidney capsule was loosened from the kidney to create a small pocket. After injection of growth factor-containing hydrogels, the number of myofibroblasts stayed the same to the contralateral (healthy) kidney, while significantly increased with the injection of saline or hydrogel alone. In another example, growth factors were delivered by UPy-modified PEG hydrogel to repair the infarcted myocardium (Bastings et al., 2014). This pH-switchable hydrogel could be injected through the long and narrow lumen of the catheter mapping system, and rapidly formed a hydrogel in contact with tissue. The growth factor-containing hydrogel reduced scar collagen in a chronic myocardial infarction pig model.

Self-healing hydrogels based on GC-DP was prepared for tissue repairs. In the application of central nervous system (CNS) repair, neurosphere-like progenitors showed better proliferation and differentiation in GC-DP hydrogel, and injection of GC-DP hydrogel combining neurospheres promoted functional recovery in a zebrafish CNS impaired model (Tseng et al., 2015). Moreover, the GC-DP hydrogel combining the optogenetic method was developed as a temporal-spatial approach to treat

TABLE 1 | Examples of self-healing hydrogels evaluated by animal models.

Self-healing mechanisms	Materials	Animal model evaluation	References
Boronate ester bonds	Alginate-boronic acid	Oral administration for drug retention	Hong et al., 2018
Coordination bonds	Dexamethasone phosphate and Ca(II)	Subcutaneous injection for drug delivery	Liu et al., 2016
Coordination bonds	Chitosan-catechol and Fe(III)	Cancer model for drug delivery	Yavvari et al., 2017
Coordination bonds and electrostatic interactions	Collagen and gold	Cancer model for drug delivery	Xing et al., 2016
Electrostatic interactions	Silicate nanoplatelets and gelatin	Liver bleeding model for hemostasis	Gaharwar et al., 2014
Hydrogen bonds	Polyglutamic acid and lysine	Skin defect model for wound healing	Zhu, S. K. et al., 2017
Hydrogen bonds	Ureidopyrimidinone-PEG	Kidney implantation for tissue repair	Dankers et al., 2012
Hydrogen bonds	Ureidopyrimidinone-PEG	Myocardial infarction model for tissue repair	Bastings et al., 2014
Hydrogen bonds	Gelatin methacrylate and tannic acid	Gastric incision model for wound closure	Liu, B. et al., 2018
Hydrogen bonds and aromatic interactions	Polydopamine nanoparticles and poly(N-isopropylacrylamide)	Skin defect model for wound healing	Han et al., 2016
Hydrogen bonds and aromatic interactions	Polydopamine, graphene oxide, and polyacrylamide	Osteochondral defect model for tissue repair	Han et al., 2017
Host-guest interactions	β-Cyclodextrin-PEI and adamantane-PEG	Myocardium injection for drug delivery	Wang L. L. et al., 2017
Host-guest interactions	Adamantane/thiol-HA and cyclodextrin/methacrylate-HA	Myocardial infarction model for tissue repair	Rodell et al., 2015a
Host-guest interactions	Adamantane-HA and β-cyclodextrin-HA	Myocardial infarction model for tissue repair	Gaffey et al., 2015
Host-guest interactions	Adamantane-HA and β-cyclodextrin-HA	Chronic kidney disease model for drug delivery	Rodell et al., 2015b
Imine bond	DF-PEG and chitosan-aniline tetramer	Subcutaneous injection for cell retention	Dong et al., 2016
Imine bond	Chondroitin sulfate-aldehyde and N-succinyl-chitosan	Subcutaneous injection for material degradation	Lü et al., 2015
Imine bond	DF-PEG-co-poly(glycerol sebacate) and chitosan-polyaniline	Skin defect model for wound healing	Zhao et al., 2017
Imine bond	Aldehyde-xanthan and carboxymethyl-chitosan	Abdominal wall defect model for tissue repair	Huang et al., 2018
Imine bond	DF-PEG and glycol chitosan	Cancer model for drug delivery	Xia et al., 2017
Imine bond	DF-PEG-co-poly(glycerol sebacate) and Chitosan-polyaniline	Liver bleeding model for hemostasis	Zhao et al., 2017
Imine bond	DF-PEG, glycol chitosan, fibrinogen, and thrombin	Hindlimb ischemia model for tissue repair	Hsieh et al., 2017
Imine bond	DF-PEG and glycol chitosan	Zebrafish neural injury model for tissue repair	Tseng et al., 2015
Imine bond	DF-PEG and glycol chitosan	Zebrafish neural injury model for drug delivery	Hsieh et al., 2018
Imine bond	DF-PEG, glycol chitosan, fibrinogen, and thrombin	Zebrafish embryos injection for angiogenesis	Hsieh et al., 2017

neurodegenerative diseases (Hsieh et al., 2018). The hydrogel containing bacteriorhodopsin plasmid and neural stem cells was injected into CNS impaired zebrafish where the neural repair was observed, particularly under green light exposure. Besides, GC-DP hydrogel was also used to induce blood capillary formation. With the incorporation of fibrin gel, a composite hydrogel could form with an interpenetrating polymer network (i.e., double network) of GC-DP and fibrin (Hsieh et al., 2017). The hydrogel induced vascular endothelial cells to form capillary-like structures, and injection of the hydrogel alone promoted angiogenesis in zebrafish and rescued the blood circulation in ischemic hindlimbs of mice.

Other Applications

Self-healing hydrogels, based on the host–guest interaction of β-cyclodextrin- and adamantine-modified HA, were used in the 3D printing of high-resolution structures through printing of shearing-thinning ink hydrogel into self-healing support hydrogel (Highley et al., 2015). The multicellular structures could be expediently patterned, such as printing of mesenchymal stem cells within an ink hydrogel into a support hydrogel containing 3T3 fibroblasts. The channel-like structure was achieved by writing the ink hydrogel into the methacrylate-modified support hydrogel, followed by UV irradiation for secondary covalent crosslinks of support hydrogel, followed by removal of the physical (i.e., host–guest) ink hydrogel. Meanwhile, the self-supporting structure was obtained by covalently crosslinking the ink hydrogel and removing the non-covalent support hydrogel. This system supported the patterning of multiple inks, cells, and channels in 3D space.

A tough self-healing hydrogel was synthesized as cell stimulators and implantable bioelectronics (Han et al., 2017). In

the study, graphene oxide was partially converted to conductive graphene through polydopamine reduction, and acrylamide monomers were polymerized *in situ* to form the hydrogel by interactions between graphene oxide, polydopamine, and polyacrylamide. Meanwhile, the free catechol groups on polydopamine imparted self-healing property and tissue adhesion to the hydrogel via various non-covalent interactions. The hydrogel could be used not only as an adhesive electrode or motion sensor but also as an *in vitro* cell stimulator and *in vivo* implantable intramuscular electrode. For example, the hydrogel electrodes were implanted into the rabbit dorsal muscle and connected to a signal detector using the transcutaneous wires. The electrodes could record the electromyographic signal when the rabbit was interfered with external stimulation.

CONCLUSIONS

Self-healing hydrogels can be classified as robust and soft hydrogels according to mechanical properties in biomedical applications. Robust self-healing hydrogels are used as soft robots (such as implantable or wearable biosensors) with extended lifetime and mechanical performance due to repairing of the damages or fatigues. Soft self-healing hydrogels with shear-thinning properties are used in cell/drug delivery and 3D printing due to injection through narrow needles and retention at target sites. To facilitate biomedical applications in the future, self-healing hydrogels need to address several major concerns including (1) designing self-healing hydrogels with good biocompatibility and appropriate mechanical properties;

(2) better characterizing the self-healing properties with various assessment tools (such as rheological measurement, mechanical analysis, or other novel tools); (3) developing theories on self-healing mechanisms and properties (such as chemistry, kinetics, and thermodynamics); and (4) translation by animal experiments and clinical trials. Moreover, because the self-healing properties of hydrogels are mostly determined in non-physiological environments, it would be challenging to verify that the known self-healing properties are well-maintained in physiological conditions such as with electrolytes, under mechanical stress, and in the presence of material–cell interaction. In addition, controllable biodegradability is important in self-healing hydrogels for tissue engineering and drug delivery. In comparison with permanent crosslinks, reversible crosslinks are broken easily to facilitate biodegradation, while reversible crosslinks recover the macro- and micro-scaled damages to restrain biodegradation. Reversible equilibriums of self-healing hydrogels should be controlled according to the various applications, such as long-term drug release and cell-adaptable materials.

AUTHOR CONTRIBUTIONS

ACKNOWLEDGMENTS

REFERENCES

Appel, E. A., Loh, X. J., Jones, S. T., Biedermann, F., Dreiss, C. A., and Scherman, O. A. (2012). Ultrahigh-water-content supramolecular hydrogels exhibiting multistimuli responsiveness. *J. Am. Chem. Soc.* 134, 11767–11773. doi: 10.1021/ja3044568

Bai, T., Liu, S., Sun, F., Sinclair, A., Zhang, L., Shao, Q., et al. (2014). Zwitterionic fusion in hydrogels and spontaneous and time-independent self-healing under physiological conditions. *Biomaterials* 35, 3926–3933. doi: 10.1016/j.biomaterials.2014.01.077

Banerjee, S. L., and Singha, N. K. (2017). A new class of dual responsive self-healable hydrogels based on a core crosslinked ionic block copolymer micelle prepared via RAFT polymerization and Diels-Alder "click" chemistry. *Soft Matter* 13, 9024–9035. doi: 10.1039/c7sm01906h

Barcan, G. A., Zhang, X., and Waymouth, R. M. (2015). Structurally dynamic hydrogels derived from 1,2-dithiolanes. *J. Am. Chem. Soc.* 137, 5650–5653. doi: 10.1021/jacs.5b02161

Bastings, M. M., Koudstaal, S., Kieltyka, R. E., Nakano, Y., Pape, A. C., Feyen, D. A., et al. (2014). A fast pH-switchable and self-healing supramolecular hydrogel carrier for guided, local catheter injection in the infarcted myocardium. *Adv. Healthc. Mater.* 3, 70–78. doi: 10.1002/adhm.201300076

Bergman, S. D., and Wudl, F. (2008). Mendable polymers. *J. Mater. Chem.* 18, 41–62. doi: 10.1039/b713953p

Canadell, J., Goossens, H., and Klumperman, B. (2011). Self-healing materials based on disulfide links. *Macromolecules* 44, 2536–2541. doi: 10.1021/ma2001492

Casuso, P., Odriozola, I., Pérez-San, A., Loinaz, I., Cabañero G., Grande, H. J., et al. (2015). Injectable and self-healing dynamic hydrogels based on

metal(I)-thiolate/disulfide exchange as biomaterials with tunable mechanical properties. *Biomacromolecules* 16, 3552–3561. doi: 10.1021/acs.biomac. 5b00980

Casuso, P., Perez-San Vicente, A., Iribar, H., Gutierrez-Rivera, A., Izeta, A., Loinaz, I., et al. (2014). Aurophilically cross-linked "dynamic" hydrogels mimicking healthy synovial fluid properties. *Chem. Commun.* 50, 15199–15201. doi: 10.1039/c4cc05735j

Chirila, T. V., Lee, H. H., Oddon, M., Nieuwenhuizen, M. M. L., Blakey, I., and Nicholson, T. M. (2014). Hydrogen-bonded supramolecular polymers as self-healing hydrogels: effect of a bulky adamantyl substituent in the ureido-pyrimidinone monomer. *J. Appl. Polym. Sci.* 131:39932. doi: 10.1002/app. 39932

Cui, J., and del Campo, A. (2012). Multivalent H-bonds for self-healing hydrogels. *Chem. Commun.* 48, 9302–9304. doi: 10.1039/c2cc34701f

Cui, J. X., Wang, D. P., Koynov, K., and del Campo, A. (2013). 2-Ureido-4-pyrimidone-based hydrogels with multiple responses. *Chemphyschem* 14, 2932–2938. doi: 10.1002/cphc.201300367

Dankers, P. Y., Hermans, T. M., Baughman, T. W., Kamikawa, Y., Kieltyka, R. E., Bastings, M. M., et al. (2012). Hierarchical formation of supramolecular transient networks in water: a modular injectable delivery system. *Adv. Mater.* 24, 2703–2709. doi: 10.1002/adma.201104072

Darabi, M. A., Khosrozadeh, A., Mbeleck, R., Liu, Y., Chang, Q., Jiang, J., et al. (2017). Skin-inspired multifunctional autonomic-intrinsic conductive self-healing hydrogels with pressure sensitivity, stretchability, and 3D printability. *Adv. Mater.* 29:1700533. doi: 10.1002/adma.201700533

Deng, G., Tang, C., Li, F., Jiang, H., and Chen, Y. (2010). Covalent cross-linked polymer gels with reversible sol–gel transition and self-healing properties. *Macromolecules* 43, 1191–1194. doi: 10.1021/ma9022197

Deng, G. H., Li, F. Y., Yu, H. X., Liu, F. Y., Liu, C. Y., Sun, W. X., et al. (2012). Dynamic hydrogels with an environmental adaptive self-healing ability and dual responsive sol-gel transitions. *ACS Macro Lett.* 1, 275–279. doi: 10.1021/mz200195n

Dong, R., Zhao, X., Guo, B., and Ma, P. X. (2016). Self-healing conductive injectable hydrogels with antibacterial activity as cell delivery carrier for cardiac cell therapy. *ACS Appl. Mater. Interfaces* 8, 17138–17150. doi: 10.1021/acsami.6b04911

Gaffey, A. C., Chen, M. H., Venkataraman, C. M., Trubelja, A., Rodell, C. B., Dinh, P. V., et al. (2015). Injectable shear-thinning hydrogels used to deliver endothelial progenitor cells, enhance cell engraftment, and improve ischemic myocardium. *J. Thorac. Cardiovasc. Surg.* 150, 1268–1276. doi: 10.1016/j.jtcvs.2015.07.035

Gaharwar, A. K., Avery, R. K., Assmann, A., Paul, A., McKinley, G. H., Khademhosseini, A., et al. (2014). Shear-thinning nanocomposite hydrogels for the treatment of hemorrhage. *ACS Nano* 8, 9833–9842. doi: 10.1021/nn503719n

Gantar, A., Drnovšek, N., Casuso, P., Pérez-San Vicente, A., Rodriguez, J., Dupin, D., et al. (2016). Injectable and self-healing dynamic hydrogel containing bioactive glass nanoparticles as a potential biomaterial for bone regeneration. *RSC Adv.* 6, 69156–69166. doi: 10.1039/c6ra17327f

Ghanian, M. H., Mirzadeh, H., and Baharvand, H. (2018). *In situ* forming, cytocompatible, and self-recoverable tough hydrogels based on dual ionic and click cross-linked alginate. *Biomacromolecules* 19, 1646–1662. doi: 10.1021/acs.biomac.8b00140

Grover, G. N., Lam, J., Nguyen, T. H., Segura, T., and Maynard, H. D. (2012). Biocompatible hydrogels by oxime click chemistry. *Biomacromolecules* 13, 3013–3017. doi: 10.1021/bm301346e

Gulyuz, U., and Okay, O. (2015). Self-healing poly(acrylic acid) hydrogels: effect of surfactant. *Macromol. Symp.* 358, 232–238. doi: 10.1002/masy.201500063

Han, L., Lu, X., Wang, M., Gan, D., Deng, W., Wang, K., et al. (2017). A mussel-inspired conductive, self-adhesive, and self-healable tough hydrogel as cell stimulators and implantable bioelectronics. *Small* 13:1601916. doi: 10.1002/smll.201601916

Han, L., Zhang, Y. N., Lu, X., Wang, K. F., Wang, Z., and Zhang, H. (2016). Polydopamine nanoparticles modulating stimuli-responsive PNIPAM hydrogels with cell/tissue adhesiveness. *ACS Appl. Mater. Interfaces* 8, 29088–29100. doi: 10.1021/acsami.6b11043

Hao, X., Liu, H., Xie, Y. J., Fang, C., and Yang, H. Y. (2013). Thermal-responsive self-healing hydrogel based on hydrophobically modified chitosan and vesicle. *Colloid Polym. Sci.* 291, 1749–1758. doi: 10.1007/s00396-013-2910-4

Harada, A., Takashima, Y., and Nakahata, M. (2014). Supramolecular polymeric materials via cyclodextrin-guest interactions. *Acc. Chem. Res.* 47, 2128–2140. doi: 10.1021/ar500109h

He, L., Fullenkamp, D. E., Rivera, J. G., and Messersmith, P. B. (2011). pH responsive self-healing hydrogels formed by boronate-catechol complexation. *Chem. Commun.* 47, 7497–7499. doi: 10.1039/c1cc11928a

He, L., Szopinski, D., Wu, Y., Luinstra, G. A., and Theato, P. (2015). Toward self-healing hydrogels using one-pot thiol–ene click and borax-diol chemistry. *ACS Macro Lett.* 4, 673–678. doi: 10.1021/acsmacrolett.5b00336

Highley, C. B., Rodell, C. B., and Burdick, J. A. (2015). Direct 3D printing of shear-thinning hydrogels into self-healing hydrogels. *Adv. Mater.* 27, 5075–5079. doi: 10.1002/adma.201501234

Hong, S. H., Kim, S., Park, J. P., Shin, M., Kim, K., Ryu, J. H., et al. (2018). Dynamic bonds between boronic acid and alginate: hydrogels with stretchable, self-healing, stimuli-responsive, remoldable, and adhesive properties. *Biomacromolecules* 19, 2053–2061. doi: 10.1021/acs.biomac.8b00144

Hou, S., Wang, X., Park, S., Jin, X., and Ma, P. X. (2015). Rapid self-integrating, injectable hydrogel for tissue complex regeneration. *Adv. Healthc. Mater.* 4, 1491–1495, 1423. doi: 10.1002/adhm.201500093

Hsieh, F.-Y., Tao, L., Wei, Y., and Hsu, S. H. (2017). A novel biodegradable self-healing hydrogel to induce blood capillary formation. *NPG Asia Mater.* 9:e363. doi: 10.1038/am.2017.23

Hsieh, F. Y., Han, H. W., Chen, X. R., Yang, C. S., Wei, Y., and Hsu, S. H. (2018). Non-viral delivery of an optogenetic tool into cells with self-healing hydrogel. *Biomaterials* 174, 31–40. doi: 10.1016/j.biomaterials.2018.05.014

Huang, J., Deng, Y., Ren, J., Chen, G., Wang, G., Wang, F., et al. (2018). Novel *in situ* forming hydrogel based on xanthan and chitosan re-gelifying in liquids for local drug delivery. *Carbohydr. Polym.* 186, 54–63. doi: 10.1016/j.carbpol.2018.01.025

Huang, Y., Lawrence, P. G., and Lapitsky, Y. (2014). Self-assembly of stiff, adhesive and self-healing gels from common polyelectrolytes. *Langmuir* 30, 7771–7777. doi: 10.1021/la404606y

Huebsch, N., Kearney, C. J., Zhao, X., Kim, J., Cezar, C. A., Suo, Z., et al. (2014). Ultrasound-triggered disruption and self-healing of reversibly cross-linked hydrogels for drug delivery and enhanced chemotherapy. *Proc. Natl. Acad. Sci. U.S.A.* 111, 9762–9767. doi: 10.1073/pnas.1405469111

Ihsan, A. B., Sun, T. L., Kuroda, S., Haque, M. A., Kurokawa, T., Nakajima, T., et al. (2013). A phase diagram of neutral polyampholyte – from solution to tough hydrogel. *J. Mater. Chem. B* 1, 4555–4562. doi: 10.1039/c3tb20790k

Kakuta, T., Takashima, Y., Nakahata, M., Otsubo, M., Yamaguchi, H., and Harada, A. (2013). Preorganized hydrogel: self-healing properties of supramolecular hydrogels formed by polymerization of host-guest-monomers that contain cyclodextrins and hydrophobic guest groups. *Adv. Mater.* 25, 2849–2853. doi: 10.1002/adma.201205321

Karimi, A. R., and Khodadadi, A. (2016). Mechanically robust 3D nanostructure chitosan-based hydrogels with autonomic self-healing properties. *ACS Appl. Mater. Interfaces* 8, 27254–27263. doi: 10.1021/acsami.6b10375

Krogsgaard, M., Andersen, A., and Birkedal, H. (2014a). Gels and threads: mussel-inspired one-pot route to advanced responsive materials. *Chem. Commun.* 50, 13278–13281. doi: 10.1039/c4cc05293e

Krogsgaard, M., Behrens, M. A., Pedersen, J. S., and Birkedal, H. (2013). Self-healing mussel-inspired multi-pH-responsive hydrogels. *Biomacromolecules* 14, 297–301. doi: 10.1021/bm301844u

Krogsgaard, M., Hansen, M. R., and Birkedal, H. (2014b). Metals & polymers in the mix: fine-tuning the mechanical properties & color of self-healing mussel-inspired hydrogels. *J. Mater. Chem. B* 2, 8292–8297. doi: 10.1039/c4tb01503g

Lee, H., Dellatore, S. M., Miller, W. M., and Messersmith, P. B. (2007). Mussel-inspired surface chemistry for multifunctional coatings. *Science* 318, 426–430. doi: 10.1126/science.1147241

Li, J., Su, Z. L., Ma, X. D., Xu, H. J., Shi, Z. X., Yin, J., et al. (2017). *In situ* polymerization induced supramolecular hydrogels of chitosan and poly(acrylic acid-acrylamide) with high toughness. *Mater. Chem. Front.* 1, 310–318. doi: 10.1039/c6qm00002a

Li, L., Yan, B., Yang, J., Chen, L., and Zeng, H. (2015). Novel mussel-inspired injectable self-healing hydrogel with anti-biofouling property. *Adv. Mater.* 27, 1294–1299. doi: 10.1002/adma.201405166

Li, Q., Barret, D. G., Messersmith, P. B., and Holten-Andersen, N. (2016). Controlling hydrogel mechanics via bio-inspired polymer-nanoparticle bond dynamics. *ACS Nano* 10, 1317–1324. doi: 10.1021/acsnano.5b06692

Li, S., Wang, L., Yu, X., Wang, C., and Wang, Z. (2018a). Synthesis and characterization of a novel double cross-linked hydrogel based on Diels-Alder click reaction and coordination bonding. *Mater. Sci. Eng. C Mater. Biol. Appl.* 82, 299–309. doi: 10.1016/j.msec.2017.08.031

Li, S., Yi, J., Yu, X., Shi, H., Zhu, J., and Wang, L. (2018b). Preparation and characterization of acid resistant double cross-linked hydrogel for potential biomedical applications. *ACS Biomater. Sci. Eng.* 4, 872–883. doi: 10.1021/acsbiomaterials.7b00818

Li, Y., Wang, X., Fu, Y., Wei, Y., Zhao, L., and Tao, L. (2018). A self-adapting hydrogel to improve the therapeutic effect in wound-healing. *ACS Appl. Mater. Interfaces* 10, 26046–26055. doi: 10.1021/acsami.8b08874

Li, Y., Zhang, Y. L., Wei, Y. N., and Tao, L. (2017). Preparation of chitosan-based injectable hydrogels and its application in 3D cell culture. *J. Vis. Exp.* 127:e56253. doi: 10.3791/56253

Lin, F., Yu, J., Tang, W., Zheng, J., Defante, A., Guo, K., et al. (2013). Peptide-functionalized oxime hydrogels with tunable mechanical properties and gelation behavior. *Biomacromolecules* 14, 3749–3758. doi: 10.1021/bm401133r

Liu, B., Wang, Y., Miao, Y., Zhang, X., Fan, Z., Singh, G., et al. (2018). Hydrogen bonds autonomously powered gelatin methacrylate hydrogels with super-elasticity, self-heal and underwater self-adhesion for sutureless skin and stomach surgery and E-skin. *Biomaterials* 171, 83–96. doi: 10.1016/j.biomaterials.2018.04.023

Liu, Q., Zhan, C., Barhoumi, A., Wang, W., Santamaria, C., McAlvin, J. B., et al. (2016). A supramolecular shear-thinning anti-inflammatory steroid hydrogel. *Adv. Mater.* 28, 6680–6686. doi: 10.1002/adma.201601147

Liu, S. L., Kang, M. M., Li, K. W., Yao, F., Oderinde, O., Fu, G. D., et al. (2018). Polysaccharide-templated preparation of mechanically-tough, conductive and self-healing hydrogels. *Chem. Eng. J.* 334, 2222–2230. doi: 10.1016/j.cej.2017.11.103

Liu, Y., Li, Z., Niu, N., Zou, J., and Liu, F. (2018). A simple coordination strategy for preparing a complex hydrophobic association hydrogel. *J. Appl. Polym. Sci.* 135:46400. doi: 10.1002/app.46400

Liu, Y. L., and Chuo, T. W. (2013). Self-healing polymers based on thermally reversible Diels-Alder chemistry. *Polym. Chem.* 4, 2194–2205. doi: 10.1039/c2py20957h

Loebel, C., Rodell, C. B., Chen, M. H., and Burdick, J. A. (2017). Shear-thinning and self-healing hydrogels as injectable therapeutics and for 3D-printing. *Nat. Protoc.* 12, 1521–1541. doi: 10.1038/nprot.2017.053

Lü, S., Gao, C., Xu, X., Bai, X., Duan, H., Gao, N., et al. (2015). Injectable and self-healing carbohydrate-based hydrogel for cell encapsulation. *ACS Appl. Mater. Interfaces* 7, 13029–13037. doi: 10.1021/acsami.5b03143

Luo, F., Sun, T. L., Nakajima, T., Kurokawa, T., Zhao, Y., Sato, K., et al. (2015). Oppositely charged polyelectrolytes form tough, self-healing, and rebuildable hydrogels. *Adv. Mater.* 27, 2722–2727. doi: 10.1002/adma.201500140

McKee, J. R., Appel, E. A., Seitsonen, J., Kontturi, E., Scherman, O. A., and Ikkala, O. (2014). Healable, stable and stiff hydrogels: combining conflicting properties using dynamic and selective three-component recognition with reinforcing cellulose nanorods. *Adv. Funct. Mater.* 24, 2706–2713. doi: 10.1002/adfm.201303699

Miyamae, K., Nakahata, M., Takashima, Y., and Harada, A. (2015). Self-healing, expansion-contraction, and shape-memory properties of a preorganized supramolecular hydrogel through host-guest interactions. *Angew. Chem. Int. Ed.* 54, 8984–8987. doi: 10.1002/anie.201502957

Mukherjee, S., Hill, M. R., and Sumerlin, B. S. (2015). Self-healing hydrogels containing reversible oxime crosslinks. *Soft Matter* 11, 6152–6161. doi: 10.1039/c5sm00865d

Murphy, E. B., and Wudl, F. (2010). The world of smart healable materials. *Prog. Polym. Sci.* 35, 223–251. doi: 10.1016/j.progpolymsci.2009.10.006

Nakahata, M., Takashima, Y., Yamaguchi, H., and Harada, A. (2011). Redox-responsive self-healing materials formed from host-guest polymers. *Nat. Commun.* 2:511. doi: 10.1038/ncomms1521

Owusu-Nkwantabisah, S., Gillmor, J. R., Switalski, S. C., and Slater, G. L. (2017). An autonomous self-healing hydrogel based on surfactant-free hydrophobic association. *J. Appl. Polym. Sci.* 134:44800. doi: 10.1002/app.44800

Pérez-San Vicente, A., Peroglio, M., Ernst, M., Casuso, P., Loinaz, I., Grande, H. J., et al. (2017). Self-healing dynamic hydrogel as injectable shock-absorbing artificial nucleus pulposus. *Biomacromolecules* 18, 2360–2370. doi: 10.1021/acs.biomac.7b00566

Qu, J., Zhao, X., Ma, P. X., and Guo, B. (2017). pH-responsive self-healing injectable hydrogel based on N-carboxyethyl chitosan for hepatocellular carcinoma therapy. *Acta Biomater.* 58, 168–180. doi: 10.1016/j.actbio.2017.06.001

Rao, Z., Inoue, M., Matsuda, M., and Taguchi, T. (2011). Quick self-healing and thermo-reversible liposome gel. *Colloids Surf. B Biointerfaces* 82, 196–202. doi: 10.1016/j.colsurfb.2010.08.038

Ren, Y., Lou, R., Liu, X., Gao, M., Zheng, H. Z., Yang, T., et al. (2016). A self-healing hydrogel formation strategy via exploiting endothermic interactions between polyelectrolytes. *Chem. Commun.* 52, 6273–6276. doi: 10.1039/c6cc02472f

Rodell, C. B., Kaminski, A. L., and Burdick, J. A. (2013). Rational design of network properties in guest–host assembled and shear-thinning hyaluronic acid hydrogels. *Biomacromolecules* 14, 4125–4134. doi: 10.1021/bm401280z

Rodell, C. B., MacArthur, J. W., Dorsey, S. M., Wade, R. J., Wang, L. L., Woo, Y. J., et al. (2015a). Shear-thinning supramolecular hydrogels with secondary autonomous covalent crosslinking to modulate viscoelastic properties *in vivo*. *Adv. Funct. Mater.* 25, 636–644. doi: 10.1002/adfm.201403550

Rodell, C. B., Rai, R., Faubel, S., Burdick, J. A., and Soranno, D. E. (2015b). Local immunotherapy via delivery of interleukin-10 and transforming growth factor beta antagonist for treatment of chronic kidney disease. *J. Control. Release* 206, 131–139. doi: 10.1016/j.jconrel.2015.03.025

Shao, C. Y., Wang, M., Chang, H. L., Xu, F., and Yang, J. (2017). A self-healing cellulose nanocrystal-poly(ethylene glycol) nanocomposite hydrogel via Diels-Alder click reaction. *ACS Sustainable Chem. Eng.* 5, 6167–6174. doi: 10.1021/acssuschemeng.7b01060

Shi, Y., Wang, M., Ma, C., Wang, Y., Li, X., and Yu, G., (2015). A conductive self-healing hybrid gel enabled by metal-ligand supramolecule and nanostructured conductive polymer. *Nano Lett.* 15, 6276–6281. doi: 10.1021/acs.nanolett.5b03069

Shin, M., and Lee, H. (2017). Gallol-rich hyaluronic acid hydrogels: shear-thinning, protein accumulation against concentration gradients, and degradation-resistant properties. *Chem. Mater.* 29, 8211–8220. doi: 10.1021/acs.chemmater.7b02267

Sileika, T. S., Barrett, D. G., Zhang, R., Lau, K. H., and Messersmith, P. B. (2013). Colorless multifunctional coatings inspired by polyphenols found in tea, chocolate, and wine. *Angew. Chem. Int. Ed.* 52, 10766–10770. doi: 10.1002/anie.201304922

Sun, T. L., Kurokawa, T., Kuroda, S., Ihsan, A. B., Akasaki, T., Sato, K., et al. (2013). Physical hydrogels composed of polyampholytes demonstrate high toughness and viscoelasticity. *Nat. Mater.* 12, 932–937. doi: 10.1038/nmat3713

Syrett, J. A., Becer, C. R., and Haddleton, D. M. (2010). Self-healing and self-mendable polymers. *Polym. Chem.* 1, 978–987. doi: 10.1039/c0py00104j

Toohey, K. S., Sottos, N. R., Lewis, J. A., Moore, J. S., and White, S. R. (2007). Self-healing materials with microvascular networks. *Nat. Mater.* 6, 581–585. doi: 10.1038/nmat1934

Tseng, T. C., Hsieh, F. Y., Theato, P., Wei, Y., and Hsu, S. H. (2017). Glucose-sensitive self-healing hydrogel as sacrificial materials to fabricate vascularized constructs. *Biomaterials* 133, 20–28. doi: 10.1016/j.biomaterials.2017.04.008

Tseng, T. C., Tao, L., Hsieh, F. Y., Wei, Y., Chiu, I. M., and Hsu, S. H. (2015). An injectable, self-Healing hydrogel to repair the central nervous system. *Adv. Mater.* 27, 3518–3524. doi: 10.1002/adma.201500762

Tuncaboylu, D. C., Argun, A., Sahin, M., Sari, M., and Okay, O. (2012a). Structure optimization of self-healing hydrogels formed via hydrophobic interactions. *Polymer (Guildf.)* 53, 5513–5522. doi: 10.1016/j.polymer.2012.10.015

Tuncaboylu, D. C., Sahin, M., Argun, A., Oppermann, W., and Okay, O. (2012b). Dynamics and large strain behavior of self-healing hydrogels with and without surfactants. *Macromolecules* 45, 1991–2000. doi: 10.1021/ma202672y

Tuncaboylu, D. C., Sari, M., Oppermann, W., and Okay, O. (2011). Tough and self-healing hydrogels formed via hydrophobic interactions. *Macromolecules* 44, 4997–5005. doi: 10.1021/ma200579v

Wang, H., and Heilshorn, S. C. (2015). Adaptable hydrogel networks with reversible linkages for tissue engineering. *Adv. Mater.* 27, 3717–3736. doi: 10.1002/adma.201501558

Wang, J. Y., Wang, D., Yan, H., Tao, L., Wei, Y., Li, Y. S., et al. (2017). An injectable ionic hydrogel inducing high temperature hyperthermia for microwave tumor ablation. *J. Mater. Chem. B* 5, 4110–4120. doi: 10.1039/c7tb00556c

Wang, L. L., Highley, C. B., Yeh, Y. C., Galarraga, J. H., Uman, S., and Burdick, J. A. (2018). Three-dimensional extrusion bioprinting of single- and double-network hydrogels containing dynamic covalent crosslinks. *J. Biomed. Mater. Res. A* 106, 865–875. doi: 10.1002/jbm.a.36323

Wang, L. L., Sloand, J. N., Gaffey, A. C., Venkataraman, C. M., Wang, Z. C., Trubelja, A., et al. (2017). Injectable, guest-host assembled polyethylenimine hydrogel for siRNA delivery. *Biomacromolecules* 18, 77–86. doi: 10.1021/acs.biomac.6b01378

Wang, Y., Park, J. P., Hong, S. H., and Lee, H. (2016). Biologically inspired materials exhibiting repeatable regeneration with self-sealing capabilities without external stimuli or catalysts. *Adv. Mater.* 28, 9961–9968. doi: 10.1002/adma.201603290

Wei, H., Du, S., Liu, Y., Zhao, H., Chen, C., Li, Z., et al. (2014). Tunable, luminescent, and self-healing hybrid hydrogels of polyoxometalates and triblock copolymers based on electrostatic assembly. *Chem. Commun.* 50, 1447–1450. doi: 10.1039/c3cc48732f

Wei, Z., He, J., Liang, T., Oh, H., Athas, J., Tong, Z., et al. (2013). Autonomous self-healing of poly(acrylic acid) hydrogels induced by the migration of ferric ions. *Polym. Chem.* 4, 4601–4605. doi: 10.1039/c3py00692a

Wei, Z., Yang, J. H., Liu, Z. Q., Xu, F., Zhou, J. X., Zrinyi, M., et al. (2015). Novel biocompatible polysaccharide-based self-healing hydrogel. *Adv. Funct. Mater.* 25, 1352–1359. doi: 10.1002/adfm.201401502

Wei, Z., Yang, J. H., Zhou, J. X., Xu, F., Zrínyi, M., Dussault, P. H., et al. (2014). Self-healing gels based on constitutional dynamic chemistry and their potential applications. *Chem. Soc. Rev.* 43, 8114–8131. doi: 10.1039/c4cs00219a

White, S. R., Sottos, N. R., Geubelle, P. H., Moore, J. S., Kessler, M. R., Sriram, S. R., et al. (2001). Autonomic healing of polymer composites. *Nature* 409, 794–797. doi: 10.1038/35057232

Xia, L. Y., Zhang, X. D., Cao, M., Chen, Z., and Wu, F. G. (2017). Enhanced fluorescence emission and singlet oxygen generation of photosensitizers embedded in injectable hydrogels for imaging guided photodynamic cancer therapy. *Biomacromolecules* 18, 3073–3081. doi: 10.1021/acs.biomac.7b00725

Xie, W., Gao, Q., Guo, Z., Wang, D., Gao, F., Wang, X., et al. (2017). Injectable and self-healing thermosensitive magnetic hydrogel for asynchronous control release of doxorubicin and docetaxel to treat triple-negative breast cancer. *ACS Appl. Mater. Interfaces* 9, 33660–33673. doi: 10.1021/acsami.7b10699

Xing, R., Liu, K., Jiao, T., Zhang, N., Ma, K., Zhang, R. Y., et al. (2016). An injectable self-assembling collagen-gold hybrid hydrogel for combinatorial antitumor photothermal/photodynamic therapy. *Adv. Mater.* 28, 3669–3676. doi: 10.1002/adma.201600284

Xu, G. Z., Xiao, Y., Cheng, L., Zhou, R. H., Xu, H., Chai, Y. M., et al. (2017). Synthesis and rheological investigation of self-healable deferoxamine grafted alginate hydrogel. *J. Polym. Sci. Pol. Phys.* 55, 856–865. doi: 10.1002/polb.24334

Yamaguchi, H., Kobayashi, Y., Kobayashi, R., Takashima, Y., Hashidzume, A., and Harada, A. (2012). Photoswitchable gel assembly based on molecular recognition. *Nat. Commun.* 3:603. doi: 10.1038/ncomms1617

Yang, B., Zhang, Y. L., Zhang, X. Y., Tao, L., Li, S. X., and Wei, Y. (2012). Facilely prepared inexpensive and biocompatible self-healing hydrogel: a new injectable cell therapy carrier. *Polym. Chem.* 3, 3235–3238. doi: 10.1039/c2py20627g

Yang, L., Li, Y. S., Gou, Y. Z., Wang, X., Zhao, X. M., and Tao, L. (2017). Improving tumor chemotherapy effect using an injectable self-healing hydrogel as drug carrier. *Polym. Chem.* 8, 3071–3076. doi: 10.1039/c7py00112f

Yang, W. J., Tao, X., Zhao, T., Weng, L., Kang, E.-T., and Wang, L. (2015). Antifouling and antibacterial hydrogel coatings with self-healing properties based on a dynamic disulfide exchange reaction. *Polym. Chem.* 6, 7027–7035. doi: 10.1039/c5py00936g

Yang, X. F., Liu, G. Q., Peng, L., Guo, J. H., Tao, L., Yuan, J. Y., et al. (2017). Highly efficient self-healable and dual responsive cellulose-based hydrogels for controlled release and 3D cell culture. *Adv. Funct. Mater.* 27:1703174. doi: 10.1002/adfm.201703174

Yavvari, P. S., Pal, S., Kumar, S., Kar, A., Awasthi, A. K., Naaz, A., et al. (2017). Injectable, self-healing chimeric catechol-Fe(III) hydrogel for localized combination cancer therapy. *ACS Biomater. Sci. Eng.* 3, 3404–3413. doi: 10.1021/acsbiomaterials.7b00741

Ye, X., Li, X., Shen, Y. Q., Chang, G. J., Yang, J. X., and Gu, Z. W. (2017). Self-healing pH-sensitive cytosine- and guanosine-modified hyaluronic acid hydrogels via hydrogen bonding. *Polymer (Guildf).* 108, 348–360. doi: 10.1016/j.polymer.2016.11.063

Yesilyurt, V., Webber, M. J., Appel, E. A., Godwin, C., Langer, R., and Anderson, D. G. (2016). Injectable self-healing glucose-responsive hydrogels with pH-regulated mechanical properties. *Adv. Mater.* 28, 86–91. doi: 10.1002/adma.201502902

Yoon, J. A., Kamada, J., Koynov, K., Mohin, J., Nicolaÿ, R., Zhang, Y., et al. (2011). Self-healing polymer films based on thiol–disulfide exchange reactions and self-healing kinetics measured using atomic force microscopy. *Macromolecules* 45, 142–149. doi: 10.1021/ma2015134

Yu, F., Cao, X., Du, J., Wang, G., and Chen, X. (2015). Multifunctional hydrogel with good structure integrity, self-healing, and tissue-adhesive property formed by combining Diels-Alder click reaction and acylhydrazone bond. *ACS Appl. Mater. Interfaces* 7, 24023–24031. doi: 10.1021/acsami.5b06896

Yu, H., Wang, Y., Yang, H., Peng, K., and Zhang, X. (2017). Injectable self-healing hydrogels formed via thiol/disulfide exchange of thiol functionalized F127 and dithiolane modified PEG. *J. Mater. Chem. B* 5, 4121–4127. doi: 10.1039/c7tb00746a

Zhang, G., Ngai, T., Deng, Y., and Wang, C. (2016). An injectable hydrogel with excellent self-healing property based on quadruple hydrogen bonding. *Macromol. Chem. Phys.* 217, 2172–2181. doi: 10.1002/macp.201600319

Zhang, H., Xia, H., and Zhao, Y. (2012). Poly(vinyl alcohol) hydrogel can autonomously self-heal. *ACS Macro Lett.* 1, 1233–1236. doi: 10.1021/mz300451r

Zhang, X., and Waymouth, R. M. (2017). 1,2-Dithiolane-derived dynamic, covalent materials: cooperative self-assembly and reversible cross-linking. *J. Am. Chem. Soc.* 139, 3822–3833. doi: 10.1021/jacs.7b00039

Zhang, Y., Tao, L., Li, S., and Wei, Y. (2011). Synthesis of multiresponsive and dynamic chitosan-based hydrogels for controlled release of bioactive molecules. *Biomacromolecules* 12, 2894–2901. doi: 10.1021/bm200423f

Zhang, Y. L., Fu, C. K., Li, Y. S., Wang, K., Wang, X., Wei, Y., et al. (2017). Synthesis of an injectable, self-healable and dual responsive hydrogel for drug delivery and 3D cell cultivation. *Polym. Chem.* 8, 537–544. doi: 10.1039/c6py01704e

Zhang, Z., Li, T. T., Chen, B., Wang, S., and Guo, Z. Y. (2017). Self-healing supramolecular hydrogel of poly(vinyl alcohol)/chitosan carbon dots. *J. Mater. Sci.* 52, 10614–10623. doi: 10.1007/s10853-017-1222-3

Zhao, J., Xu, R., Luo, G., Wu, J., and Xia, H. (2016). A self-healing, re-moldable and biocompatible crosslinked polysiloxane elastomer. *J. Mater. Chem. B* 4, 982–989. doi: 10.1039/c5tb02036k

Zhao, X., Wu, H., Guo, B., Dong, R., Qiu, Y., and Ma, P. X. (2017). Antibacterial anti-oxidant electroactive injectable hydrogel as self-healing wound dressing with hemostasis and adhesiveness for cutaneous wound healing. *Biomaterials* 122, 34–47. doi: 10.1016/j.biomaterials.2017.01.011

Zheng, Y., Hashidzume, A., and Harada, A. (2013). pH-responsive self-assembly by molecular recognition on a macroscopic scale. *Macromol. Rapid Commun.* 34, 1062–1066. doi: 10.1002/marc.201300324

Zheng, Y., Hashidzume, A., Takashima, Y., Yamaguchi, H., and Harada, A. (2012). Temperature-sensitive macroscopic assembly based on molecular recognition. *ACS Macro Lett.* 1, 1083–1085. doi: 10.1021/mz300338d

Zhu, C., Zhao, J., Kempe, K., Wilson, P., Wang, J., Velkov, T., et al. (2017). A hydrogel-based localized release of colistin for antimicrobial treatment of burn wound infection. *Macromol. Biosci.* 17:1600320. doi: 10.1002/mabi.201600320

Zhu, D., Wang, H., Trinh, P., Heilshorn, S. C., and Yang, F. (2017). Elastin-like protein-hyaluronic acid (ELP-HA) hydrogels with decoupled mechanical and biochemical cues for cartilage regeneration. *Biomaterials* 127, 132–140. doi: 10.1016/j.biomaterials.2017.02.010

Zhu, S. K., Wang, J. X., Yan, H. R., Wang, Y. Y., Zhao, Y. C., Feng, B., et al. (2017). An injectable supramolecular self-healing bio-hydrogel with high stretchability, extensibility and ductility, and a high swelling ratio. *J. Mater. Chem. B* 5, 7021–7034. doi: 10.1039/c7tb01183k

Zou, W., Dong, J., Luo, Y., Zhao, Q., and Xie, T. (2017). Dynamic covalent polymer networks: from old chemistry to modern day innovations. *Adv. Mater.* 29:1600320. doi: 10.1002/adma.201606100

Check for updates

Facile Fabrication of Sandwich Structural Membrane With a Hydrogel Nanofibrous Mat as Inner Layer for Wound Dressing Application

Xueqian Yin[1], Ya Wen[1], Yajing Li[1,2], Pengqing Liu[3], Zhongming Li[3], Yidong Shi[1], Jianwu Lan[1], Ronghui Guo[1] and Lin Tan[1,3]*

[1] College of Light Industry, Textile and Food Engineering, Sichuan University, Chengdu, China, [2] College of Architecture & Environment, Sichuan University, Chengdu, China, [3] College of Polymer Science and Engineering, Sichuan University, Chengdu, China

A common problem existing in wound dressing is to integrate the properties of against water erosion while maintaining a high water-uptake capacity. To tackle this issue, we imbedded one layer of hydrogel nanofibrous mat into two hydrophobic nanofibrous mats, thereafter, the sandwich structural membrane (SSM) was obtained. Particularly, SSM is composed of three individual nanofibrous layers which were fabricated through sequential electrospinning technology, including two polyurethane/antibacterial agent layers, and one middle gelatin/rutin layer. The obtained SSM is characterized in terms of morphology, component, mechanical, and functional performance. In addition to the satisfactory antibacterial activity against *Staphylococcus aureus* and *Escherichia coli*, and antioxidant property upon scavenging DPPH free radicals, the obtained SSM also shows a desirable thermally regulated water vapor transmission rate. More importantly, such SSM can be mechanically stable and keep its intact morphology without appearance damage while showing a high water-absorption ratio. Therefore, the prepared sandwich structural membrane with hydrogel nanofibrous mat as inner layer can be expected as a novel wound dressing.

Keywords: sandwich structure, hydrogel nanofibrous mat, antibacterial activity, antioxidant activity, wound dressing application

INTRODUCTION

Hydrogel-based wound dressings are effective materials for the treatment of chronic wound due to the excellent exudates absorption and retaining properties, which allow them to modulate the fluid balance at the site of wound bed and maintain an microenvironment close to that present in native tissue (Fan et al., 2014; Sun et al., 2017; Zhao et al., 2017). Currently, most hydrogels are synthesized in terms of film, powder, particle and bulk 3D constructs. However, some drawbacks existing in those types of hydrogels when applying them as wound dressing materials, such as low gas and liquid permeation, insufficient surface area, poor structural integration (Ravichandran et al., 2014; Chen et al., 2015; Sun et al., 2017). Recently, hydrogel nanofibrous mats which

can combine the advantages of both nanofibers and hydrogels have received increasing attention due to their desirable gas/liquid permeability, high surface area, highly porous structure, and excellent water uptake capacity(Brunelle et al., 2017; Sun et al., 2017; Zhao et al., 2017).

Electrospinning is an efficient and versatile technique to produce diversified nanofibers, and hundreds of polymers and their composites have been successfully processed into fibrous structure through electrospinning (Lin et al., 2012; Valizadeh and Mussa, 2014; Ahmed et al., 2015). Recently, several electrospun hydrogel nanofibrous mats, e.g., poly(vinylalcohol) (Bhowmick and Koul, 2016; Oh et al., 2016), Poly-(N-vinyl-2-pyrrolidone) (Kurniawan et al., 2016), poly(acrylic acid)-silica (Wang et al., 2016), poly(N-isopropylacrylamide) (Wen et al., 2015; Yao et al., 2015) have been reported, and the obtained hydrogel nanofibrous mats were mostly proposed to be applied as wound dressing and tissue scaffold. Nevertheless, the maintenance of intact hydrogel nanofibrous structure should be further improved during the functions performing due to the intrinsic poor mechanical stability (Fan et al., 2014; Gonzalez et al., 2014; Wang et al., 2015; Wu et al., 2017), thus additional bottom and top protection barriers for hydrogel nanofibrous layer are necessary (Xia et al., 2015; Kim et al., 2017). Regarding the wound dressing application, susceptible to water erosion and bacterial infection are fatal for wound healing, the membranes possessing two hydrophobic surfaces and one inner hydrophilic layer have greatly promising prospects in wound dressing application accordingly, while each layer can have and perform its own function separately, such as antibacterial property, high water uptake capacity, water resistance against erosion (Fan et al., 2014; Xu et al., 2015; Zhao et al., 2017). In other words, sandwich structure may be an ideal candidate for wound dressing fabrication. However, the conventional electrospun nanofibrous membrane is single layer or double layers. Obviously, the former type has the same wettability for its both surfaces, and the problem of relatively low adhesive force between two individual layers exists in latter type (Tan et al., 2015c; Trinca et al., 2017). Therefore, the fabrication of sandwich structural membrane with hydrogel nanofibrous mat may address the above concerns.

Both electrospun polyurethane and gelatin are popular materials for wound dressings application (Li et al., 2016; Resmi et al., 2016; Sahraro et al., 2016; Nian et al., 2018). Polyurethane (PU) currently is one of the most widely applied synthetic polymers. Compared with conventional polymers, PU possesses comprehensive excellent performances on following aspects, including hydrophobic property, easy preparation, recyclability, and good mechanical features, such as the stretching capability and elasticity (Janik and Marzec, 2015; Kucinska-Lipka et al., 2015); Gelatin (GE) is a natural protein which is derived from the partial and irreversible hydrolysis of collagen, and it also has been extensively employed as a hydrogel polymer (Zhao et al., 2015, 2018), but the poor intrinsic mechanical property of gelatin hinders its application, and the primary way to exert the functions of gelatin is to combine with other polymers (Tan et al., 2015c; Feng et al., 2016; Trinca et al., 2017).

Herein, we put forward the concept of fabricating one novel sandwich structural membrane (SSM) consisting of two hydrophobic electrospun PU layers as bottom and top surfaces, respectively, and one hydrophilic inner layer of gelatin hydrogel nanofibrous mat. Additionally, in order to accelerate the potential wound healing process, both antibacterial activity and free radicals scavenging capacity are introduced into such SSM. We demonstrate that the facilely fabricated SSM shows good performance on antibacterial activity, antioxidant property, water vapor transmission rate, mechanical and water uptake capacity. Therefore, the fabricated SSM in this study can be highly recommended as an ideal cover dressing for promoting wound healing.

MATERIALS AND METHODS

Materials

Polyurethane and antibacterial agent N-halamine (N-chloro-2,2,6,6-tetramethyl-4-piperidinyl, Ca) were synthesized according to the previous reports, and the synthesis information of Ca is presented in **Figure S1** (Tan et al., 2015a; Dong et al., 2017). Rutin was purchased from Shanghai Aladdin Biochemical Polytron Technologies Inc.; Gelatin (Type A) from porcine skin was purchased from Sigma Aldrich. N, N-dimethylacetamide (DMAc) and other solvents were purchased from Chengdu Kelong reagent company and used directly without further purification. Dehydrated polycaprolactone diol (PCL, Mn = 4,000 g/mol) was obtained from Perstop U.K. Ltd (United Kindom). 4,4-methylene bis(phenylisocyanate) (MDI), 1,4-Butanediol (BDO) and dibutyltin dilaurate (DBTDL) were purchased from Sigma Aldrich (Unnithan et al., 2015).

Synthesis of Polyurethane

The applied polyurethane used for electrospinning in this study was synthesized according to our previous method. In particular, the obtained PU composed of PCL, MDI, and chain extender BDO. The reaction to prepare prepolymer was conducted in a 1,000 mL conical flask equipped with a mechanical stirrer. PCL (∼492 g) mixed with MDI (∼24 g) for 2 h at 80°C, and followed by the chain extension reaction with BDO (∼100 g) for another 2 h under same temperature. The whole isocyanate group content was excessive by 3 mol%, and the hard segment content is around 20%. All the chemicals used in the synthesis process should be dehydrated with 4 Å molecular sieves in advance (Tan et al., 2015a).

Preparation of Gelatin-Rutin (GE-R) and Polyurethane-Antibacterial Agent (PU-Ca) Solution

Firstly, 24 wt% gelatin solution was prepared by dissolving gelatin powder into a binary solvent consisting of water and formic acid with the mass ratio of 8:2 accordingly and the homogenous solution was obtained after stirring at room temperature for 3 h; Thereafter, a calculated amount of rutin powder (10 wt% of gelatin) was added to the solution for another 2 h stirring under the same condition. Similarly, PU-Ca dissolved in DMAc was prepared under constant stirring at 80°C for 4 h, the concentration of PU was fixed at 20 wt%, and the ratio of Ca was 10 wt% of PU content.

Fabrication of Electrospun Sandwich Structural Membrane (SSM)

SSM was prepared using a manual assembly electrospinning system. The bottom and top layers were fabricated by spinning PU-Ca solution, and the inner hydrogel nanofibrous layer was made from GE-R solution, two voltage gradients of around 1.0 and 1.8 kV/cm were applied for PU-Ca solution and GE-R solution, respectively, and the feeding rate of 1 mL/h was fixed during electrospinning process under an ambient condition (Relative humidity = 50 ± 5%, Working temperature = 22∼26°C). In the course of spinning process, we controlled the thickness of the electrospun membrane through feeding ratio, spinning time and the width for nanofiber collection, and the thickness was measured with the aid of a micrometer (Mitutoyo, Japan). The PU-Ca/GE-R/PU-Ca sandwich structure was constructed through sequential electrospinning. In our study, two SSMs were prepared by adjusting the thickness ratio among the three layers, particularly including 1:4:1 and 2:2:2, and we named such two SSMs in short as "SSM141" and "SSM222," respectively. In addition, the PU-Ca and GE-R nanofibrous mats were prepared as comparisons. SSM141, SSM222, and GE-R nanofibrous mats were crosslinked by saturated glutaraldehyde vapor for 15 min and followed by placing in a vacuum desiccator to remove residual crosslinker.
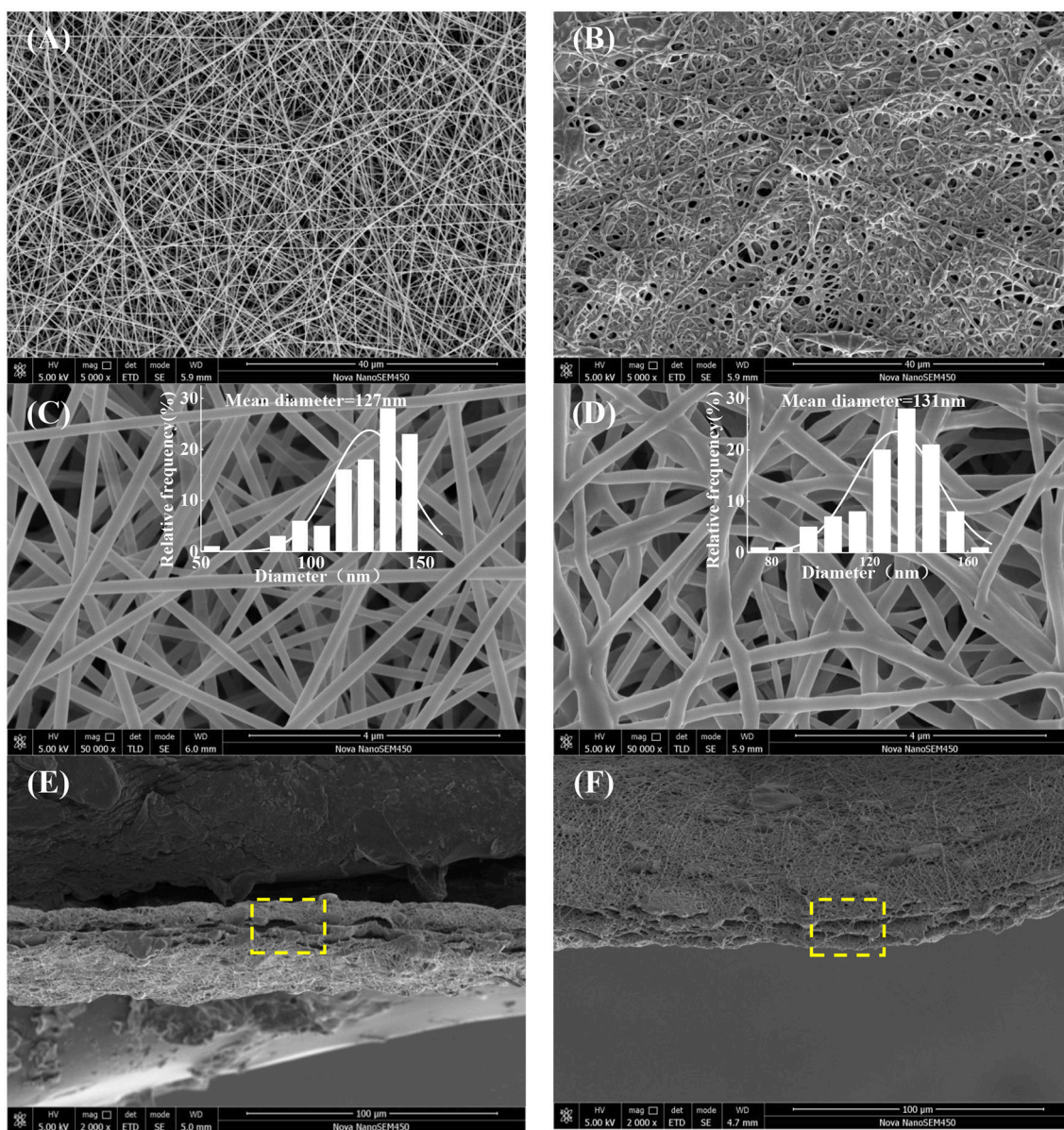
FIGURE 1 | Surface images and fibers diameter distribution (*ImageJ*) of GE-R **(A,C)**, and PU-Ca **(B,D)**, and cross-sectional images of SSM141 **(E)**, and SSM222 **(F)**.

Characterizations

The surface and cross-section morphologies of nanofibrous mats were characterized by scanning electron microscope (SEM, Hitachi SU3500, Japan), and all specimens were sputter-coated

FIGURE 2 | FT-IR spectrum of each component of SSM.

with gold for 20 s before observation. Nanofiber diameter distribution was determined by measuring the diameters of 100 randomly selected nanofibers in SEM images with the aid of *ImageJ* software; The chemical structure and conformation of nanofibrous mats were analyzed by attenuated total reflectance model based Fourier transform infrared (ATR-FTIR, Tracer-100, Japan) spectroscopy in the range of 650–4,000 cm^{-1} at room temperature; Thermal decomposition behavior was investigated by thermogravimetric analysis (DTG-60, Shimadzu, Japan) with a heating scan from 30 to 800°C, and the flow rate of nitrogen gas was fixed at 50 mL/min; Mechanical properties was investigated using an electronic single yarn strength meter (YM061,China). The width of specimens employed was 3 mm and the distance between two clamps was 20 mm, the stretching speed was 10 mm/min, and each sample was measured at least 10 times, the average values of breaking force (cN) and elongation at break (%) were recorded; Water contact angle (WCA) of the fabricated membranes surface was measured through a contact angle tester (Harke-SPCAX1, China) using the sessile drop method, and at least five individual values were collected and averaged.

Water-Absorption Ratio and Water Vapor Transmission Rate (WVTR) Investigation

WAR was evaluated by immersing samples in PBS buffer (pH = 7.4) for 12 h, and then weighted them after removing the surface water using wiping paper; WVTR was determined based on evaporation of water vapor through the testing nanofibrous mats under the temperature of 21 and 37°C with a continuous % RH, including 35, 55, and 75%. WVTR was monitored by measuring the weight loss (mg) of the cups by functions of unit area (cm^2) and time (h), the cups without samples were applied as comparisons. Tests of both WAR and WVTR were performed in triplicate.

Antibacterial Activity Assessment

Antibacterial activity of SSM against *Staphylococcus aureus* and *Escherichia coli* was investigated based on agar disk diffusion susceptibility. The samples were cut into discs with the size of 1.5*1.5 cm^2, and sterilized by ultraviolet irradiation 15 min for
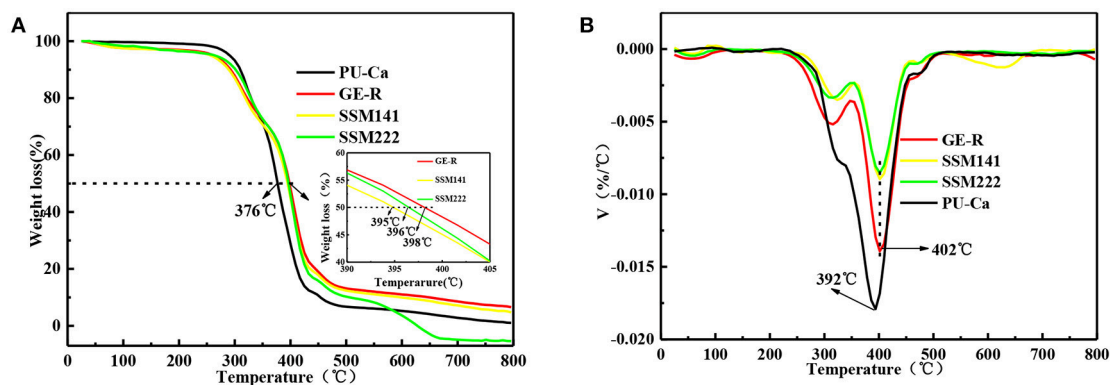
FIGURE 3 | Thermal decomposition **(A)** and DTG **(B)** curves of different electrospun membranes.

both surfaces separately in a laminar flow hood. Gram-negative *E. coli* and Gram positive *S. aureus* were selected as representative bacteria and were cultivated overnight in an incubator, and the sterilized samples were placed on the surface of agar plates coated with the *E. coli* and *S. aureus* already diluted by PBS buffer. Subsequently, the plates were incubated at 37°C overnight, and then inhibition zones were observed and photographed.

DPPH Radical Scavenging Activity

The antioxidant activity of SSM were determined according to 1,1-diphenyl-2-picrylhydrazyl (DPPH) free radical-scavenging

assays. Specifically, a piece of nanofibrous mat with the size of $1.5*1.5$ cm^2 was immersed in 4 mL DPPH ethanol solution (1.5 mg/mL), scavenging activity assay was carried out by recording the absorbance at 516 nm of DPPH solution at six specific time points, including 2, 4, 8, 16, 32, and 64 min after the mixture reaction, and the lower average absorbance value indicates better antioxidant activity.

RESULTS AND DISCUSSION

Morphological Analysis

SEM images of surface and cross-section of electrospun nanofibrous membranes are presented in **Figure 1**. Firstly, all the as-fabricated nanofibrous mats show desirable fiber morphology and size homogeneity without beads (**Figures 1A–D**), while slow evaporation of DMAc, bending deformation, entanglement of the nanofibers and resulted in the compacted homogenous structure (**Figure 1B**), and the average diameter of GE-R and PU-Ca are 127 and 131 nm, respectively. Secondly, the obvious sandwich structure can be observed, and the distinct boundary exists between the adjacent two layers, while interconnected porous structure due to the entanglement of nanofibers are visible from the cross-sectional sites (**Figures 1E,F**). Unlike the conventional bilayered nanofibrous mats, such kind of sandwich structure can ensure the integration of nanofibrous membrane during the application, in other words, under the protection of bottom and top layers which are hydrophobic and materials-homogenous, such SSM can prevent the mutual stripping, collapse and effusion under the circumstance of water erosion or others. Additionally, the highly porous structure is highly beneficial to the circulation of oxygen gas and water vapor. More importantly, the wound exudates can freely access to the inner hydrogel nanofibrous layer through the porous pathway and stay inside the layer up to the saturated absorption.

FT-IR Characterization and Thermal Property Investigation

As shown in **Figure 2**, the typical strong peaks of relevant bonds indicate the blending and electrospinning process did
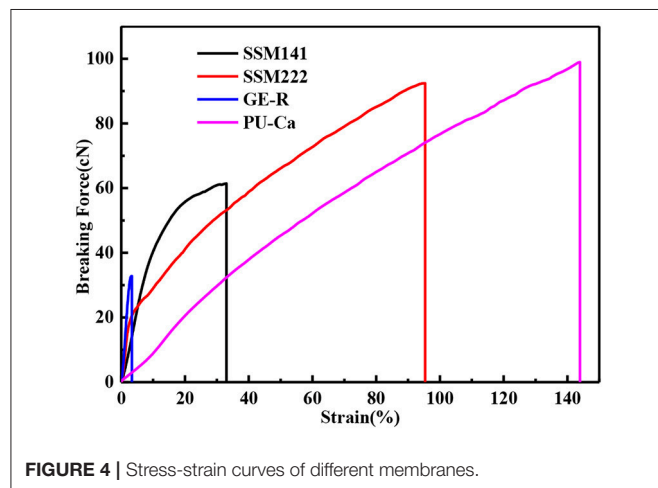
FIGURE 4 | Stress-strain curves of different membranes.

TABLE 1 | The average tensile strength, thickness, elongation at break of different membranes.

Sample	Membrane thickness/μm	Breaking force/cN	Elongation at break/%
GE-R	47.40 ± 0.89	32.66 ± 0.19	3.89 ± 0.88
SSM141	47.60 ± 1.58	60.36 ± 1.51	29.6 ± 4.67
SSM222	49.20 ± 1.22	95.57 ± 4.44	99.22 ± 6.05
PU-Ca	48.40 ± 1.58	98.67 ± 0.40	140.60 ± 4.57
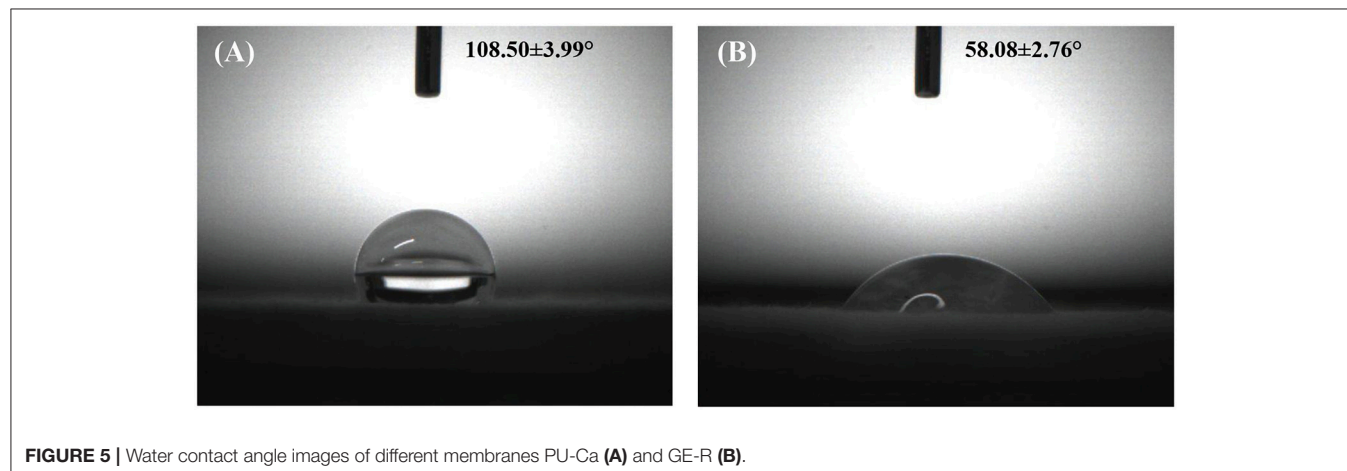
FIGURE 5 | Water contact angle images of different membranes PU-Ca **(A)** and GE-R **(B)**.

FIGURE 6 | WAR of different electrospun membranes under ambient condition.
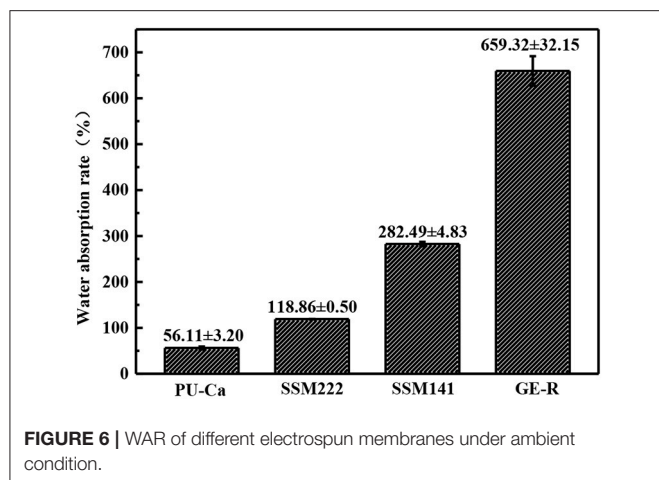
not influence the structure of each component. Particularly, it can be clearly observed that the characteristic peak at ~1,642 cm^{-1} represents the C=O stretching vibration of peptide bonds in the backbone of gelatin, and the peak at ~1,536 cm^{-1} corresponds to the N-H bending and C-N stretching vibration; Additionally, the sharp peaks at ~1,722 cm^{-1} and broad peak at 2,942 cm^{-1} can be ascribed to C=O stretching vibration of urethane groups and stretching vibration of –NH and –OH groups of PU, respectively (Tan et al., 2015b). After they blended with rutin or antibacterial agent Ca, and even after the formation of SSM, the above typical peaks did not shift, thus, it can be concluded that all the components maintain their own native structure after the physical blending and electrospinning.

The thermal decomposition behavior was also studied, and the decomposition curves are shown in **Figure 3**, **Figures S2A,B**. Regarding the semi-decomposition temperature (SDT) and maximum decomposition temperatures (MDT), 167, 374, 396°C and 181, 382, 408°C are recorded for Ca, PU-Ca, and PU, that means the thermal stability of PU decreases over 20°C after blending with Ca; In contrast, the stability of gelatin was significantly improved after blending with rutin in terms of SDT and MDT, e.g. the MDT of GE-R reach to 326°C, while only 276°C was recorded for the MDT of gelatin (**Figures S2C,D**). Additionally, from **Figures 3A,B**, both SSMs shows desirable thermal stability with near 400°C of SDT and above 400°C of MDT. In addition, there is no obvious difference between SSM141 and SSM222 in terms of SDT and MDT, indicating that the change of the thickness ratio of each layer has little influence on the thermal stability of the sandwich structural nanofibrous membranes, and such desirable thermal stability can endow the possible thermal sterilization of SSM before use.

Mechanical Properties

A certain mechanical strength can cater to the motorial behavior of skin, while weak mechanical strength may cause the collapse of wound dressings and then fail to protect

the wound bed. **Figure 4** shows the representative stress-strain curves of different electrospun membranes. In this study, breaking force and elongation were recorded to evaluate the mechanical properties, and the data were summarized in **Table 1**. Obviously, GE-R has the lowest breaking force (~33 cN) as well as the breaking elongation (~4.0%), thus gelatin in combination with other polymers, e.g., PU, for wound dressing application is preferable. From the testing results, SSMs show much better mechanical property compared with that of GE-R electrospun membrane, the reason can be mainly attributed to the presence of PU-Ca layers, and higher composition ratio of PU-Ca endows SSM better mechanical property, i.e., SSM222 have desirable breaking force of around 96 cN and elongation of around 99%. Thus, the obtained SSM can withstand the mechanical deformation resulted from the motorial behavior.

Surface Wettability

Surface wettability is an important property for wound dressing which can influence not only the biological response but the defense performance against water erosion. **Figure 5** shows the WCA values of two individual layer surfaces which consist the final SSMs, and the layer of PU-Ca is hydrophobic with a WCA value of 108.50 ± 3.99°, while the hydrogel nanofibrous layer of GE-R exhibits relative hydrophilic with a WCA value of 58.08 ± 0.76°. The WCA values of SSM141 and SSM222 were shown in **Figure S3**, and they have little difference with pristine PU-Ca layer, indicating that the inner layer of the hydrogel nanofiber has no significant effect on the surface wettability of SSM. Consequently, the bottom and top layers of the fabricated SSMs can effectively defense the water or wound fluids erosion and keep the structural integrity of SSMs during the application, and the inner hydrogel nanofibrous layer can absorb the wound fluids which can freely access through the nanofibrous pathway.

WAR and WVTR Study

Both WAR and WVTR are critical factors for the wound management, and both of them play their own role separately and synergistically. Particularly, WAR is applied to evaluate the exudates retaining capacity of the wound dressing, and WVTR will influence the wounds dehydration or accumulation of exudates. In virtue of desirable WAR and WVTR, an ideal moisture microenvironment will exist around the site of wound bed, thus promote the wound healing process.

WAR and WVTR are calculated according to following Equation (1) and Equation (2). In Equation (1), W_1 represents the weight after the suction, and W_0 represents the original weight of the sample.

$$WAR(\%) = \frac{W_1 - W_0}{W_0} \times 100\% \qquad (1)$$

$$WVTR(mg.cm^{-2}.h^{-1}) = \frac{Water\ weight\ change\ (mg)}{Exposure\ area\ (cm^2) \times exposure\ time(h)} \qquad (2)$$
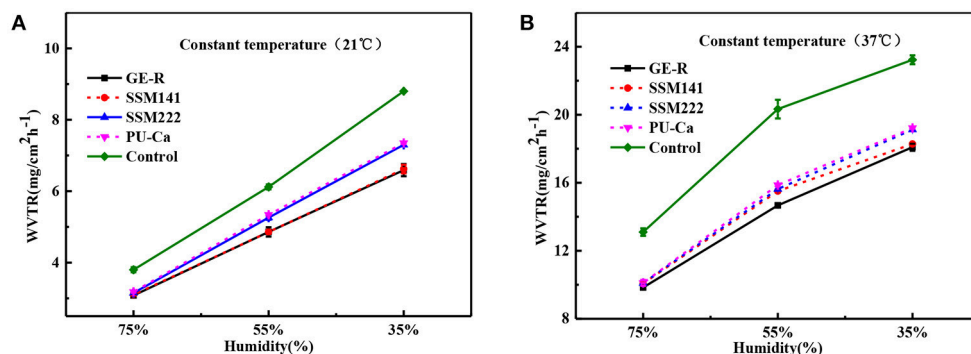
FIGURE 7 | WVTR curves by the function of humidity under constant temperature 21°C **(A)** and constant temperature 37°C **(B)**.

TABLE 2 | WVTR and WAR of different electrospun membranes.

Samples	Thickness (μm)	WVTR/21°C (mg/cm^2.h^{-1}) Humidity(%)			WVTR/37°C (mg/cm^2.h^{-1}) Humidity(%)			WAR(%)
		35%	55%	75%	35%	55%	75%	
GE-R	47.40 ± 0.89	6.59 ± 0.17	4.86 ± 0.13	3.08 ± 0.03	18.09 ± 0.21	14.67 ± 0.02	9.84 ± 0.07	659.32 ± 32.15
SSM141	47.60 ± 1.58	6.62 ± 0.12	4.86 ± 0.05	3.10 ± 0.02	18.28 ± 0.09	15.51 ± 0.09	10.08 ± 0.09	282.49 ± 2.83
SSM222	49.20 ± 1.22	7.30 ± 0.005	5.26 ± 0.06	3.15 ± 0.03	19.13 ± 0.04	15.63 ± 0.04	10.10 ± 0.15	118.8600.50
PU-Ca	48.60 ± 1.58	7.35 ± 0.03	5.34 ± 0.01	3.18 ± 0.02	19.22 ± 0.03	15.86 ± 0.04	10.11 ± 0.17	56.11 ± 3.20
Control	NA	8.80 ± 0.16	6.12 ± 0.07	3.8 ± 0.07	23.23 ± 0.26	20.33 ± 0.55	13.10 ± 0.22	NA
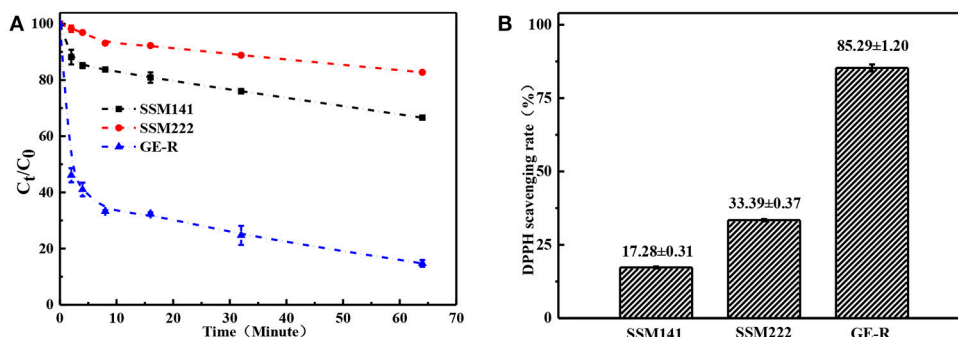
FIGURE 8 | Antioxidant performance of different electrospun membranes. **(A)** Scavenging rate-time curve of different membranes; **(B)** Scavenging rate histogram of different membranes.

The thickness of the obtained nanofibrous membranes are around 50 μm. As shown in **Figure 6**, the WAR values of PU-Ca, SSM222, SSM141, and GE-R are around 56, 119, 282, and 659%, respectively. The WAR of SSM222 and SSM141 increased by 2 and 5 times higher than that of PU-Ca membrane, which indicates the incorporation of hydrogel nanofibrous mat can significantly increase the WAR, and the thicker of GE-R layer incorporated in such sandwich structural membrane renders higher WAR owning to the intrinsic hygroscopicity of gelatin. Therefore, the accumulation of exudates around the wound beds can be avoided and the risk of potential bacteria infection will be reduced. Whatever normal skin or injured skin, body fluid will evaporate through the micropores of skin,

while the injured skin normally shows higher WVTR of 1.16–21.41 mg.cm^{-2}.h^{-1} compared to that of normal skin (Saeed et al., 2017). Thus, porous structure with suitable WVTR of wound dressing is essential and required. **Figure 7** and **Figure S4** show the successive recorded WVTR values of different electrospun membranes under different temperature and humidity. It can be clearly seen that the WVTR values for all electrospun membranes reasonably increase with temperature increasing under constant humidity, while WVTR decreases with increasing the ambient humidity. From **Table 2**, all WVTR values of SSMs, lowest value of 3.10 ± 0.02 mg/cm^2.h^{-1} and the highest value of 19.13 ± 0.04 mg/cm^2.h^{-1}, are within the body fluids evaporation range of injured skin, which can indicate that the fabricated SSM can meet
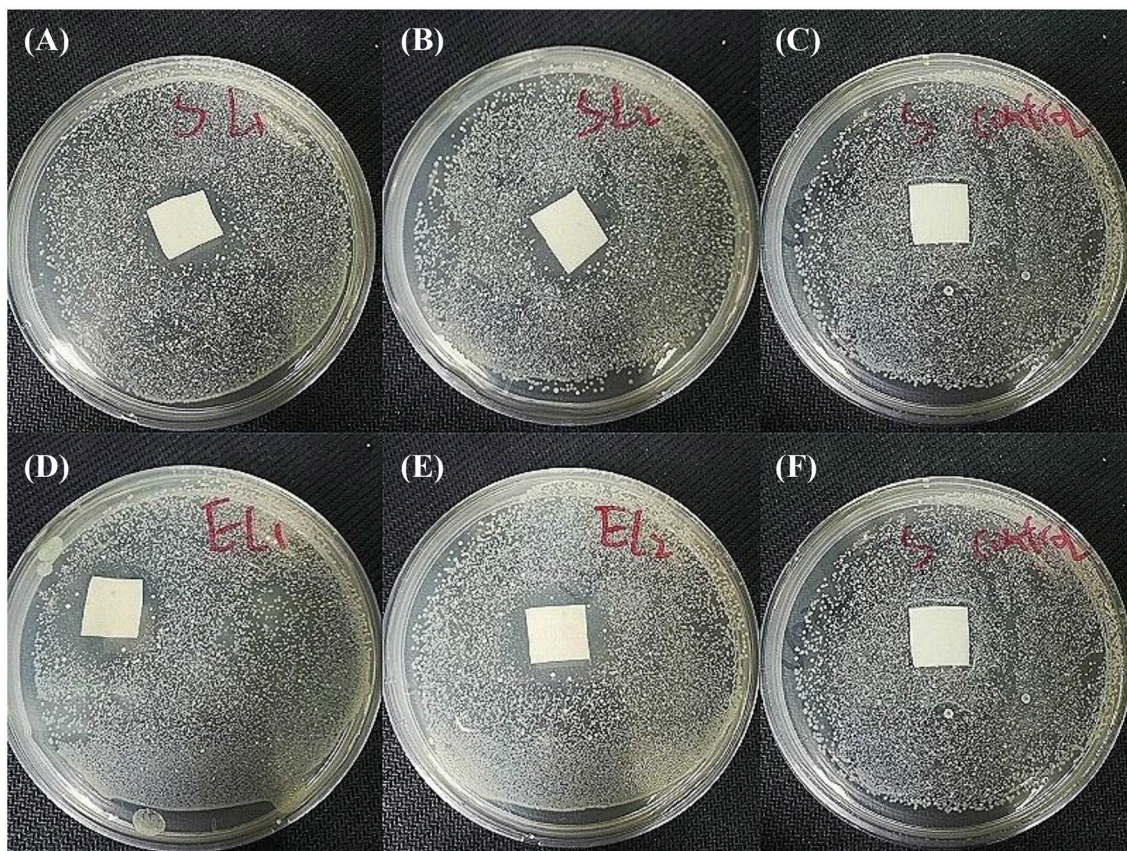
FIGURE 9 | Antibacterial activity investigation results. SSM141against *S. aureus* **(A)** and *E. coli* **(D)**. SSM222 against *S. aureus* **(B)** and *E. coli* **(E)**, and pristine PU against *S. aureus* **(C)** and *E. coli* **(F)** as the comparisons.

the requirement on managing the wound fluids as a qualified wound dressing.

Antioxidant Property

Antioxidant property of the fabricated sandwich structural membrane was evaluated in term of the capacity on scavenging free radicals, and the scavenging ratio of DPPH free radicals (SRDPPH) was calculated according to the following Equation (3):

$$SRDPPH(\%) = \frac{A_0 - A_t}{A_0} \times 100\% \qquad (3)$$

Where A_0 is the original absorbance of DPPH, A_t is the absorbance of the DPPH at the specific measuring time. Antioxidant property refers to the ability of scavenging free radicals, and it should be a crucial property for wound dressing which can protect human skin or wound bed from free radicals damage. Antioxidant performance was monitored through measuring the absorbance of DPPH-contained solution at 516 nm, which was also accompanied by a color change from deep purple to yellow. **Figure 8** demonstrates the antioxidant activity of SSM prepared with different contents of rutin, and higher content of rutin renders the higher SRDPPH, that means

higher content of GE-R layer can be incorporated to prepare SSM with better antioxidant performance. In addition, the SRDPPH was recorded by the function of time (**Figure 8B**), and the slope of the curve can reflect the scavenging rate of DPPH free radicals. We can clearly observe that the oxidant performance of all the samples include one initial fast SRDPPH stage with a sharp slope and one slower stage. In other words, the electrospun membranes can initially scavenge the DPPH free radicals quickly then reach a plateau gradually.

Antibacterial Activity

Antibacterial activity is essential to a qualified wound dressing, that's because a longer healing process will be required once the wound bed is infected by bacteria. **Figure 9** shows the antibacterial activity of two SSMs against *E. coli* and *S. aureus*. Compared with the pristine PU membrane, PU-Ca (**Figure S5**), SSM141 and SSM222 have satisfactory antibacterial activity by the evidence of obvious inhibition zones. In addition, we observed that the inhibition zones against *E. coli* is slightly larger than those against *S. aureus*, the possible reason can be attributed to the thicker cell wall of the *Gram*-positive negative bacteria, and thus the encapsulated antibacterial monomer

N-halamine (Ca) can more effectively kill the *Gram*-negative bacteria.

CONCLUSION

In this study, we have successfully fabricated a novel type of electrospun SSM with a hydrogel nanofibrous mat as the inner layer through lay-by-layer deposition. The obtained SSM has two hydrophobic surfaces (PU-Ca) which can prevent the water erosion, and simultaneously has a high water-uptake capacity because of the hydrophilic hydrogel nanofibrous layer (GE-R), thus the structural integrity can be effectively maintained during the application. Additionally, the SSM also displays favorable antibacterial activity against *E. coli* and *S. aureus*, antioxidant activity in terms of scavenging capacity of DPPH free radicals, and a desirable thermally regulated WVTR. More importantly, the functions and properties can be highly adjusted owing to the nanofibrous sandwich structure, and the incorporated functions can be also performed individually, such as the thickness of inner hydrogel nanofibrous layer, wettability of each layer, mechanical strength and antioxidant period. We believe that such type of SSM can work competently as a wound dressing, and more functional SSMs can be prepared based on this concept.

REFERENCES

Ahmed, F. E., Lalia, B. S., and Hashaikeh, R. (2015). A review on electrospinning for membrane fabrication: challenges and applications. *Desalination* 356, 15–30. doi: 10.1016/j.desal.2014.09

Bhowmick, S., and Koul, V. (2016). Assessment of PVA/silver nanocomposite hydrogel patch as antimicrobial dressing scaffold: synthesis, characterization and biological evaluation. *Mater. Sci. Eng. C* 59, 109–119. doi: 10.1016/j.msec.2015.10.003

Brunelle, A. R., Horner, C. B., and Nam, J. (2017). Electrospun thermosensitive hydrogel scaffold for enhanced chondrogenesis of human mesenchymal stem cells. *Acta Biomater.* 66, 166–176. doi: 10.1016/j.actbio.2017.11.020

Chen, G., Chen, J., Yang, B., Li, L., Luo, X., Zhang, X., et al. (2015). Combination of aligned PLGA/Gelatin electrospun sheets, native dental pulp extracellular matrix and treated dentin matrix as substrates for tooth root regeneration. *Biomaterials* 52, 56–70. doi: 10.1016/j.biomaterials.2015.02.011

Dong, A., Wang, Y. J., Gao, Y., Gao, T., and Gao, G. (2017). Chemical insights into antibacterial N-Halamines. *Chem. Rev.* 117, 4806–4862. doi: 10.1021/acs.chemrev.6b00687

Fan, Z., Liu, B., Wang, J., Zhang, S., Lin, Q., Gong, P., et al. (2014). A novel wound dressing based on Ag/Graphene polymer hydrogel: effectively kill bacteria and accelerate wound healing. *Adv. Funct. Mater.* 24, 3933–3943. doi: 10.1002/adfm.201304202

Feng, Q., Wei, K., Lin, S., Xu, Z., Sun, Y., Shi, P., et al. (2016). Mechanically resilient, injectable, and bioadhesive supramolecular gelatin hydrogels crosslinked by weak host-guest interactions assist cell infiltration and in situ tissue regeneration. *Biomaterials* 101, 217–228. doi: 10.1016/j.biomaterials.2016.05.043

Gonzalez, J. S., Ludueña, L. N., Ponce, A., and Alvarez, V. A. (2014). Poly(vinyl alcohol)/cellulose nanowhiskers nanocomposite hydrogels for potential wound dressings. *Mater. Sci. Eng. C Mater. Biol. Appl.* 34, 54–61. doi: 10.1016/j.msec.2013.10.006

Janik, H., and Marzec, M. (2015). A review: fabrication of porous polyurethane scaffolds. *Mater. Sci. Eng. C* 48, 586–591. doi: 10.1016/j.msec.2014.12.037

Kim, J. W., Kim, M. J., Ki, C. S., Kim, H. J., and Park, Y. H. (2017). Fabrication of bi-layer scaffold of keratin nanofiber and gelatin-methacrylate hydrogel: implications for skin graft. *Int. J. Biol. Macromol.* 105(Pt 1), 541–548. doi: 10.1016/j.ijbiomac.2017.07.067

Kucinska-Lipka, J., Gubanska, I., Janik, H., and Sienkiewicz, M. (2015). Fabrication of polyurethane and polyurethane based composite fibres by the electrospinning technique for soft tissue engineering of cardiovascular system. *Mater. Sci. Eng. C Mater. Biol. Appl.* 46, 166–176. doi: 10.1016/j.msec.2014.10.027

Kurniawan, A., Gunawan, F., Nugraha, A. T., Ismadji, S., and Wang, M. J. (2016). Biocompatibility and drug release behavior of curcumin conjugated gold nanoparticles from aminosilane-functionalized poly(N-vinyl-2-pyrrolidone) electrospun nanofibrous mats. *Int. J. Pharm.* 516, 158–169. doi: 10.1016/j.ijpharm.2016.10.067

Li, H., Wang, M., Williams, G. R., Wu, J., Sun, X., Lv, Y., et al. (2016). Electrospun gelatin nanofibers loaded with vitamins A and E as antibacterial wound dressing materials. *RSC Adv.* 6, 50267–50277. doi: 10.1039/c6ra05092a

Lin, J., Wang, X., Ding, B., Yu, J., Sun, G., and Wang, M. (2012). Biomimicry via Electrospinning. *Crit. Rev. Solid State Mater. Sci.* 37, 94–114. doi: 10.1080/10408436.2011.627096

Nian, L., Cao, A., Wang, J., Tian, H., Liu, Y., Gong, L., et al. (2018). Viscoelastic and functional properties of Cod-bone gelatin in the presence of xylitol and stevioside. *Front. Chem.* 6:111. doi: 10.3389/fchem.2018.00111

Oh, S. H., An, D. B., Kim, T. H., and Lee, J. H. (2016). Wide-range stiffness gradient PVA/HA hydrogel to investigate stem cell differentiation behavior. *Acta Biomater.* 35, 23–31. doi: 10.1016/j.actbio.2016.02.016

Ravichandran, R. K., Sundaramurthi, D., Gandhi, S., Sethuraman, S., and Krishnan, U. M. (2014). Bioinspired hybrid mesoporous silica–gelatin sandwich construct for bone tissue engineering. *Microporous Mesoporous Mater.* 187, 53–62. doi: 10.1016/j.micromeso.2013.12.018

Resmi, R., Unnikrishnan, S., Krishnan, L. K., and Kalliyana Krishnan, V. (2016). Synthesis and characterization of silver nanoparticle incorporated gelatin-hydroxypropyl methacrylate hydrogels for wound dressing applications. *J. Appl. Polym. Sci.* 134, 1–9. doi: 10.1002/app.44529

Saeed, S. M., Mirzadeh, H., Zandi, M., and Barzin, J. (2017). Designing and fabrication of curcumin loaded PCL/PVA multi-layer nanofibrous electrospun structures as active wound dressing. *Prog. Biomater.* 6, 39–48. doi: 10.1007/s40204-017-0062-1

Sahraro, M., Yeganeh, H., and Sorayya, M. (2016). Guanidine hydrochloride embedded polyurethanes as antimicrobial and absorptive wound dressing membranes with promising cytocompatibility. *Mater. Sci.Eng. C Mater. Biol. Appl.* 59, 1025–1037. doi: 10.1016/j.msec.2015.11.038

Sun, X., Lang, Q., Zhang, H., Cheng, L., Zhang, Y., Pan, G., et al. (2017). Electrospun photocrosslinkable hydrogel fibrous scaffolds for rapid *in vivo* vascularized skin flap regeneration. *Adv. Funct. Mater.* 27:1604617. doi: 10.1002/adfm.201604617

Tan, L., Gan, L., Hu, J., Zhu, Y., and Han, J. (2015a). Functional shape memory composite nanofibers with graphene oxide filler. *Composites Part A* 76, 115–123. doi: 10.1016/j.compositesa.2015.04.015

Tan, L., Hu, J., Huang, H., Han, J., and Hu, H. (2015b). Study of multi-functional electrospun composite nanofibrous mats for smart wound healing. *Int. J. Biol. Macromol.* 79, 469–476. doi: 10.1016/j.ijbiomac.2015.05.014

Tan, L., Hu, J., and Zhao, H. (2015c). Design of bilayered nanofibrous mats for wound dressing using an electrospinning technique. *Mater. Lett.* 156, 46–49. doi: 10.1016/j.matlet.2015.04.119

Trinca, R. B., Westin, C. B., Silva, J. A. F. D., and Moraes, M. (2017). Electrospun multilayer chitosan scaffolds as potential wound dressings for skin lesions. *Eur. Polym. J.* 88, 161–170. doi: 10.1016/j.eurpolymj.2017.01.021

Unnithan, A. R., Sasikala, A. R., Murugesan, P., Gurusamy, M., Wu, D., Park, C. H., et al. (2015). Electrospun polyurethane-dextran nanofiber mats loaded with Estradiol for post-menopausal wound dressing. *Int. J. Biol. Macromol.* 77, 1–8. doi: 10.1016/j.ijbiomac.2015.02.044

Valizadeh, A., and Mussa, F. S. (2014). Electrospinning and electrospun nanofibres. *Iet Nanobiotechnol.* 8, 83–92. doi: 10.1049/iet-nbt.2012.0040

Wang, L., Wu, Y., Guo, B., and Ma, P. X. (2015). Nanofiber Yarn/Hydrogel core–shell scaffolds mimicking native skeletal muscle tissue for guiding 3d myoblast alignment, elongation, and differentiation. *Acs Nano* 9, 9167–9179. doi: 10.1021/acsnano.5b03644

Wang, M., Li, X., Hua, W., Shen, L., Yu, X., and Wang, X. (2016). Electrospun Poly(acrylic acid)/Silica hydrogel nanofibers scaffold for highly efficient adsorption of Lanthanide ions and its photoluminescence performance. *ACS Appl. Mater. Interf.* 8, 23995–24007. doi: 10.1021/acsami.6b08294

Wen, J. Z., Ning, A., Jian, H. Y., Zhou, J., and Yong, M. C. (2015). Tough Al-alginate/Poly(N-isopropylacrylamide) hydrogel with tunable lcst for soft robotics. *ACS Appl. Mater. Interf.* 7, 1758–1764. doi: 10.1021/am507339r

Wu, Y., Wang, L., Guo, B., and Ma, P. X. (2017). Interwoven aligned conductive nanofiber Yarn/Hydrogel composite scaffolds for engineered

3d cardiac anisotropy. *ACS Nano* 11, 5646–5659. doi: 10.1021/acsnano.7b01062

Xia, Q., Liu, Z., Wang, C., Zhang, Z., Xu, S., and Han, C. C. (2015). A biodegradable trilayered barrier membrane composed of sponge and electrospun layers: hemostasis and antiadhesion. *Biomacromolecules* 16, 3083–3092. doi: 10.1021/acs.biomac.5b01099

Xu, R., Luo, G., Xia, H., He, W., Zhao, J., Liu, B., et al. (2015). Novel bilayer wound dressing composed of silicone rubber with particular micropores enhanced wound re-epithelialization and contraction. *Biomaterials* 40, 1–11. doi: 10.1016/j.biomaterials.2014.10.077

Yao, C., Liu, Z., Yang, C., Wang, W., Ju, X. J., Xie, R., et al. (2015). Poly(N-isopropylacrylamide)-Clay nanocomposite hydrogels with responsive bending property as temperature-controlled manipulators. *Adv. Funct. Mater.* 25, 2980–2991. doi: 10.1002/adfm.201500420

Zhao, X., Guo, B., Wu, H., Liang, Y., and Ma, P. X. (2018). Injectable antibacterial conductive nanocomposite cryogels with rapid shape recovery for noncompressible hemorrhage and wound healing. *Nat. Commun.* 9:2784. doi: 10.1038/s41467-018-04998-9

Zhao, X., Li, P., Guo, B., and Ma, P. X. (2015). Antibacterial and conductive injectable hydrogels based on quaternized chitosan-graft-polyaniline/oxidized dextran for tissue engineering. *Acta Biomater.* 26, 236–248. doi: 10.1016/j.actbio.2015.08.006

Zhao, X., Wu, H., Guo, B., Dong, R., Qiu, Y., and Ma, P. X. (2017). Antibacterial anti-oxidant electroactive injectable hydrogel as self-healing wound dressing with hemostasis and adhesiveness for cutaneous wound healing. *Biomaterials* 122, 34–47. doi: 10.1016/j.biomaterials.2017.01.011

Rational Design of Self-Healing Tough Hydrogels: A Mini Review

Wenda Wang, Ravin Narain* and Hongbo Zeng*

Department of Chemical and Materials Engineering, University of Alberta, Edmonton, AB, Canada

Hydrogels are three-dimensional cross-linked polymer networks which can absorb and retain large amount of water. As representative soft materials with tunable chemical, physical and biological properties, hydrogels with different functions have been developed and utilized in a broad range of applications, from tissue engineering to soft robotics. However, conventional hydrogels usually suffer from weak mechanical properties and they are easily deformed or damaged when they are subjected to mechanical forces. The accumulation of the damage may lead to the permanent structural change and the loss of the functional properties of the hydrogels. Therefore, it is important to develop mechanically robust hydrogels with autonomous self-healing property in order to extend their lifespan for various applications. In this mini review, we focus on the discussion about the appropriate molecular design of the hydrogel network for achieving self-healing and excellent mechanical properties, respectively as well as the corresponding self-healing and toughening mechanisms. We conclude with perspectives on the remaining challenges in the field as well as the recommendations for future development.

Keywords: hydrogels, synthesis, self-healing, tough hydrogels, functional hydrogels

INTRODUCTION

Hydrogels are three-dimensional networks consisting of cross-linked polymer chains, which form matrices with high water content (Annabi et al., 2014). Over the past few years, significant progress has been achieved in the development of functional hydrogels with tunable chemical, physical and biological properties for various applications, including tissue engineering (Eke et al., 2017; Wang J. et al., 2017), controlled drug delivery systems (Zhang et al., 2011; Chen et al., 2018), sensors and actuators (Lei et al., 2017; Yuk et al., 2017), soft electronics (Lin et al., 2016; Cai et al., 2017), etc. However, conventional hydrogels usually suffer from poor mechanical properties and are easily deformed or damaged when they are subjected to mechanical forces. The propagation and accumulation of the damage would affect the integrity of the hydrogels and cause the loss of the functionalities, which may limit the lifespan of the hydrogels. Therefore, it is desirable to develop mechanically robust hydrogels possessing the self-healing capability in order to not only prolong the life-time of the materials but also increase the durability and the reliability of the hydrogels in certain applications by avoiding accumulation of cracks or damages (**Graphical Abstract**).

Self-healing hydrogels are the hydrogels which can automatically heal damages and restore themselves to normality without the intervention of an external stimuli (Taylor and In Het Panhuis, 2016). Based on different self-healing mechanisms, the self-healing hydrogels can be divided into two categories, chemically and physically self-healing hydrogels. Different design strategies can be employed for fabricating hydrogels with self-healing ability. Chemically self-healing hydrogels

GRAPHICAL ABSTRACT | Design of self-healing tough hydrogel.
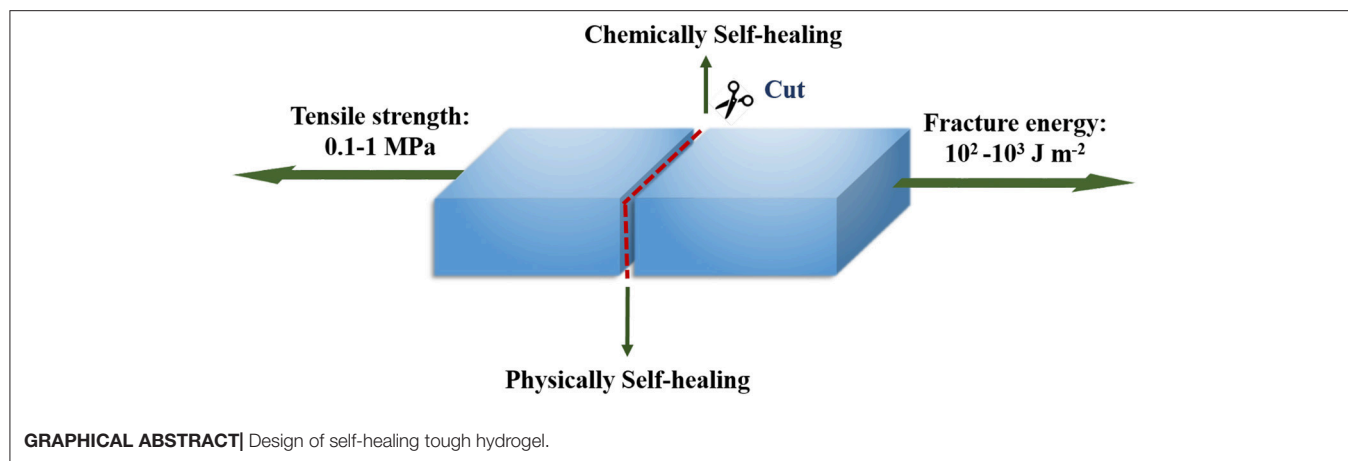
reform the network through dynamic covalent bonds or reversible chemical reactions, commonly including phenylboronic ester bonds (Wang et al., 2016; Guo et al., 2017), dynamic imine bonds (dynamic Schiff base) (Zhao et al., 2017; Liu et al., 2018), disulfide bonds (Yang X. et al., 2017; Yu et al., 2017), reversible radical reaction (Ida et al., 2016), Diels-Alder reaction (Shao et al., 2017), etc. Physically self-healing hydrogels re-establish the structure through dynamic non-covalent interactions such as hydrogen bonding (Ren et al., 2017), hydrophobic interaction (Xiong et al., 2017), host-guest interaction (Zhang M. et al., 2012), metal-coordination (Andersen et al., 2018), or a combination of multiple intermolecular interactions (Liao et al., 2017; Shao et al., 2018). For both types of self-healing hydrogels, special functional groups are required to be incorporated into the polymer chains for desirable chemical reactions or physical interactions, which mediate the self-healing process, to occur in the damaged region.

Conventional hydrogels are considered to be mechanically weak (toughness $<10 \, \text{J m}^{-2}$), which limits certain applications such as tissue engineering (cartilages or tendon), since these tissues are natural hydrogels possessing high toughness (1,000 J m^{-2}) and high tensile strength (30 MPa) (Taylor and In Het Panhuis, 2016). The brittleness (low toughness) of the conventional hydrogels comes from two reasons. Conventionally, hydrogels are synthesized by free radical polymerization of water-soluble monomers and cross-linkers. Due to the difference in reactivity between the reagents, highly random (heterogeneous) cross-linked network is typically produced. The heterogeneity will lead to uneven stress distribution and stress localization when the hydrogel experiences force loading, which accounts for the brittleness (Naficy et al., 2011). Besides, the conventional hydrogels lack of mechanisms which allow the mechanical energy to be dissipated through the hydrogel upon force loading, which is another reason for the brittleness (Chung et al., 2017). It is generally agreed that the hydrogels with tensile strength of 0.1–1 MPa and fracture energy of 10^2-10^3 J m^{-2} can be considered as tough hydrogels (Chen et al., 2016). To improve the mechanical properties of the conventional hydrogels, one can either increase the homogeneity of the cross-linked network

[tetra-PEG hydrogels (Ishii et al., 2017; Yang N. et al., 2017), radiation cross-lined hydrogels (Xu et al., 2018)] or design the hydrogels with special structure (double network (DN) hydrogels (Li et al., 2016; Liu and Li, 2016), nanocomposite hydrogels (Jiang et al., 2017; Qin et al., 2017)etc., which allows mechanical energy to be dissipated through the hydrogel.

In this mini-review, we briefly discuss different design strategies for developing self-healing and tough hydrogels, respectively. Examples from recent literature will be illustrated accordingly. Finally, we conclude with a perspective on remaining challenges in the field and the recommendations for future development.

DESIGN STRATEGIES FOR SELF-HEALING HYDROGELS

Chemically Self-Healing Hydrogels

In conventional hydrogels, the polymer networks are usually cross-linked by covalent bonds which are irreversible and too stable for dynamic chemistry to occur for self-healing (Wei et al., 2014). The chemically self-healing hydrogels reform the network through dynamic covalent bonds or reversible chemical reactions, typically including phenylboronic ester bonds, dynamic imine bonds (dynamic Schiff base), disulfide bonds, reversible radical reaction, Diels-Alder reaction, etc. (**Figure 1A**).

Phenylboronic Ester Complexation

Phenylboronic ester is the dynamic complex formed based on boronic acid-diol interaction. The dynamic nature (self-healing ability) of the complexation strongly depends on the pK$_a$ value of various phenylboronic acids. Langer et al. reported an injectable self-healing glucose-responsive hydrogel which was constructed by phenylboronic acid-terminated four-armed poly(ethylene glycol) (PEG) and diol-terminated four-armed PEG (Yesilyurt et al., 2016). It was found that the self-healing behavior and the mechanical property of the hydrogels are closely associated with the pK$_a$ value of the terminal phenylboronic acid group. When the hydrogel was formed at pH greater than the pK$_a$ value of
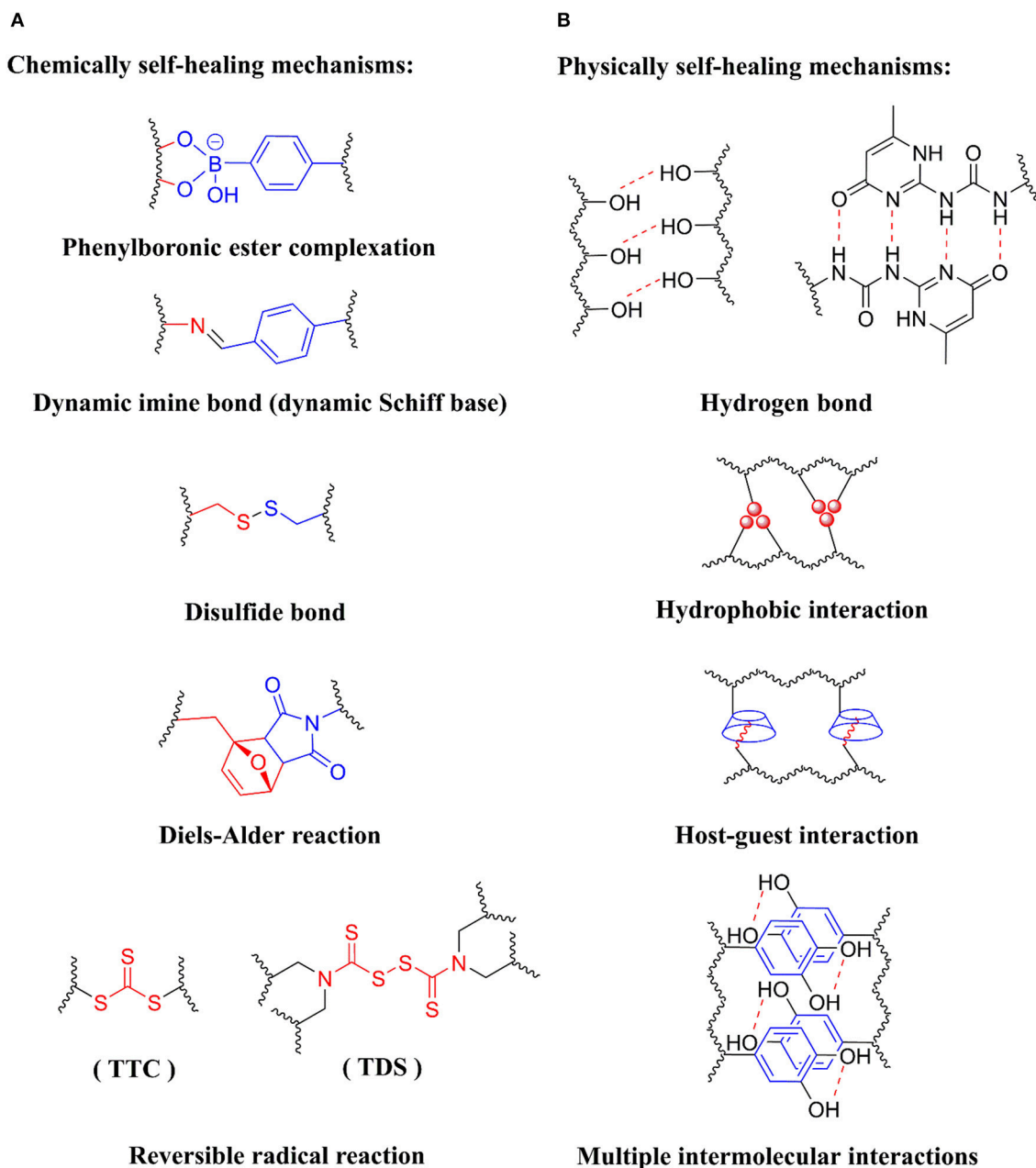
FIGURE 1 | Different strategies for designing self-healing hydrogels. **(A)** Chemically self-healing mechanisms, including phenylboronic ester complexation, dynamic imine bond (dynamic Schiff base), disulfide bond, Diels-Alder reaction and reversible radical reaction, **(B)** Physically self-healing mechanisms, including hydrogen bond, hydrophobic interaction, host-guest interaction and multiple intermolecular interactions.

the terminal phenylboronic acid group, the gel was rigid and brittle and the self-healing ability was found to decrease with increasing the pH. However, when the hydrogel was formed around the pK_a value of the terminal phenylboronic acid group, the hydrogels showed excellent self-healing ability. When the pH is below the pK_a value, there is no gel formation observed. The stability (self-healing ability) of phenylboronic ester complex also depends on the conformation of the diol groups in the

polymer chains. Schiller et al. determined binding constants between phenylboronic acid and different polysaccharides with different diol conformations (Axthelm et al., 2017). It was found that phenylboronic acid has a higher affinity for the *cis*-diol groups than that for the *trans*-diol groups. Therefore, the self-healing ability of the hydrogel is expected to be enhanced when *cis*-diol is incorporated into the polymers used to construct hydrogel network since the boron-*cis*-diol complexation is more

thermodynamically stable and more likely to be reformed after being destructed. The self-healing hydrogels which based on phenylboronic ester complexation have been applied to a wide range of biomedical applications. Narain et al. developed a series of self-healing hydrogels for applications such as glucose sensing (Kotsuchibashi et al., 2013), drug delivery (Chen et al., 2018) and 3D cell cultivation (Wang et al., 2016).

Dynamic Imine Bond (Schiff Base)

Dynamic imine bonds (dynamic Schiff base) are formed between the aldehyde groups and the primary amine groups. Wei et al. reported a series of self-healing hydrogels based on dynamic Schiff base during the past few years (Zhang et al., 2011; Tseng et al., 2015; Hsieh et al., 2017; Yang X. et al., 2017; Zhang Y. et al., 2017). In most of their work, a benzaldehyde-difunctionalized poly(ethylene glycol) (DF-PEG) was synthesized. Self-healing hydrogels with different properties and applications can be constructed by simply mixing the DF-PEG solution with either natural polymer solutions or synthetic polymer solutions such as glycol chitosan solution (Zhang et al., 2011), amine-modified carboxyethyl cellulose solution (Yang X. et al., 2017), etc. Such self-healing hydrogels can be used in wide biomedical applications such as 3D cell cultivation (Zhang Y. et al., 2017), controlled release of biomolecules (Zhang et al., 2011), blood capillary formation (Hsieh et al., 2017), central nervous system repair (Tseng et al., 2015), etc. Guo et al. also developed self-healing hydrogels which employs dynamic Schiff base for biomedical applications such as cutaneous wound healing (Zhao et al., 2017), cell delivery carrier for cardiac cell therapy (Dong et al., 2016) and drug delivery carrier for hepatocellular carcinoma therapy (Qu et al., 2017). Interestingly, similar to the phenylboronic ester complex, the self-healing ability of the hydrogels based on dynamic Schiff base is also pH dependent. Therefore, appropriate pH condition needs to be met when constructing the hydrogel with desirable self-healing property.

Disulfide Bond

Disulfide bond is another dynamic covalent bond which is often adopted to make the hydrogel self-healable. The dynamic feature of the disulfide bond is based on the thiol/disulfide exchange reactions which are sensitive to heat, photo-irradiation and mechanical stress. Waymouth et al. developed a self-healing hydrogel which was constructed by an ABA triblock copolymer (Zhang and Waymouth, 2017). The A-block of the polymer contains pendent dithiolane groups which can be cross-linked through reversible ring opening polymerization induced by disulfide exchange reactions between the 1,2-dithiolanes and dithiols. The as-prepared hydrogel underwent reversible sol-gel transition in the presence of external stimuli such as temperature and pH. The hydrogel was able to restore itself after rheological deformation up to a strain value of 800%. Such hydrogel is a promising candidate for stimuli-responsive drug delivery. Wang et al. developed a self-healing hydrogel coating which based on disulfide bond with antibacterial and antifouling properties (Yang et al., 2015). The as-prepared hydrogel coating has great potential as an effective and durable coating in long-term applications for biomaterials.

Other Dynamic Chemical Bonds and Reactions

Diels-Alder reaction is one of the "click chemistry" which occurs between a diene and a dienophile (Gregoritza et al., 2017; Guaresti et al., 2018). Yang et al. reported a self-healable cellulose nanocrystal-poly(ethylene glycol) (CNC-PEG) nanocomposite hydrogel via Diels-Alder reaction. The hydrogel possessed both excellent self-healing property and mechanical properties, which can be potentially used for tissue engineering (Shao et al., 2017). Chen et al. reported that the self-healing hydrogel based on Diels-Alder reaction was completely self-healed after 7 h (Wei et al., 2013). For the self-healing hydrogels based on the reversible radical reaction, functional groups such as trithiocarbonate (TTC) units (Amamoto et al., 2011), thiuramdisulfide (TDS) units (Amamoto et al., 2012), etc., need to be integrated into the polymer network. The reversible radical reaction can be triggered by external stimuli such as photo irradiation for the hydrogels to be self-healed (Wei et al., 2014).

Physically Self-Healing Hydrogels

This section focuses on designing physically self-healing hydrogels based on dynamic non-covalent interactions, including hydrogen bonds, hydrophobic interaction, host-guest interaction and multiple intermolecular interactions (**Figure 1B**).

Hydrogen Bond

Hydrogen bonding is one of the most commonly used strategies to construct physically self-healing hydrogels. Zhao et al. prepared a poly(vinyl alcohol) (PVA) hydrogel through facile freezing/thawing method (Zhang H. et al., 2012). It was found that the hydrogel showed excellent self-healing behavior only when the polymer concentration is >35 wt %, which indicates that sufficient number of hydroxyl groups are required to promote the regeneration of enough hydrogen bonds across the interface for the hydrogel to be self-healed. The conformation of hydrogen bond donors and acceptors is another factor which may affect the formation of hydrogen bonds and influence the self-healing performance. Wang et al. designed a self-healing hydrogel which contains ureido pyrimidinone (UPy) moieties (Zhang G. et al., 2017). The UPy moieties can be dimerized through quadruple hydrogen bonds. The hydrogel showed excellent self-healing performance due to the multiple hydrogen bonds formed in the network. Gu et al. prepared a self-healing hydrogel which was formed through hydrogen bonding between the cytosine (C) and guanosine (G) modified hyaluronic acid (HA) (Ye et al., 2017). The as-prepared hydrogel could be applied for short-term injectable drug delivery, tissue engineering and regenerative medicine.

Hydrophobic Interaction

Hydrophobic interaction serves as another strategy to design physically self-healing hydrogels. In these hydrogels, hydrophobic monomers are incorporated into the hydrogel network together with the hydrophilic monomers. Hydrophobic associations or hydrophobic domains will be formed within the hydrogel through self-assemble. By carefully controlling the hydrophobe content in the hydrogel, the resulting hydrogel can be self-healed through strong hydrophobic interactions.

Okay et al. reported several self-healing hydrogels which were based on hydrophobic interactions and the resulting hydrogels showed excellent self-healing properties (Tuncaboylu et al., 2011; Mihajlovic et al., 2017). Owusu-Nkwantabisah et al. developed a thermoresponsive self-healing hydrogel which incorporated poly(N-isopropylacrylamide) (PNIPAM) nanogels (Owusu-Nkwantabisah et al., 2017). The as-prepared hydrogel showed rapid self-healing behavior through hydrophobic interaction upon raising the temperature. Such hydrogel can be potentially applied for temperature sensors, thermo-switchable windows in biomedical applications.

Host-Guest Interaction

Host-guest interaction is one of the supramolecular interactions which is also widely employed to construct physically self-healing hydrogels. The interaction usually involves two or more molecules forming complex through various dynamic non-covalent interactions such as hydrogen bonds, electrostatic interactions, van der Waals forces, etc., (Wei et al., 2014). Typical examples of the host molecules including, cyclodextrin (CD) (Loebel et al., 2017), cucurbituril (CB) (Xu et al., 2017), crown ether (CE) (Zhang M. et al., 2012), etc., which have been used to make self-healing hydrogels for different applications. The internal cavity of these molecules allows them to accommodate various guest molecules with different binding affinity (Nakahata et al., 2011). Therefore, one should carefully choose the host-guest pair since the self-healing ability strongly depends on the binding affinity between the host and guest molecules. Guo et al. developed several conductive self-healing hydrogels which are based on host-guest interaction. Such hydrogels can be potentially used for a wide range of biomedical applications where electroactivity is in need such as bio sensors (Deng et al., 2018) and carriers for therapeutic agents (Wu et al., 2014).

Multiple Intermolecular Interactions

In order to achieve shorter self-healing time and higher self-healing efficiency, multiple intermolecular interactions are employed to endow the hydrogel with self-healing property. Mussel-inspired self-healing hydrogels are typical examples which contain polydopamine (PDA) within their structure. PDA based materials are well known for their remarkable adhesive property through synergestic effect of various interactions such as hydrogen bonds, metal-catechol coordination, cation–π interactions, π-π interactions, etc., (Li et al., 2015b). Zeng et al. reported several mussel-inspired self-healing hydrogels with antifouling and antimicrobial properties (Li et al., 2015c, 2017). The hydrogels showed excellent self-healing performance and such hydrogels have great potential in wound healing application.

DESIGN STRATEGIES FOR TOUGH HYDROGELS

Homogeneous Tough Hydrogels

Tetra-PEG hydrogel is a typical example of homogeneous hydrogels (**Figure 2A**). Sakai et al. did pioneering work on developing tetra-PEG tough hydrogel (Sakai et al., 2008). In

FIGURE 2 | Typical strategies for designing tough hydrogels. **(A)** Tetra-PEG hydrogel, **(B)** double network hydrogel (DN hydrogel), **(C)** nanocomposite hydrogel (NC hydrogel).
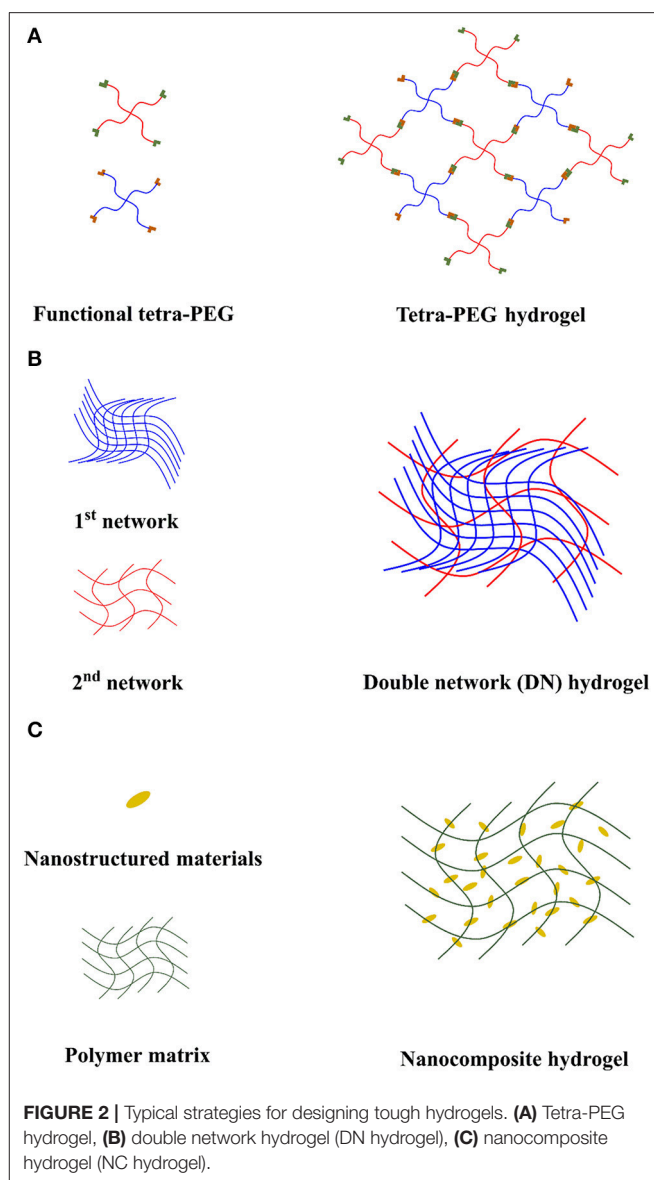
2008, the first tetra-PEG hydrogel was developed. Two tetra-PEG macro-monomers with the same arm length and different end group were synthesized. The hydrogel was fabricated by simply mixing two tetra-PEG solutions to allow crosslinking reactions between the end groups. The mechanical property of the developed hydrogel was compared with that of agarose gel and acrylamide gel by compression test. It was found that tetra-PEG hydrogel prepared at 1:1 mole ratio of two macro-monomers experienced the highest compression strength of ∼2.5 MPa. The enhanced toughness of the hydrogel results from the homogenously cross-linked network, which can not only avoid stress concentration in certain regions but also allows the stress to be distributed evenly (Naficy et al., 2011).

Homogeneously cross-linked hydrogels can also be fabricated through radiation cross-linking method instead of chemical cross-linking method. Wang et al. synthesized a polyacrylic

acid (PAA) and polyacrylamide (PAAm) hydrogel through γ-radiation-induced polymerization (Wang et al., 2011). It was found that the mechanical property of the PAA-PAAm hydrogel was superior to those produced by the classical chemical polymerization using a crosslinking agent. This may be due to the non-selective initiation effect of the monomers when a high-energy irradiation source is in presence, which could lead to a more homogeneous hydrogel network and improve the mechanical properties of the hydrogel.

Double-Network Tough Hydrogels (DN Hydrogels)

Double-network hydrogels (DN hydrogels) are considered as one class of tough hydrogels which employ mechanical energy dissipation mechanism (**Figure 2B**). The high strength and toughness of the DN hydrogels are resulted from their unique contrasting network structure and strong network entanglement (Chen et al., 2016). The first network is often designed to be tightly cross-linked and serves as the minor component of the DN hydrogel. The second network is designed to be loosely cross-linked and it is the major component of the DN hydrogel (Gong, 2010). Gong et al. reported the first DN hydrogel in 2003 (Gong et al., 2003), in which the poly(2-acrylamido-2-methylpropanesulfonic acid)/poly(acrylamide) (PAMPS/PAM) DN hydrogel showed fracture stress of 17.2 MPa which is 20 times higher than that of either PAMPS or PAM single network hydrogel. Brown and Tanaka proposed the toughening mechanism of the DN hydrogel (Brown, 2007; Tanaka, 2007). During the fracture process, the tightly cross-linked PAMPS network is firstly fragmented into micro-clusters and they act as the cross-linking points which are able to hold and stabilize the loosely cross-linked PAM network. The brittle PAMPS network serves as the "sacrificial bonds" which allows energy to be dissipated during the formation of the micro-cracks. However, the largest disadvantage of the DN hydrogel developed by Gong et al. is that the brittle PAMPS network is irreversibly cross-linked and the fracture of the PAMPS network is permanent. Such DN hydrogel will lose its toughness once the first polymer network is ruptured. Later, Suo et al. reported a DN hydrogel which composed of a dynamically cross-linked alginate network based on the ionic interactions between Ca^{2+} and carboxylic groups ($COOH^{-}$) on the alginate as the first "sacrificial network" and a chemically cross-linked PAM network as the second network (Sun et al., 2012). The DN hydrogel not only showed superior mechanical property but also recovered most of its mechanical properties after first force loading. Due to the excellent mechanical properties, DN hydrogels attract great interest in biomedical applications. Guo et al. developed biocompatible functional hydrogels with excellent mechanical properties for potential applications of tissue implantation (Li et al., 2015a) and drug delivery (Zhao et al., 2014).

Nanocomposite Hydrogels (NC Hydrogels)

Nanocomposite (NC hydrogels) are the hydrogels formed between nano-scaled materials and polymer chains (**Figure 2C**). The concept of NC hydrogel was established by Haraguchi and Takehisa (2002). In this work, they developed a

novel NC hydrogel which contains clay and poly(N-isopropyl acrylamide) (PNIPAM) chains. The hydrogels was formed by *in-situ* free radical polymerization of the NIPAM monomers in well-dispersed clay aqueous solution without using chemical cross-linkers. A mechanism was proposed for the hydrogel formation: First, the initiator could bind to the surface of clay through electrostatic interactions which allows polymer chains to be grafted from the clay nanosheets. In addition, the nucleophilic N(H)CO in PNIPAm chains could coordinate with the Si on the clay. Therefore, the clay nanosheets can act as multifunctional cross-linkers which allow multiple polymer chains to be attached through various interactions. The clay/PNIPAM NC hydrogels possessed excellent mechanical properties with tensile stress of 0.109 MPa and elongation ratio of 1,424%. The outstanding mechanical properties of the NC hydrogel is due to the synergistic effect of the multiple reversible intermolecular interactions between nanomaterials and polymer chains for mechanical energy dissipation (Haraguchi, 2007) and the homogeneity of the well-dispersed nanomaterials within the hydrogel network for even distribution of stress (Chung et al., 2017).

It is worth mentioning that through special design of NC hydrogels, one can fabricate hydrogels with both outstanding mechanical properties and excellent self-healing properties. Lu et al. adopted mussel-inspired surface chemistry to modify the surfaces of the nanomaterials with polydopamine (PDA) and developed a series of tough self-healing NC hydrogels for various applications such as reduced graphene oxide (rGO)/polyacrylamide (PAM) NC hydrogels for implantable bioelectronics (Han et al., 2017b), nanoclay/PAM NC hydrogels for wound healing (Han et al., 2017a), carbon black nanoparticle (CBNP)/PAM NC hydrogels for electricity conduction (Han et al., 2017d), etc. With the modification of PDA, multiple reversible intermolecular interactions from PDA are introduced into the hydrogel system, which not only improve the mechanical properties but also endow the hydrogel with self-healing capability. Similarly, Shao et al. developed a tough self-healing NC hydrogel which based on tannic acid-coated cellulose nanocrystals (TA@CNCs) for wearable strain sensor (Shao et al., 2018). The TA@CNCs act as dynamic bridges in the hydrogel network, which lead to rapid self-healing performance as well as reliable mechanical properties of the as-prepared hydrogel.

CONCLUDING REMARKS

Mechanically robust hydrogels with self-healing properties present many advantages over conventional hydrogels as they can be utilized in a broad range of areas such as stretchable electronics (Pu et al., 2017; Jing et al., 2018; Hong et al., 2019), sensors and actuators (Francis et al., 2017; Tudor et al., 2017), cartilage repair (Han et al., 2017c; Lolli et al., 2018), with extended life-time and enhanced durability and reliability. Although the field of study shows great promise, there are still challenges to be tackled.

Generally, the self-healing ability of the hydrogels weakens and the time required for the healing process increases with the improvement of the mechanical properties of the hydrogels as

summarized by Panhui et al. (Taylor and In Het Panhuis, 2016). Therefore, the development of mechanically robust hydrogels which can be self-healed on the time scale of seconds or minutes should be considered. One possible approach is to introduce multiple chemically or physically self-healing mechanisms into the NC hydrogels/DN hydrogels in order to enhance the self-healing efficiency without sacrificing the mechanical properties.

The fundamental understanding of different self-healing and toughening mechanisms is crucial for designing and optimizing the self-healing tough hydrogels. Both theoretical and experimental studies are needed to understand the self-healing and toughening mechanisms at the atomic-scale or molecular-scale. For instance, Zeng et al. used a surface forces apparatus (SFA) to quantitatively study the polymer interactions which account for the self-healing behavior of the hydrogel (Yan et al., 2017). Such non-destructive *in situ* testing method is highly needed for elucidating the molecular interaction mechanisms of various hydrogel materials.

It is also necessary to develop self-healing tough hydrogels into multifunctional "smart" materials, which should integrate other properties such as electrical conductivity (Wu et al., 2017),

temperature responsivity (Zubik et al., 2017), photo responsivity (Wang R. et al., 2017), etc., into a single hydrogel system. Such hydrogels can be promisingly applied in different applications such as sensors and actuators. When the hydrogels are endowed with the stimuli responsive properties, one should ensure the chemical and mechanical stability of the hydrogels as the change of environmental conditions may affect the intrinsic properties of the hydrogels. The intermolecular and surface interactions of various components in the hydrogel systems essentially determine the properties and performances of the hydrogel systems, which should be well taken in the rational design of the self-healing tough hydrogels.

AUTHOR CONTRIBUTIONS

WW wrote the manuscript. RN and HZ helped to revise the manuscript.

ACKNOWLEDGMENTS

REFERENCES

Amamoto, Y., Kamada, J., Otsuka, H., Takahara, A., and Matyjaszewski, K. (2011). Repeatable photoinduced self-healing of covalently cross-linked polymers through reshuffling of trithiocarbonate units. *Angewandte Chemie Int. Ed.* 50, 1660–1663. doi: 10.1002/anie.201003888

Amamoto, Y., Otsuka, H., Takahara, A., and Matyjaszewski, K. (2012). Self-healing of covalently cross-linked polymers by reshuffling thiuram disulfide moieties in air under visible light. *Adv. Mater.* 24, 3975–3980. doi: 10.1002/adma.201201928

Andersen, A., Krogsgaard, M., and Birkedal, H. (2018). Mussel-inspired self-healing double-cross-linked hydrogels by controlled combination of metal coordination and covalent cross-linking. *Biomacromolecules* 19, 1402–1409. doi: 10.1021/acs.biomac.7b01249

Annabi, N., Tamayol, A., Uquillas, J. A., Akbari, M., Bertassoni, L. E., Cha, C., et al. (2014). 25th Anniversary Article: rational design and applications of hydrogels in regenerative medicine. *Adv. Mater.* 26, 85–124. doi: 10.1002/adma.201303233

Axthelm, J., Askes, S. H. C., Elstner, M., G, U. R., Görls, H., Bellstedt, P., et al. (2017). Fluorinated boronic acid-appended pyridinium salts and 19f nmr spectroscopy for diol sensing. *J. Am. Chem. Soc.* 139, 11413–11420. doi: 10.1021/jacs.7b01167

Brown, H. R. (2007). A model of the fracture of double network gels. *Macromolecules* 40, 3815–3818. doi: 10.1021/ma062642y

Cai, G., Wang, J., Qian, K., Chen, J., Li, S., and Lee, P. S. (2017). Extremely stretchable strain sensors based on conductive self-healing dynamic cross-links hydrogels for human-motion detection. *Adv. Sci.* 4:1600190. doi: 10.1002/advs.201600190

Chen, Q., Chen, H., Zhu, L., and Zheng, J. (2016). Engineering of tough double network hydrogels. *Macromol. Chem. Phys.* 217, 1022–1036. doi: 10.1002/macp.201600038

Chen, Y., Wang, W., Wu, D., Nagao, M., Hall, D. G., Thundat, T., et al. (2018). Injectable self-healing zwitterionic hydrogels based on dynamic benzoxaborole-sugar interactions with tunable mechanical properties. *Biomacromolecules* 19, 596–605. doi: 10.1021/acs.biomac.7b01679

Chung, H.-J., Charaya, H., Liu, L., and Li, X. (2017). "Tough Hydrogels: Toughening Mechanisms and Their Utilization in Stretchable Electronics and

in Regenerative Medicines," in *Hybrid Organic-Inorganic Interfaces*, eds M. H. Delville and A. Taubert (Edmonton, AB: Wiley).

Deng, Z., Guo, Y., Zhao, X., Ma, P. X., and Guo, B. (2018). Multifunctional stimuli-responsive hydrogels with self-healing, high conductivity, and rapid recovery through host–guest interactions. *Chem. Mater.* 30, 1729–1742. doi: 10.1021/acs.chemmater.8b00008

Dong, R., Zhao, X., Guo, B., and Ma, P. X. (2016). Self-healing conductive injectable hydrogels with antibacterial activity as cell delivery carrier for cardiac cell therapy. *ACS Appl. Mater. Interfaces* 8, 17138–17150. doi: 10.1021/acsami.6b04911

Eke, G., Mangir, N., Hasirci, N., MacNeil, S., and Hasirci, V. (2017). Development of a UV crosslinked biodegradable hydrogel containing adipose derived stem cells to promote vascularization for skin wounds and tissue engineering. *Biomaterials* 129, 188–198. doi: 10.1016/j.biomaterials.2017.03.021

Francis, W., Dunne, A., Delaney, C., Florea, L., and Diamond, D. (2017). Spiropyran based hydrogels actuators—Walking in the light. *Sensors Actuators B* 250, 608–616. doi: 10.1016/j.snb.2017.05.005

Gong, J. P. (2010). Why are double network hydrogels so tough? *Soft Matter* 6, 2583–2590. doi: 10.1039/B924290B

Gong, J. P., Katsuyama, Y., Kurokawa, T., and Osada, Y. (2003). Double-network hydrogels with extremely high mechanical strength. *Adv. Mater.* 15, 1155–1158. doi: 10.1002/adma.200304907

Gregoritza, M., Messmann, V., Abstiens, K., Brandl, F. P., and Goepferich, A. M. (2017). Controlled antibody release from degradable thermoresponsive hydrogels cross-linked by diels–alder chemistry. *Biomacromolecules* 18, 2410–2418. doi: 10.1021/acs.biomac.7b00587

Guaresti, O., García–Astrain, C., Aguirresarobe, R. H., Eceiza, A., and Gabilondo, N. (2018). Synthesis of stimuli–responsive chitosan–based hydrogels by Diels–Alder cross–linking 'click' reaction as potential carriers for drug administration. *Carbohydrate Polymers* 183, 278–286. doi: 10.1016/j.carbpol.2017.12.034

Guo, R., Su, Q., Zhang, J., Dong, A., Lin, C., and Zhang, J. (2017). Facile Access to multisensitive and self-healing hydrogels with reversible and dynamic boronic ester and disulfide linkages. *Biomacromolecules* 18, 1356–1364. doi: 10.1021/acs.biomac.7b00089

Han, L., Lu, X., Liu, K., Wang, K., Fang, L., Weng, L. T., et al. (2017a). Mussel-inspired adhesive and tough hydrogel based on nanoclay confined dopamine polymerization. *ACS Nano* 11, 2561–2574. doi: 10.1021/acsnano.6b05318

Han, L., Lu, X., Wang, M., Gan, D., Deng, W., Wang, K., et al. (2017b). A mussel-inspired conductive, self-adhesive, and self-healable tough hydrogel as cell stimulators and implantable bioelectronics. *Small* 13:1601916. doi: 10.1002/smll.201601916

Han, L., Xu, J., Lu, X., Gan, D., Wang, Z., Wang, K., et al. (2017c). Biohybrid methacrylated gelatin/polyacrylamide hydrogels for cartilage repair. *J. Mater. Chem. B* 5, 731–741. doi: 10.1039/C6TB02348G

Han, L., Yan, L., Wang, K., Fang, L., Zhang, H., Tang, Y., et al. (2017d). Tough, self-healable and tissue-adhesive hydrogel with tunable multifunctionality. *NPG Asia Mater.* 9, e372–e372. doi: 10.1038/am.2017.33

Haraguchi, K. (2007). Nanocomposite hydrogels. *Curr. Opin. Solid State Mater. Sci.* 11, 47–54. doi: 10.1016/j.cossms.2008.05.001

Haraguchi, K., and Takehisa, T. (2002). Nanocomposite Hydrogels: a unique organic–inorganic network structure with extraordinary mechanical, optical, and swelling/de-swelling properties. *Adv. Mater.* 14, 1120–1124. doi: 10.1002/1521-4095(20020816)14:163.0.CO;2-9

Hong, K. S., Sungmook, J., Seon, Y. I., Chihak, L., Youngsu, O., and Jae-Min, H. (2019). Ultrastretchable conductor fabricated on skin-like hydrogel–elastomer hybrid substrates for skin electronics. *Adv. Mater.* 30:e1800109. doi: 10.1002/adma.201800109

Hsieh, F.-Y., Tao, L., Wei, Y., and Hsu, S.-H. (2017). A novel biodegradable self-healing hydrogel to induce blood capillary formation. *NPG Asia Mater.* 9, e363–e363. doi: 10.1038/am.2017.23

Ida, S., Kimura, R., Tanimoto, S., and Hirokawa, Y. (2016). End-crosslinking of controlled telechelic poly(N-isopropylacrylamide) toward a homogeneous gel network with photo-induced self-healing. *Polymer J.* 49:237. doi: 10.1038/pj.2016.112

Ishii, S., Kokubo, H., Hashimoto, K., Imaizumi, S., and Watanabe, M. (2017). Tetra-PEG network containing ionic liquid synthesized via michael addition reaction and its application to polymer actuator. *Macromolecules* 50, 2906–2915. doi: 10.1021/acs.macromol.6b02750

Jiang, H., Zhang, G., Feng, X., Liu, H., Li, F., Wang, M., et al. (2017). Room-temperature self-healing tough nanocomposite hydrogel crosslinked by zirconium hydroxide nanoparticles. *Composites Sci. Tech.* 140, 54–62. doi: 10.1016/j.compscitech.2016.12.027

Jing, X., Mi, H.-Y., Peng, X.-F., and Turng, L.-S. (2018). Biocompatible, self-healing, highly stretchable polyacrylic acid/reduced graphene oxide nanocomposite hydrogel sensors via mussel-inspired chemistry. *Carbon* 136, 63–72. doi: 10.1016/j.carbon.2018.04.065

Kotsuchibashi, Y., Agustin, R. V. C., Lu, J.-Y., Hall, D. G., and Narain, R. (2013). Temperature, pH, and glucose responsive gels via simple mixing of boroxole- and glyco-based polymers. *ACS Macro Lett.* 2, 260–264. doi: 10.1021/mz400076p

Lei, Z., Wang, Q., Sun, S., Zhu, W., and Wu, P. (2017). A bioinspired mineral hydrogel as a self-healable, mechanically adaptable ionic skin for highly sensitive pressure sensing. *Adv. Mater.* 29:1700321. doi: 10.1002/adma.201700321

Li, H., Hao, D., Fan, J., Song, S., Guo, X., Song, W., et al. (2016). A robust double-network hydrogel with under sea water superoleophobicity fabricated via one-pot, one-step reaction. *J. Mater. Chem. B* 4, 4662–4666. doi: 10.1039/C6TB00818F

Li, L., Ge, J., Ma, P. X., and Guo, B. (2015a). Injectable conducting interpenetrating polymer network hydrogels from gelatin-graft-polyaniline and oxidized dextran with enhanced mechanical properties. *RSC Adv.* 5, 92490–92498. doi: 10.1039/c5ra19467a

Li, L., Smitthipong, W., and Zeng, H. (2015b). Mussel-inspired hydrogels for biomedical and environmental applications. *Polymer Chem.* 6, 353–358. doi: 10.1039/c4py01415d

Li, L., Yan, B., Yang, J., Chen, L., and Zeng, H. (2015c). Novel mussel-inspired injectable self-healing hydrogel with anti-biofouling property. *Adv. Mater.* 27, 1294–1299. doi: 10.1002/adma.201405166

Li, L., Yan, B., Yang, J., Huang, W., Chen, L., and Zeng, H. (2017). Injectable self-healing hydrogel with antimicrobial and antifouling properties. *ACS Appl. Mater. Interfaces* 9, 9221–9225. doi: 10.1021/acsami.6b16192

Liao, M., Wan, P., Wen, J., Gong, M., Wu, X., Wang, Y., et al. (2017). Wearable, healable, and adhesive epidermal sensors assembled from mussel-inspired conductive hybrid hydrogel framework. *Adv. Funct. Mater.* 27:1703852. doi: 10.1002/adfm.201703852

Lin, S., Yuk, H., Zhang, T., Parada, G. A., Koo, H., Yu, C., et al. (2016). Stretchable hydrogel electronics and devices. *Adv. Mater.* 28, 4497–4505. doi: 10.1002/adma.201504150

Liu, J., Zhang, X., Chen, X., Qu, L., Zhang, L., Li, W., et al. (2018). Stimuli-responsive dendronized polymeric hydrogels through Schiff-base chemistry showing remarkable topological effects. *Polymer Chem.* 9, 378–387. doi: 10.1039/C7PY01865G

Liu, S., and Li, L. (2016). Recoverable and self-healing double network hydrogel based on κ-carrageenan. *ACS Appl. Mater. Interfaces* 8, 29749–29758. doi: 10.1021/acsami.6b11363

Loebel, C., Rodell, C. B., Chen, M. H., and Burdick, J. A. (2017). Shear-thinning and self-healing hydrogels as injectable therapeutics and for 3D-printing. *Nat. Protoc.* 12, 1521–1541. doi: 10.1038/nprot.2017.053

Lolli, A., Sivasubramaniyan, K., Vainieri, M. L., Eglin, D., Wexselblatt, E., Yayon, A., et al. (2018). Hyaluronan-based hydrogel delivering antimiR-221 for the guidance of endogenous cartilage repair. *Osteoarthritis Cartilage* 26:S163. doi: 10.1016/j.joca.2018.02.355

Mihajlovic, M., Staropoli, M., Appavou, M.-S., Wyss, H. M., Pyckhout-Hintzen, W., and Sijbesma, R. P. (2017). Tough supramolecular hydrogel based on strong hydrophobic interactions in a multiblock segmented copolymer. *Macromolecules* 50, 3333–3346. doi: 10.1021/acs.macromol.7b00319

Naficy, S., Brown, H. R., Razal, J. M., Spinks, G. M., and Whitten, P. G. (2011). Progress toward robust polymer hydrogels. *Aust. J. Chem.* 64, 1007–1025. doi: 10.1071/CH11156

Nakahata, M., Takashima, Y., Yamaguchi, H., and Harada, A. (2011). Redox-responsive self-healing materials formed from host–guest polymers. *Nat. Commun.* 2:511. doi: 10.1038/ncomms1521

Owusu-Nkwantabisah, S., Gillmor, J., Switalski, S., Mis, M. R., Bennett, G., Moody, R., et al. (2017). Synergistic thermoresponsive optical properties of a composite self-healing hydrogel. *Macromolecules* 50, 3671–3679. doi: 10.1021/acs.macromol.7b00355

Pu, X., Liu, M., Chen, X., Sun, J., Du, C., Zhang, Y., et al. (2017). Ultrastretchable, transparent triboelectric nanogenerator as electronic skin for biomechanical energy harvesting and tactile sensing. *Sci. Adv.* 3:e1700015. doi: 10.1126/sciadv.1700015

Qin, H., Zhang, T., Li, H.-N., Cong, H.-P., Antonietti, M., and Yu, S.-H. (2017). Dynamic au-thiolate interaction induced rapid self-healing nanocomposite hydrogels with remarkable mechanical behaviors. *Chem* 3, 691–705. doi: 10.1016/j.chempr.2017.07.017

Qu, J., Zhao, X., Ma, P. X., and Guo, B. (2017). pH-responsive self-healing injectable hydrogel based on N-carboxyethyl chitosan for hepatocellular carcinoma therapy. *Acta Biomater.* 58, 168–180. doi: 10.1016/j.actbio.2017.06.001

Ren, Y., Zhang, Y., Sun, W., Gao, F., Fu, W., Wu, P., et al. (2017). Methyl matters: an autonomic rapid self-healing supramolecular poly(N-methacryloyl glycinamide) hydrogel. *Polymer* 126, 1–8. doi: 10.1016/j.polymer.2017.08.016

Sakai, T., Matsunaga, T., Yamamoto, Y., Ito, C., Yoshida, R., Suzuki, S., et al. (2008). Design and Fabrication of a High-Strength Hydrogel with Ideally Homogeneous Network Structure from Tetrahedron-like Macromonomers. *Macromolecules* 41, 5379–5384. doi: 10.1021/ma800476x

Shao, C., Wang, M., Chang, H., Xu, F., and Yang, J. (2017). A Self-Healing Cellulose nanocrystal-poly(ethylene glycol) nanocomposite hydrogel via diels–alder click reaction. *ACS Sust. Chem. Eng.* 5, 6167–6174. doi: 10.1021/acssuschemeng.7b01060

Shao, C., Wang, M., Meng, L., Chang, H., Wang, B., Xu, F., et al. (2018). Mussel-inspired cellulose nanocomposite tough hydrogels with synergistic self-healing, adhesive, and strain-sensitive properties. *Chem. Mater.* 30, 3110–3121. doi: 10.1021/acs.chemmater.8b01172

Sun, J.-Y., Zhao, X., Illeperuma, W. R. K., Chaudhuri, O., Oh, K. H., Mooney, D. J., et al. (2012). Highly stretchable and tough hydrogels. *Nature* 489:133. doi: 10.1038/nature11409

Tanaka, Y. (2007). A local damage model for anomalous high toughness of double-network gels. *EPL (Europhysics Letters)* 78:56005. doi: 10.1209/0295-5075/78/56005

Taylor, D. L., and In Het Panhuis, M. (2016). Self-healing hydrogels. *Adv. Mater.* 28, 9060–9093. doi: 10.1002/adma.201601613

Tseng, T. C., Tao, L., Hsieh, F. Y., Wei, Y., Chiu, I. M., and Hsu, S. H. (2015). An injectable, self-healing hydrogel to repair the central nervous system. *Adv. Mater.* 27, 3518–3524. doi: 10.1002/adma.201500762

Tudor, A., Saez, J., Florea, L., Benito-Lopez, F., and Diamond, D. (2017). Poly(ionic liquid) thermo-responsive hydrogel microfluidic actuators. *Sensors Actuators B* 247, 749–755. doi: 10.1016/j.snb.2017.03.045

Tuncaboylu, D. C., Sari, M., Oppermann, W., and Okay, O. (2011). Tough and self-healing hydrogels formed via hydrophobic interactions. *Macromolecules* 44, 4997–5005. doi: 10.1021/ma200579v

Wang, J., Zhang, F., Tsang, W. P., Wan, C., and Wu, C. (2017). Fabrication of injectable high strength hydrogel based on 4-arm star PEG for cartilage tissue engineering. *Biomaterials* 120, 11–21. doi: 10.1016/j.biomaterials.2016.12.015

Wang, R., Yang, Z., Luo, J., Hsing, I.-M., and Sun, F. (2017). B_{12}-dependent photoresponsive protein hydrogels for controlled stem cell/protein release. *Proc. Natl. Acad. Sci.* 114, 5912–5917. doi: 10.1073/pnas.1621350114

Wang, X., Wang, H., and Brown, H. R. (2011). Jellyfish gel and its hybrid hydrogels with high mechanical strength. *Soft. Matter* 7, 211–219. doi: 10.1039/C0SM00632G

Wang, Y., Li, L., Kotsuchibashi, Y., Vshyvenko, S., Liu, Y., Hall, D., et al. (2016). Self-healing and injectable shear thinning hydrogels based on dynamic oxaborole-diol covalent cross-linking. *ACS Biomater. Sci. Eng.* 2, 2315–2323. doi: 10.1021/acsbiomaterials.6b00527

Wei, Z., Yang, J. H., Du, X. J., Xu, F., Zrinyi, M., Osada, Y., et al. (2013). Dextran-based self-healing hydrogels formed by reversible diels–alder reaction under physiological conditions. *Macromol. Rapid Commun.* 34, 1464–1470. doi: 10.1002/marc.201300494

Wei, Z., Yang, J. H., Zhou, J., Xu, F., Zrinyi, M., Dussault, P. H., et al. (2014). Self-healing gels based on constitutional dynamic chemistry and their potential applications. *Chem. Soc. Rev.* 43, 8114–8131. doi: 10.1039/c4cs00219a

Wu, Q., Wei, J., Xu, B., Liu, X., Wang, H., Wang, W., et al. (2017). A robust, highly stretchable supramolecular polymer conductive hydrogel with self-healability and thermo-processability. *Sci. Rep.* 7:41566. doi: 10.1038/srep41566

Wu, Y., Guo, B., and Ma, P. X. (2014). Injectable electroactive hydrogels formed via host–guest interactions. *ACS Macro Lett.* 3, 1145–1150. doi: 10.1021/mz500498y

Xiong, C., Peng, K., Tang, X., Ye, Z., Shi, Y., and Yang, H. (2017). CO2-responsive self-healable hydrogels based on hydrophobically-modified polymers bridged by wormlike micelles. *RSC Adv.* 7, 34669–34675. doi: 10.1039/C7RA06418G

Xu, Q., A, S., McMichael, P., Creagh-Flynn, J., Zhou, D., Gao, Y., et al. (2018). Double-cross-linked hydrogel strengthened by UV irradiation from a hyperbranched PEG-based trifunctional polymer. *ACS Macro Lett.* 7, 509–513. doi: 10.1021/acsmacrolett.8b00138

Xu, W., Song, Q., Xu, J.-F., Serpe, M. J., and Zhang, X. (2017). Supramolecular hydrogels fabricated from supramonomers: a novel wound dressing material. *ACS Appl. Mater. Interfaces* 9, 11368–11372. doi: 10.1021/acsami.7b02850

Yan, B., Huang, J., Han, L., Gong, L., Li, L., Israelachvili, J. N., et al. (2017). Duplicating dynamic strain-stiffening behavior and nanomechanics of biological tissues in a synthetic self-healing flexible network hydrogel. *ACS Nano* 11, 11074–11081. doi: 10.1021/acsnano.7b05109

Yang, N., Yang, H., Shao, Z., and Guo, M. (2017). Ultrastrong and tough supramolecular hydrogels from multiurea linkage segmented copolymers with tractable processablity and recyclability. *Macromol. Rapid Commun.* 38:1700275. doi: 10.1002/marc.201700275

Yang, W. J., Tao, X., Zhao, T., Weng, L., Kang, E.-T., and Wang, L. (2015). Antifouling and antibacterial hydrogel coatings with self-healing properties based on a dynamic disulfide exchange reaction. *Polymer Chem.* 6, 7027–7035. doi: 10.1039/C5PY00936G

Yang, X., Liu, G., Peng, L., Guo, J., Tao, L., Yuan, J., et al. (2017). Highly Efficient self-healable and dual responsive cellulose-based hydrogels for controlled release and 3D cell culture. *Adv. Funct. Mater.* 27:1703174. doi: 10.1002/adfm.201703174

Ye, X., Li, X., Shen, Y., Chang, G., Yang, J., and Gu, Z. (2017). Self-healing pH-sensitive cytosine- and guanosine-modified hyaluronic acid hydrogels via hydrogen bonding. *Polymer* 108, 348–360. doi: 10.1016/j.polymer.2016.11.063

Yesilyurt, V., Webber, M. J., Appel, E. A., Godwin, C., Langer, R., and Anderson, D. G. (2016). Injectable self-healing glucose-responsive hydrogels with pH-regulated mechanical properties. *Adv. Mater.* 28, 86–91. doi: 10.1002/adma.201502902

Yu, H., Wang, Y., Yang, H., Peng, K., and Zhang, X. (2017). Injectable self-healing hydrogels formed via thiol/disulfide exchange of thiol functionalized F127 and dithiolane modified PEG. *J. Mater. Chem. B* 5, 4121–4127. doi: 10.1039/C7TB00746A

Yuk, H., Lin, S., Ma, C., Takaffoli, M., Fang, N. X., and Zhao, X. (2017). Hydraulic hydrogel actuators and robots optically and sonically camouflaged in water. *Nature Commun.* 8:14230. doi: 10.1038/ncomms14230

Zhang, G., Chen, Y., Deng, Y., Ngai, T., and Wang, C. (2017). Dynamic supramolecular hydrogels: regulating hydrogel properties through self-complementary quadruple hydrogen bonds and thermo-switch. *ACS Macro Lett.* 6, 641–646. doi: 10.1021/acsmacrolett.7b00275

Zhang, H., Xia, H., and Zhao, Y. (2012). Poly(vinyl alcohol) hydrogel can autonomously self-heal. *ACS Macro Lett.* 1, 1233–1236. doi: 10.1021/mz300451r

Zhang, M., Xu, D., Yan, X., Chen, J., Dong, S., Zheng, B., et al. (2012). Self-Healing supramolecular gels formed by crown ether based host–guest interactions. *Angewandte Chemie Int. Ed.* 51, 7011–7015. doi: 10.1002/anie.201203063

Zhang, X., and Waymouth, R. M. (2017). 1,2-Dithiolane-derived dynamic, covalent materials: cooperative self-assembly and reversible cross-linking. *J. Am. Chem. Soc.* 139, 3822–3833. doi: 10.1021/jacs.7b00039

Zhang, Y., Fu, C., Li, Y., Wang, K., Wang, X., Wei, Y., et al. (2017). Synthesis of an injectable, self-healable and dual responsive hydrogel for drug delivery and 3D cell cultivation. *Polymer Chem.* 8, 537–544. doi: 10.1039/c6py01704e

Zhang, Y., Tao, L., Li, S., and Wei, Y. (2011). Synthesis of multiresponsive and dynamic chitosan-based hydrogels for controlled release of bioactive molecules. *Biomacromolecules* 12, 2894–2901. doi: 10.1021/bm200423f

Zhao, J., Zhao, X., Guo, B., and Ma, P. X. (2014). Multifunctional interpenetrating polymer network hydrogels based on methacrylated alginate for the delivery of small molecule drugs and sustained release of protein. *Biomacromolecules* 15, 3246–3252. doi: 10.1021/bm5006257

Zhao, X., Wu, H., Guo, B., Dong, R., Qiu, Y., and Ma, P. X. (2017). Antibacterial anti-oxidant electroactive injectable hydrogel as self-healing wound dressing with hemostasis and adhesiveness for cutaneous wound healing. *Biomaterials* 122, 34–47. doi: 10.1016/j.biomaterials.2017.01.011

Zubik, K., Singhsa, P., Wang, Y., Manuspiya, H., and Narain, R. (2017). Thermo-responsive poly(N-Isopropylacrylamide)-cellulose nanocrystals hybrid hydrogels for wound dressing. *Polymers* 9:119. doi: 10.3390/polym9040119

Conflict of Interest Statement: The authors declare that the research was conducted in the absence of any commercial or financial relationships that could be construed as a potential conflict of interest.

Functional Hydrogels With Tunable Structures and Properties for Tissue Engineering Applications

Xiaomeng Li[1,2], Qingqing Sun[3], Qian Li[1,2], Naoki Kawazoe[4] and Guoping Chen[4*]

[1] School of Mechanics and Engineering Science, Zhengzhou University, Zhengzhou, China, [2] National Center for International Joint Research of Micro-nano Moulding Technology, Zhengzhou University, Zhengzhou, China, [3] Center for Functional Sensor and Actuator, National Institute for Materials Science, Tsukuba, Japan, [4] Research Center for Functional Materials, National Institute for Materials Science, Tsukuba, Japan

Tissue engineering (TE) has been used as an attractive and efficient process to restore the original tissue structures and functions through the combination of biodegradable scaffolds, seeded cells, and biological factors. As a unique type of scaffolds, hydrogels have been frequently used for TE because of their similar 3D structures to the native extracellular matrix (ECM), as well as their tunable biochemical and biophysical properties to control cell functions such as cell adhesion, migration, proliferation, and differentiation. Various types of hydrogels have been prepared from naturally derived biomaterials, synthetic polymers, or their combination, showing their promise in TE. This review summarizes the very recent progress of hydrogels used for TE applications. The strategies for tuning biophysical and biochemical properties, and structures of hydrogels are first introduced. Their influences on cell functions and promotive effects on tissue regeneration are then highlighted.

Keywords: functional hydrogels, tissue engineering, physical properties, chemical properties, microstructures

INTRODUCTION

Tissue engineering (TE) has emerged as a useful approach to treat tissue damages caused by diseases and trauma, which has shown many advantages as compared to conventional treatment strategies. To afford desirable therapeutic outcome, scaffolds prepared from various kinds of biomaterials have been used for TE to accommodate sufficient amount of cells and to control cell functions (Chen and Kawazoe, 2016a,b; Chen et al., 2018).

Among of different types of scaffolds, hydrogels have attracted more and more attention in the TE field owing to their similarity to *in vivo* cellular microenvironment and tunable physiochemical properties (Drury and Mooney, 2003). Hydrogels are generally prepared by translating hydrophilic polymers solution into 3D network structure via physical or chemical crosslinking. During this process, hydrogels can encapsulate cells homogeneously and provide cells a 3D microenvironment similar to the native extracellular matrix (ECM) (Tibbitt and Anseth, 2009). Cell behaviors and functions *in vivo* are affected by the stimuli that are produced by the surrounding ECM. In a similar way, the structures and physiochemical properties of hydrogels provide critical cues to control the functions of embedded cells and thus guide tissue regeneration.

The structures and physiochemical properties of hydrogels can be designed and controlled through selecting different biomaterials, crosslinking methods and fabrication strategies. This review summarizes the latest developments of functional hydrogels for TE applications. At first, the

materials and crosslinking methods used for hydrogel preparation are introduced. And then, the approaches to tune the structure and physiochemical properties of hydrogels and their effects on cell functions and tissue regeneration are compared. Finally, the challenges and future perspectives of functional hydrogels are discussed.

MATERIALS AND CROSSLINKING METHODS FOR FUNCTIONAL HYDROGELS PREPARATION

There are several criterias to prepare hydrogels for TE applications. Firstly, the materials and crosslinking agents should be compatible toward living cells and biological factors (e.g., growth factors). Secondly, the preparation process should be easily occured under mild conditions. Thirdly, the products from hydrogel degradation should be non-toxic to cells and tissues. The materials and crosslinking methods used for hydrogel preparation for TE are summarized in **Table 1**.

Hydrogel Construction Materials

Materials used to prepare TE hydrogels can be briefly classified into natural and synthetic polymers. Hydrogels prepared from natural polymers possess intrinsic advantages, such as high biocompatibility, biodegradability and similar microenvironment to that of native tissues. Natural polymers used for hydrogel preparation include protein-based materials (such as gelatin, collagen, fibrin, and silk fibroin) and polysaccharide-based materials (such as hyaluronic acid (HA), chondroitin sulfate (CS), alginate, chitosan and so on). Collagen, as the main ECM component of various tissue, is an attractive material for hydrogels preparation (Heo et al., 2016). It's derivative, gelatin, is also a frequently used protein-based material for hydrogel formation, which has higher solubility and lower cost when compared with collagen (Zhao et al., 2016). Gelatin-based hydrogels are good candidates for various TE. For example, injectable gelatin methacryloyl (GelMA) hydrogels are prepared for cartilage TE (Li et al., 2016). The chondrocytes 3D cultured in these hydrogels have shown excellent viabilities and desirable functions. HA as a glycosaminoglycan is commonly prevalent in body liquid and native ECM (Shendi et al., 2016). Therefore, it has been used to prepare various kinds of hydrogels for cartilage, skin, and many other TE. For example, it has been reported that HA molecular can bond with mesenchymal stem cells (MSCs) through CD44 receptors and promote the chondrogenesis (Chung and Burdick, 2008). CS is a sulfated glycosaminoglycan with a linear structure existing in cartilage tissue ECM (Levett et al., 2014). Chondrocytes cultured in CS hydrogels have round morphology, enhanced gene expression, and secretion of cartilaginous ECM (Levett et al., 2014; Zhu et al., 2014). Other polysaccharide-based materials, such as alginate (obtaining from bacteria and brown seaweed) and chitosan (derived from chitin that is produced from the shells of crabs and shrimps), are also commonly used for hydrogel preparation due to their biocompatibility, degradability and easy modification (Kim et al., 2016; Hunt et al., 2017).

On the other hand, synthetic polymers have also exhibited wide usage due to their controllability, reproducibility, and good mechanical properties (Guan et al., 2017). Representative synthetic polymers used for TE hydrogels include poly(ethylene glycol) (PEG), poly(vinyl alcohol) (PVA),poly (N-isopropylacrylamide) (PNIPAM) (Haq et al., 2017), and polyacrylamide (PAM) (Darnell et al., 2013). PEG and PVA have low toxicity, making them widely used for cell-laden hydrogels and drug carriers (Kim et al., 2016; You et al., 2018). However, due to the lack of biological activity, the biocompatibility of these synthetic polymers is compromised relative to natural materials. Hybridization with natural materials is an efficient and easy-going approach to integrate the advantages of natural and synthetic component. It has been reported that the biocompatibilities of PAM, PVA, PNIPAM, and PEG hydrogels are significantly improved after blend with gelatin (Gao et al., 2015; Kim et al., 2016; Navaei et al., 2016b; Han et al., 2017). The cell spreading, and proliferation in these hybrid hydrogels are enhanced compared with the cells 3D cultured in synthetic hydrogels. Besides, the hybridization of different natural materials can also exhibit novel attractive properties. For example, alginate is interpenetrated and crosslinked into photopolymerized gelatin hydrogel network to generate alginate/gelatin hybrid hydrogel (Pacelli et al., 2018). Such a hydrogel is confirmed to have the function of promoting bone tissue regeneration due to the good biocompatibility and enhanced mechanical property.

Crosslinking Methods

There are various methods for crosslinking of hydrophilic polymers chains to form hydrogels, which usually are selected depending on the materials chemistry and expected functions. In general, they can be classified into physical and chemical crosslinking methods.

Physical Crosslinking Methods

Physically crosslinked hydrogels can be prepared at very mild conditions without the utilization of crosslinking agents that often cause toxicity to cells or may affect the activity of biological molecules encapsulated in hydrogels (Hennink and Van Nostrum, 2012). There are many methods to prepare physically crosslinked hydrogels for TE applications, such as ionic interaction, guest-host interaction and thermo-gelation.

Ionic crosslinking

Ionic crosslinking method is frequently used to encapsulate cells and drugs due to the mild crosslinking procedures (Goosen et al., 1985; Gombotz and Wee, 2012). The most representative hydrogels formed by ionic crosslinking is alginate hydrogel. The crosslinking is through the exchange of sodium ions from guluronic acid units with divalent cations such as calcium to form junction zones (Gacesa, 1988). This physically crosslinked alginate hydrogel not only has shown a biocompatible property but also has many other functions, such as self-healing and stress relaxation, due to the reversible dissociation and re-bonding between α-L-guluronic acid in alginate and calcium ions. However, the stability of ionic hydrogel should be considered

TABLE 1 | Materials and crosslinking methods for functional hydrogels preparation.

Materials		Characteristics	Crosslinking methods		TE applications	References
			Physical crosslinking	**Chemical crosslinking**		
Natural Materials	Gelatin		Guest-host		Cartilage TE	Feng et al., 2016
		GelMA		Photo	Cartilage, tendon TE	Yang et al., 2016; Li et al., 2017b
		GelMA	Thermal	Photo	Corneal TE	Rizwan et al., 2017
		Gelatin-hydroxyphenylpropionic acid (Gtn-HPA)		Enzymatic	Cartilage TE	Wang et al., 2014; Le Thi et al., 2017
	Collagen			Photo	Meniscus TE	Heo et al., 2016
	HA	Adamantane-functionalized HA	Guest-host		Cartilage TE	Wei et al., 2016
		HA-vinyl sulfone		Michael addition	Neural engineering	Shendi et al., 2016
		Maleimide-functionalized HA and furan-functionalized HA		Diels-Alder	Adipose TE	Fan et al., 2015a
		Methacrylated HA (MeHA)		Photo	Meniscus, nucleus pulposus TE	Kim et al., 2015; Koh et al., 2017
	Chondroitin sulfate	Furfurylamine grafted chondroitin sulfate		Diels-Alder	Bone TE	Bai et al., 2017
		Methacrylated chondroitin sulfate		Photo	Cartilage TE	Levett et al., 2014; Abbadessa et al., 2016
	Alginate		Ionic		Cartilage, retinal and bone TE	Chaudhuri et al., 2016; Hunt et al., 2017; Lee et al., 2017
		Methacrylated alginate		Photo	Bone TE	Ho et al., 2016
	Dextran	Dextran bifunctionalized with methacrylate and aldehyde		Photo	Vascular TE	Liu and Chan-Park, 2009
		Azadibenzocyclooctyne-modified dextran and azide-modified dextran		Alkyne-azide	Cartilage TE	Wang et al., 2017b
	Agarose		Thermal		Osteochondral, skin TE	Sheehy et al., 2013; Miguel et al., 2014
	Chitosan	Chitosan-g-poly(N-isopropylacrylamide)	Thermal		Cardiac, cartilage TE	Baei et al., 2016; Mellati et al., 2017
		Methacrylated glycol chitosan		Photo	Bone TE	Kim et al., 2016
Synthetic and Hybrid Materials	PEG	Norbornene-terminated PEG		Michael addition	Cartilage, vascular TE	Mahadevaiah et al., 2015; Sridhar et al., 2015; Wang et al., 2017a
		Thiol-norbornene PEG, PEG diacrylate (PEGDA)		Photo	Cartilage TE Heart valve TE	Zhang et al., 2015; Neumann et al., 2016
	PAM/Gelatin	PAM and GelMA		Photo	Cartilage TE	Han et al., 2017
	PVA/Gelatin		Thermal		Cartilage TE	Kim et al., 2016
	PNIPAM/Gelatin	PNIPAAm-based copolymer, thiol-modified gelatin	Thermal	Michael addition	Cardiac TE	Navaei et al., 2016b
	PEG/Gelatin	PEG dimethacrylate, GelMA		Photo	Bone, cartilage TE	Gao et al., 2015
	PEG/Chitosan	Glycol chitosan, benzaldehyde functioned PEG		Schiff-base	Neural engineering, vascular TE	Tseng et al., 2015; Hsieh et al., 2017
	PEG/HA	Amino-terminated PEG, aldehyde HA		Schiff-base	Adipose TE	Fan et al., 2015b
		Furylamine and tyramine functional HA; Dimaleimide PEG		Diels-Alder/Enzymatic	Cartilage TE	Mahadevaiah et al., 2015
	Gelatin/HA	GelMA/MeHA		Photo	Skin, neural TE	Eke et al., 2017; Magarinos et al., 2018
	Gelatin/Alginate	Oxidized alginate, gelatin		Schiff-base	Muscle TE	Baniasadi et al., 2016
		GelMA and alginate		Photo	Bone TE	Lewandowska-Łancucka et al., 2017
		GelMA, alginate	Ionic	Photo	Bone TE	Pacelli et al., 2018

when using under physiological conditions. For instance, calcium crosslinked alginate hydrogel will lose stability in 0.9 wt% sodium chloride solution due to the exchange of calcium ions by sodium ions (Martinsen et al., 1989).

Guest-host chemistry

The guest-host chemistry holds great potential for hydrogels preparation, because the low cytotoxicity and specific selectivity. In this reaction, host molecules can selectively recognize and physically bind to certain guest molecules to form crosslinked network. The interaction includes hydrophobic association, hydrogen bonding, electrostatic interaction, van der Waals forces, and so on (Steed et al., 2007). Cyclodextrin, as one macrocycle, has hydrophobic interior cavities that have a high affinity for specific hydrophobic guest moieties. Specifically, guest–host pair, adamantane (guest) and β-cyclodextrin (host), is widely used to synthesize corresponding macromers. The guest-host bonding can translate mixed solution into hydrogels easily (Rodell et al., 2016). In another study, acrylate β-cyclodextrin can build guest-host binding with the benzene ring of gelatin to form supramolecular hydrogels. These hydrogels have very good bio-adhesive property and sustainable release of hydrophobic drugs, which is promising for TE of bone, cartilage and tendon (Feng et al., 2016).

Thermo-gelation

Thermo-gelation is to build a physically crosslinked network by altering the temperature. For example, the crystalline nature of PVA has been applied to fabricate physically crosslinked hydrogel by several repeating cycles of freezing and thawing (Hassan and Peppas, 2000). These physically crosslinked PVA hydrogels are reported to have many characteristics, such as high swelling degree and mechanical strength. Gelatin solution becomes hydrogel due to the intermolecular hydrogen bonding formation when the temperature drops below the upper critical solution temperature (UCST). In contrast, some other macromer, such as PNIPAM, becomes hydrogel when temperature increases above the lower critical solution temperature (LCST) due to the balance between hydrogen bonding and hydrophobic effects (Ashraf et al., 2016). These temperature-responsive polymers can transform phases between sol and gel near physiological temperature, which enables the hydrogels injectable. PNIPAM-based injectable hydrogel has been used to encapsulate cardiomyocytes and the encapsulated cells exhibit high viability and mature phenotypes (Navaei et al., 2016b).

Chemical Crosslinking Methods

Chemically crosslinked hydrogels have a better performance at stability than physically crosslinked hydrogels due to stronger binding energy and substantially improved flexibility. Hydrogel-forming water-soluble polymers have many functional groups, such as OH, COOH, and NH_2. 3D network can be established by covalent bonding between these functional groups using glutaraldehyde and EDC/NHS (Balakrishnan et al., 2013; Omobono et al., 2015; Cheaburu Yilmaz et al., 2017). However, the toxicity of crosslinking agents and process limit the TE

applications. For example, small molecular crosslinkers like glutaraldehyde and carbodiimides have been reported to be toxic and are not recommended to fabricate cell-laden hydrogels (Balakrishnan, 2016). To meet the requirements for TE, several available strategies for functional hydrogel preparation will be discussed below.

Photopolymerization

Photopolymerization has been widely used for hydrogel fabrications due to its biocompatibility and spatiotemporal controllability. Usually, macromers are modified with photoreactive moieties, such as methacrylate or acrylate groups. The photoreactive macromer solution with photoinitiator can be crosslinked under UV or visible light. The photoinitiators can generate free radicals that are transferred to the photoreactive carbon double bond groups in the modified macromers to start chain polymerization. However, under high photo exposure, photoinitiator will generate a large number of free radicals which may react with intracellular molecules to induce cell damage. This problem can be addressed by decreasing the light energy and amount of photoinitiator (Bryant et al., 2000; Fedorovich et al., 2009). High density of methacrylate groups has been reported to protect encapsulated cells by quenching free radicals (Bartnikowski et al., 2015). The method can be used for the preparation of hydrogels from various kinds of polymers and a variety of cell types can be encapsulated into the hydrogels for TE applications (Park et al., 2003; Chen et al., 2018). One of the most frequently used macromers is GelMA, which retains cell adhesive peptide sequence (arginine-glycine-aspartic acid, RGD) and matrix metalloproteinase (MMP) degradable peptide (Yue et al., 2015).

Enzyme-enabled crosslinking

Enzyme-enabled crosslinking is highly selective for a specific enzyme and can be achieved under mild physiological conditions (Ulijn, 2006). Transglutaminase and horse radish peroxidase are two commonly used enzymes. Transglutaminase catalyzes trans-amidation reaction that introduces N ϵ-(γ- glutamyl)lysine cross-links in proteins, converting protein solution into 3D hydrogel network (Chen et al., 2003). Horse radish peroxidase can build networks between polymers by oxidative coupling of hydroxyphenylpropionic acid moieties (Wang et al., 2014). Besides selectivity, this enzyme-mediated crosslinking approach also exhibits rapid gelation and easily tunable mechanical properties by varying the concentration of horse radish peroxidase and H_2O_2 (Ren et al., 2015).

Click chemistry

Click chemistry has the characters of high efficiency, high yield, and proceeding with no side products, which make the method wildly studied. TE application requires the reaction to proceed under physiological conditions. The typical click reaction is thiol-ene radical reaction which is hindered by inhibitory capacity of oxygen and shows complicated volume relaxation and stress development compared with classical radical photopolymerization (Hoyle and Bowman, 2010). Other representative chick chemistry includes Diels-Alder reaction,

azide-alkyne cycloaddition chemistry (Xu and Bratlie, 2018) and Michal addition. Strain-promoted azide-alkyne cycloaddition (SPAAC) click chemistry has drawn increasing attention recently due to the mild reaction conditions and bioorthogonality (Xu et al., 2014). An injectable and degradable PEG-based hydrogel has been prepared via the bioorthogonal SPAAC click chemistry (Jiang et al., 2015). Michael addition reaction is the nucleophilic addition of a carbanion or a nucleophile to an α, β-unsaturated carbonyl compound. Michael addition-mediated hydrogels can be prepared under physiological conditions, making this kind of hydrogels injectable (Sun et al., 2017). For example, HA with thiol functional groups can form a 3D network with PEG vinylsulfone macromers via Michael addition. The gelation time can be controlled by the degree of functionalization and the ratio of the two functional groups (Jin et al., 2010).

Schiff base reaction

Schiff base reaction has been widely used to form hydrogels via the coupling between aldehyde and amine groups in polymer chains. These hydrogels have been reported to have self-healing capacity due to the dynamic equilibrium of the linkages. For example, glycol chitosan and benzaldehyde functioned PEG have been synthesized and used to form a hydrogel with self-healing property for central nervous regeneration (Tseng et al., 2015). Proliferation rate and differentiation tendency of neurosphere-like progenitors are enhanced in the self-healing hydrogel.

The above-described materials and crosslinking reactions have their respective merits and demerits. While, rational combination of natural and synthetic polymers or different crosslinking methods may afford an optimized approach to improve the hydrogel functions. For example, enzymatic crosslinking and Diels-Alder click chemistry can be induced into HA/PEG hydrogels for cartilage TE (Mahadevaiah et al., 2015). Both biocompatibility and mechanical property are improved by blending of HA and PEG polymers. The enzymatic crosslinking provides a suitable gelation speed for injectability, while the click reaction generates second crosslinking that renders an outstanding shape memory and anti-fatigue property. All these characters are required for cartilage TE.

CONTROL OF PHYSICAL PROPERTIES

Physical properties of hydrogels, such as mechanical strength, stiffness, stress relaxation, self-healing, and degradation, can be controlled at different levels to meet the specific requirements for TE. These physical properties have obvious effects on cell functions, and thus should be investigated and reviewed. The hydrogels prepared with different physical properties, and their effects on cell functions, as well as their applications for TE are summarized in **Table 2**.

Mechanical Strength and Stiffness

Conventional hydrogels normally possess breakable characters that will decrease their stability and thus cannot be utilized for specific tissue application such as bone, cartilage and tendon. To overcome this issue, two effective strategies have been developed. One is the hybridization of hydrogels with other polymers,

nanoparticles or nanofibers. For example, regenerated silk fibroin and chitin nanofiber have been used to improve the mechanical strength of GelMA hydrogels by β-sheet folding and self-assembly, respectively. The hydrogel elastic modulus increases by one-thousand folds and strain-to-failure enhances by around 200% after chitin nanofiber assembly (Hassanzadeh et al., 2016). The hydrogels also demonstrate good cell viability, promotive cell differentiation and stable vasculature formation. Collagen-based hydrogels with a 10-fold increase in stiffness have been realized after mixing with very low amount of chemical functionalized nanoparticles working as crosslinker epicenters to make collagen chains crosslinked on the surface of nanoparticles (Jaiswal et al., 2015). Due to the interaction between nanoparticles and polymer chains, the mechanical properties of hybrid hydrogels can be enhanced. The other strategy is to prepare interpenetrating polymer network (IPN) hydrogels with high resistance to wear and high fracture strength, which has gained a lot of attention recently (Dragan, 2014). Double networks (DN) are introduced in hydrogels to enhance mechanical property for cartilage TE (Gong et al., 2003; Yasuda et al., 2009; Fukui et al., 2014). The feature of DN hydrogels is the formulation of first densely crosslinked hydrogel and second loosely network. The first network serves as sacrificial bonds to disperse the stress, while the second polymer chains work as hidden length that can extend to sustain large deformation (Haque et al., 2012). Similarly, ionic crosslinked chitosan with low molecular weight is used to work as the second crosslinking component to enhance the mechanical strength of the UV initiated PAM hydrogel (Yang et al., 2018).

Macroscopically, the mechanical property is important to maintain the scaffold stability to bear loads and fulfill the defects. Meanwhile, at microscopic level, the mechanical signals play a critical role in affecting cell activities and fates. For example, matrix stiffness has been reported to affect cell spreading, migration, proliferation and differentiation (Wen et al., 2014). Stiffness of hydrogels can be tuned by changing the crosslinking density, crosslinker length and molecular weight of the precursors (Slaughter et al., 2009; Li et al., 2016, 2017b). Differentiation of mesenchymal stem cells (MSCs) cultured on 2D matrix surface depends on substrate stiffness (Engler et al., 2006). MSCs cultured in hydrogels with stiffness of lower (0.1–1 kPa), intermediate (8–17 kPa) or higher ranges (34 kPa) can differentiate into neural, myogenic or osteogenic phenotypes, respectively. However, the microenvironment provided to the cells in 3D culture differs from that in the traditional 2D system (Baker and Chen, 2012). Osteogenic differentiation of murine MSCs is enhanced in RGD modified alginate, agarose and PEG diacrylate (PEGDA) with intermediate stiffness (11–30 kPa) (Huebsch et al., 2010) (**Figure 1A**). Influence of stiffness on chondrogenic, vascular and neural differentiation has also been studied (Banerjee et al., 2009; Bian et al., 2013; Mahadevaiah et al., 2015). For instance, to investigate the influence of stiffness on the maintaining of chondrocyte phenotype, GelMA hydrogels with different stiffness but the same RGD density are prepared by changing the degree of methacryloyl substitution while using the same GelMA concentration. Bovine articular chondrocytes are encapsulated and cultured in the GelMA hydrogel with low, medium and high stiffness. The chondrocytes encapsulated in

TABLE 2 | Physical properties of hydrogels and their performance as TE scaffolds.

Physical properties	Materials	Approaches	Applications and performance	References
Mechanical strength	GelMA	Chitin nanofibers, Nanoparticles blending	Strain-to-failure increased 200% after chitin nanofiber assembly; stiffness of collagen-based hydrogel increased 10-fold after addition of functionalized nanoparticles.	Jaiswal et al., 2015; Hassanzadeh et al., 2016
	PAMPS/PDMAAm	Double network	High strength PAMPS/PDMAAm gel could induce spontaneous hyaline cartilage regeneration in the osteochondral defect.	Yasuda et al., 2009; Fukui et al., 2014
Stiffness	RGD modified alginate, agarose, and PEGDA	Tuning of Ca^{2+} or polymer concentration	Intermediate stiffness promoted the osteogenic differentiation of murine MSCs.	Huebsch et al., 2010
	Four-arm maleimide-functionalized PEG and four-arm thiol-functionalized PEG	By using different PEG concentration	The proliferation, self-renewal and vascular differentiation of stem cells were enhanced in lower stiffness hydrogel.	Mahadevaiah et al., 2015
	MeHA	Tuning of macromer concentration or UV exposure time	Low stiffness of HA hydrogel promoted chondrogenic differentiation of MSCs. Highly crosslinked HA hydrogel promoted hypertrophic conversion of encapsulated MSCs.	Bian et al., 2013
	Gel-HPA	Altering macromer and/or H_2O_2 concentration	Medium stiffness showed superior stimulus for maintaining of chondrogenic phenotype, high stiffness promoted collagen type II gene expression.	Wang et al., 2014
	GelMA	Using the same macromer concentration with different methacryloyl substitution	High stiffness environment was beneficial for maintaining of chondrogenic gene expression.	Li et al., 2016
Stress relaxation	RGD-alginate	Tuning of stress-relaxation by using alginate with different molecular weight or PEG spacer	Fast stress relaxation promoted MSC spreading and osteogenic differentiation.	Chaudhuri et al., 2016
	Alginate	Same as above	Slow relaxing environment restricted cell volume expansion, up-regulated the gene related to matrix degradation and cell death.	Lee et al., 2017
	HA, Collagen I	Dynamic crosslinking of HA-ALD and HA-BLD, combined with collagen	Fast relaxation promoted cell spreading and focal adhesion formation.	Lou et al., 2018
Self-healing	Glycol chitosan, benzaldehyde functioned PEG	Reversible Schiff-base reaction	Self-healing hydrogel could increase proliferation and neural differentiation of neural stem cells, and enhanced capillary inducing capacity of vascular endothelial cells.	Tseng et al., 2015; Hsieh et al., 2017
		Dynamic acylhydrazone bond and DA click covalent crosslinking	Increasing the viability, decreasing apoptosis of MSCs and promoting bone regeneration	Lü et al., 2017
Degradation	GelMA	Collagenase degradable photocrosslinked gelatin hydrogel	Valvular interstitial cells had more spreading morphology in collagenase treated GelMA hydrogel than untreated hydrogel.	Benton et al., 2009
	Sulfated HA	Slowing the degradation of HA hydrogel by sulfated modification	The low degradation was beneficial for chondrogenesis of MSCs.	Feng et al., 2017
	HA functionalized with both maleimide and methacrylate	Thiol-ene crosslinking via MMP degradable crosslinker and photocrosslinking	Differentiation of MSC was directed by degradation-mediated cellular traction.	Khetan et al., 2013
	PEG-derivative	Hydrogel crosslinked by PEG derivative containing nitrobenzyl ether moieties could be degradable by photo exposure.	MSC spreading was enhanced after photodegradation.	Kloxin et al., 2010
	PEG-derivative	Modification of ends of PEG with oligo (lactic acid) and acryloyl, hydrolysis of the ester bonds altered the degradation	The high degradation enhanced osteogenesis of MSCs.	Peng et al., 2018
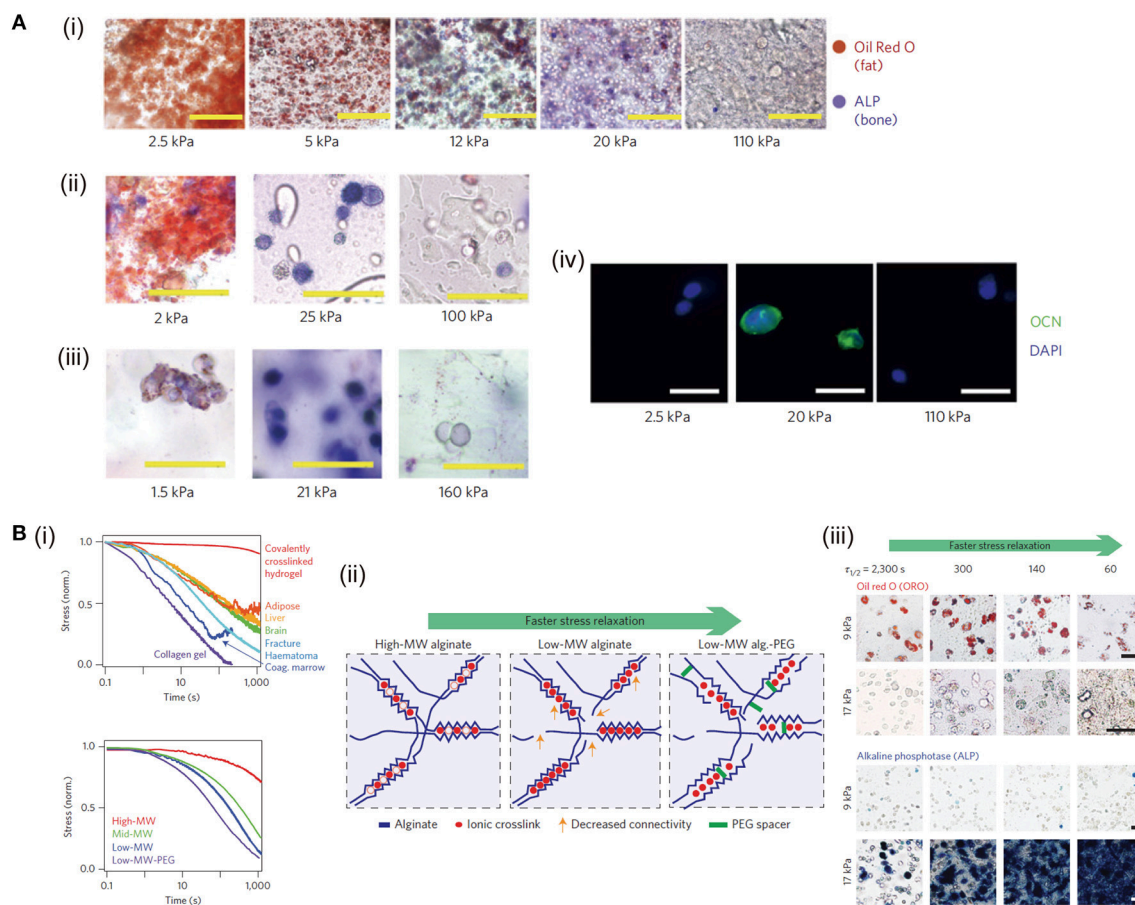
FIGURE 1 | Control of stiffness and stress relaxation of hydrogels and their influence on cell functions: **(A)** MSC differentiation affected by the stiffness of RGD-modified alginate (i), RGD-modified agarose (ii), and RGD-modified PEGDA (iii) hydrogels. Alkaline phosphatase (ALP) activity (fast blue; osteogenic biomarker, blue) and neutral lipid accumulation (oil red O; adipogenic biomarker, red) staining of MSCs after 1 week of culture. Osteocalcin (OCN, green) and nuclear counterstain 4′,6-diamidino-2-phenylindole (DAPI, blue) staining in alginate hydrogel (iv). Scale bars: (i) 100 μm, (ii)–(iii) 50 μm and (iv) 20 μm, respectively. Reproduced with the permission from Huebsch et al. (2010), Copyright © 2010, Springer Nature. **(B)** Stress relaxation properties of living tissues and prepared hydrogels (i). Decreasing molecular weight (MW) of alginate and coupling PEG spacers both are predicted to increase the rate of stress relaxation (ii). MSCs cultured in hydrogels at indicated initial modulus and timescale of stress relaxation undergo adipogenic and osteogenic differentiation (Oil Red O staining and alkaline phosphatase staining) for 7 days (iii). Scale bars are 25 μm. Reproduced with the permission from Chaudhuri et al. (2016), Copyright © 2016, Springer Nature.

high stiffness hydrogel exhibit round cell morphology and high chondrogenic gene expression, while chondrocytes cultured in low stiffness counterparts show elongated morphology and low chondrogenic gene expression (Li et al., 2016).

Stress Relaxation

Stress relaxation is another important mechanical property for hydrogels, which also is a common behavior of tissue matrix. It has been reported that ionic and covalent hydrogels both exhibit stress relaxation through uncoupling-reforming of crosslinks and migration of water, respectively (Zhao et al., 2010). Ionic hydrogels have faster stress relaxation and easier modulation than that of covalent hydrogels. Sodium alginate has been commonly used to form hydrogels with tunable stress relaxation. In a previous study, RGD modified alginate has been used to prepare soft but highly stress-relaxing substrate. Cells cultured in this substrate spread similarly to the cell on the surface of stiff elastic substrates (Chaudhuri et al., 2015). The stress relaxation of covalently crosslinked PAM hydrogel, physically crosslinked collagen hydrogel and living tissues like adipose, liver, brain and an initial fracture haematoma are compared by measuring the stress change when fixing the strain at 15% (Chaudhuri et al., 2016). The results indicate that the stress relaxation of collagen hydrogel is faster than that of living tissues and PAM hydrogel, while that of PAM is slowest. RGD coupled alginate with different molecular weights and PEG spacers are used to prepare hydrogels with different stress relaxation properties independent of initial elastic modulus and matrix degradation. Fast stress relaxation enhances cell spreading, proliferation and osteogenic differentiation of stem cell through integrin-RGD binding and clustering (**Figure 1B**). Stress relaxation has also been demonstrated to have the capability to alter chondrocyte phenotype and matrix deposition via modulating cell volume expansion (Lee et al., 2017). Slow relaxing environment restricts

cell volume, leading to interleukin-1β secretion increase, which in turn up-regulates the genes related to matrix degradation and cell death. To fully mimic the mechanical and structural cues of native ECM, HA crosslinked with dynamic covalent bonds and fibrillar collagen type I are used to prepare IPN hydrogel with tunable stress relaxation (Lou et al., 2018). Cell spreading, fiber remodeling and focal adhesion formation are enhanced in the faster relaxation hydrogels.

Self-Healing

Self-healing hydrogel is able to intrinsically and automatically heal the breaks, making itself back to original shape and mechanical property. This property is directly based on the reversible or dynamic crosslinking chemistry (Taylor and in het Panhuis, 2016). One of the representative self-healing hydrogels is prepared by glycol chitosan and benzaldehyde functionalized PEG via Schiff-base reaction (Tseng et al., 2015). The proliferation rate and differentiation tendency of neurosphere-like progenitors cultured in this self-healing hydrogel are enhanced (**Figure 2A**). Thrombin crosslinked fibrinogen can build a 3D network structure, which is used to prepare IPN structure after mixing with the above-mentioned chitosan-PEG hydrogel (Hsieh et al., 2017). This hydrogel encapsulated with vascular endothelial cells shows excellent self-healing and capillary-inducing capacity. Injection of this

hydrogel promotes angiogenesis in zebrafish and mice. Dynamic acylhydrazone bond and Diels-Alder click covalent crosslinking are combined to prepare self-healing hydrogels with desirable mechanical property (Lü et al., 2017). These hydrogels increase the viability, reduces apoptosis of MSCs, and enhances bone regeneration in cranial bone defects. Guest-host crosslinking has also been used to prepare self-healing hydrogels. Cyclodextrin conjugated in one polymer backbone can work as the host to engulf hydrophobic moieties of another polymer chain to achieve self-healing. This self-healing property can further be selectively improved when the stimuli-responsive moiety, such as polyacrylamide-ferrocene with a reversible hydrophobic-charge transition at reduced/oxidized state, is included in the above hydrogels (Nakahata et al., 2011).

Degradation

Covalently crosslinked hydrogels can undergo degradation through ester hydrolysis, enzymatic hydrolysis or photolytic cleavage of the polymer chains (Kharkar et al., 2013). Based on these mechanisms, hydrogels could be designed with good biodegradability and desirable degradation rate, working as temporary supports and being degraded and replaced by the regenerating tissues gradually (Bryant et al., 2004). For example, the photocrosslinkable PVA/PEG hybrid hydrogels with controlled degradation profiles have been used for cartilage TE.
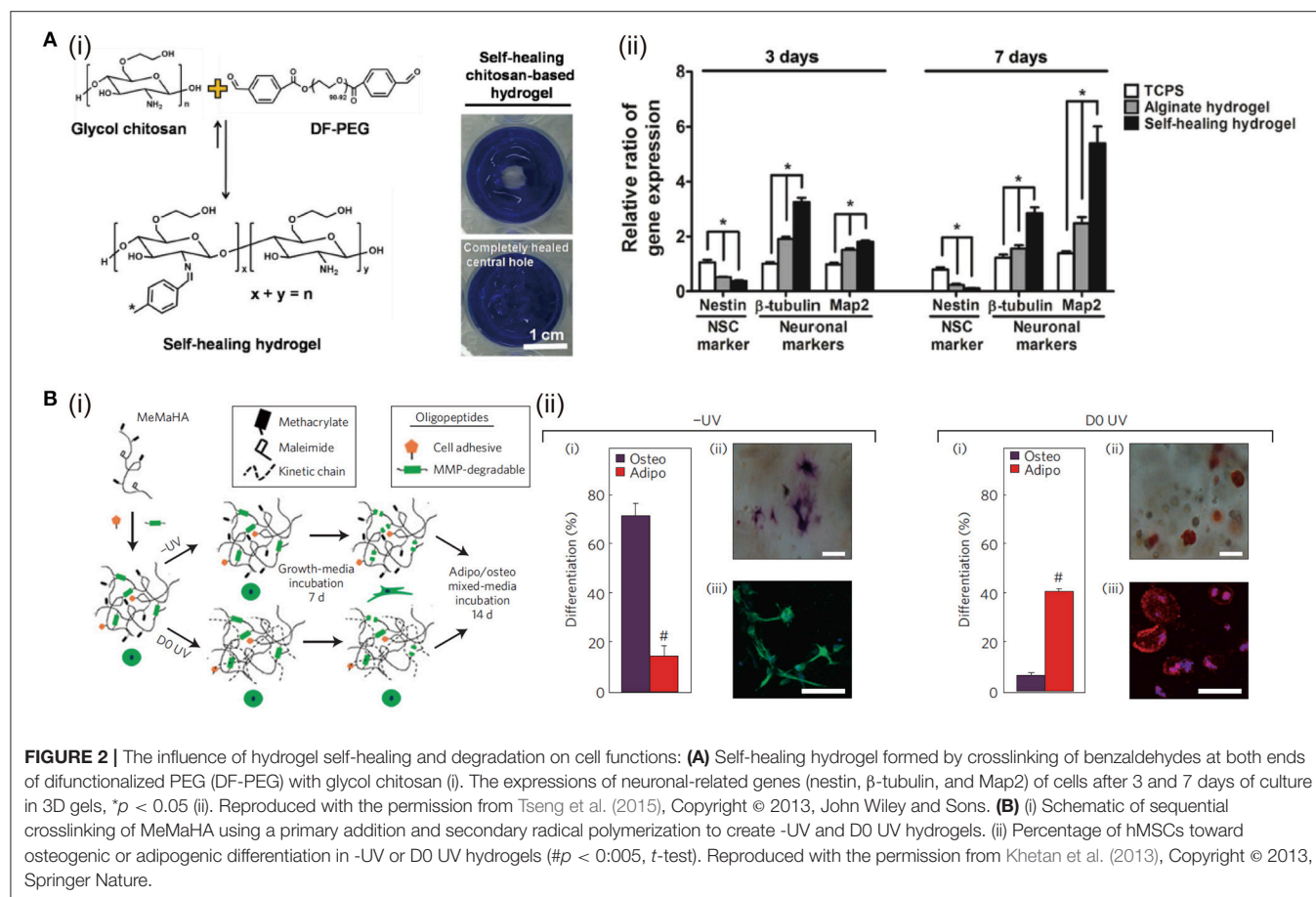
FIGURE 2 | The influence of hydrogel self-healing and degradation on cell functions: **(A)** Self-healing hydrogel formed by crosslinking of benzaldehydes at both ends of difunctionalized PEG (DF-PEG) with glycol chitosan (i). The expressions of neuronal-related genes (nestin, β-tubulin, and Map2) of cells after 3 and 7 days of culture in 3D gels, *$p < 0.05$ (ii). Reproduced with the permission from Tseng et al. (2015), Copyright © 2013, John Wiley and Sons. **(B)** (i) Schematic of sequential crosslinking of MeMaHA using a primary addition and secondary radical polymerization to create -UV and D0 UV hydrogels. (ii) Percentage of hMSCs toward osteogenic or adipogenic differentiation in -UV or D0 UV hydrogels (#$p < 0:005$, t-test). Reproduced with the permission from Khetan et al. (2013), Copyright © 2013, Springer Nature.

The degradation time can be tuned from less than 1 to 34 days by altering the ratio of PVA to PEG. The results show that the DNA and GAG contents increase with culture time and the neocartilaginous tissue at 6 weeks is homogeneously distributed in the PVA/PEG hydrogel with the ratio of 1:3, indicating the importance of degradation for TE (Martens et al., 2003). When implanted *in vivo*, HA-based hydrogel often shows too fast degradation to meet the requirement for cartilage tissue repair. To solve this limitation, sulfate groups are conjugated to HA to decelerate the hyaluronidase degradation rate. Sulfated HA displays slow degradation and enhances protein binding ability, promoting chondrogenesis of hMSCs with reduced hypertrophy (Feng et al., 2017).

Degradation of the hydrogel is a chemical process, but it can work as a dynamically physical stimulus to affect cell behaviors and functions for cell-matrix interaction, such as cell spreading, migration, proliferation, and differentiation, to further mimic the native ECM and improve the tissue regeneration. For example, photo-responsive hydrogels can be prepared from PEG derivatives containing nitrobenzyl ether photolabile moieties. When human mesenchymal stem cells (hMSCs) are cultured in the photodegradable hydrogel, cell spreading is enhanced after light exposure (Kloxin et al., 2010). Degradation of hydrogel is always accompanied with decrease of stiffness, making it complicated to discriminate the influences of degradation and stiffness. To decouple the influence from mechanical property of degradable hydrogels, hydrogels are designed to degrade while their mechanical properties remain unchanged. For example, HA functionalized with both maleimide and methacrylate is used to prepare hydrogels by thiol-ene crosslinking via MMP degradable crosslinker and photo-initiated crosslinking of the methacrylate. The MMP-cleavable peptide crosslinker permits cell-mediated degradation. The photo-initiated crosslinking can dynamically control the secondary crosslinking at the very beginning or

after a period of cultivation. The stiffness of hydrogels with or without UV exposure is controlled at the same level by changing the molecular weight of HA macromers. When hMSCs are cultured in the tuned hydrogels, they exhibit different osteogenic and adipogenic differentiation. The results indicate that hMSCs differentiation is directed by degradation-mediated cellular traction, independent of the matrix mechanics. (Khetan et al., 2013) (**Figure 2B**).

CONTROL OF CHEMICAL PROPERTIES

The composition of hydrogels can highly affect the cell behaviors including viability, adhesion, spreading, proliferation, and differentiation (Ruoslahti and Pierschbacher, 1987). Hydrogel composition can be controlled by choosing different precursors and preparation methods. The methods used to tune chemical properties of functional hydrogels are summarized in **Table 3**.

Cell adhesion ligand is a crucial biochemical component in ECM, because many types of cells have to adhere to their microenvironment through cell surface integrin to perform the relative functions and maintain their viability (Huettner et al., 2018). Naturally derived proteins, like collagen and gelatin, retain many cell adhesion ligands. However, polysaccharide-based natural materials and synthetic polymers are lack of these ligands. Hence, bioactive peptide modification has been used to improve the biochemical property of non-adhesive hydrogels. RGD peptide, as one of the potent adhesion ligands, plays an important role on cell adhesion and other functions. To study the impact of dynamic presentation of RGD in matrix on cell functions, a light-responsive PEGDA hydrogel is synthesized, in which a protecting group is used to temporally and spatially control the RGD presentation by transdermal light exposure (**Figure 3A**). PEGDA hydrogels

TABLE 3 | Control of chemical properties of hydrogels for TE applications.

Original hydrogels	Approaches	Applications and Performance	References
HA, alginate, chitosan, and PEG	Modifying hydrogel precursors with RGD peptides	Promoted cell adhesion and viability, enhanced cell proliferation and differentiation	Lee et al., 2015; Kim et al., 2016; Long et al., 2017; Sun et al., 2017
Polyacrylamide	Hybridization with GelMA	Improved biocompatibility of synthetic hydrogels	Han et al., 2017
PEG	Hybridization with HA	Increased chondrocyte number and sGAG and collagen production	Skaalure et al., 2014; Fu et al., 2017
PEG	Covalently tethered transforming growth factor-beta 1 (TGF-β1) to PEG hydrogel through thiol-ene reaction	Increased chondrogenic matrix deposition by immobilization of TGF-β1	Sridhar et al., 2014; Mao et al., 2017
GelMA	Hybridization with nanosilicates	Promoted osteogenic differentiation of preosteoblasts in a growth-factor-free microenvironment	Xavier et al., 2015
GelMA Collagen/Alginate	Hybridization with multiwalled CNTs Gold nanorod	Improved cell adhesion and maturation; enhanced cardiac tissue regeneration, exhibiting strong spontaneous and stimulated synchronous beating	Shin et al., 2013; Navaei et al., 2016a; Izadifar et al., 2018
Polyacrylamide	Hybridization with graphene oxide	Enhanced proliferation and myogenic differentiation of C2C12 cells, and combining electrical stimulation further enhanced myogenic gene expression	Jo et al., 2017

with RGD peptides and light-induced uncaged RGD peptides support high number of adherent cells. On the other hand, PEGDA hydrogels without RGD modifications or with caged RGD support few adherent cells and the cells have round morphology. Besides, it has been reported that RGD peptides can be introduced to polymers, such as HA (Lee et al., 2015), alginate (Sun et al., 2017), chitosan (Kim et al., 2016), and PEG (Long et al., 2017), by chemical binding to fabricated bioactive hydrogels. These functionalized hydrogels show improved biological properties to promote cell adhesion, spreading, proliferation, and differentiation. For instance, RGD peptides promote the survival of MSCs in PEG hydrogels and induce the chondrogenic differentiation (Salinas and Anseth, 2008). RGD ligands in hydrogels increase the chondrogenic gene expression when the hydrogel matrices are loaded with dynamic mechanical force (Steinmetz and Bryant, 2011). Moreover, RGD density affects the redifferentiation of chondrocytes (Schuh et al., 2012).

Hybridization with natural polymers is another facile way to tune the biochemical property of hydrogels, which can change the composition of hydrogels in favor of promotion of cell function and TE. For example, GelMA is used to hybridize with PAM to prepare a photopolymerized hydrogel for cartilage tissue regeneration. Cells cultured in the hybrid hydrogel exhibit higher viability and proliferation rate than those cultured in pure PAM hydrogel (Han et al., 2017). What's more, HA/PEG hybrid hydrogel prepared via the SPAAC crosslinking shows excellent biocompatibility (Fu et al., 2017), which may be due to the fact that HA can bond to some receptors on cell membrane to affect both chondrocyte survival pathway and apoptotic pathway (Knudson and Knudson, 2004).

Besides hybridization with natural polymers or modification with biological moieties to improve the biochemical properties of hydrogels for TE, loading of growth factors and nanoparticles have been frequently adapted to improve hydrogel functions. Growth factors play important roles in cell growth, cell function determination, tissue regeneration, and organ development (Parker et al., 2016; Yan et al., 2018). Therefore, immobilization of growth factors in hydrogels will significantly improve the functionality of hydrogels. There are two strategies for
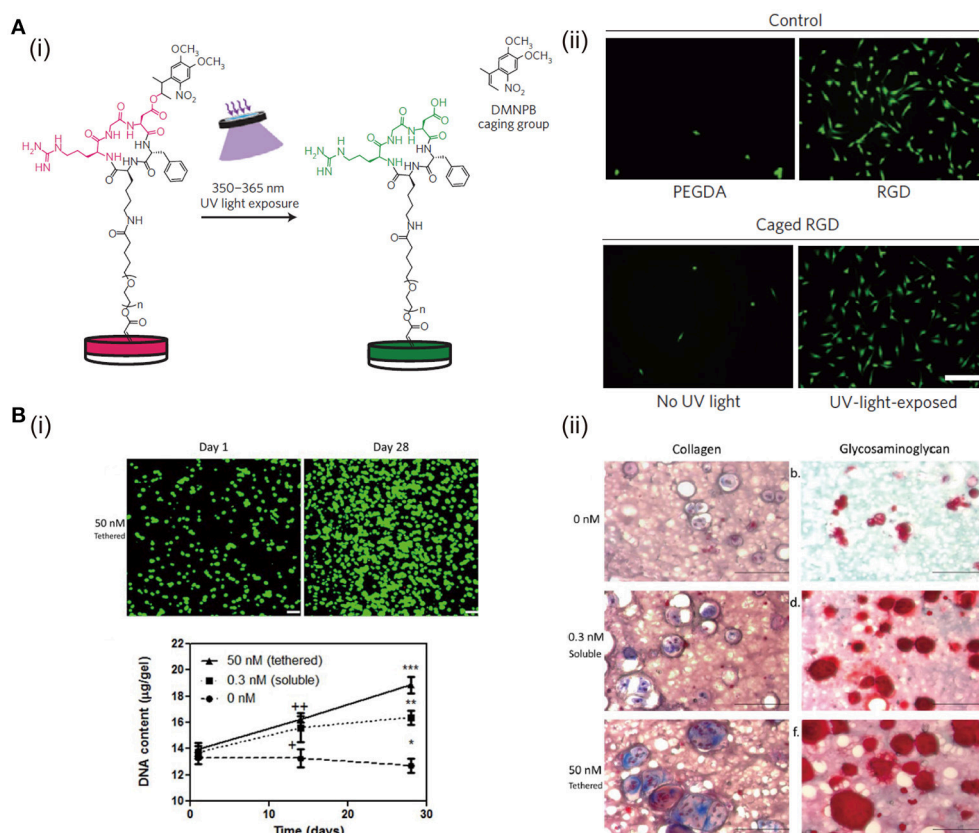
FIGURE 3 | The effects of RGD peptides and growth factors in hydrogels on cell functions: **(A)** Schematic representation of the activation of caged RGD peptides in PEGDA hydrogels under light exposure (i). Cell adhesion and spreading can be enhanced after culture in hydrogels with RGD peptides and UV-light-exposed caged RGD peptides (ii). Reproduced with the permission from Lee et al. (2015), Copyright © 2015, Springer Nature. **(B)** ECM production of chondrocytes is enhanced after culture in PEG hydrogels with covalently tethered TGF-β. DNA content of chondrocytes exposed to 50 nM tethered TGF-β is the highest (i). Chondrogenic matrix (collagen and glycosaminoglycan) deposition is enhanced when exposing to TGF-β. The matrix produced in 50 nM (tethered) group is higher than that in 0.3 nM (soluble) group (ii). Reproduced with the permission from Sridhar et al. (2014), Copyright © 2014, John Wiley and Sons.

immobilizing growth factors in hydrogels, namely physical, and chemical immobilization (Nguyen and Alsberg, 2014). Heparin can bind many types of growth factors through the strong electrostatic interactions. The immobilization of fibroblast growth factor-2 and vascular endothelial growth factor in heparin-modified PEG hydrogels has been shown to boost angiogenesis (Zieris et al., 2010). Compared with physical immobilization, chemical immobilization can further improve the stability, prolong the release of growth factors, and reduce the required amount. For example, transforming growth factor-beta 1 (TGF-β1) is covalently tethered to PEG hydrogel through thiol-ene reaction (Sridhar et al., 2014; Mao et al., 2017). Chondrocytes cultured in PEG hydrogel immobilized with TGF-β1 show higher DNA content and chondrogenic matrix production than the cells cultured in PEG hydrogel with soluble TGF-β1 (**Figure 3B**).

A variety of nanoparticles have also been incorporated into different kinds of natural or synthetic polymer networks to prepare nanocomposite hydrogels for TE. The incorporation of nanoparticles can provide not only higher mechanical properties, but also the possibility to tune biochemical characteristics of the 3D network. For examples, nanosilicates are incorporated into GelMA hydrogels to obtain a bioactive nanocomposite (Xavier et al., 2015). Not only the mechanical strength of the hydrogel is enhanced, osteogenic differentiation of preosteoblasts is also promoted (**Figure 4**). In another study, nanosized hydroxyapatite is incorporated into a PEG hydrogel aiming to produce highly tough matrix for bone TE. After incorporation, the morphologies of these hydrogels show highly interconnected porous structures. What's more, the presence of hydroxyapatite nanoparticles can provide osteoblast cells adhesion and bioactive attachment sites compared with pure PEG hydrogels (Gaharwar et al., 2011). For cardiac tissue regeneration, conductive nanoparticles like carbon nanotubes are added into GelMA hydrogels, resulting in improved cell adhesion and maturation (Shin et al., 2013). The percentage of cell retention and viability on carbon nanotubes nanocomposite GelMA hydrogel is higher than those on pristine GelMA. The mature cell/hydrogel sheet with very good electrophysiological and mechanical properties exhibits strong spontaneous and stimulated synchronous beating.

STRUCTURAL CONTROL OF HYDROGELS

Microstructure is another critical factor to affect cell activities and functions because the optimized architecture of engineered tissue has the function to organize multiple cell types for TE (Stevens et al., 2013). Hydrogels with microarchitectures are briefly classified into microporous, channel-bearing, double-ring, multilayered, and hierarchically structured ones. The structure types of functional hydrogels and their influence on cell functions and tissue regeneration are summarized in **Table 4**.

Microporous Hydrogels

The structure of bulk hydrogels is dense polymers with absorbed water and nano-sized pores within the network (Hoffman, 2012), in which, the nano-sized pores are too small to promote cell migration, proliferation and ECM diffusion. Thereby,

FIGURE 4 | Schematic illustration of fabrication of nanocomposite hydrogels from GelMA and nanosilicates by photocrosslinking **(A)**. Nanosilicate-loaded gelatin hydrogels can support cell adhesion and spreading (live/dead staining) and enhance inorganic calcium deposition in normal and osteoconductive media (Alizarin Red S staining) **(B)**. Reproduced with the permission from Xavier et al. (2015), Copyright © 2015, American Chemical Society.
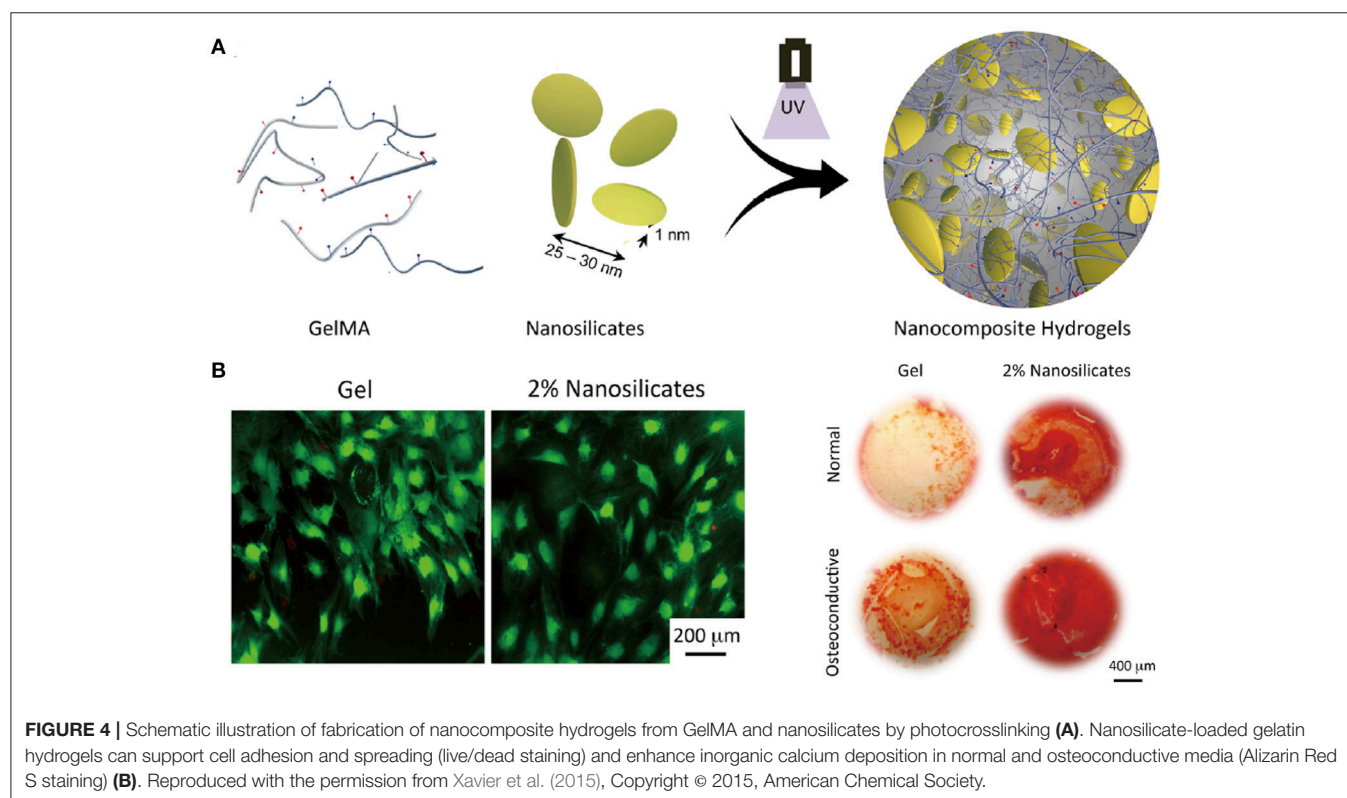
TABLE 4 | Structural control of hydrogels and TE applications.

Structural hydrogels	Materials	Approaches	Applications and Performance	References
Porous structure	Alginate HA	Mixing with gelatin particles prepared by water/oil emulsion	Chondrogenic matrix secretion and gene expression were improved in alginate and HA porous hydrogels.	Fan and Wang, 2015; Leong et al., 2016
	GelMA	Mixing with gelatin cubes prepared by mesh-cutting	Chondrocytes migration and proliferation were enhanced in porous structures.	Li et al., 2017a
	GelMA	Gelatin, alginate, and HA porogens prepared by water/oil emulsion can be degraded to specific stimuli including temperature, chelating and enzymatic digestion, respectively.	Increased cell proliferation and spreading, and enhanced type II and X collagen production happened in the hydrogel with dynamic pore formation	Han et al., 2013
Channel structure	2-hydroxyethyl methacrylate, agarose or GelMA	Embedding PVA sacrificial templates	High cell viability in bulk hydrogel was achieved by this channel structures.	Tocchio et al., 2015
	Gelatin	Embedding and dissolving solvent-spun PNIPAM microfibers		Lee et al., 2016
	Agarose/alginate/PEG/ Fibrin/Matrigel	Carbohydrate-glass fibers were 3D printed and removed after surround hydrogel formation.	Good biocompatibility and enhanced nutrition diffusion.	Miller et al., 2012
Double-ring structure	GelMA and hydroxyapatite	Osteon-like concentric double-ring structure was prepared via photolithography and self-assembly.	HUVECs and MG63s were encapsulated in the inner and outer ring, working as blood vessel tubule and bone, respectively.	Zuo et al., 2015; Wei et al., 2017
Bilayered structure	Transglutaminase factor XIII crosslinked PEG hydrogels	Chondrocytes and MSCs were encapsulated in different hydrogel layers functionalized with TGF-β3 or BMP-2.	Endochondral bone or stable cartilage can be developed at an ectopic site without the need of a predifferentiation process *in vitro*.	Stüdle et al., 2018
	Agarose	Chondrocytes and MSCs were encapsulated in the top and bottom layer agarose hydrogel for osteochondral TE.	Coculture of chondrocytes and MSCs in different environment showed potential for osteochondral TE.	Sheehy et al., 2013
	PEG-derivative	Top layer with low RGD concentration and soft stiffness was designed for chondrogenesis of MSC; bottom layer was prepared with high RGD concentration and high stiffness for osteogenesis of MSC.	Spatial presentation of physiochemical cues combined with dynamic mechanical stimulation could regulate the differentiation of MSCs.	Steinmetz et al., 2015
Hierarchical structure	PEG-derivative	Hierarchical vessels were fabricated by multiphoton lithography.	Human bone marrow-derived hS5 stromal cells exhibited high viability for a long culture period.	Arakawa et al., 2017
	POMaC and collagen	POMaC made scaffold with nanopores and micro-holes was prepared by using 3D stamping technique.	The incorporation of nanopores and micro-holes enhanced permeability, and permits intercellular crosstalk and extravasation.	Zhang et al., 2016

microporous structures have been proposed. The effects of different pore structures and pore size ranges have been studied for cell culture and TE (Zhang et al., 2014; Chen et al., 2016). Various technologies including solvent casting, particle leaching, freeze-drying, and gas foaming can be used to adjust hydrogel porosity (Annabi et al., 2010). Among them, stimuli-responsive porogens, such as gelatin, alginate and HA, are used to create cell-laden hydrogels with tunable porosity. These porogens can be removed by specific stimuli including temperature, chelating, and enzymatic digestion, respectively (Han et al., 2013). Similarly, gelatin microspheres fabricated by water/oil emulsion are used to generate micropores in alginate (Leong et al., 2016) and HA (Fan and Wang, 2015) hydrogels. Plenty

of micropores are left after gelatin microbeads are dissolved at 37°C. Chondrocytes cultured in the porous hydrogels show high proliferation and ECM secretion. Gelatin microparticles have also been used to prepare microporous hydrogels for bone TE (Vo et al., 2016). The pore-forming gelatin microparticles can be used not only for generation of micropores, but also for introduction of living cells in the micropores. Cell-laden gelatin microcubes are prepared by a mesh-cutting method and used to prepare microporous hydrogels with promotive capacity of cell proliferation (Li et al., 2017a). Chondrocytes cultured in the microporous hydrogels show high proliferation and cells prefer to migrate into the microporous cavities (**Figure 5A**).

Channel-Bearing Hydrogels

Cells must reside with $100–200\,\mu m$ from adjacent capillary blood vessels to remain viable or else they will undergo necrosis due to insufficient oxygenation and nutrition diffusion (Carmeliet and Jain, 2000). Therefore, hydrogels with micro-channels are highly needed to vascularize artificial tissue or study cell behaviors in a vascular structure, in particular for the regeneration of large and complex tissues and organs. Multiple strategies and techniques have been developed for preparation of channel-bearing hydrogels for TE applications.

PVA-based sacrificial templates are fabricated into branched fluidic architectures by casting (Tocchio et al., 2015). The architecture obtained after washing exhibits promoted regeneration of hierarchically branched endothelium and high cell viability inside bulk hydrogels formed by 2-hydroxyethyl methacrylate, agarose or GelMA. To prepare

a complex capillary-like micro-channel vascular structure, solvent-spun PNIPAM microfibers are fabricated and used as temperature-responsive templates (Lee et al., 2016). The PNIPAM microfibers are spun and maintained at a temperature above $32°C$. Cell-suspended gelatin precursor solution is kept at $37°C$ prior to embedding the templates. After complete gelation of the gelatin hydrogel, the PNIPAM microfibers are removed by immersion in cell culture medium at room temperature to generate the capillary-like micro-channel vascular structure. Cell viability is higher than 96% during 7 days of cultivation in the perfused micro-channel hydrogel. Carbohydrate-glass microfibers are printed to induce vascular architecture in bulk hydrogels, which can be removed by cell medium perfusion (Miller et al., 2012). The micro-channel hydrogels demonstrate good biocompatibility and enhanced nutrition diffusion. Combination of carbohydrate glass material with 3D printing provides independent control of vascular network
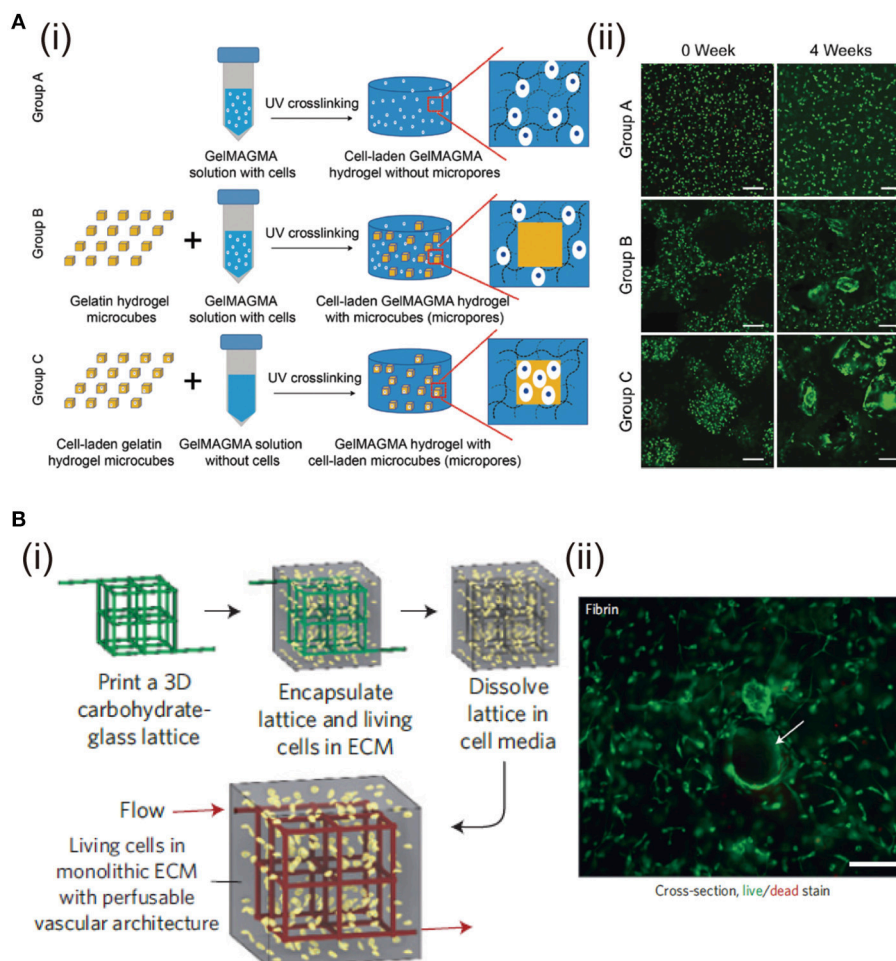
FIGURE 5 | Fabrication of porous and channel hydrogels and the effects on cell functions. **(A)** Preparation scheme of GelMAGMA hydrogels with or without microporous structures. (i). Live/dead staining of chondrocytes in the hydrogels after UV crosslinking (0 week) and after 28 days of *in vitro* culture (4 weeks) (ii). Scale bar: 200 mm. Reproduced with the permission from Li et al. (2017a), Copyright © 2017, Royal Society of Chemistry. **(B)** Fabrication of hydrogel with channel structure by dissolving 3D printed carbohydrate-glass lattice (i). Representative live/dead image of HUVEC and 10T1/2 co-cultured in the interstitial space of a fibrin gel (ii). Cells survive and spread near open channels (highlighted with white arrow). Scale bar: 200 μm. Reproduced with the permission from Miller et al. (2012) Copyright © 2012, Springer Nature.

geometry, endothelialization, and extravascular tissue formation (**Figure 5B**).

Double-Ring Structural Hydrogels

Osteon-like concentric double-ring structure is prepared with hybrid hydrogels of GelMA and hydroxyapatite via photolithography technology and self-assembly (Zuo et al., 2015). Human umbilical endothelial cells (HUVECs) are encapsulated in the inner ring to mimic blood vessel tubules, while human osteoblast-like cells (MG63s) are located in the outer ring as bone part (**Figure 6A**). Expression of angiogenesis-related and osteogenesis-related genes is promoted. Osteon-like fibers with HUVECs and MG63s separately encapsulated are constructed with the combination of photolithography

and microfluidic chip techniques (Wei et al., 2017). RGD modified alginate precursor with photoreactive functionalization is used for the hydrogel preparation because the modified alginate possesses cell adhesive sites and UV/Ca^{2+} crosslinkable properties. This not only satisfies cell proliferation but enhances the relative gene expression and protein secretion in the osteon-like architecture.

Multilayered Hydrogels

ECM composition and structure of cartilage and bone tissues have an obvious difference. The biochemical and biophysical microenvironments surrounding the cells in cartilage and bone are also different. To regenerate full-thickness articular cartilage defects, bilayered hydrogel architecture is designed.
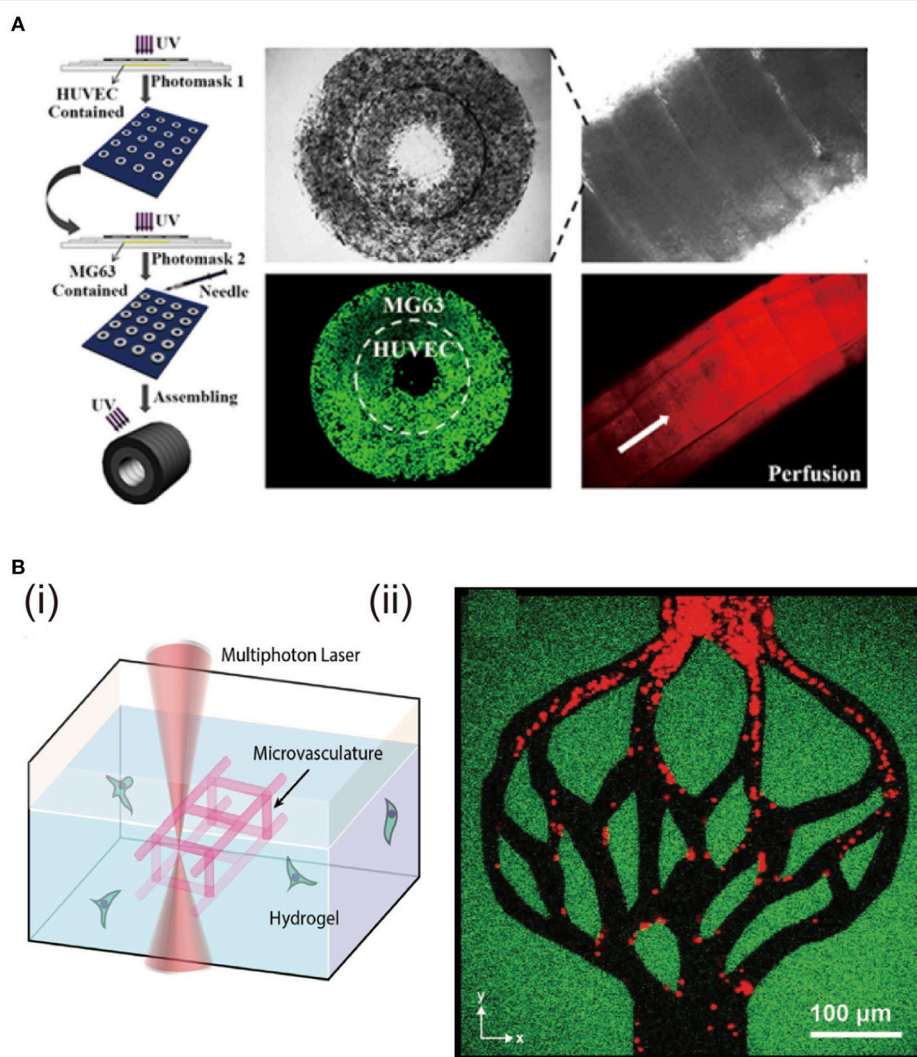
FIGURE 6 | Fabrication of double-ring and hierarchically structural hydrogels and the effects on cell functions. **(A)** Fabrication of hydrogels with osteon-like double-ring structure by photolithograph and self-assembly. Cell viability of MG63s and HUVECs encapsulated in the outer ring and inner ring of the osteon-like module. Reproduced with the permission from Zuo et al. (2015), Copyright © 2015, American Chemical Society. **(B)** Degradation of the hydrogel through oNB photocleavage (i). Creation of hydrogels with hierarchical vascular structure by programmable photodegradation (ii). Reproduced with the permission from Arakawa et al. (2017), Copyright © 2017, John Wiley and Sons.

For example, bilayered agarose hydrogels are prepared for osteochondral tissue repair (Sheehy et al., 2013). The top hydrogel layer is encapsulated with chondrocytes, while the bottom layer is seeded with MSCs. After 49 days of *in vitro* cultivation, the top layer promotes production of cartilaginous ECM, while the hypertrophy of MSCs encapsulated in the bottom layer is decreased. The results indicate the bilayered structure has a great potential for spatially separated coculture of chondrocyte and MSCs and osteochondral tissue regeneration. Bilayered structure can also provide tunable biochemical and mechanical microenvironment for differentiation of MSCs. For example, the top hydrogel layer fabricated with low RGD concentration and soft matrix can promote chondrogenesis of MSCs, while, the bottom layer designed to have high RGD amount and stiff mechanical property can promote osteogenesis of MSCs (Steinmetz et al., 2015).

Hierarchically Structured Hydrogels

Hierarchical architecture exists in living tissues. For example, blood vessels possess many scales of size to adapt to tissue requirements. They include large arteries, smaller arterioles and smallest capillaries, which have the functions to permit large blood volume flow and support mass transport via diffusion (Michiels, 2003). The above mentioned methodologies for channel structures have limitations to introduce such hierarchical structures in cell-laden hydrogel constructs, especially for the size of diameter less than 150 μm (Lee et al., 2014). Multiphoton lithography-assisted photoscission, as a cytocompatible fabrication strategy, is used to create hierarchical vessels spanning nearly all the size ranges in the human body (Arakawa et al., 2017) (**Figure 6B**). The hydrogel network is crosslinked by azide-alkyne cycloaddition between PEG tetrabicyclononyne and diazide-functionalized peptide. The photo degradation is based on the ortho-nitrobenzyl ester (oNB) moiety that undergoes photolysis upon exposure to pulsed near-infrared light (DeForest and Tirrell, 2015). Human bone marrow-derived hS5 stromal cells are encapsulated inside the hydrogel, followed by preparation of photodegradable vessels. The hS5 cells are viable during the whole culture period. This complex and hierarchical structures can maintain cell viability and functions, which is essential for regeneration of heterogeneous tissues. Furthermore, the hierarchical vascular structure is promising for investigation of endothelialization and blood-capillary interaction in the various environments.

3D stamping technique can also be used to prepare hydrogels with hierarchical structures. AngioChip with hierarchical vascular and porous architecture is prepared by this method (Zhang et al., 2016). Nanopores and micro-holes are fabricated into the vascular walls to promote molecular exchange and cell migration. The permeability for large molecular (70 kDa TRITC-dextran) of AngioChip with micro-holes is more than 4 times higher than that of the counterparts without micro-holes. A confluent endothelium is exhibited on the microchannel surface and endothelial sprouts are observed through the micro-holes. Human embryonic stem cell-derived hepatocytes and hMSCs are encapsulated in a collagen matrix and seeded into the parenchymal space to engineer the AngioChip. Urea secretion per cell from this hierarchical construct is much higher than that of collagen sandwich control. Furthermore, this complex hierarchical structural AngioChip is also used for *in vitro* regeneration of cardiac tissue models and implantation for direct surgical anastomosis. Due to the complex and hierarchical architectures, cell viabilities and relative functions are enhanced.

CONCLUSION AND OUTLOOKS

Control of the structures and physiochemical properties of hydrogels is important for their utilization in TE. Cells first sense the signals from surrounding hydrogel matrix, which makes the physiochemical properties of hydrogel critical for cell functions. Various structures of hydrogels can further alter the microenvironments and provide the possibility of flow stimulus by micro-channel structure or co-culture microenvironment by spatially layered structures. A variety of preparation methods and functional hydrogels have been developed for TE of various tissues and organs. Despite of these progresses, hydrogels with further improved biochemical and biophysical properties, as well as biomimetic structures are deserved to be further studied. The explored hydrogels until now have some similar but not completely matched functions to the *in vivo* cell-surrounding microenvironments. Dynamically responsive biophysical and biochemical stimuli and spatiotemporally controlled architecture may become the main direction of design and preparation of functional hydrogels to realize the complete functionality for TE applications.

AUTHOR CONTRIBUTIONS

All authors listed have made a substantial, direct and intellectual contribution to the work, and approved it for publication.

ACKNOWLEDGMENTS

REFERENCES

Abbadessa, A., Blokzijl, M. M., Mouser, V., Marica, P., Malda, J., Hennink, W., et al. (2016). A thermo-responsive and photo-polymerizable chondroitin sulfate-based hydrogel for 3D printing applications. *Carbohydr. Polym.* 149, 163–174. doi: 10.1016/j.carbpol.2016.04.080

Annabi, N., Nichol, J. W., Zhong, X., Ji, C., Koshy, S., Khademhosseini, A., et al. (2010). Controlling the porosity and microarchitecture of hydrogels for tissue engineering. *Tissue Eng. B Rev.* 16, 371–383. doi: 10.1089/ten.teb.2009.0639

Arakawa, C. K., Badeau, B. A., Zheng, Y., and DeForest, C. A. (2017). Multicellular vascularized engineered tissues through user-programmable biomaterial photodegradation. *Adv. Mat.* 29:1703156. doi: 10.1002/adma.201703156

Ashraf, S., Park, H.-K., Park, H., and Lee, S.-H. (2016). Snapshot of phase transition in thermoresponsive hydrogel PNIPAM: role in drug delivery and tissue engineering. *Macromol. Res.* 24, 297–304. doi: 10.1007/s13233-016-4052-2

Baei, P., Jalili-Firoozinezhad, S., Rajabi-Zeleti, S., Tafazzoli-Shadpour, M., Baharvand, H., and Aghdami, N. (2016). Electrically conductive gold nanoparticle-chitosan thermosensitive hydrogels for cardiac tissue engineering. *Mat. Sci. Eng. C* 63, 131–141. doi: 10.1016/j.msec.2016.02.056

Bai, X., Lü, S., Cao, Z., Ni, B., Wang, X., Ning, P., et al. (2017). Dual crosslinked chondroitin sulfate injectable hydrogel formed via continuous Diels-Alder (DA) click chemistry for bone repair. *Carbohydr. Polym.* 166, 123–130. doi: 10.1016/j.carbpol.2017.02.062

Baker, B. M., and Chen, C. S. (2012). Deconstructing the third dimension–how 3D culture microenvironments alter cellular cues. *J. Cell Sci.* 125, 3015–3024. doi: 10.1242/jcs.079509

Balakrishnan, B. (2016). "Injectable hydrogels by chemical crosslinking," in *Injectable Hydrogels for Regenerative Engineering*, ed. L. S. Nair (Singapore: World Scientific), 155–200.

Balakrishnan, B., Joshi, N., and Banerjee, R. (2013). Borate aided Schiff's base formation yields in situ gelling hydrogels for cartilage regeneration. *J. Mater. Chem. B* 1, 5564–5577. doi: 10.1039/c3tb21056a

Banerjee, A., Arha, M., Choudhary, S., Ashton, R. S., Bhatia, S. R., Schaffer, D. V., et al. (2009). The influence of hydrogel modulus on the proliferation and differentiation of encapsulated neural stem cells. *Biomaterials* 30, 4695–4699. doi: 10.1016/j.biomaterials.2009.05.050

Baniasadi, H., Mashayekhan, S., Fadaoddini, S., and Haghirsharifzamini, Y. (2016). Design, fabrication and characterization of oxidized alginate–gelatin hydrogels for muscle tissue engineering applications. *J. Biomater. Appl.* 31, 152–161. doi: 10.1177/0885328216634057

Bartnikowski, M., Bartnikowski, N., Woodruff, M., Schrobback, K., and Klein, T. (2015). Protective effects of reactive functional groups on chondrocytes in photocrosslinkable hydrogel systems. *Acta Biomater.* 27, 66–76. doi: 10.1016/j.actbio.2015.08.038

Benton, J. A., DeForest, C. A., Vivekanandan, V., and Anseth, K. S. (2009). Photocrosslinking of gelatin macromers to synthesize porous hydrogels that promote valvular interstitial cell function. *Tissue Eng. A* 15, 3221–3230. doi: 10.1089/ten.tea.2008.0545

Bian, L., Hou, C., Tous, E., Rai, R., Mauck, R. L., and Burdick, J. A. (2013). The influence of hyaluronic acid hydrogel crosslinking density and macromolecular diffusivity on human MSC chondrogenesis and hypertrophy. *Biomaterials* 34, 413–421. doi: 10.1016/j.biomaterials.2012.09.052

Bryant, S. J., Bender, R. J., Durand, K. L., and Anseth, K. S. (2004). Encapsulating chondrocytes in degrading PEG hydrogels with high modulus: engineering gel structural changes to facilitate cartilaginous tissue production. *Biotechnol. Bioeng.* 86, 747–755. doi: 10.1002/bit.20160

Bryant, S. J., Nuttelman, C. R., and Anseth, K. S. (2000). Cytocompatibility of UV and visible light photoinitiating systems on cultured NIH/3T3 fibroblasts in vitro. *J. Biomater. Sci. Polym. Ed.* 11, 439–457. doi: 10.1163/156856200743805

Carmeliet, P., and Jain, R. K. (2000). Angiogenesis in cancer and other diseases. *Nature* 407:249. doi: 10.1038/35025220

Chaudhuri, O., Gu, L., Darnell, M., Klumpers, D., Bencherif, S. A., Weaver, J. C., et al. (2015). Substrate stress relaxation regulates cell spreading. *Nat. Commun.* 6:6365. doi: 10.1038/ncomms7365

Chaudhuri, O., Gu, L., Klumpers, D., Darnell, M., Bencherif, S. A., Weaver, J. C., et al. (2016). Hydrogels with tunable stress relaxation regulate stem cell fate and activity. *Nat. Mater.* 15:326. doi: 10.1038/nmat4489

Cheaburu Yilmaz, C. N., Pamfil, D., Vasile, C., Bibire, N., Lupuşoru, R.-V., Zamfir, C.-L., et al. (2017). Toxicity, biocompatibility, pH-responsiveness and methotrexate release from PVA/hyaluronic acid cryogels for psoriasis therapy. *Polymers* 9:123. doi: 10.3390/polym9040123

Chen, G., and Kawazoe, N. (2016a). "Polymeric and biomimetic ECM scaffolds for tissue engineering," in *Polymeric Biomaterials for Tissue Regeneration*, ed. C. Gao (Singapore: Springer), 41–56.

Chen, G., and Kawazoe, N. (2016b). "Preparation of polymer scaffolds by ice particulate method for tissue engineering," in *Biomaterials Nanoarchitectonics*, ed. M. Ebara (Amsterdam: Elsevier), 77–95.

Chen, G., Kawazoe, N., and Ito, Y. (2018). "Photo-crosslinkable hydrogels for tissue engineering applications," in *Photochemistry for Biomedical Applications*, ed. Y. Ito (Singapore: Springer), 277–300.

Chen, S., Zhang, Q., Nakamoto, T., Kawazoe, N., and Chen, G. (2016). Gelatin scaffolds with controlled pore structure and mechanical property for cartilage tissue engineering. *Tissue Eng. C Methods* 22, 189–198. doi: 10.1089/ten.tec.2015.0281

Chen, T., Small, D. A., McDermott, M. K., Bentley, W. E., and Payne, G. F. (2003). Enzymatic methods for in situ cell entrapment and cell release. *Biomacromolecules* 4, 1558–1563. doi: 10.1021/bm034145k

Chung, C., and Burdick, J. A. (2008). Influence of three-dimensional hyaluronic acid microenvironments on mesenchymal stem cell chondrogenesis. *Tissue Eng. A* 15, 243–254. doi: 10.1089/ten.tea.2008.0067

Darnell, M. C., Sun, J. Y., Mehta, M., Johnson, C., Arany, P. R., Suo, Z., et al. (2013). Performance and biocompatibility of extremely tough alginate/polyacrylamide hydrogels. *Biomaterials* 34, 8042–8048. doi: 10.1016/j.biomaterials.2013.06.061

DeForest, C. A., and Tirrell, D. A. (2015). A photoreversible protein-patterning approach for guiding stem cell fate in three-dimensional gels. *Nat. Mater.* 14:523. doi: 10.1038/nmat4219

Dragan, E. S. (2014). Design and applications of interpenetrating polymer network hydrogels. A review. *Chem. Eng. J.* 243, 572–590. doi: 10.1016/j.cej.2014.01.065

Drury, J. L., and Mooney, D. J. (2003). Hydrogels for tissue engineering: scaffold design variables and applications. *Biomaterials* 24, 4337–4351. doi: 10.1016/S0142-9612(03)00340-5

Eke, G., Mangir, N., Hasirci, N., MacNeil, S., and Hasirci, V. (2017). Development of a UV crosslinked biodegradable hydrogel containing adipose derived stem cells to promote vascularization for skin wounds and tissue engineering. *Biomaterials* 129, 188–198. doi: 10.1016/j.biomaterials.2017.03.021

Engler, A. J., Sen, S., Sweeney, H. L., and Discher, D. E. (2006). Matrix elasticity directs stem cell lineage specification. *Cell* 126, 677–689. doi: 10.1016/j.cell.2006.06.044

Fan, C., and Wang, D. A. (2015). Effects of permeability and living space on cell fate and neo-tissue development in hydrogel-based scaffolds: a study with cartilaginous model. *Macromol. Biosci.* 15, 535–545. doi: 10.1002/mabi.201400453

Fan, M., Ma, Y., Zhang, Z., Mao, J., Tan, H., and Hu, X. (2015a). Biodegradable hyaluronic acid hydrogels to control release of dexamethasone through aqueous Diels–Alder chemistry for adipose tissue engineering. *Mater. Sci. Eng. C* 56, 311–317. doi: 10.1016/j.msec.2015.04.004

Fan, M., Zhang, Z., Mao, J., and Tan, H. (2015b). Injectable multi-arm poly (ethylene glycol)/hyaluronic acid hydrogels for adipose tissue engineering. *J. Macromol. Sci. A* 52, 345–352. doi: 10.1080/10601325.2015.1018804

Fedorovich, N. E., Oudshoorn, M. H., van Geemen, D., Hennink, W. E., Alblas, J., and Dhert, W. J. (2009). The effect of photopolymerization on stem cells embedded in hydrogels. *Biomaterials* 30, 344–353. doi: 10.1016/j.biomaterials.2008.09.037

Feng, Q., Lin, S., Zhang, K., Dong, C., Wu, T., Huang, H., et al. (2017). Sulfated hyaluronic acid hydrogels with retarded degradation and enhanced growth factor retention promote hMSC chondrogenesis and articular cartilage integrity with reduced hypertrophy. *Acta Biomater.* 53, 329–342. doi: 10.1016/j.actbio.2017.02.015

Feng, Q., Wei, K., Lin, S., Xu, Z., Sun, Y., Shi, P., et al. (2016). Mechanically resilient, injectable, and bioadhesive supramolecular gelatin hydrogels crosslinked by weak host-guest interactions assist cell infiltration and in situ tissue regeneration. *Biomaterials* 101, 217–228. doi: 10.1016/j.biomaterials.2016.05.043

Fu, S., Dong, H., Deng, X., Zhuo, R., and Zhong, Z. (2017). Injectable hyaluronic acid/poly (ethylene glycol) hydrogels crosslinked via strain-promoted azide-alkyne cycloaddition click reaction. *Carbohydr. Polym.* 169, 332–340. doi: 10.1016/j.carbpol.2017.04.028

Fukui, T., Kitamura, N., Kurokawa, T., Yokota, M., Kondo, E., Gong, J. P., et al. (2014). Intra-articular administration of hyaluronic acid increases the volume of the hyaline cartilage regenerated in a large osteochondral defect by implantation of a double-network gel. *J. Mater. Sci. Mater. Med.* 25, 1173–1182. doi: 10.1007/s10856-013-5139-3

Gacesa, P. (1988). Alginates. *Carbohydr. Polym.* 8, 161–182. doi: 10.1016/0144-8617(88)90001-X

Gaharwar, A. K., Dammu, S. A., Canter, J. M., Wu, C. J., and Schmidt, G. (2011). Highly extensible, tough, and elastomeric nanocomposite hydrogels from poly (ethylene glycol) and hydroxyapatite nanoparticles. *Biomacromolecules* 12, 1641–1650. doi: 10.1021/bm200027z

Gao, G., Schilling, A. F., Hubbell, K., Yonezawa, T., Truong, D., Hong, Y., et al. (2015). Improved properties of bone and cartilage tissue from 3D inkjet-bioprinted human mesenchymal stem cells by simultaneous deposition and photocrosslinking in PEG-GelMA. *Biotechnol. Lett.* 37, 2349–2355. doi: 10.1007/s10529-015-1921-2

Gombotz, W. R., and Wee, S. F. (2012). Protein release from alginate matrices. *Adv. Drug Deliv. Rev.* 64, 194–205. doi: 10.1016/j.addr.2012.09.007

Gong, J. P., Katsuyama, Y., Kurokawa, T., and Osada, Y. (2003). Double-network hydrogels with extremely high mechanical strength. *Adv. Mater.* 15, 1155–1158. doi: 10.1002/adma.200304907

Goosen, M. F., O'Shea, G. M., Gharapetian, H. M., Chou, S., and Sun, A. M. (1985). Optimization of microencapsulation parameters: semipermeable microcapsules as a bioartificial pancreas. *Biotechnol. Bioeng.* 27, 146–150. doi: 10.1002/bit.260270207

Guan, X., Avci-Adali, M., Alarçin, E., Cheng, H., Kashaf, S. S., Li, Y., et al. (2017). Development of hydrogels for regenerative engineering. *Biotechnol. J.* 12:1600394. doi: 10.1002/biot.201600394

Han, L., Xu, J., Lu, X., Gan, D., Wang, Z., Wang, K., et al. (2017). Biohybrid methacrylated gelatin/polyacrylamide hydrogels for cartilage repair. *J. Mater. Chem. B* 5, 731–741. doi: 10.1039/C6TB02348G

Han, L. H., Lai, J. H., Yu, S., and Yang, F. (2013). Dynamic tissue engineering scaffolds with stimuli-responsive macroporosity formation. *Biomaterials* 34, 4251–4258. doi: 10.1016/j.biomaterials.2013.02.051

Haq, M. A., Su, Y., and Wang, D. (2017). Mechanical properties of PNIPAM based hydrogels: a review. *Mater. Sci. Eng. C* 70, 842–855. doi: 10.1016/j.msec.2016.09.081

Haque, M. A., Kurokawa, T., and Gong, J. P. (2012). Super tough double network hydrogels and their application as biomaterials. *Polymer* 53, 1805–1822. doi: 10.1016/j.polymer.2012.03.013

Hassan, C. M., and Peppas, N. A. (2000). "Structure and applications of poly (vinyl alcohol) hydrogels produced by conventional crosslinking or by freezing/thawing methods," in *Biopolymers· PVA Hydrogels, Anionic Polymerisation Nanocomposites*, ed. D. Y. Godovsky (Berlin: Springer), 37–65.

Hassanzadeh, P., Kazemzadeh-Narbat, M., Rosenzweig, R., Zhang, X., Khademhosseini, A., Annabi, N., et al. (2016). Ultrastrong and flexible hybrid hydrogels based on solution self-assembly of chitin nanofibers in gelatin methacryloyl (GelMA). *J. Mater. Chem. B* 4, 2539–2543. doi: 10.1039/C6TB00021E

Hennink, W., and Van Nostrum, C. F. (2012). Novel crosslinking methods to design hydrogels. *Adv. Drug Deliv. Rev.* 64, 223–236. doi: 10.1016/j.addr.2012.09.009

Heo, J., Koh, R. H., Shim, W., Kim, H. D., Yim, H. G., and Hwang, N. S. (2016). Riboflavin-induced photo-crosslinking of collagen hydrogel and its application in meniscus tissue engineering. *Drug Deliv. Transl. Res.* 6, 148–158. doi: 10.1007/s13346-015-0224-4

Ho, S. S., Vollmer, N. L., Refaat, M. I., Jeon, O., Alsberg, E., Lee, M. A., et al. (2016). Bone morphogenetic protein-2 promotes human mesenchymal stem cell survival and resultant bone formation when entrapped in photocrosslinked alginate hydrogels. *Adv. Healthc. Mater.* 5, 2501–2509. doi: 10.1002/adhm.201600461

Hoffman, A. S. (2012). Hydrogels for biomedical applications. *Adv. Drug Deliv. Rev.* 64, 18–23. doi: 10.1016/j.addr.2012.09.010

Hoyle, C. E., and Bowman, C. N. (2010). Thiol–ene click chemistry. *Angew. Chem. Int. Ed.* 49, 1540–1573. doi: 10.1002/anie.200903924

Hsieh, F.-Y., Tao, L., Wei, Y., and Hsu, S.-H. (2017). A novel biodegradable self-healing hydrogel to induce blood capillary formation. *Npg Asia Mater.* 9:e363. doi: 10.1038/am.2017.23

Huebsch, N., Arany, P. R., Mao, A. S., Shvartsman, D., Ali, O. A., Bencherif, S. A., et al. (2010). Harnessing traction-mediated manipulation of the cell/matrix interface to control stem-cell fate. *Nat. Mater.* 9:518. doi: 10.1038/nmat2732

Huettner, N., Dargaville, T. R., and Forget, A. (2018). Discovering cell-adhesion peptides in tissue engineering: beyond RGD. *Trends Biotechnol.* 6, 372–383. doi: 10.1016/j.tibtech.2018.01.008

Hunt, N. C., Hallam, D., Karimi, A., Mellough, C. B., Chen, J., Steel, D. H., et al. (2017). 3D culture of human pluripotent stem cells in RGD-alginate hydrogel improves retinal tissue development. *Acta Biomater.* 49, 329–343. doi: 10.1016/j.actbio.2016.11.016

Izadifar, M., Chapman, D., Babyn, P., Chen, X., and Kelly, M. E. (2018). UV-assisted 3D bioprinting of nanoreinforced hybrid cardiac patch for myocardial tissue engineering. *Tissue Eng. C Methods* 24, 74–88. doi: 10.1089/ten.tec.2017.0346

Jaiswal, M. K., Xavier, J. R., Carrow, J. K., Desai, P., Alge, D., and Gaharwar, A. K. (2015). Mechanically stiff nanocomposite hydrogels at ultralow nanoparticle content. *ACS Nano* 10, 246–256. doi: 10.1021/acsnano.5b03918

Jiang, H., Qin, S., Dong, H., Lei, Q., Su, X., Zhuo, R., et al. (2015). An injectable and fast-degradable poly (ethylene glycol) hydrogel fabricated via bioorthogonal strain-promoted azide–alkyne cycloaddition click chemistry. *Soft Matter* 11, 6029–6036. doi: 10.1039/C5SM00508F

Jin, R., Teixeira, L. M., Krouwels, A., Dijkstra, P. J., Van Blitterswijk, C., Karperien, M., et al. (2010). Synthesis and characterization of hyaluronic acid–poly (ethylene glycol) hydrogels via Michael addition: an injectable biomaterial for cartilage repair. *Acta Biomater.* 6, 1968–1977. doi: 10.1016/j.actbio.2009.12.024

Jo, H., Sim, M., Kim, S., Yang, S., Yoo, Y., Park, J.-H., et al. (2017). Electrically conductive graphene/polyacrylamide hydrogels produced by mild chemical reduction for enhanced myoblast growth and differentiation. *Acta Biomater.* 48, 100–109. doi: 10.1016/j.actbio.2016.10.035

Kharkar, P. M., Kiick, K. L., and Kloxin, A. M. (2013). Designing degradable hydrogels for orthogonal control of cell microenvironments. *Chem. Soc. Rev.* 42, 7335–7372. doi: 10.1039/C3CS60040H

Khetan, S., Guvendiren, M., Legant, W. R., Cohen, D. M., Chen, C. S., and Burdick, J. A. (2013). Degradation-mediated cellular traction directs stem cell fate in covalently crosslinked three-dimensional hydrogels. *Nat. Mater.* 12:458. doi: 10.1038/nmat3586

Kim, D. H., Martin, J. T., Elliott, D. M., Smith, L. J., and Mauck, R. L. (2015). Phenotypic stability, matrix elaboration and functional maturation of nucleus pulposus cells encapsulated in photocrosslinkable hyaluronic acid hydrogels. *Acta Biomater.* 12, 21–29. doi: 10.1016/j.actbio.2014.10.030

Kim, S., Cui, Z. K., Fan, J., Fartash, A., Aghaloo, T. L., and Lee, M. (2016). Photocrosslinkable chitosan hydrogels functionalized with the RGD peptide and phosphoserine to enhance osteogenesis. *J. Mater. Chem. B* 4, 5289–5298. doi: 10.1039/C6TB01154C

Kloxin, A. M., Tibbitt, M. W., Kasko, A. M., Fairbairn, J. A., and Anseth, K. S. (2010). Tunable hydrogels for external manipulation of cellular microenvironments through controlled photodegradation. *Adv. Mater.* 22, 61–66. doi: 10.1002/adma.200900917

Knudson, C. B., and Knudson, W. (2004). Hyaluronan and CD44: modulators of chondrocyte metabolism. *Clin. Orthop. Relat. Res.* 427, S152–S162. doi: 10.1097/01.blo.0000143804.26638.82

Koh, R. H., Jin, Y., Kang, B. J., and Hwang, N. S. (2017). Chondrogenically primed tonsil-derived mesenchymal stem cells encapsulated in riboflavin-induced photocrosslinking collagen-hyaluronic acid hydrogel for meniscus tissue repairs. *Acta Biomater.* 53, 318–328. doi: 10.1016/j.actbio.2017.01.081

Le Thi, P., Lee, Y., Nguyen, D. H., and Park, K. D. (2017). *In situ* forming gelatin hydrogels by dual-enzymatic cross-linking for enhanced tissue adhesiveness. *J. Mater. Chem. B* 5, 757–764. doi: 10.1039/C6TB02179D

Lee, H. P., Gu, L., Mooney, D. J., Levenston, M. E., and Chaudhuri, O. (2017). Mechanical confinement regulates cartilage matrix formation by chondrocytes. *Nat. Mater.* 16:1243. doi: 10.1038/nmat4993

Lee, J. B., Wang, X., Faley, S., Baer, B., Balikov, D. A., Sung, H. J., et al. (2016). Development of 3D microvascular networks within gelatin hydrogels using thermoresponsive sacrificial microfibers. *Adv. Healthc. Mater.* 5, 781–785. doi: 10.1002/adhm.201500792

Lee, T. T., García, J. R., Paez, J. I., Singh, A., Phelps, E. A., Weis, S., et al. (2015). Light-triggered *in vivo* activation of adhesive peptides regulates cell adhesion, inflammation and vascularization of biomaterials. *Nat. Mater.* 14:352. doi: 10.1038/nmat4157

Lee, V. K., Kim, D. Y., Ngo, H., Lee, Y., Seo, L., Yoo, S. S., et al. (2014). Creating perfused functional vascular channels using 3D bio-printing technology. *Biomaterials* 35, 8092–8102. doi: 10.1016/j.biomaterials.2014.05.083

Leong, W., Kremer, A., and Wang, D. A. (2016). Development of size-customized hepatocarcinoma spheroids as a potential drug testing platform using a sacrificial gelatin microsphere system. *Mater. Sci. Eng. C* 63, 644–649. doi: 10.1016/j.msec.2016.03.046

Levett, P. A., Melchels, F. P., Schrobback, K., Hutmacher, D. W., Malda, J., and Klein, T. J. (2014). A biomimetic extracellular matrix for cartilage tissue engineering centered on photocurable gelatin, hyaluronic acid and chondroitin sulfate. *Acta Biomater.* 10, 214–223. doi: 10.1016/j.actbio.2013. 10.005

Lewandowska-Łancucka, J., Mystek, K., Mignon, A., Van Vlierberghe, S., Łatkiewicz, A., and Nowakowska, M. (2017). Alginate-and gelatin-based bioactive photocross-linkable hybrid materials for bone tissue engineering. *Carbohydr. Polym.* 157, 1714–1722. doi: 10.1016/j.carbpol.2016. 11.051

Li, X., Chen, S., Li, J., Wang, X., Zhang, J., Kawazoe, N., et al. (2016). 3D culture of chondrocytes in gelatin hydrogels with different stiffness. *Polymers* 8:269. doi: 10.3390/polym8080269

Li, X., Chen, Y., Kawazoe, N., and Chen, G. (2017a). Influence of microporous gelatin hydrogels on chondrocyte functions. *J. Mater. Chem. B* 5, 5753–5762. doi: 10.1039/C7TB01350G

Li, X., Zhang, J., Kawazoe, N., and Chen, G. (2017b). Fabrication of highly crosslinked gelatin hydrogel and its influence on chondrocyte proliferation and phenotype. *Polymers* 9:309. doi: 10.3390/polym9080309

Liu, Y., and Chan-Park, M. B. (2009). Hydrogel based on interpenetrating polymer networks of dextran and gelatin for vascular tissue engineering. *Biomaterials* 30, 196–207. doi: 10.1016/j.biomaterials.2008.09.041

Long, J., Kim, H., Kim, D., Lee, J. B., and Kim, D. H. (2017). A biomaterial approach to cell reprogramming and differentiation. *J. Mater. Chem. B* 5, 2375–2389. doi: 10.1039/C6TB03130G

Lou, J., Stowers, R., Nam, S., Xia, Y., and Chaudhuri, O. (2018). Stress relaxing hyaluronic acid-collagen hydrogels promote cell spreading, fiber remodeling, and focal adhesion formation in 3D cell culture. *Biomaterials* 154, 213–222. doi: 10.1016/j.biomaterials.2017.11.004

Lü, S., Bai, X., Liu, H., Ning, P., Wang, Z., Gao, C., et al. (2017). An injectable and self-healing hydrogel with covalent cross-linking *in vivo* for cranial bone repair. *J. Mater. Chem. B* 5, 3739–3748. doi: 10.1039/C7TB00776K

Magarinos, A. M., Pedron, S., Creixell, M., Kilinc, M., Tabansky, I., Pfaff, D. W., et al. (2018). The feasibility of encapsulated embryonic medullary reticular cells to grow and differentiate into neurons in functionalized gelatin-based hydrogels. *Front. Mater.* 5:40. doi: 10.3389/fmats.2018. 00040

Mahadevaiah, S., Robinson, K. G., Kharkar, P. M., Kiick, K. L., and Akins, R. E. (2015). Decreasing matrix modulus of PEG hydrogels induces a vascular phenotype in human cord blood stem cells. *Biomaterials* 62, 24–34. doi: 10.1016/j.biomaterials.2015.05.021

Mao, H., Kim, S. M., Ueki, M., and Ito, Y. (2017). Serum-free culturing of human mesenchymal stem cells with immobilized growth factors. *J. Mater. Chem. B* 5, 928–934. doi: 10.1039/C6TB02867E

Martens, P. J., Bryant, S. J., and Anseth, K. S. (2003). Tailoring the degradation of hydrogels formed from multivinyl poly (ethylene glycol) and poly (vinyl alcohol) macromers for cartilage tissue engineering. *Biomacromolecules* 4, 283–292. doi: 10.1021/bm025666v

Martinsen, A., Skjåk-Bræk, G., and Smidsrød, O. (1989). Alginate as immobilization material: I. Correlation between chemical and physical properties of alginate gel beads. *Biotechnol. Bioeng.* 33, 79–89. doi: 10.1002/bit.260330111

Mellati, A., Fan, C. M., Tamayol, A., Annabi, N., Dai, S., Bi, J., et al. (2017). Microengineered 3D cell-laden thermoresponsive hydrogels for mimicking cell morphology and orientation in cartilage tissue engineering. *Biotechnol. Bioeng.* 114, 217–231. doi: 10.1002/bit.26061

Michiels, C. (2003). Endothelial cell functions. *J. Cell. Physiol.* 196, 430–443. doi: 10.1002/jcp.10333

Miguel, S. P., Ribeiro, M. P., Brancal, H., Coutinho, P., and Correia, I. J. (2014). Thermoresponsive chitosan–agarose hydrogel for skin regeneration. *Carbohydr. Polym.* 111, 366–373. doi: 10.1016/j.carbpol.2014. 04.093

Miller, J. S., Stevens, K. R., Yang, M. T., Baker, B. M., Nguyen, D. H. T., Cohen, D. M., et al. (2012). Rapid casting of patterned vascular networks for perfusable engineered three-dimensional tissues. *Nat. Mater.* 11:768. doi: 10.1038/nmat3357

Nakahata, M., Takashima, Y., Yamaguchi, H., and Harada, A. (2011). Redox-responsive self-healing materials formed from host–guest polymers. *Nat. Commun.* 2:511. doi: 10.1038/ncomms1521

Navaei, A., Saini, H., Christenson, W., Sullivan, R. T., Ros, R., and Nikkhah, M. (2016a). Gold nanorod-incorporated gelatin-based conductive hydrogels for engineering cardiac tissue constructs. *Acta Biomater.* 41, 133–146. doi: 10.1016/j.actbio.2016.05.027

Navaei, A., Truong, D., Heffernan, J., Cutts, J., Brafman, D., Sirianni, R. W., et al. (2016b). PNIPAAm-based biohybrid injectable hydrogel for cardiac tissue engineering. *Acta Biomater.* 32, 10–23. doi: 10.1016/j.actbio.2015. 12.019

Neumann, A. J., Quinn, T., and Bryant, S. J. (2016). Nondestructive evaluation of a new hydrolytically degradable and photo-clickable PEG hydrogel for cartilage tissue engineering. *Acta Biomater.* 39, 1–11. doi: 10.1016/j.actbio.2016. 05.015

Nguyen, M. K., and Alsberg, E. (2014). Bioactive factor delivery strategies from engineered polymer hydrogels for therapeutic medicine. *Prog. Polym. Sci.* 39, 1235–1265. doi: 10.1016/j.progpolymsci.2013.12.001

Omobono, M. A., Zhao, X., Furlong, M. A., Kwon, C. H., Gill, T. J., Randolph, M. A., et al. (2015). Enhancing the stiffness of collagen hydrogels for delivery of encapsulated chondrocytes to articular lesions for cartilage regeneration. *J. Biomed. Mater. Res. A* 103, 1332–1338. doi: 10.1002/jbm.a. 35266

Pacelli, S., Rampetsreiter, K., Modaresi, S., Subham, S., Chakravarti, A. R., Lohfeld, S., et al. (2018). Fabrication of a double crosslinked interpenetrating polymeric network (IPN) hydrogel surface modified with polydopamine to modulate osteogenic differentiation of adipose-derived stem cells. *ACS Appl. Mater. Interfaces.* 10, 24955–24962. doi: 10.1021/acsami.8b 05200

Park, Y. D., Tirelli, N., and Hubbell, J. A. (2003). Photopolymerized hyaluronic acid-based hydrogels and interpenetrating networks. *Biomaterials* 24, 893–900. doi: 10.1016/S0142-9612(02)00420-9

Parker, J., Mitrousis, N., and Shoichet, M. S. (2016). Hydrogel for simultaneous tunable growth factor delivery and enhanced viability of encapsulated cells *in vitro*. *Biomacromolecules* 17, 476–484. doi: 10.1021/acs.biomac. 5b01366

Peng, Y., Liu, Q., He, T., Ye, K., Yao, X., and Ding, J. (2018). Degradation rate affords a dynamic cue to regulate stem cells beyond varied matrix stiffness. *Biomaterials* 78, 467–480. doi: 10.1016/j.biomaterials.2018. 04.021

Ren, K., He, C., Xiao, C., Li, G., and Chen, X. (2015). Injectable glycopolypeptide hydrogels as biomimetic scaffolds for cartilage tissue engineering. *Biomaterials* 51, 238–249. doi: 10.1016/j.biomaterials.2015.02.026

Rizwan, M., Peh, G. S., Ang, H. P., Lwin, N. C., Adnan, K., Mehta, J. S., et al. (2017). Sequentially-crosslinked bioactive hydrogels as nano-patterned substrates with customizable stiffness and degradation for corneal tissue engineering applications. *Biomaterials* 120, 139–154. doi: 10.1016/j.biomaterials.2016.12.026

Rodell, C. B., Highley, C. B., Chen, M. H., Dusaj, N. N., Wang, C., Han, L., et al. (2016). Evolution of hierarchical porous structures in supramolecular guest–host hydrogels. *Soft Matter* 12, 7839–7847. doi: 10.1039/C6SM 01395C

Ruoslahti, E., and Pierschbacher, M. D. (1987). New perspectives in cell adhesion: RGD and integrins. *Science* 238, 491–498. doi: 10.1126/science. 2821619

Salinas, C. N., and Anseth, K. S. (2008). The enhancement of chondrogenic differentiation of human mesenchymal stem cells by enzymatically regulated RGD functionalities. *Biomaterials* 29, 2370–2377. doi: 10.1016/j.biomaterials.2008.01.035

Schuh, E., Hofmann, S., Stok, K., Notbohm, H., Müller, R., and Rotter, N. (2012). Chondrocyte redifferentiation in 3D: the effect of adhesion site density and substrate elasticity. *J. Biomed. Mater. Res. A* 100, 38–47. doi: 10.1002/jbm.a.33226

Sheehy, E. J., Vinardell, T., Buckley, C. T., and Kelly, D. J. (2013). Engineering osteochondral constructs through spatial regulation of endochondral ossification. *Acta Biomater.* 9, 5484–5492. doi: 10.1016/j.actbio.2012.11.008

Shendi, D., Dede, A., Yin, Y., Wang, C., Valmikinathan, C., and Jain, A. (2016). Tunable, bioactive protein conjugated hyaluronic acid hydrogel for neural engineering applications. *J. Mater. Chem. B* 4, 2803–2818. doi: 10.1039/C5TB02235E

Shin, S. R., Jung, S. M., Zalabany, M., Kim, K., Zorlutuna, P., and Kim, S. B., et al. (2013). Carbon-nanotube-embedded hydrogel sheets for engineering cardiac constructs and bioactuators. *ACS Nano* 7, 2369–2380. doi: 10.1021/nn305559j

Skaalure, S. C., Dimson, S. O., Pennington, A. M., and Bryant, S. J. (2014). Semi-interpenetrating networks of hyaluronic acid in degradable PEG hydrogels for cartilage tissue engineering. *Acta Biomater.* 10, 3409–3420. doi: 10.1016/j.actbio.2014.04.013

Slaughter, B. V., Khurshid, S. S., Fisher, O. Z., Khademhosseini, A., and Peppas, N. A. (2009). Hydrogels in regenerative medicine. *Adv. Mater.* 21, 3307–3329. doi: 10.1002/adma.200802106

Sridhar, B. V., Brock, J. L., Silver, J. S., Leight, J. L., Randolph, M. A., and Anseth, K. S. (2015). Development of a cellularly degradable PEG hydrogel to promote articular cartilage extracellular matrix deposition. *Adv. Healthc. Mater.* 4, 702–713. doi: 10.1002/adhm.201400695

Sridhar, B. V., Doyle, N. R., Randolph, M. A., and Anseth, K. S. (2014). Covalently tethered TGF-β1 with encapsulated chondrocytes in a PEG hydrogel system enhances extracellular matrix production. *J. Biomed. Mater. Res. A* 102, 4464–4472. doi: 10.1002/jbm.a.35115

Steed, J. W., Turner, D. R., and Wallace, K. (2007). *Core Concepts in Supramolecular Chemistry and Nanochemistry*. Chichester: John Wiley & Sons.

Steinmetz, N. J., Aisenbrey, E. A., Westbrook, K. K., Qi, H. J., and Bryant, S. J. (2015). Mechanical loading regulates human MSC differentiation in a multi-layer hydrogel for osteochondral tissue engineering. *Acta Biomater.* 21, 142–153. doi: 10.1016/j.actbio.2015.04.015

Steinmetz, N. J., and Bryant, S. J. (2011). The effects of intermittent dynamic loading on chondrogenic and osteogenic differentiation of human marrow stromal cells encapsulated in RGD-modified poly (ethylene glycol) hydrogels. *Acta Biomater.* 7, 3829–3840. doi: 10.1016/j.actbio.2011.06.031

Stevens, K. R., Ungrin, M., Schwartz, R., Ng, S., Carvalho, B., Christine, K., et al. (2013). InVERT molding for scalable control of tissue microarchitecture. *Nat. Commun.* 4:1847. doi: 10.1038/ncomms2853

Stüdle, C., Vallmajó-Martín, Q., Haumer, A., Guerrero, J., Centola, M., Mehrkens, A., et al. (2018). Spatially confined induction of endochondral ossification by functionalized hydrogels for ectopic engineering of osteochondral tissues. *Biomaterials* 171, 219–229. doi: 10.1016/j.biomaterials.2018.04.025

Sun, J., Wei, D., Yang, K., Yang, Y., Liu, X., Fan, H., et al. (2017). The development of cell-initiated degradable hydrogel based on methacrylated alginate applicable to multiple microfabrication technologies. *J. Mater. Chem. B* 5, 8060–8069. doi: 10.1039/C7TB01458A

Taylor, D. L., and in het Panhuis, M. (2016). Self-healing hydrogels. *Adv. Mater.* 28, 9060–9093. doi: 10.1002/adma.201601613

Tibbitt, M. W., and Anseth, K. S. (2009). Hydrogels as extracellular matrix mimics for 3D cell culture. *Biotechnol. Bioeng.* 103, 655–663. doi: 10.1002/bit.22361

Tocchio, A., Tamplenizza, M., Martello, F., Gerges, I., Rossi, E., Argentiere, S., et al. (2015). Versatile fabrication of vascularizable scaffolds for large tissue engineering in bioreactor. *Biomaterials* 45, 124–131. doi: 10.1016/j.biomaterials.2014.12.031

Tseng, T. C., Tao, L., Hsieh, F. Y., Wei, Y., Chiu, I. M., and Hsu, S. H. (2015). An injectable, self-healing hydrogel to repair the central nervous system. *Adv. Mater.* 27, 3518–3524. doi: 10.1002/adma.201500762

Ulijn, R. V. (2006). Enzyme-responsive materials: a new class of smart biomaterials. *J. Mater. Chem.* 16, 2217–2225. doi: 10.1039/b601776m

Vo, T. N., Shah, S., Lu, S., Tatara, A., Lee, E., Roh, T., et al. (2016). Injectable dual-gelling cell-laden composite hydrogels for bone tissue engineering. *Biomaterials* 83, 1–11. doi: 10.1016/j.biomaterials.2015.12.026

Wang, J., Zhang, F., Tsang, W. P., Wan, C., and Wu, C. (2017a). Fabrication of injectable high strength hydrogel based on 4-arm star PEG for cartilage tissue engineering. *Biomaterials* 120, 11–21. doi: 10.1016/j.biomaterials.2016.12.015

Wang, L. S., Du, C., Toh, W. S., Wan, A. C., Gao, S. J., and Kurisawa, M. (2014). Modulation of chondrocyte functions and stiffness-dependent cartilage repair using an injectable enzymatically crosslinked hydrogel with tunable mechanical properties. *Biomaterials* 35, 2207–2217. doi: 10.1016/j.biomaterials.2013.11.070

Wang, X., Li, Z., Shi, T., Zhao, P., An, K., Lin, C., et al. (2017b). Injectable dextran hydrogels fabricated by metal-free click chemistry for cartilage tissue engineering. *Mater. Sci. Eng. C* 73, 21–30. doi: 10.1016/j.msec.2016.12.053

Wei, D., Sun, J., Bolderson, J., Zhong, M., Dalby, M. J., Cusack, M., et al. (2017). Continuous fabrication and assembly of spatial cell-laden fibers for a tissue-like construct via a photolithographic-based microfluidic chip. *ACS Appl. Mater. Interfaces* 9, 14606–14617. doi: 10.1021/acsami.7b00078

Wei, K., Zhu, M., Sun, Y., Xu, J., Feng, Q., Lin, S., et al. (2016). Robust biopolymeric supramolecular "host– guest macromer" hydrogels reinforced by in situ formed multivalent nanoclusters for cartilage regeneration. *Macromolecules* 49, 866–875. doi: 10.1021/acs.macromol.5b02527

Wen, J. H., Vincent, L. G., Fuhrmann, A., Choi, Y. S., Hribar, K. C., Taylor-Weiner, H., et al. (2014). Interplay of matrix stiffness and protein tethering in stem cell differentiation. *Nat. Mater.* 13:979. doi: 10.1038/nmat4051

Xavier, J. R., Thakur, T., Desai, P., Jaiswal, M. K., Sears, N., Cosgriff-Hernandez, E., et al. (2015). Bioactive nanoengineered hydrogels for bone tissue engineering: a growth-factor-free approach. *ACS Nano* 9, 3109–3118. doi: 10.1021/nn507488s

Xu, J., Feng, E., and Song, J. (2014). Bioorthogonally cross-linked hydrogel network with precisely controlled disintegration time over a broad range. *J. Am. Chem. Soc.* 136, 4105–4108. doi: 10.1021/ja4130862

Xu, Z., and Bratlie, K. M. (2018). Click chemistry and material selection for *in situ* fabrication of hydrogels in tissue engineering applications. *ACS Biomater. Sci. Eng.* 4, 2276–2291. doi: 10.1021/acsbiomaterials.8b00230

Yan, H. J., Casalini, T., Hulsart-Billström, G., Wang, S., Oommen, O. P., Salvalaglio, M., et al. (2018). Synthetic design of growth factor sequestering extracellular matrix mimetic hydrogel for promoting *in vivo* bone formation. *Biomaterials* 161, 190–202. doi: 10.1016/j.biomaterials.2018.01.041

Yang, G., Lin, H., Rothrauff, B. B., Yu, S., and Tuan, R. S. (2016). Multilayered polycaprolactone/gelatin fiber-hydrogel composite for tendon tissue engineering. *Acta Biomater.* 35, 68–76. doi: 10.1016/j.actbio.2016.03.004

Yang, Y., Wang, X., Yang, F., Wang, L., and Wu, D. (2018). Highly elastic and ultratough hybrid ionic–covalent hydrogels with tunable structures and mechanics. *Adv. Mater.* 30:1707071. doi: 10.1002/adma.201707071

Yasuda, K., Kitamura, N., Gong, J. P., Arakaki, K., Kwon, H. J., Onodera, S., et al. (2009). A novel double-network hydrogel induces spontaneous articular cartilage regeneration *in vivo* in a large osteochondral defect. *Macromol. Biosci.* 9, 307–316. doi: 10.1002/mabi.200800223

You, S., Li, J., Zhu, W., Yu, C., Mei, D., and Chen, S. (2018). Nanoscale 3D printing of hydrogels for cellular tissue engineering. *J. Mater. Chem. B* 6, 2187–2197. doi: 10.1039/C8TB00301G

Yue, K., Trujillo-de Santiago, G., Alvarez, M. M., Tamayol, A., Annabi, N., and Khademhosseini, A. (2015). Synthesis, properties, and biomedical applications of gelatin methacryloyl (GelMA) hydrogels. *Biomaterials* 73, 254–271. doi: 10.1016/j.biomaterials.2015.08.045

Zhang, B., Montgomery, M., Chamberlain, M. D., Ogawa, S., Korolj, A., Pahnke, A., et al. (2016). Biodegradable scaffold with built-in vasculature for organ-on-a-chip engineering and direct surgical anastomosis. *Nat. Mater.* 15:669. doi: 10.1038/nmat4570

Zhang, Q., Lu, H., Kawazoe, N., and Chen, G. (2014). Pore size effect of collagen scaffolds on cartilage regeneration. *Acta Biomater.* 10, 2005–2013. doi: 10.1016/j.actbio.2013.12.042

Zhang, X., Xu, B., Puperi, D. S., Yonezawa, A. L., Wu, Y., Tseng, H., et al. (2015). Integrating valve-inspired design features into poly (ethylene glycol) hydrogel scaffolds for heart valve tissue engineering. *Acta Biomater.* 14, 11–21. doi: 10.1016/j.actbio.2014.11.042

Zhao, X., Huebsch, N., Mooney, D. J., and Suo, Z. (2010). Stress-relaxation behavior in gels with ionic and covalent crosslinks. *J. Appl. Phys.* 107:063509. doi: 10.1063/1.3343265

Zhao, X., Lang, Q., Yildirimer, L., Lin, Z. Y., Cui, W., Annabi, N., et al. (2016). Photocrosslinkable gelatin hydrogel for epidermal tissue engineering. *Adv. Healthc. Mater.* 5, 108–118. doi: 10.1002/adhm.201500005

Zhu, Y., Wu, H., Sun, S., Zhou, T., Wu, J., and Wan, Y. (2014). Designed composites for mimicking compressive mechanical properties of

articular cartilage matrix. *J. Mech. Behav. Biomed. Mater.* 36, 32–46. doi: 10.1016/j.jmbbm.2014.04.003

Zieris, A., Prokoph, S., Levental, K. R., Welzel, P. B., Grimmer, M., Freudenberg, U., et al. (2010). FGF-2 and VEGF functionalization of starPEG–heparin hydrogels to modulate biomolecular and physical cues of angiogenesis. *Biomaterials* 31, 7985–7994. doi: 10.1016/j.biomaterials.2010. 07.021

Zuo, Y., Liu, X., Wei, D., Sun, J., Xiao, W., Zhao, H., et al. (2015). Photo-cross-linkable methacrylated gelatin and hydroxyapatite hybrid hydrogel for modularly engineering biomimetic osteon. *ACS Appl. Mater. Interfaces* 7:10386–10394. doi: 10.1021/acsami.5b01433

Preparation and Characterization of Chitosan/β-Glycerophosphate Thermal-Sensitive Hydrogel Reinforced by Graphene Oxide

Han Qin, Jian Wang, Tong Wang, Xiaomeng Gao, Qianbing Wan* and Xibo Pei*

State Key Laboratory of Oral Diseases, Department of Prosthodontics, National Clinical Research Center for Oral Diseases, West China Hospital of Stomatology, Sichuan University, Chengdu, China

Thermal-sensitive hydrogel based on chitosan (CS) and β-glycerophosphate (GP) has shown good biocompatibility and biodegradability. But the application of such hydrogel is limited due to its poor mechanical property. Recently, graphene oxide(GO) is widely used as a reinforcement agent to prepare nanocomposites with different polymers for improving the properties of the materials. In this study, CS/GP-based hydrogels with different weight ratio of GO/CS (0.5, 1, 2%) were fabricated. The gelation time of the hydrogels at body temperature was evaluated by tube inverting method. The gelation process during heating was monitored by rheological measurement. The morphology, porosities, chemical structure, swelling properties of the lyophilized hydrogels were investigated by scanning electron microscopy, liquid displacement method, Fourier transform infrared spectroscopy and gravimetric method. Mechanical property of the hydrogels was analyzed by rheological measurement and unconfined compression test. MC3T3-E1 mouse pre-osteoblast cell line was used to assess the biological properties of the hydrogels. The results obtained from those assessments revealed that the addition of GO into CS/GP improved the properties of the prepared hydrogels without changing the high porous and interconnected microstructure and swelling ability of the hydrogels. The gelation time at body temperature was significantly reduced by nearly 20% with the addition of small amount of GO (0.5% weight ratio of CS). The mechanical properties of the hydrogels containing GO were improved significantly over that of CS/GP. The storage (G′)/loss (G″) moduli of the hydrogels with GO were 1.12 to 1.69 times that of CS/GP at the gelling temperature. The Young's modulus of 0.5%GO/CS/GP hydrogel is 1.76 times that of CS/GP. Moreover, the 0.5%GO/CS/GP hydrogel revealed remarkable biological affinity such as cellular attachment, viability and proliferation. All of these results suggest that 0.5%GO/CS/GP hydrogel has great potential for practical application in biomedical field.

Keywords: thermal-sensitive, hydrogel, chitosan, β-glycerophosphate, graphene oxide

INTRODUCTION

Hydrogels have some unique physical properties, which make them widely used in biomedical fields such as tissue engineering, wound dressing and drug delivery systems (Bhattarai et al., 2010). A good candidate to form hydrogel is chitosan (CS), a copolymer of β[1,4]-linked 2-acetamido-2-deoxy-D-glucopyranose and 2-amino-2-deoxy-D-glucopyranosea. This biopolymer with polycationic structure is generally obtained by alkaline deacetylation from chitin which is the second most abundant polysaccharide in nature after celluse (Rinaudo, 2006). Because of its non-toxicity, biocompatibility, biodegradability, antibacterial ability, and low immunogenicity, chitosan has attracted large interest in biological application such as tissue engineering, drug delivery and wound healing (Riva et al., 2011; Zhao et al., 2015, 2018; Dong et al., 2016). These admirable characteristics of chitosan is ascribed to its unique chemical structure. For example, the polysaccharide unit of chitosan resembles the structure of glycosaminoglycans (GAGs), which is the major component of the extracellular matrix (ECM) of bone and cartilage (Khor and Lim, 2003). The cationic character of chitosan enables it to form complexes with anionic molecules, including proteoglycans, GAGs, growth factors, receptors and adhesion proteins that help to regulate cellular activity (Lehr et al., 1992; Dutta et al., 2011). In addition, chitosan can create networks with highly porous and interconnected pore structure which is helpful for cell adhesion, proliferation, and differentiation as it enhances the diffusion of nutrients and provide room for neovascularization (Dutta et al., 2011). Hence, chitosan can be used to form hydrogels as scaffolds or substrate for tissue engineering.

Generally, chitosan hydrogels can be prepared by either covalently or ionically crosslinking methods with the addition of different crosslinkers. Covalently cross-linked hydrogels possess a stable and permanent network structure as irreversible chemical bonding are formed. However, covalent cross-linkers such as glutaraldehyde are usually toxic to organism. And the chemical crosslinking makes hydrogels hard to degrade. On the other hand, ionically cross-linked hydrogels are formed by reversible links and generally considered biocompatible, exhibiting a higher swelling sensitivity to pH changes compared with covalently cross-linked chitosan hydrogels (Berger et al., 2004). Because chitosan is a polycationic polymer, one of the anionic molecules—β-glycerophosphate (GP) can be used as an ionic crosslinking agent. It is an organic compound naturally found in the body and has been used as an osteogenic supplement for culturing human bone marrow stem cells (Zhou et al., 2015). Chitosan/β-Glycerophosphate (CS/GP) is an *in situ* thermal-sensitive gelling system, which maintains fluidity at low temperature (room temperature or below) and becomes gel at higher temperature (body temperature) (Berger et al., 2004; Zhou et al., 2015). With this characteristics, CS/GP hydrogel has attracted great attention as it does not require an surgical operation when implanted (Zheng et al., 2010). However, the usage of the material is usually limited due to its poor mechanical properties. Hence, many studies aimed at improving its mechanical functionality by blending CS/GP system with

other nanomaterials, such as nano-attapulgite (Wang and Chen, 2016), nano-hydroxyapatite (Huang et al., 2011; Chen et al., 2016), nanosilver (Tsai et al., 2011), carbon nanotubes(CNTs) (Gholizadeh et al., 2017) and etc.

In addition to those nanofillers, a recently attractive material has yet not been studied as a reinforcing agent in CS/GP system—graphene. Graphene is expected for application in various fields because of its exceptional physico-chemical properties (Zhu et al., 2010). It is considered as a promising nanofiller as it possesses high aspect ratio which is a very useful parameter for improving the properties of materials, such as thermal, electrical and mechanical properties (Stankovich et al., 2006; Cote et al., 2009; Salavagione et al., 2009; Vickery et al., 2009). Compared with its allotrope CNTs, graphene offers enhanced mechanical properties to the composite, due to the planar structure and the aspect ratio, which allows better stress transfer within the host medium during the loading process (Mittal et al., 2015). Moreover, graphene-based materials promote stem cell attachment and growth, and enhance osteogenic differentiation, indicating its application as an alternative material for bone regeneration research (Dubey et al., 2015). A widely used form of graphene is graphene oxide (GO), which is amphiphilic due to the multiple oxygen-containing groups such as hydroxyls, epoxides, and carboxyls on its surface (Li et al., 2008; Marcano et al., 2010). These functional groups (oxygen-containing) allow GO to disperse at an individual sheet and highly negatively charged in aqueous solution, which makes it possible to form special interaction between GO and protonated polymers such as CS. Meanwhile, these functional groups (oxygen-containing) as well as the large aromatic (π-configuration) interface endow GO with the ability to interact with proteins, peptides, or DNA via chemical bonding or physical adsorption (Shin et al., 2016). Adding GO into CS to form films or scaffolds have been reported with improved properties, including mechanical strength in both wet and dry state, storage modulus, and thermal stability (Fan et al., 2010; Yang et al., 2010; Depan et al., 2011; Han et al., 2011; Dinescu et al., 2014). Because of the advantages of graphene and its derivatives and previous studies of CS and GO mentioned above, we considered adding graphene oxide into CS/GP system to improve the properties of CS/GP hydrogel.

In the present work, GO/CS/GP hydrogels with different GO/CS weight ratios were prepared as the amount of GO in nanocomposites plays an important role to the properties of materials. Meanwhile, the physical, chemical and biological properties of each hydrogel were evaluated. We expect to develop a composite hydrogel of GO/CS/GP with suitable mechanical properties while maintaining biological functionality for biomedical applications.

MATERIALS AND METHODS

Materials

β-Glycerophosphate disodium salt was obtained from Sigma-Aldrich Co.(US). Medium molecular weight chitosan(molecular weight≈21,0000 Da, deacetylation degree≥95%) was purchased from Tokyo Chemical Industry Co., Ltd. Acetic acid (chemical reagents of analytical grade) was provided by Baoxin

Bio-Technology Co., Ltd. (Chengdu, China). Single-layered graphene oxide, purity>99%, diameter of 0.5–5 μm, thickness of 0.8–1.2 nm was purchased from Nanjing/Jiangsu XFNANO Materials Tech Co., Ltd. (Nanjing, China).

Preparation of the Hydrogels

To prepare 10 mL GO/CS/GP hydrogel, the following steps were implemented. Firstly, 200 mg CS powder was dissolved in 6 mL acetic acid (0.75%v/v) and vigorously stirred for 1 h; prescribed amount (1, 2 or 4 mg) of GO sheets were dispersed in 2 mL distilled water and treated by ultrasonication for 1 h; 600 mg GP was dissolved in 2 mL distilled water. Secondly, GO dispersion was added into the CS solution and stirred for 1 h until complete mixture. Finally, the GP solution was added dropwise to the GO/CS mixed solution under constant stirring. As the control group, the CS/GP hydrogel was prepared following the same steps above except that the GO dispersion was replaced by 2 mL distilled water. According to the weight ratio of GO and CS, the samples were grouped as CS/GP, 0.5%GO/CS/GP, 1%GO/CS/GP, and 2%GO/CS/GP. The total concentrations of the components in each hydrogel groups were shown in **Table 1**.

Gelation Time Determination

Appropriate gelation time of the hydrogel is of much importance for the clinical or biomedical application. The test tube inverting method was used to measure the gelation time at constant temperature of 37°C in a water bath (Zhao et al., 2009; Mirahmadi et al., 2013). One milliliter of each sample ($n = 5$) was added into test tubes at room temperature, then incubated in the water bath. The fluidity of the samples was observed every 30 s by tilting the tube. The time at which flow stopped was taken as the gelation time and the values were recorded.

Rheological Measurement

To analyze the rheological properties of the hydrogels in the gelling process, rheology tests was performed with a rheometer (HAKKE Viscotester IQ Air 260-100, Thermofish, US), which required about 2 mL of the solution per sample. Samples of all groups were inserted into the rheometer. Oscillatory measurements were performed at 1 Hz, while the temperature was elevated at the rate of 2°C/min from 10 to 60°C. During the gelling process, the dynamic rheological properties such as the dynamic elastic (storage) modulus (G′) and the viscous (loss) modulus (G″) were measured by oscillatory shear measurement. The gelation temperature was determined as the crossover point of the elastic (G′) and viscous (loss) moduli (G″) (δ = 45°).

Scanning Electron Microscopy (SEM)

After gelation, all samples were frozen in a refrigerator at −20°C for 2 h and then lyophilized in a freeze drier at −80°C for 24 h. Afterwards, the samples were sputter coated with gold and scanning electron microscopy (SEM) (Inspect F50, FEI, Hillsboro, OR, US) was used to evaluate the surface morphology, pore morphology, and pore size distribution of the samples. The average pore size of each sample were obtained using the software Digimizer, 20 pores were considered.

Porosity Determination

The porosities of the hydrogels were measured using liquid displacement method. Briefly, initial weight and volume of the lyophilized hydrogels ($n = 5$) were measured and recorded (W and V, respectively). Then, the gels were immersed in dehydrated alcohol for 24 h until they were fully saturated. After removal of the surface liquid, the gels were weighted again (W'). The porosities were calculated using the equation below (Gholizadeh et al., 2017):

$$Porosity(\%) = [(W' − W)/(V × \rho)] × 100\%$$

Where ρ is the density of alcohol.

Fourier-Transform Infrared (FTIR) Spectroscopy

The FTIR spectra of CS, GO, GP and all the lyophilized samples were recorded in KBr pellets with a Nicolet FT-IR 6700 spectrophotometer (Thermo Nicolet Corp., Madison, WI, US). An IR spectral range of 400–4,000 cm^{-1} was analyzed.

In vitro Swelling Kinetic Analysis

The water uptake ability of the hydrogels was measured by classical gravimetric method (Mirahmadi et al., 2013; Gholizadeh et al., 2017). Each sample ($n = 5$) of lyophilized hydrogels was weighed (W_d) and immersed into the distilled water at 37°C for 12 h. At appropriate intervals (10, 20, 30 min, 1, 2, … 12 h), samples were retrieved and blotted with filter paper to remove the surface solution and weighed again (W_w). The water uptake ratio (E_u) at each interval was calculated as below (Mirahmadi et al., 2013; Gholizadeh et al., 2017):

$$E_u = [(W_w − W_d)/W_d]$$

Mechanical Properties

The compressive mechanical property of the hydrogels was tested by a universal tensile testing machine (SANS CMT4000) at room temperature under a 9 N load cell. Dimensions of the samples were measured carefully using a digital caliper. The state of the hydrogel samples was examined with crosshead speed of 2 mm/min until reaching 20% strain. At least four specimens were tested for each group. Force and deformation data were collected by the test instrument and were converted to stress and strain values. Elastic modulus was determined from the slope of the linear portion of the stress–strain curve for all samples.

TABLE 1 | Total concentrations of component in each hydrogel group.

Group	Chitosan wt %	GO wt %	GO/CS weight ratio %	GP wt %
CS/GP	2	0	0	6
0.5%GO/CS/GP	2	0.01	0.5	6
1%GO/CS/GP	2	0.02	1	6
2%GO/CS/GP	2	0.04	2	6

Cell Studies

The cell studies were conducted using the mouse pre-osteoblast cell line MC3T3-E1. Alpha-minimum essential medium (α-MEM, HyClone, USA) supplemented with 10% fetal bovine serum (FBS, HyClone, USA) and 1% penicillin–streptomycin was used to culture the cells.

Sterile hydrogels were prepared according to the steps mentioned above (Preparation of the hydrogels) in aseptic environment. The CS powder and GO sheets were sterilized by ultraviolet ray radiation before dissolved in acetic acid and dispersed in distilled water. The GP solutions and acetic acid were sterilized by using $0.22\,\mu m$ filtration.

The hydrogel solutions were placed in 24-well plates (0.5 mL for each well) and incubated in a humidified incubator at 37°C. After gelation, all the hydrogels were washed three times with cell culture medium every 30 min and then MC3T3-E1 cells were seeded into the hydrogels (5×10^4 cells/well). 1 mL complete medium was added to each well. Culture medium was changed every 2 days.

Cell Attachment

SEM was used to study the attachment and morphology of the cells on the hydrogels. The culture medium was removed from the cell-gel constructs after cells were cultured on the gels for 24 h. The cell-gel constructs were washed twice with PBS, followed by fixation with 2.5 vol.% glutaraldehyde for 2 h at 4°C. After removing the fixatives, the constructs were dried with a graded series of ethanol and sputter coated with gold. Then the samples were observed by SEM.

Cell Proliferation

CCK-8 test was used for cell proliferation assessment. After culturing for 1, 4, and 7 days, cell culture medium of the samples ($n = 4$) was removed and 350 μL fresh culture medium with 35 μL CCK-8 reagent was added to each sample. After incubated at 37°C for 2 h, 100 μL medium of each well was transferred to 96-well plate. The absorbance values were measured using a microplate reader (Bio-Rad, USA) at wavelength of 450 nm. The results obtained were expressed as optical density (OD) after blank subtraction.

Cell Viability and Morphology

Fluorescent inverted microscopy was used to study the viability and morphology of MC3T3-E1 on the hydrogels using live/dead staining kit Calcein-AM/Propidium iodide (Calcein-AM/PI, Sigma, USA). Cells were cultured on the gels for 1 d and 5 d, then culture medium was removed and cell-gel constructs in each well were washed twice with PBS. Onemilliliter dye (10 μg/mL in PBS) was added into each well. After incubation for 45 min, the dye was removed and the constructs were washed once with PBS. The samples were observed with fluorescence inverted microscope (IX 71, Olympus, Japan) under blue fluorescent light (490 nm) and green fluorescent light (545 nm), respectively. Live cells were stained green and nucleus of dead cells were colored red.

Statistics

At least three samples were tested for each experiment and all data were reported as mean ± SD. Statistical analysis was carried out using one-way analysis of variance (ANOVA) for the comparison of groups and results were set as significant for $p < 0.05$.

RESULTS

Gelation Time

Figure 1 showed the gelation time of the hydrogels at 37°C. All the samples were converted to gels around physiological temperature in <10 min but the time durations were different. CS/GP became gel in 9 ± 0.41 min, while 0.5%GO/CS/GP became gel in 7.25 ± 0.29 min. The gelation time was reduced about 20% ($p < 0.05$) by adding a small amount of GO (0.5% weight ratio of CS) into the CS/GP. Gelling time appeared to display an apparent decrease with the increase of GO/CS ratio. 1%GO/CS/GP and 2%GO/CS/GP became gels in 6.63 ± 0.25 min(1%GO/CS/GP) and 4.88 ± 0.25 min(2%GO/CS/GP), respectively.

Rheological Measurement

The results of rheology tests were showed in **Figure 2**. There were three regions in the curves according to the temperature range upon the heating process. In region 1, the samples showed a viscoelastic fluidlike behavior ($G' < G''$), and both G' and G'' moduli decreased as the temperature increased, which is the common behavior of a polymer solution. In the next region (region 2), both storage modulus (G') and loss modulus (G'') abruptly increased during heating due to the fast formation of the three-dimensional network. However, the growing rate of G' was much larger than that of G'' in this region, indicating that the development of the gel structure contributed
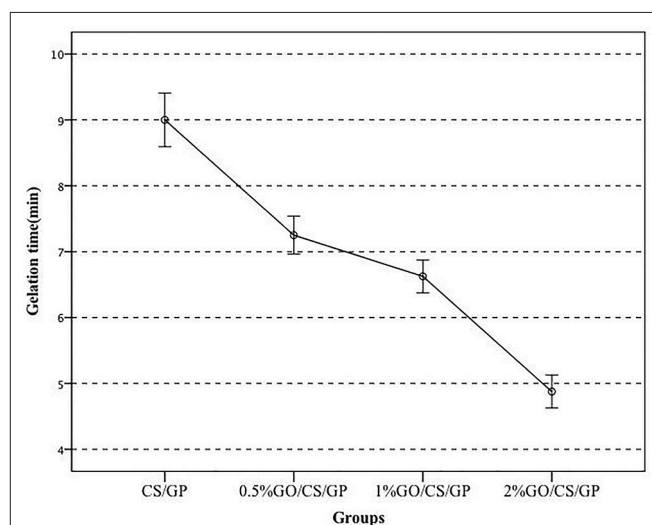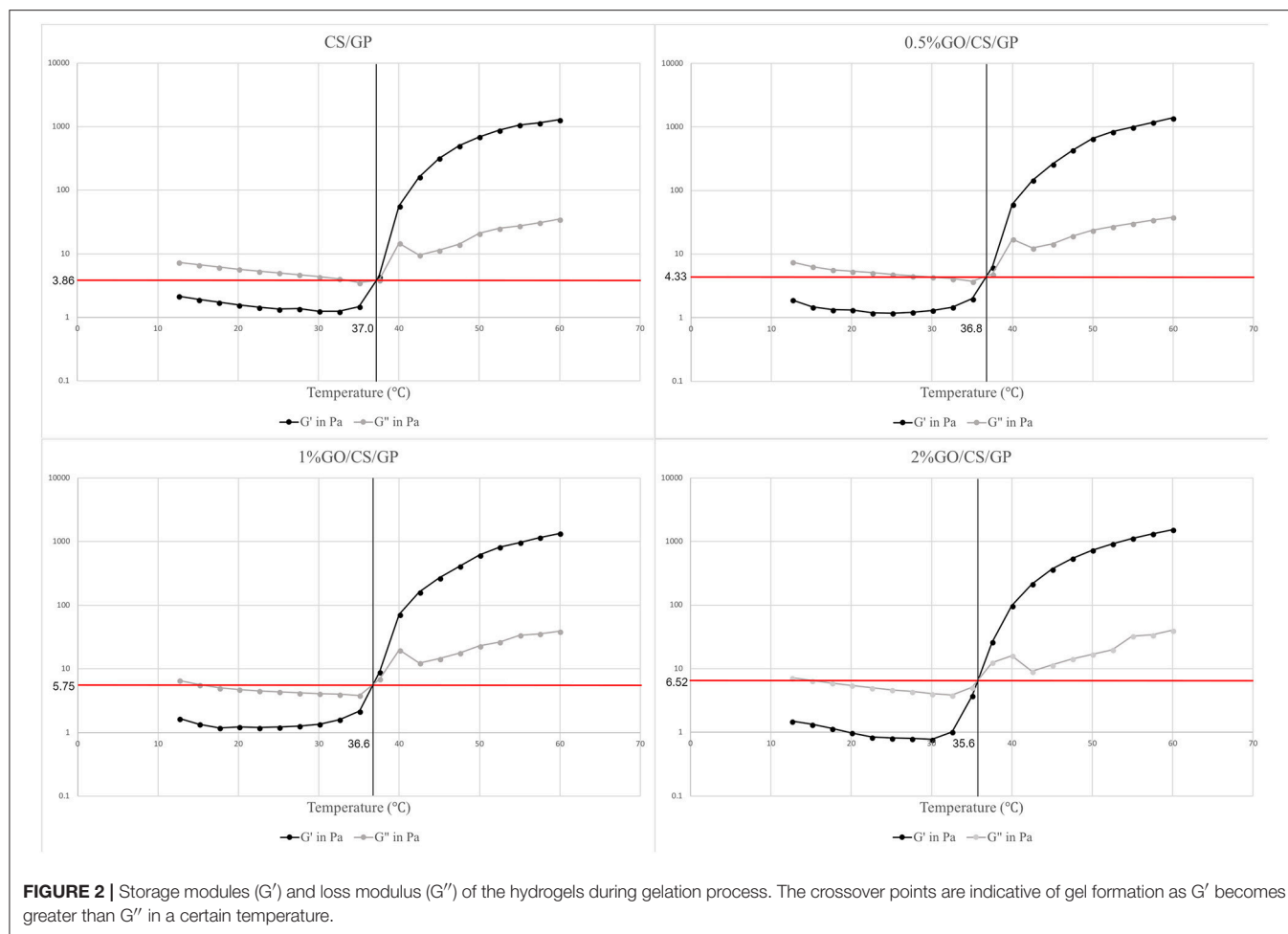

FIGURE 1 | The gelation time of the hydrogels with different content of GO at 37°C.

FIGURE 2 | Storage modules (G′) and loss modulus (G″) of the hydrogels during gelation process. The crossover points are indicative of gel formation as G′ becomes greater than G″ in a certain temperature.

to the stiffening of the system. The gelation temperature was determined at the crosspoint of storage (G′) and loss (G″) moduli ranging from 35.7 to 37.0°C. The slight difference of gelation temperature of the hydrogels may attribute to the existence of graphene oxide. At the gelling point, the storage (G′)/ loss (G″) moduli showed a positive correlation with the amount of GO. The storage (G′)/ loss (G″) moduli of CS/GP, 0.5%GO/CS/GP, 1%GO/CS/GP and 2%GO/CS/GP at the gelling point were 3.86, 4.33, 5.75, and 6.52 Pa, respectively. In the last zone (region 3), the gelation process became much slower because of the lower diffusivity resulted from the increasing viscosity during the network formation.

Morphology Observation

The high porous homogeneous and interconnected structure of the lyophilized hydrogels were revealed by scanning electron microscopy (**Figure 3**). The microstructure of the hydrogels containing GO were similar to that of CS/GP, irrespective of the amount of GO. The average pore sizes of each hydrogel were presented in **Table 2**. The average pore size of CS/GP was 56.61 ± 18.82 μm, while the average pore size of 0.5%GO/CS/GP was 58.83 ± 19.85 μm. With the adding amount of GO, the average pore sizes were substantially increased to 65.26 ± 15.32 μm

(1%GO/CS/GP) and 69.61 ± 19.72 μm (2%GO/CS/GP). The interconnecting pores and canals of the hydrogels were uniform and coherent, which makes fast liquid convection. Porosity measurement was conducted by liquid displacement method and the results are presented in **Table 2**. All the hydrogels had porosities in the range 80% to 90%. The porosity of the CS/GP was the lowest (81 ± 3%), whereas, by the addition of small amount of GO (0.5% weight ratio of CS) into the gelling system, the porosity was increased to 83 ± 2%. The porosities of 1%GO/CS/GP and 2%GO/CS/GP were 84 ± 3% and 88 ± 3%, respectively.

Water Uptake

The water uptake abilities of the hydrogels were displayed in **Figure 4**. The swelling ratios of all the four hydrogels showed a similar trend of time-dependent increasing in the initial 4 h and then remained unchanged in the following 8 h, which indicated the hydrogels had reached their equilibrium state. In general, the water uptakes ratios of all the hydrogels were above 8 after immersion for 10 min and increased with time. At equilibrium state, the E_u of CS/GP was 9.23 ± 0.83, while E_u of 0.5%GO/CS/GP was 8.68 ± 0.33. However, there was no significant difference among E_u values of the groups.
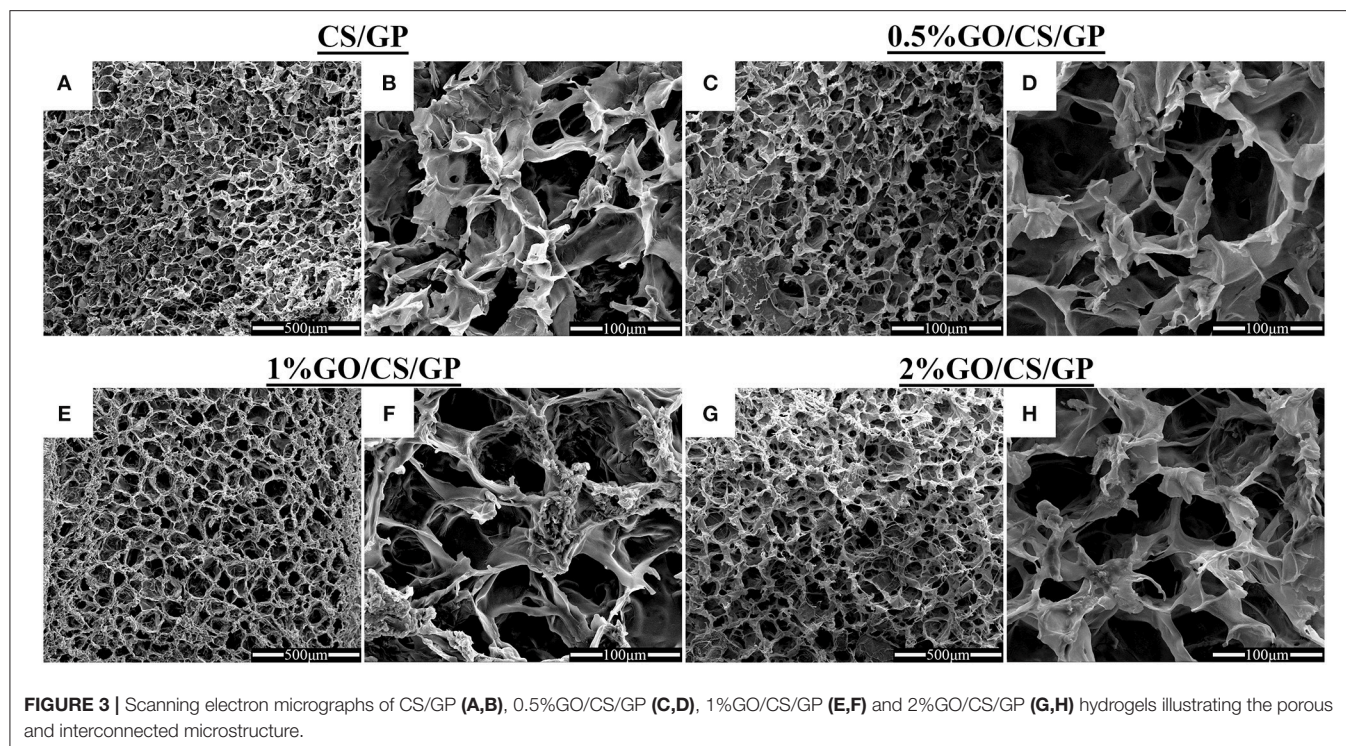
FIGURE 3 | Scanning electron micrographs of CS/GP **(A,B)**, 0.5%GO/CS/GP **(C,D)**, 1%GO/CS/GP **(E,F)** and 2%GO/CS/GP **(G,H)** hydrogels illustrating the porous and interconnected microstructure.

TABLE 2 | Summary of the physical properties of lyophilized hydrogels.

Group/properties	Average pore diameter (μm)	Porosity (%)
CS/GP	56.61 ± 18.82	81 ± 3
0.5%GO/CS/GP	58.83 ± 19.85	83 ± 2
1%GO/CS/GP	65.26 ± 15.32	84 ± 3
2%GO/CS/GP	69.61 ± 19.72	88 ± 3

FTIR Spectra of the Hydrogels

The differences in chemical structures of GP, GO, CS, CS/GP, 0.5%GO/CS/GP, 1%GO/CS/GP, and 2%GO/CS/GP determined by FTIR were shown in **Figure 5**. In the spectrum of GO, the peaks at 1,730 and 1,628 cm^{-1} represented C=O stretch of the carboxylic group and the C–C stretching mode of the sp^2 carbon skeletal network, respectively. In regard to CS, two characteristic absorbance bands centered at 1,653 and 1,597 cm^{-1} corresponded to the C=O stretching vibration of –NHCO– (amide I) and the N–H bending of –NH$_2$ (amide II), respectively. The spectrums of all the lyophilized hydrogels were similar, showing lower wavenumbers of amide I (1,643 cm^{-1}) and amino groups (1,550 cm^{-1}). This could be interpreted by the electrostatic interaction between protonated CS and negative charged GP (Zhou et al., 2008; Assaad et al., 2015). For the hydrogels containing GO, the disappearing of the peak at 1,730 cm^{-1} which related to C=O stretch could be explained by the synergistic effect of H-bonding between CS and the oxygen-containing groups in GO and electrostatic interaction between polycationic CS and the negatively charged GO (Yang et al., 2010).

Mechanical Testing

Results of unconfined compression test on the hydrogels were shown in **Figures 6**, **7**. Stress-strain profiles (**Figure 6**) showed that all the hydrogels exhibited a linear strain-stress relationship from 0 to 20% strain. Determination of the linear modulus (**Figure 7**) revealed that 0.5%GO/CS/GP hydrogel was 1.76 times stiffer than CS/GP hydrogel ($p < 0.05$). 0.5%GO/CS/GP hydrogel had a modulus of 6.96 ± 0.43 kPa while CS/GP hydrogel had the modulus of 3.95 ± 0.68 kPa. The modulus of the hydrogels displayed a positive correlation with the content of GO as the modulus of 1%GO/CS/GP and 2%GO/CS/GP were 8.21 ± 0.49 and 11.61 ± 2.19 kPa, respectively.

Cellular Assay

The SEM micrographs in **Figure 8** illustrated cellular attachment on the surface of the hydrogels. The porous structure could not be observed as the dehydration treatment before SEM made the hydrogel shrink to a film. Most of the cells on the surface of the CS/GP and 0.5%GO/CS/GP hydrogels showed a spindle shape, which was the typical morphology of MC3T3-E1, indicating that the cells were still spreading and growing. While there were more cells on the surface 1%GO/CS/GP and 2%GO/CS/GP hydrogels that showed a spherical shape, indicating the cells were not completely attached to the substrate.

The results of CCK-8 assay of the samples at day 1, 4, and 7 were shown in **Figure 9**, revealing the proliferation of cells grown in all the hydrogels over the incubation period. However, there were differences among the OD values of groups at 4 d and 7 d, indicating the proliferation of cells was influenced by GO. At day 1, there was no significant difference of the OD values among the
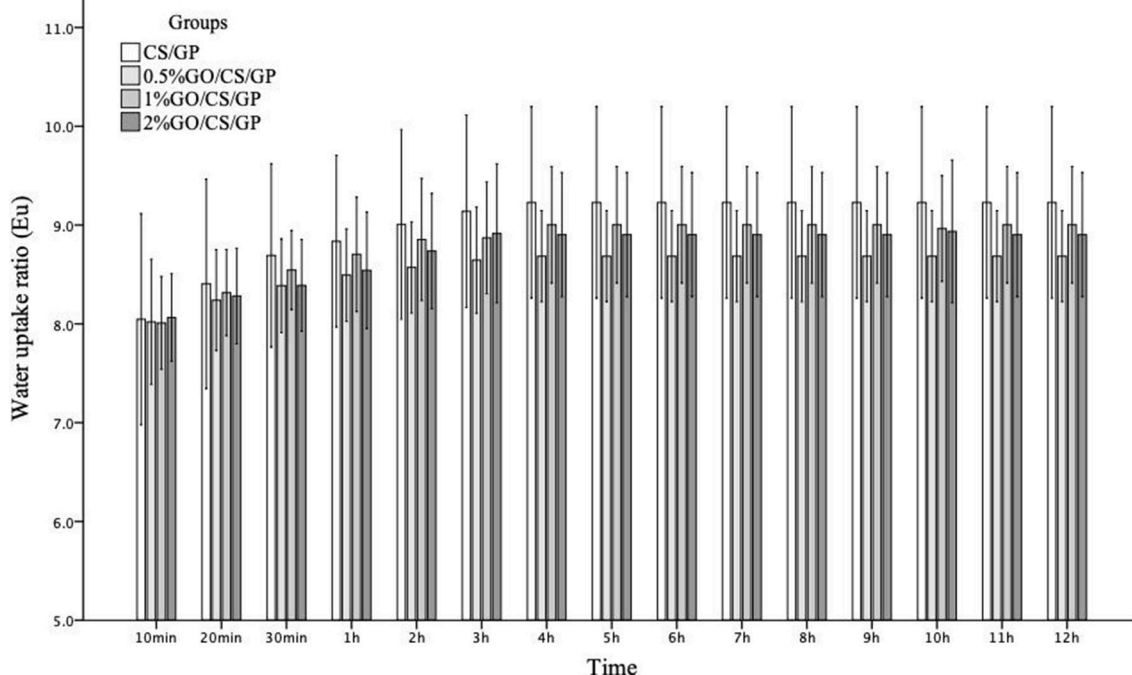
FIGURE 4 | The water uptake ratios of CS/GP, 0.5%GO/CS/GP, 1%GO/CS/GP, 2%GO/CS/GP with time.
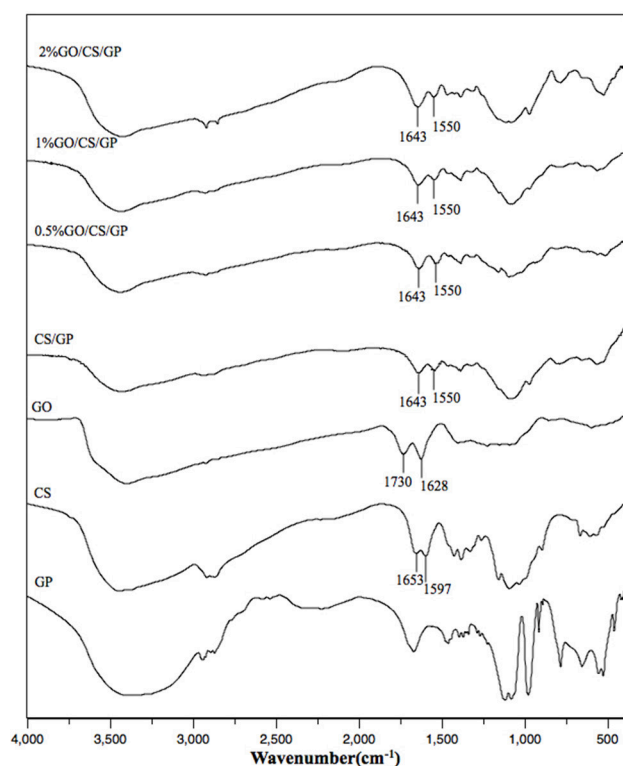
FIGURE 5 | The FTIR spectrum of CS/GP, 0.5%GO/CS/GP, 1%GO/CS/GP, 2%GO/CS/GP, CS, GO, GP.
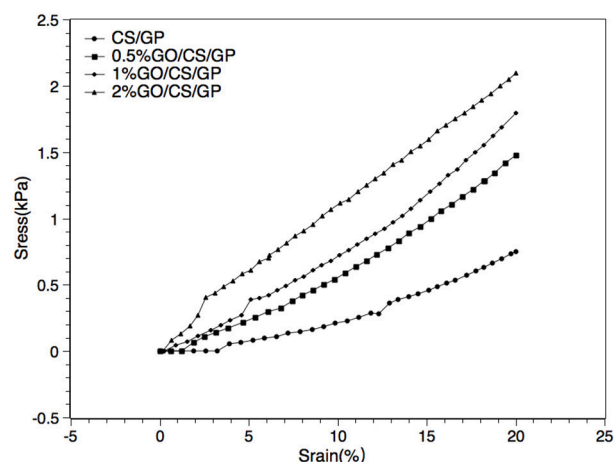
FIGURE 6 | Representative strain–stress curves of CS/GP, 0.5%GO/CS/GP, 1%GO/CS/GP, 2%GO/CS/GP.

samples. At day 4 and 7, the OD values of 2%GO/CS/GP were significant lower than the other three samples. At day 7, the OD value of group 1%GO/CS/GP was lower than those of CS/GP and 0.5%GO/CS/GP, and the OD value of 2%GO/CS/GP was even lower.

Results of live/dead (**Figure 10**) staining revealed that most cells survived in all hydrogels, but there was no obvious difference in cell morphology and viability among the groups at d 1.
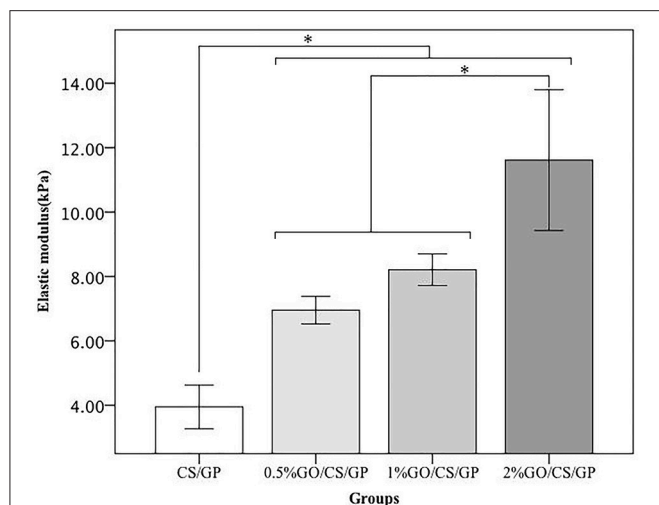
FIGURE 7 | Elastic modulus obtained by unconfined compressive mechanical tests. *Statistically significant differences existing among the groups.

FIGURE 9 | CCK-8 cellular proliferation assays of CS/GP 0.5%GO/CS/GP, 1%GO/CS/GP and 2%GO/CS/GP. *Statistically significant differences existing among the groups.

FIGURE 8 | Scanning electron micrographs of cellular adhesion on CS/GP**(A)**, 0.5%GO/CS/GP**(B)**, 1%GO/CS/GP**(C)**, and 2%GO/CS/GP**(D)** after incubation for 24 h. White arrows indicate cells with spindle shape, black arrows indicate cells with spherical shape.

DISCUSSION

In the present study, chitosan/β-Glycerophosphate hydrogels with different content of graphene oxide were fabricated through thermal-induced gelation at physiological pH and temperature, indicating that such materials can be possibly used as injectable *in situ* scaffold for tissue engineering.

Mechanism of Gel Formation

GP is a key factor for gel formation. Previous studies reported that higher content of GP induced faster hydrogel formation or gelation at lower temperature (Cho et al., 2006). However, it h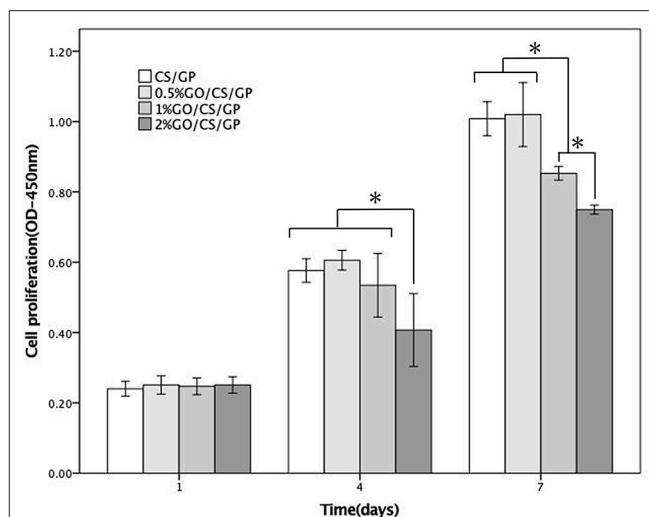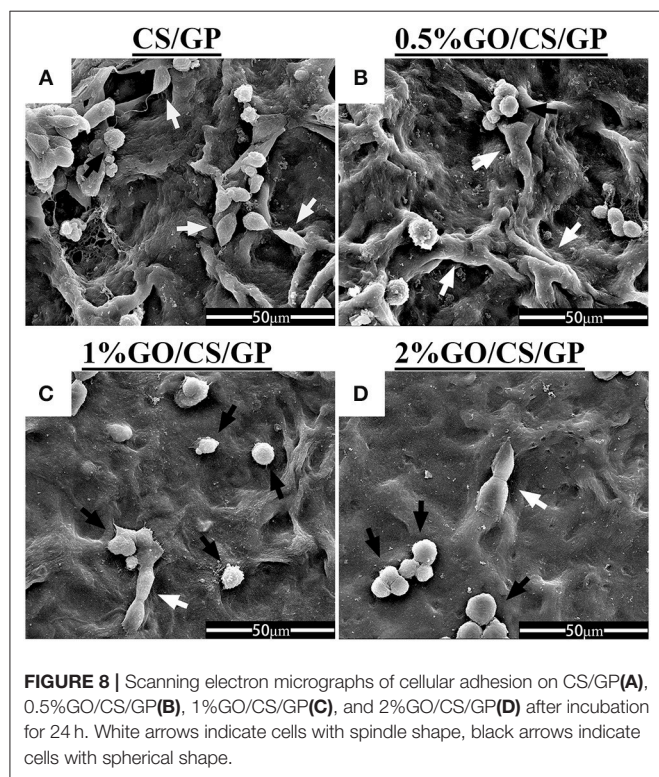as also been suggested that high concentrations of GP can be detrimental to cell viability and proliferation (Ahmadi and de Bruijn, 2008; Wang and Stegemann, 2010). The reason may be that high concentrations of GP avoidably dissolves and diffuses into the surrounding culture medium or tissue fluid, causing osmosis pressure change, which will lead to cell activity decrease or even cell death (Song et al., 2017). In order to initiate the gelling process at body temperature while avoiding causing cytotoxicity, the concentration of 6 wt% GP was chosen to prepare hydrogel in this work. The gelation mechanism of CS/GP system has been explained by many studies in literature. Briefly, there are three effective interactions involved in the sol/gel transition: (1) the electrostatic attractions between chitosan and β-glycerolphosphate via amino and the phosphate groups, respectively, (2) the chitosan interchain hydrogen bonding, and (3) the chitosan–chitosan hydrophobic interactions which could be enhanced by the structuring action of glycerol on water (Cho et al., 2006; Ahmadi and de Bruijn, 2008; Zhou et al., 2015). When adding GO, the molecular mechanism of gelation involves multiple interactions between CS, GP, GO and water (**Figure 11**). In addition to the three interactions mentioned above, in GO/CS/GP system, electrostatic attraction, hydrogen

After 5 days, it could be observed that cells in CS/GP and 0.5%GO/CS/GP spread better and showed a typically spindle-shaped morphology. There were less live cells in 1%GO/CS/GP and 2%GO/CS/GP and the proportion of spherical-shaped cells was higher. These images suggest that hydrogel containing small amount of GO (0.5%) showed no difference in cell attachment, viability and proliferation compared with CS/GP hydrogel.

FIGURE 10 | Fluorescence micrographs stained by Calcein-AM/PI illustrating the cellular viability on the hydrogels after incubation for 1 day and 5 days. Live cells were stained green and nucleus of dead cells were colored red.
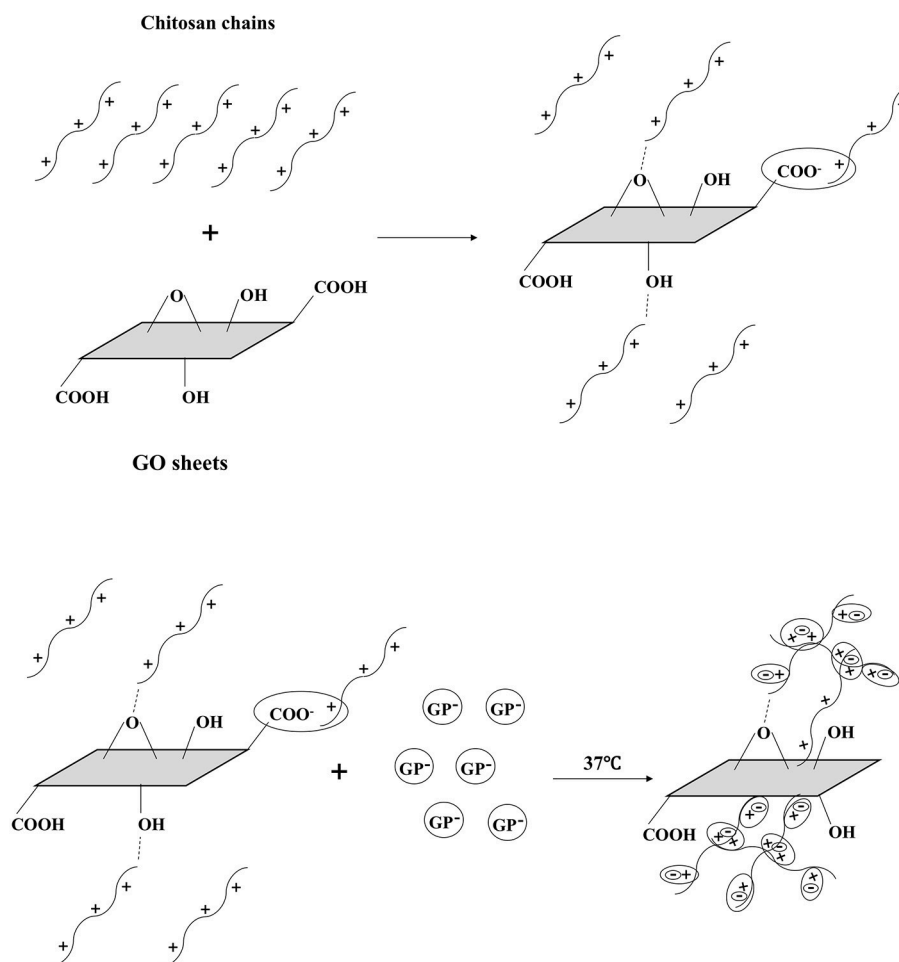
FIGURE 11 | Schematic illustration of gel formation at 37°C. GO and CS were interacted by H-bonding and electrostatic bonding in the homogeneous codispersion. With the addition of GP, the repulsion of pronated CS was weakening due to the CS-GP electrostatic attractions via amino and the phosphate groups. When the temperature rises, the hydrophobic effect of CS chains becomes dominant. CS chains entangle with each other and the gel forms. GO sheets reinforce the hydrophobic effect, inducing the faster gelation.

bonding and hydrophobic interaction also exist between GO and CS. When mixing GO dispersion and CS acetic acid solution, because of polycationic nature of CS in acid media and the negative charge on the surface of GO, electrostatic attraction can be achieved. Hydrogen bonding can be formed between the amino and hydroxyl groups in the unit of CS and the oxygen-containing groups on the GO. These two interactions between CS and GO could induce the truly homogeneous codispersion on the molecular scale (Yang et al., 2010). It has been confirmed that the hydrophobic effect is the main driving force for the heat-induced gelation of CS/GP system since the ratio of $-NH_3^+$ in chitosan and $-OPO(O^-)^2$ in GP reduces and the hydrogen bonding are not predominant (Zhou et al., 2015). In the presence of GO, the sp^2 bonded substrate could reinforce the hydrophobic effect of the system upon heating. As it shown in the rheological test and gelation time determination, hydrogel containing more GO had lower gelation temperature and faster gelation process.

Properties of the Hydrogels

The results of rheological tests revealed that the gelling process of all groups started around the body temperature and the results of gelation time indicated that all the hydrogels could be formed in several minutes at 37°C, which is of much importance in clinical application. When injecting the heat-induced *in situ* gelling system into irregular-shaped bone defect (e.g., oral and maxillofacial region), the material could well adjust to defect zone due to its fluidity. Appropriate gel formation speed gives the practitioner enough time to inject or shape the gel to an ideal form. And the practitioner does not have to waste too much time on waiting for the gelation before the next surgery step. The gelation time of the hydrogels (several minutes) in this study was approximately equal to or less than the time needed for putting bone substitute into the bone defect and laying a membrane above it, which is a routine procedure of guided bone regeneration (GBR) technique in oral implantation. From the perspective of operability, the thermal-sensitive hydrogels offer a more convenient and less time-consuming alternative procedure compared with traditional treatments.

The SEM images demonstrated highly porous structure of the hydrogels. The interconnecting and stable internal channel system provides space for embedded cells (Mirahmadi et al., 2013). Appropriate pore size, porosity and desirable water uptake ability are beneficial for cell adhesion, ingrowth and proliferation. The pore diameters and porosities in all the types of hydrogels in this study were found to be appropriate for bone tissue engineering applications (Amaral et al., 2009; Depan et al., 2011). An interesting phenomenon was that the average pore diameters and the porosities of the hydrogels were not in relation to the water uptake abilities. The former two were in positive correlation to the amount of GO, while the latter was not. Nevertheless, the results of water uptake proved satisfactory water-absorbing ability of the hydrogels.

Proper mechanical properties are required for scaffolds in order to maintain their structure for tissues ingrowth. Previous studies reported the elastic modulus of CS/GO composite film prepared by solution casting method was increased even by adding a small amount of GO compared with the pure CS film as

control (Fan et al., 2010; Han et al., 2011). In this work, results of rheological measurement and unconfined compression test revealed that the mechanical properties of the hydrogels were improved by the addition of GO. The storage (G′)/loss (G″) moduli of the hydrogels with GO evaluated by rheology test were 1.12 to 1.69 times that of CS/GP at the gelling temperature. The elastic modulus of hydrogels containing different amounts of GO have been increased by 1.76 to 2.94 times compared with pure CS/GP hydrogel. GO has a large specific surface to volume ratio and a unique two-dimensional structure which probably imposes a higher degree of geometric constraint with regard to the mobility of polymer chains, influencing binding interactions between molecules and subsequently enhances elastic modulus (Han et al., 2011). The properties of GO/CS/GP (including 0.5, 1, 2%) were acceptable for tissue engineering applications.

Biological Assays

Besides physical and chemical properties, the cytocompatibility of biomaterials is of much importance for tissue engineering as scaffolds are expected to promote cellular adhesion, proliferation and differentiation. CS is a well-known biopolymer for its biocompatibility and biodegradability. Because of its ability to support cell growth and to integrate with surrounding ECM, chitosan has been widely studied in biomedical field. GP is an organic compound naturally found in the body and has been shown as an osteogenic supplement for culturing bone marrow stem cells (Zhou et al., 2015). However, it has also been reported that high concentrations of GP, in particular above 10wt% can be detrimental to cell proliferation (Zhu et al., 2010). In this study, the concentration of GP was relatively low (6 wt%), and all the hydrogels were immersed in complete cell culture medium for three times, half an hour for each time before seeding cells into them in order to remove the diffused GP, preventing possible toxicity caused by GP. Results of the biological assessment in this study revealed that the CS/GP promoted cellular adhesion and proliferation for MC3T3-E1. However, the cytocompatibility and toxicity of GO are controversial. Some investigators indicated that GO demonstrated biocompatibility in a number of studies aiming for biomedical applications while the other reported adverse biological responses and cytotoxicity (Gurunathan and Kim, 2016; Ou et al., 2016). In current study, results of CCK-8 assay showed that cells kept proliferating in the incubation with the hydrogels but there was a difference among the groups. Cells incubated in the hydrogel with low content of GO (0.5%GO/CS/GP) exhibited a similar proliferation rate with cells in the hydrogel without GO, while the hydrogels with higher contents of GO (1%GO/CS/GP and 2% GO/CS/GP) had an inhibiting effect on the cell attachment and proliferation. The live/dead staining images of samples also revealed that there were less live cells on the hydrogels with higher content GO (1%GO/CS/GP and 2% GO/CS/GP) after 5 days. The concentrations of GO in each hydrogel sample were 100 μg/mL (0.5%GO/CS/GP), 200 μg/mL (1%GO/CS/GP) and 400 μg/mL (0.5%GO/CS/GP), respectively. For cell incubation, the final concentrations of GO in each well of the culture plate were one third of those in hydrogels as the volume of culture

medium been calculated. The results were consistent with studies concerning the dose-dependent toxicity of GO. A study reported that GO nanosheets at the concentration of $20\,\mu g/mL$ had no toxicity in A549 within 2 h, but a higher concentration ($85\,\mu g/mL$) reduced the cellular viability to 50 % within 24 h (Chang et al., 2011). Another study also demonstrated that GO had no obvious cytotoxicity at low concentrations for 96 h on human neuroblastoma SH-SY5Y cell line, but the viability of cells sharply decreased to 20 % after treatment with 100 mg/mL GO for 96 h of incubation (Lv et al., 2012). It is important to bear in mind that the toxicity of GO is influenced by many physicochemical properties such as lateral dimensions, surface area, surface chemistry, surface charge, layer number, purity, particulate state and shape. In this study, the dose-dependent adverse effects of GO on the cellular viability and proliferation cells may be attributed to the dispersed GO. As the physical interactions between GO and CS can be interrupted by water, different ions and molecules of the culture medium or released from cells, the GO sheets would disperse in the medium again. Given that the lateral diameter of GO used in this work was too large to be taken up by the cells, the dispersed GO may influence the growth of cells by cutting through cell membranes directly or binding with the proteins of the medium through π-π stacking, preventing them absorbed by the cells (Akhavan and Ghaderi, 2010; Zhou and Gao, 2014). For the GO entangled by CS, there would be less opportunity to expose its sharp margin and hexagonal lattice. Hence, hydrogels with higher content of GO that may release more dispersed GO had an adverse effect on cell viability. The cytocompatibility of 0.5%GO/CS/GP was acceptable for biomedical application.

CONCLUSION

The thermal-sensitive chitosan/β-glycerophosphate hydrogels reinforced by graphene oxide were fabricated at physiological pH and temperature. The hydrogels possessed highly porous structure with good ability of water uptake, which favors living cells ingrowth and water convection. The presence of GO within the hydrogel stiffened the scaffolds because of its large surface to volume ratio and a unique two-dimensional structure. The biocompatibility was associated with the content of GO assessed by SEM, CCK-8 test and live/dead staining. The hydrogel with lower content of GO (0.5%GO/CS/GP) not only had an enhanced mechanical property but also favored for cell attachment, viability and proliferation, exhibiting potentiality for application in regenerative medicine such as being used as *in situ* gel-forming materials for tissue engineering.

REFERENCES

Ahmadi, R., and de Bruijn, J. D. (2008). Biocompatibility and gelation of chitosan–glycerol phosphate hydrogels. *J. Biomed. Mater. Res. A.* 86, 824–832. doi: 10.1002/jbm.a.31676

Akhavan, O., and Ghaderi, E. (2010). Toxicity of graphene and graphene oxide nanowalls against bacteria. *ACS Nano.* 4, 5731–5736. doi: 10.1021/nn101390x

Amaral, I. F., Unger, R. E., Fuchs, S., Mendonca, A. M., Sousa, S. R., Barbosa, M. A., et al. (2009). Fibronectin-mediated endothelialisation of chitosan porous matrices. *Biomaterials* 30, 5465–5475. doi: 10.1016/j.biomaterials.2009.06.056

Assaad, E., Maire, M., and Lerougea, S. (2015). Injectable thermosensitive chitosan hydrogels with controlled gelation kinetics and enhanced mechanical resistance. *Carbohyd. Polym.* 130, 87–96. doi: 10.1016/j.carbpol.2015.04.063

Berger, J., Reist, M., Mayer, J. M., Felt, O., Peppas, N. A., and Gurny, R. (2004). Structure and interactions in covalently and ionically crosslinked chitosan hydrogels for biomedical applications. *Eur. J. Pharm. Biopharm.* 57, 19–34. doi: 10.1016/S0939-6411(03)00161-9

Bhattarai, N., Gunn, J., and Zhang, M. (2010). Chitosan-based hydrogels for controlled, localized drug delivery. *Adv. Drug Deliv. Rev.* 62, 83–99. doi: 10.1016/j.addr.2009.07.019

Chang, Y. L., Yang, S. T., Liu, J. H., Dong, E., Wang, Y. W., Cao, A., et al. (2011). *In vitro* toxicity evaluation of graphene oxide on A549 cells. *Toxicol. Lett.* 200, 201–210. doi: 10.1016/j.toxlet.2010.11.016

Chen, Y. T., Zhang, F. L., Fu, Q., Liu, Y., Wang, Z. J., and Qi, N. M. (2016). *In vitro* proliferation and osteogenic differentiation of human dental pulp stem cells in injectable thermo-sensitive chitosan/β-glycerophosphate/ hydroxyapatite hydrogel. *J. Biomater. Appl.* 31, 317–327. doi: 10.1177/0885328216661566

Cho, J. Y., Heuzey, M. C., Bégin, A., and Carreau, P. J. (2006). Chitosan and glycerophosphate concentration dependence of solution behaviour and gel point using small amplitude oscillatory rheometry. *Food Hydrocol.* 20, 936–945. doi: 10.1016/j.foodhyd.2005.10.015

Cote, L. J., Cruz-Silva, R., and Huang, J. X. (2009). Flash reduction and patterning of graphite oxide and its polymer composite. *J. Am. Chem. Soc.* 131, 11027–11032. doi: 10.1021/ja902348k

Depan, D., Girase, B., Shah, J. S., and Misra, R. D. K. (2011). Structure–process–property relationship of the polar graphene oxide-mediated cellular response and stimulated growth of osteoblasts on hybrid chitosan network structure nanocomposite scaffolds. *Acta Biomater.* 7, 3432–3445. doi: 10.1016/j.actbio.2011.05.019

Dinescu, S., Ionita, M., Pandele, A. M., Galateanu, B., Iovu, H., Ardelean, A., et al. (2014). *In vitro* cytocompatibility evaluation of chitosan/graphene oxide 3D scaffold composites designed for bone tissue engineering. *Biomed. Mater. Eng.* 24, 2249–2256. doi: 10.3233/BME-141037

Dong, R., Zhao, X., Guo, B., and Ma, P. X. (2016). Self-healing conductive injectable hydrogels with antibacterial activity as cell delivery carrier for cardiac cell therapy. ACS Appl. Mater. Interfaces 8, 17138–17150. doi: 10.1021/acsami.6b04911

Dubey, N., Bentini, R., Islam, I., Cao, T., Neto, A. H. C., and Rosa, V. (2015). Graphene: a versatile carbon-based material for bone tissue engineering. Stem Cells Int. 2015:804213. doi: 10.1155/2015/804213

Dutta, P. K., Rinki, K., and Dutta, J. (2011). Chitosan: a promising biomaterial for tissue engineering scaffolds. Adv. Polym. Sci. 244, 45–80. doi: 10.1007/12_2011_112

Fan, H., Wang, L., Zhao, K., Li, N., Shi, Z., Ge, Z., et al. (2010). Fabrication, mechanical properties, and biocompatibility of graphene-reinforced chitosan composites. Biomacromolecules 11, 2345–2351. doi: 10.1021/bm100470q

Gholizadeh, S., Moztarzadeh, F., Haghighipour, N., Ghazizadeh, L., Baghbani, F., Shokrgozar, M. A., et al. (2017). Preparation and characterization of novel functionalized multiwalled carbon nanotubes/chitosan/β-Glycerophosphate scaffolds for bone tissue engineering. Int. J. Biol. Macromol. 97, 365–372. doi: 10.1016/j.ijbiomac.2016.12.086

Gurunathan, S., and Kim, J. H. (2016). Synthesis, toxicity, biocompatibility, and biomedical applications of graphene and graphene-related materials. Int. J. Nanomed. 11, 1927–1945. doi: 10.2147/IJN.S105264

Han, D. L., Yan, L. F., Chen, W. F., and Li, W. (2011). Preparation of chitosan/graphene oxide composite film with enhanced mechanical strength in the wet state. Carbohyd Polym. 83, 653–658. doi: 10.1016/j.carbpol.2010.08.038

Huang, Z., Feng, Q. L., Yu, B., and Li, S. J. (2011). Biomimetic properties of an injectable chitosan/nano-hydroxyapatite/collagen composite. Mat. Sci. Eng. Mater. 31, 683–687. doi: 10.1016/j.msec.2010.12.014

Khor, E., and Lim, L. Y. (2003). Implantable applications of chitin and chitosan. Biomaterials 24, 2339–2349. doi: 10.1016/S0142-9612(03)00026-7

Lehr, C. M., Bouwstra, J. A., Schacht, E. H., and Junginger, H. E. (1992). In vitro evaluation of mucoadhesive properties of chitosan and some other natural polymers. Int. J. Pharm. 78, 43–48. doi: 10.1016/0378-5173(92)90353-4

Li, D., Muller, M. B., Gilje, S., Kaner, R. B., and Wallace, G. G. (2008). Processable aqueous dispersions of graphene nanosheets. Nat. Nanotechnol. 3, 101–105. doi: 10.1038/nnano.2007.451

Lv, M., Zhang, Y. J., Liang, L., Wei, M., Hu, W. B., Li, X. M., et al. (2012). Effect of graphene oxide on undifferentiated and retinoic acid-differentiated SH-SY5Y cells line. Nanoscale 4, 3861–3866. doi: 10.1039/c2nr30407d

Marcano, D. C., Kosynkin, D. V., Berlin, J. M., Sinitskii, A., Sun, Z., Slesarev, A., et al. (2010). Improved synthesis of graphene oxide. ACS Nano. 4, 4806–4814. doi: 10.1021/nn1006368

Mirahmadi, F., Tafazzoli-Shadpour, M., Shokrgozar, M. A., and Bonakda, S. (2013). Enhanced mechanical properties of thermosensitive chitosan hydrogel by silk fibers for cartilage tissue engineering. Mat. Sci. Eng. Mater. 33, 4786–4794. doi: 10.1016/j.msec.2013.07.043

Mittal, G., Dhand, V., Rhee, K. Y., Park, S., and Lee, W. R. (2015). A review on carbon nanotubes and graphene as fillers in reinforced polymer nanocomposites. J. Ind. Eng. Chem. 21, 11–25. doi: 10.1016/j.jiec.2014.03.022

Ou, L. L., Song, B., Liang, H. M., Liu, J., Feng, X. L., Deng, B., et al. (2016). Toxicity of graphene-family nanoparticles: a general review of the origins and mechanisms. Part Fibre Toxicol. 13:57. doi: 10.1186/s12989-016-0168-y

Rinaudo, M. (2006). Chitin and chitosan: properties and applications. Prog. Polym. Sci. 31, 603–632. doi: 10.1016/j.progpolymsci.2006.06.001

Riva, R., Ragelle, H., des Rieux, A., Duhem, N., Jerome, C., and Preat, V. (2011). Chitosan and chitosan derivatives in drug delivery and tissue engineering. Adv. Polym. Sci. 244, 19–44. doi: 10.1007/12_2011_137

Salavagione, H. J., Martinez, G., and Gomez, M. A. (2009). Synthesis of poly(vinyl alcohol)/reduced graphite oxide nanocomposites with improved thermal and electrical properties. J. Mater. Chem. 19, 5027–5032. doi: 10.1039/b904232f

Shin, S. R., Li, Y. C., Jang, H. L., Khoshakhlagh, P., Akbari, M., Nasajpour, A., et al. (2016). Graphene-based materials for tissue engineering. Adv. Drug Deliver. Rev. 105, 255–274. doi: 10.1016/j.addr.2016.03.007

Song, K. D., Li, L. Y., Yan, X. Y., Zhang, W., Zhang, Y., Wang, Y. W., et al. (2017). Characterization of human adipose tissue-derived stem cells in vitro

culture and in vivo differentiation in a temperature-sensitive chitosan/β-glycerophosphate/collagen hybrid hydrogel. Mat. Sci. Eng. C Mater. 70, 231–240. doi: 10.1016/j.msec.2016.08.085

Stankovich, S., Dikin, D. A., Dommett, G. H. B., Kohlhaas, K. M., Zimney, E. J., Stach, E. A., et al. (2006). Graphene-based composite materials. Nature 442, 282–286. doi: 10.1038/nature04969

Tsai, M. L., Chang, H. W., Yu, H. C., Lin, Y. S., and Tsai, Y. D. (2011). Effect of chitosan characteristics and solution conditions on gelation temperatures of chitosan/β-glycerophosphate/nanosilver hydrogels. Carbohydr Polym. 84, 1337–1343. doi: 10.1016/j.carbpol.2011.01.035

Vickery, J. L., Patil, A. J., and Mann, S. (2009). Fabrication of graphene polymer nanocomposites with higher-order three-dimensional architectures. Adv. Mater. 21, 2180–2183. doi: 10.1002/adma.200803606

Wang, L., and Stegemann, J. P. (2010). Thermogelling chitosan and collagen composite hydrogels initiated with β-glycerophosphate for bone tissue engineering. Biomaterials 31, 3976–3985. doi: 10.1016/j.biomaterials.2010.01.131

Wang, Q., and Chen, D. (2016). Synthesis and characterization of a chitosan based nanocomposite injectable hydrogel. Carbohydr. Polym. 136, 1228–1237. doi: 10.1016/j.carbpol.2015.10.040

Yang, X., Tu, Y., Li, L., Shang, S., and Tao, X. M. (2010). Well-dispersed chitosan/graphene oxide nanocomposites. ACS Appl. Mater. Interfaces. 2, 1707–1713. doi: 10.1021/am100222m

Zhao, Q. S., Ji, Q. X., Xing, K., Li, X. Y., Liu, C. S., and Chen, X. G. (2009). Preparation and characterics of novel porous hydrogel films based on chitosan and glycerophosphate. Carbohyd. Polym. 76, 410–416. doi: 10.1016/j.carbpol.2008.11.020

Zhao, X., Guo, B., Wu, H., Liang, Y., and Ma, P. X. (2018). Injectable antibacterial conductive nanocomposite cryogels with rapid shape recovery for noncompressible hemorrhage and wound healing. Nat. Commun. 9:2784. doi: 10.1038/s41467-018-04998-9

Zhao, X., Li, P., Guo, B., and Ma, P. X. (2015). Antibacterial and conductive injectable hydrogels based on quaternized chitosan-graft-polyaniline/oxidized dextran for tissue engineering. Acta Biomater. 26, 236–248. doi: 10.1016/j.actbio.2015.08.006

Zheng, L., Ao, Q., Han, H., Zhang, X., and Gong, Y. (2010). Evaluation of the chitosan/glycerol-beta-phosphate disodium salt hydrogel application in peripheral nerve regeneration. Biomed. Mater. 5:35003. doi: 10.1088/1748-6041/5/3/035003

Zhou, H. Y., Chen, X. G., Kong, M., Liu, C. S., Cha, D. S., and Kennedy, J. F. (2008). Effect of molecular weight and degree of chitosan deacetylation on the preparation and characteristics of chitosan thermosensitive hydrogel as a delivery system. Carbohyd. Polym. 73, 265–273. doi: 10.1016/j.carbpol.2007.11.026

Zhou, H. Y., Jiang, L. J., Cao, P. P., Li, J. B., and Chen, X. G. (2015). Glycerophosphate-based chitosan thermosensitive hydrogels and their biomedical applications. Carbohydr. Polym. 117, 524–536. doi: 10.1016/j.carbpol.2014.09.094

Zhou, R., and Gao, H. (2014). Cytotoxicity of graphene: recent advances and future perspective. Wires Nanomed. Nanobio. 6, 452–474. doi: 10.1002/wnan.1277

Zhu, Y., Murali, S., Cai, W., Li, X., Suk, J. W., Potts, J. R., et al. (2010). Graphene and graphene oxide: synthesis, properties, and applications. Adv. Mater. 22, 3906–3924. doi: 10.1002/adma.201001068

Monomer-Induced Customization of UV-Cured Atelocollagen Hydrogel Networks

He Liang [1,2], Stephen J. Russell [1], David J. Wood [2] and Giuseppe Tronci [1,2]*

[1] Clothworkers' Centre for Textile Materials Innovation for Healthcare, School of Design, University of Leeds, Leeds, United Kingdom, [2] Biomaterials and Tissue Engineering Research Group, School of Dentistry, St. James's University Hospital, University of Leeds, Leeds, United Kingdom

The covalent functionalization of type I atelocollagen with either 4-vinylbenzyl or methacrylamide residues is presented as a simple synthetic strategy to achieve customizable, cell-friendly UV-cured hydrogel networks with widespread clinical applicability. Molecular parameters, i.e., the type of monomer, degree of atelocollagen functionalization and UV-curing solution, have been systematically varied and their effect on gelation kinetics, swelling behavior, elastic properties, and enzymatic degradability investigated. UV-cured hydrogel networks deriving from atelocollagen precursors functionalized with equivalent molar content of 4-vinylbenzyl ($F_{4VBC} = 18 \pm 1$ mol.%) and methacrylamide ($F_{MA} = 19 \pm 2$ mol.%) adducts proved to display remarkably-different swelling ratio ($SR = 1963 \pm 58$–5202 ± 401 wt.%), storage modulus ($G' = 17 \pm 3$–390 ± 99 Pa) and collagenase resistance ($\mu_{rel} = 18 \pm 5$–56 ± 5 wt.%), similarly to the case of UV-cured hydrogel networks obtained with the same type of methacrylamide adduct, but varied degree of functionalization ($F_{MA} = 19 \pm 2 - 88 \pm 1$ mol.%). UV-induced network formation of 4VBC-functionalized atelocollagen molecules yielded hydrogels with increased stiffness and enzymatic stability, attributed to the molecular rigidity of resulting aromatized crosslinking segment, whilst no toxic response was observed with osteosarcoma G292 cells. Although to a lesser extent, the pH of the UV-curing solution also proved to affect macroscopic hydrogel properties, likely due to the altered organization of atelocollagen molecules during network formation. By leveraging the knowledge gained with classic synthetic networks, this study highlights how the type of monomer can be conveniently exploited to realize customizable atelocollagen hydrogels for personalized medicine, whereby the structure-property relationships can be controlled to meet the requirements of unmet clinical applications.

Keywords: type I atelocollagen, covalent network, UV-curing, monomer, 4-vinylbenzyl chloride, methacrylic anhydride

INTRODUCTION

As a simple mimetic of the extracellular matrix (ECM) of biological tissues hydrogels have been widely applied in the biomedical field (Zhang and Khademhosseini, 2017), for applications including regenerative medicine (Heller et al., 2013), wound care (Konieczynska et al., 2016), and controlled drug delivery (Chen et al., 2017). The high swelling in aqueous medium makes hydrogels

inherently soft, so that molecular manipulation of their constituent building blocks (Nimmo and Shoichet, 2011) is key to enable customized properties and functions for personalized medicine.

At the molecular scale, hydrogels typically consist of hydrophilic polymer networks, crosslinked via either physical or covalent linkages, whilst short amino acidic sequences have also been proven to generate water-swollen supramolecular structures (Koch et al., 2018). Although various synthetic polymers have been employed (Aggeli et al., 2003; Fairbanks et al., 2009; Bulman et al., 2015; Qin et al., 2015, 2018; Sridhar et al., 2015; Gharaei et al., 2016), a great deal of attention has recently been paid to the use of natural, ECM-extracted, biopolymers as building blocks of multifunctional hydrogels (Van Vlierberghe et al., 2011; Head et al., 2016). The selection of biopolymer-based building blocks is attractive since it ensures that the resulting material has biomimetic features from the molecular up to the macroscopic scale, due to the presence of cell-binding sequences, fiber-forming biopolymer capability (with resulting fiber dimensions comparable to the ones found in the ECM) (Younesi et al., 2014), and the water-swollen macroscopic state, respectively. In comparison to synthetic polymers, however, ensuring customization and reliable structure-property relationships in biopolymer-based systems is highly challenging, due to the inherent batch-to-batch variability and the hardly-controllable secondary interactions between biopolymer chains (Salchert et al., 2004; Yang et al., 2016). Leveraging the knowledge gained with classic polymers, the synthesis of covalently-crosslinked hydrogel networks made of linear biopolymers, e.g., hyaluronic acid (Burdick and Prestwich, 2011), has been successful aiming to achieve defined structure-property relationships (Tronci et al., 2010). Other than linear biopolymers, such a level of customization is still hardly realized when employing biopolymers with increased organizational complexity, such as collagen, because of the inherently-limited chemical accessibility and solubility. Customization of these building blocks would on the other hand enable the formation of systems with superior biofunctionality and widespread clinical applicability. Type I collagen is one the most abundant structural proteins of connective tissues, and it constitutes the main organic component of bone, skin and tendon (Grant et al., 2009). As the most abundant collagen in humans, type I collagen-based hydrogels have been widely employed for therapeutics and diagnostics, with multiple commercial products being routinely used in the clinic (Neel et al., 2013). Other than its hierarchical, water-insoluble organization found in biological tissues, collagen *ex vivo* is predominantly extracted in the form of a water-soluble triple helix, due to the extraction-induced breakdown of covalent crosslinks of collagen found *in vivo*. To enable applicability of the extracted water-soluble product in physiological conditions, restoration of *in vivo*-like covalent crosslinks *ex vivo* is a promising strategy. Reaction of side chain terminations with bifunctional segments, e.g., diisocyanates (Olde Damink et al., 1995a; Kishan et al., 2015), diacids (Duan et al., 2014; Tronci et al., 2015b), and dialdehydes (Olde Damink et al., 1995b; Haugh et al., 2011), or carbodiimide-induced intramolecular crosslinking (Everaerts et al., 2008; Yunoki and Matsuda, 2008) proved to induce some adjustment in the mechanical properties

of resulting collagen materials. At the same time, the use of toxic reagents and the relatively-long reaction time prevent the application of these synthetic strategies for the delivery of cell-friendly, *in-situ* forming hydrogels (Lee et al., 2013) or to achieve material customization at the bed side. Another challenge associated with above-mentioned strategies is that the enzymatic degradability of resulting collagen materials is still relatively quick, so that the requirements of specific clinical application, e.g., in guided bone regeneration, cannot be entirely fulfilled (Calciolari et al., 2018). Ultimately, above-mentioned crosslinking strategies are often associated with unwanted side reactions, so that defined structure-property relationships are hardly-developed (Yunoki and Matsuda, 2008; Tronci et al., 2010; Duan et al., 2014).

Rather than one-step crosslinking reactions, photoinduced network formations mechanisms have been recently investigated for the development of *in situ*-forming, cell-encapsulating collagen hydrogels (Brinkman et al., 2003). Derivatization of collagen triple helices with photoactive, e.g., methacrylamide, groups has been widely demonstrated to rapidly generate covalent networks via photoinduced free radical crosslinking (Gaudet and Shreiber, 2012) and UV-induced thiol-ene (Holmes et al., 2017) click reactions. Although resulting systems proved to display varied storage modulus (Gaudet and Shreiber, 2012; Ravichandran et al., 2016), collagen hydrogel customization often relies on the incorporation of a synthetic copolymer, e.g., polyethylene glycol (PEG), in the crosslinked network. Whist this approach affords wide tailoring in macroscopic properties, incorporation of the synthetic phase may affect the biofunctionality of resulting system. In an effort to expand the customizability of collagen hydrogels and avoid the use of copolymers, functionalization of collagen with 4-vinylbenzyl residues has recently been reported. UV-cured 4VBC-functionalized collagen triple helices proved to display significantly increased compression properties with respect to methacrylated variants (Tronci et al., 2016a), whereby the introduction of 4VBC aromatic rings was found to impact on the activity of matrix metalloproteinases (MMPs) *in vitro* (Tronci et al., 2016b; Liang et al., 2018). Although insightful, these studies did not systematically investigate the effect of the type of monomer and respective degree of functionalization on the macroscopic properties of resulting hydrogels, due to the limited chemical accessibility of the protein backbone. On the other hand, systematic investigations on the effect of covalently-coupled monomer and respective degree of functionalization on network properties could open up new avenues aiming to develop simple synthetic routes yielding customizable collagen systems for personalized medicine.

This study therefore is focused on the synthesis of photoactive atelocollagen precursors and consequent UV-cured networks, whereby the effects of (i) type of monomer, (ii) the degree of atelocollagen functionalization, and (iii) UV-curing aqueous solution were addressed. Pepsin-solubilized type I telopeptide-free collagen, i.e., atelocollagen, was selected as a purified, minimally-antigenic building block with comparable chemical composition, and dichroic properties with respect to acid-extracted type I collagen (Lynn et al., 2004; Tronci et al., 2016b). Firstly, photoactive atelocollagen precursors with comparable

molar content, but different type of photoactive adduct, i.e., either 4-vinylbenzyl or methacrylamide adduct, were considered. Secondly, photoactive atelocollagen precursors with varied molar content of the same type of photoactive, i.e., methacrylamide, adduct were addressed. Ultimately, the aqueous solution employed for the solubilization of functionalized atelocollagen, i.e., hydrochloric acid, acetic acid and phosphate buffered saline solution, was also varied during network formation to investigate the effect of environmental conditions on resulting hydrogels. Hydrogel networks were prepared via UV-induced free radical crosslinking of photoactive atelocollagen precursors in the presence of 2-hydroxy-1-[4-(2-hydroxyethoxy) phenyl]-2-methyl-1-propanone (I2959), which was used as a water-soluble, cell-friendly photoinitiator (Holmes et al., 2017). Resulting UV-cured hydrogel networks were characterized with regards to their gelation kinetics, swelling and compression properties, enzymatic degradability, and cytotoxicity, aiming to establish defined structure-property relationships, and systematic material customization.

MATERIALS AND METHODS

Materials

Pepsin-extracted type I bovine atelocollagen (AC, 6 mg·mL^{-1}) solutions in 10 mM hydrochloric acid (HCl) were purchased from Collagen Solutions PLC (Glasgow, UK). 4-vinylbenzyl chloride (4VBC), methacrylic anhydride (MA), and triethylamine (TEA) were purchased from Sigma-Aldrich. I2959 and deuterium oxide were purchased from Fluorochem Limited (Glossop, UK). Ninhydrin 99% was supplied by Alfa-Aesar (Massachusetts, USA). Polysorbate 20, absolute ethanol and diethyl ether were purchased from VWR internationals. All other chemicals were purchased from Sigma-Aldrich unless specified.

Synthesis of Photoactive Precursors

To achieve the MA-functionalized products, AC solutions (6 mg·mL^{-1} in 10 mM HCl) were diluted to a concentration of 3 mg·mL^{-1} via addition of 10 mM HCl and equilibrated to pH 7.5. MA and TEA were added at varied molar ratios with respect to the molar lysine content in AC ([MA][Lys]$^{-1}$ = 0.1–25). When an MA/Lys molar ratio of 0.1–1 was selected, TEA was added with a 10 molar ratio with respect to the collagen lysine content. When an MA/Lys molar ratio of 25 was selected, an equimolar monomer content of TEA was added ([TEA] = [MA]). After 24 h, the functionalization reaction was stopped by precipitating the reacting mixture in 10-volume excess of absolute ethanol. Following at least 8-h incubation in ethanol, the reacted, ethanol-precipitated product was recovered by centrifugation and air dried. The 4VBC-functionalized AC was prepared following the above protocol, whereby polysorbate 20 (PS-20) was added prior to the functionalization reaction in order to mediate the solubility of 4VBC in water. Hence, the diluted (3 mg·mL^{-1}) and pH-equilibrated AC solution was supplemented with 1 wt.% PS−20 (with respect to the weight of the diluted AC solution) prior to addition of 4VBC and TEA at a fixed molar ratio of 25 ([4VBC]·[Lys]$^{-1}$ = 25; [4VBC] = [TEA]).

Characterization of Reacted AC Products

TNBS assay ($n = 3$) was used to measure the derivatization of amino to vinyl groups and respective degree of AC functionalization, as previously reported (Tronci et al., 2016b; Liang et al., 2018). Briefly, 11 mg of dry samples was mixed with 1 mL of 4 wt.% NaHCO$_3$ and 1 mL of 0.5 wt.% TNBS solution. The mixture was reacted at 40°C for 4 h, followed by addition of 3 mL of 6 N HCl for one more hour to induce complete sample dissolution. The solution was then cooled down to room temperature, diluted with 5 mL of distilled water, and extracted (×3) with 15 mL diethyl ether to remove any non-reacted TNBS species. An aliquot of 5 mL was collected and diluted in 15 mL of distilled water and the reading was recorded using an UV-Vis spectrophotometer (Model 6305, Jenway) against the blank. The molar content of primary free amino groups (largely attributed to the side chains of lysine) was calculated via Equation 1:

$$\frac{mol(Lys)}{g(AC)} = \frac{2 \times Abs\,(346\,nm) \times 0.02}{1.46 \times 10^4 \times b \times x} \tag{1}$$

where $Abs\,(346\,nm)$ is the UV absorbance value recorded at 346 nm, 2 is the dilution factor, 0.02 is the volume of the sample solution (in liters), 1.46×10^4 is the molar absorption coefficient for 2,4,6-trinitrophenyl lysine (in M^{-1} cm^{-1}), b is the cell path length (1 cm), and x is the weight of the dry sample. The degree of functionalization (F) was calculated via Equation 2:

$$F = \left(1 - \frac{mol(Lys)_{funct.}}{mol(Lys)_{AC}}\right) \times 100 \tag{2}$$

where $mol(Lys)_{AC}$ and $mol(Lys)_{funct.}$ represent the total molar content of free amino groups in native and functionalized atelocollagen, respectively.

Further confirmation of AC functionalization was assessed via Ninhydrin assay ($n = 3$). Briefly, 10 mg of the dry sample was mixed with 4 mL of distilled water and 1 mL of 8 wt.% Ninhydrin solution in acetone. The mixture was reacted at 100°C for 15 min and the reaction terminated by cooling in ice and adding 1 mL of 50% ethanol (v/v). The molar content of amino groups was measured by reading the absorbance at 570 nm against the blank. A standard curve calibration was prepared by measuring solutions containing known amount of atelocollagen.

TNBS and ninhydrin assays were ultimately coupled with ^{1}H-NMR spectroscopy (JEOL ECA, 600 MHz). ^{1}H-NMR spectra of native, MA- and 4VBC-functionalized AC were recorded following dissolution of 5 mg of dry sample in 1 mL of 10 mM deuterium chloride.

Synthesis of UV-Cured AC Networks

Either MA- or 4VBC-functionalized AC products were dissolved at a fixed concentration of 0.8 wt.% in either 10 mM HCl (pH 2.1), 17.4 mM acetic acid (AcOH, pH 3.4) or 10 mM phosphate buffered saline (PBS, pH 7.5) solutions supplemented with 1 wt.% I2959 photo-initiator. Resulting AC solutions (0.8 wt.% functionalized AC, 0.992 wt.% I2959) were centrifuged at 3000 rpm for 5 min to remove any air bubble and then cast onto a 24 well plate (Corning Costar, 0.8 g per well). Well

plates were irradiated with a UV lamp (346 nm, 8 mW cm^{-2}, Spectroline) for 30 min on both top and bottom side, leading to the formation of hydrogels. Irradiation intensities were measured with an International Light IL1400A radiometer equipped with a broadband silicon detector (model SEL033), a 10× attenuation neutral density filter (model QNDS1), and a quartz diffuser (model W). The UV-cured hydrogels were carefully removed from the plate and washed in distilled water (15 min, ×3), followed by dehydration *via* an ascending series of ethanol and air drying.

Quantification of Swelling Ratio and Gel Content

Dry UV-cured samples ($n = 4$) of known mass (m_d) were individually incubated in PBS (10 mM, pH 7.5, 1.5 mL) at room temperature for 24 h. The swelling ratio (SR) was calculated by Equation 3:

$$SR = \frac{m_s - m_d}{m_s} \times 100 \tag{3}$$

where m_s is the mass of the PBS-equilibrated UV-cured sample.

The gel content ($n = 4$) was measured to investigate the overall portion of the covalent hydrogel network insoluble in 17.4 mM acetic acid solution (Liang et al., 2018). Dry collagen networks (m_d: 10 mg−20 mg) were individually incubated in 2 mL of 17.4 mM AcOH for 24 h. Resulting samples were further air dried and weighed. The gel content (G) was calculated by Equation 4:

$$G = \frac{m_1}{m_d} \times 100 \tag{4}$$

where m_1 is the dry mass of collected samples.

Compression Test

PBS-equilibrated hydrogel discs (Ø: 14 mm; h: 5–6 mm, $n = 3$) were compressed at room temperature with a compression rate of 3 mm·min^{-1} (Instron ElectroPuls E3000). A 250 N load cell was operated up to complete sample compression. Stress-compression curves were recorded and the compression modulus quantified as the slope of the plot linear region at 25-30% strain.

Degradation Tests

Dry samples (n=4) of either UV-cured AC network or native AC were incubated for 4 days (37°C, pH 7.5) in 1 mL of 50 mM [tris(hydroxymethyl)-methyl-2-aminoethane sulfonate] (TES) buffer containing 0.36 mM calcium chloride and supplemented with 5 CDU of collagenase type I from *Clostridium histolyticum* (125 CDU·mg^{-1}). Following 4-day incubation, the samples were washed in distilled water, dehydrated via an ascending series of ethanol solutions and air dried. The relative mass (μ_{rel}) of samples was determined according to Equation 5:

$$\mu_{rel} = \frac{m_4}{m_d} \times 100 \tag{5}$$

where m_4 and m_d are the masses of the dry partially-degraded and dry freshly-synthesized samples, respectively.

UV-Curing Rheological Measurements

The UV-induced kinetics of network formation ($n = 3$) was measured by a modular compact rotational rheometer (MCR 302, Anton Paar, Austria) equipped with a UV curing module (Ominicure 1500, Excelitus Technologies). Functionalized atelocollagen products (0.8 wt.%) were dissolved in I2959-supplemented aqueous solutions (1 wt.% I2959), followed by time sweep measurement at a strain of 0.1% and frequency of 1 Hz. Values of storage (G') and loss (G'') modulus were recorded during time sweep measurements under irradiation with UV light. The oscillatory shear was applied to a transparent glass parallel plate (Ø 25 mm) and the gap between the plates was 300 μm. UV light (365 nm, 8 mW·cm^{-2}) was initiated after 5 s of shear oscillation at 21°C. The gelation time (τ) was determined by the temporal interval between the UV activation and complete gelation.

Cell Culture Study

G292 cells were cultured in Dulbecco's modified Eagle's medium (DMEM), supplemented with 10% fetal bovine serum (FBS), 1% glutamine, and 2.5 mg·mL^{-1} penicillin–streptomycin, in a humidified incubator at 37°C and 5% CO$_2$. Cells were passaged every 3 days with 0.25% trypsin/0.02% EDTA. UV-cured samples were individually synthesized on to a 24-well plate, extensively washed in distilled water and dehydrated in an ascending series of ethanol-distilled water [0, 20, 40, 60, 80, (3×) 100 vol.% EtOH] to remove any acidic or ethanol residues. Prior to cell seeding, hydrogels were disinfected in a 70 vol.% ethanol solution under UV light and washed in PBS (3×, 10 min) to remove any acidic or ethanol residues. G292 cells (8·10^3 cells·mL^{-1}) were seeded on top of the sample (following UV disinfection) and incubated at 37°C for up to 7 days. After incubation, samples ($n = 6$) were washed with PBS (×3) and transferred to a new 24-well plate before adding the dying agent of Calcein AM and Ethidium homodimer-1. The sample plate was then incubated for 20 minutes away from light. Live /dead stained hydrogels were placed onto a glass slide for fluorescence microscopy imaging (Leica DMI6000 B).Cells grown on tissue culture treated plastics were used as positive control (Nunc, UK). Other than live/dead staining, cell viability was assessed at selected time points using Alamar Blue assay (ThermoFisher Scientific, UK) according to the manufacturer's guidance. VP-SEM (Hitachi S-3400N VP) combined with Deben cool stage control (Model: LT3299) was also employed for high resolution imaging of cell attachment on hydrated samples after 7-day incubation under low pressure (60–70 Pa).

Statistical Analysis

Data are presented as mean ± standard deviation (SD). Statistical analysis was carried out with the Student's *t*-test. A p value lower than 0.05 was considered to be significantly different.

RESULTS AND DISCUSSION

In the following, the synthesis and characterization of UV-cured hydrogel networks made of either 4-vinylbenzylated or methacrylated atelocollagen is presented. The effects

of covalently-coupled monomer, degree of atelocollagen functionalization and UV-curing aqueous solution was investigated, aiming to draw controlled structure-property relationships. The synthesis of the covalent networks was linked to the degree of functionalization of respective photoactive AC solutions, whilst respective UV-induced gelation kinetics was assessed in either acidic or basic conditions. Resulting UV-cured networks were characterized with regards to rheological properties, gel content, swelling ratio, compression modulus, enzymatic degradability, and cellular tolerability.

The sample nomenclature is as follows: functionalized AC samples are coded as "XXXYY," where "XXX" identifies the type of monomer introduced on to the AC backbone, i.e., either 4VBC or MA; and "YY" describes the monomer/Lys molar ratio used in the functionalization reaction. UV-cured samples are coded as "XXXYY(Z)*," where "XXX" and "YY" have the same meaning as previously discussed; "Z" indicates the UV-curing aqueous solution used to dissolve the functionalized AC sample, i.e., either 10 mM HCl (H), 17.4 mM acetic acid (A) or 10 mM PBS (P); "*" identifies a UV-cured hydrogel sample.

Synthesis of Functionalized AC Precursors

Following reaction with either 4VBC or MA, the degree of functionalization (F) consequent to the covalent coupling of photoactive adducts on to the AC backbone was determined. Since network formation was pursued via UV-induced free radical crosslinking mechanism, the introduction of photoactive adducts was expected to be directly related to the crosslink density and macroscopic properties of respective AC networks. The reaction of AC with selected monomers proceeds via lysine-initiated nucleophilic substitution (**Figure S1**) leading to the consumption of free amino groups and derivatization with either 4-vinylbenzyl or methacrylamide adducts. TNBS (Bubnis and Ofner, 1992) and ninhydrin (Starcher, 2001) assays are two colorimetric assays widely employed for the determination of amino groups in proteins. Both assays have recently been employed for the characterization of reacted gelatin (Billiet et al., 2013; Kishan et al., 2015) and acid-solubilized collagen (Ravichandran et al., 2016; Tronci et al., 2016a,b; Liang et al., 2018) products, proving to correlate well with ^{1}H-NMR spectroscopy. Both TNBS and ninhydrin assays were therefore selected in this study to measure the molar content of free amino groups in both native and reacted pepsin-solubilized AC samples, so that F could be indirectly quantified.

An overall content of primary amino groups of $2.89 \cdot 10^{-4}$ mol·g^{-1} was recorded on native atelocollagen via TNBS assay. Both colorimetric methods revealed a comparable and decreased molar content of amino groups in both MA- and 4VBC-reacted atelocollagen samples (**Table 1**), in line with previous reports (Jia et al., 2012; Tronci et al., 2016b); whilst monomer-related geminal protons could not be clearly detected in ^{1}H-NMR spectra of sample MA0.3 and 4VBC25 due to the overlapping with AC species (**Figure S2**). The range of MA/Lys molar ratio selected during the functionalization reaction proved to directly impact on the degree of atelocollagen methacrylation ($F_{MA} = 4 \pm 1 - 88 \pm 1$ mol.%), whilst an insignificant variation in the molar content

TABLE 1 | TNBS assay quantification of the amino group molar content and degree of functionalization (F) in atelocollagen products ($n = 2$) following reaction with either 4VBC or MA at varied monomer/Lys molar ratios.

Sample ID	Molar ratio / [Monomer][Lys]$^{-1}$	Amine groups/ mol·g^{-1} ($\times 10^{-4}$)		F /mol.% [a]
		TNBS	**Ninhydrin**	
4VBC25	25	2.38 ± 0.02	2.38 ± 0.01	18 ± 1
MA0.1	0.1	2.77 ± 0.03	n.a.	4 ± 1
MA0.3	0.3	2.34 ± 0.06	2.40 ± 0.13	19 ± 2
MA0.5	0.5	2.07 ± 0.14	n.a.	28 ± 5
MA1	1	1.63 ± 0.11	n.a.	44 ± 4
MA25	25	0.36 ± 0.01	0.44 ± 0.04	88 ± 1

The quantification of amino group molar content was confirmed via Ninydrin assay ($n = 2$). n.a., not applicable.
[a] *F was calculated considering an overall molar content of amino groups of 2.89×10^{-4} mol·g^{-1} in native AC, as revealed by TNBS assay.*

of covalently-coupled 4VBC adducts ($F_{4VBC} = 18 \pm 1$ mol.%) was observed in respective products (data not shown). The different trend in degree of functionalization observed in MA- with respect to 4VBC-reacted samples is attributed to the decreased reactivity and solubility of 4VBC in aqueous environment, as reported in previous publications (Tronci et al., 2016a), which was partially mitigated in this study by the addition of PS-20 in the reacting mixture.

Despite the different reactivity of MA with respect to 4VBC, the range of F observed in resulting MA-functionalized AC is in line with the results reported in previous publications (Brinkman et al., 2003; Gaudet and Shreiber, 2012; Ravichandran et al., 2016) with collagen-based materials.

Billiet et al. analyzed the covalent coupling of (meth)acrylic anhydride to bovine type B gelatin and achieved up to ca. 80 mol.% methacrylation (Billiet et al., 2013). Ravichandran et al. reported a degree of porcine collagen methacrylation of 57–87 mol% (Ravichandran et al., 2016), and similar results ($F = 39$–86 mol.%) were obtained by Chaikof et al. with acid-soluble rat tail collagen (Brinkman et al., 2003). Compared to the latter case, the results presented in this work with pepsin-soluble collagen suggest that the removal of telopeptides does not significantly impact on the molar content of free amino groups and functionalization capability of resulting atelocollagen product, in line with a previous report (Tronci et al., 2016b).

In order to systematically investigate how above-mentioned differences at the molecular scale of AC precursors were reflected on the macroscale of resulting UV-cured networks, it was therefore of interest to systematically vary either the type of covalently-coupled monomer (whilst keeping respective degree of AC functionalization constant) or the degree of functionalization (with the same type of covalently-coupled monomer). Accordingly, samples MA0.3 ($F_{MA} = 19 \pm 2$ mol.%), 4VBC25 ($F_{4VBC} = 18 \pm 1$ mol.%), and MA25 ($F_{MA} = 88 \pm 1$ mol.%) were selected for further investigations, and dissolved in either hydrochloric acid, acetic acid or PBS, as commonly-used solvent for collagen, prior to UV curing.

UV-Induced Network Formation and Time-Sweep Photorheometry

AC samples functionalized with methacrylamide residues (**Figure 1A**) formed a clear solution in both acidic and PBS solutions, whilst sample 4VBC25 (**Figure 1B**) could only be dissolved in 10 mM HCl (pH 2.1) and 17.4 mM AcOH (pH 3.4). The insolubility of the 4VBC-Functionalized AC product in PBS agrees with previous reports (Tronci et al., 2015a) and may be attributed to secondary interactions developed between aromatic 4-vinylbenzyl residues following atelocollagen functionalization and sample drying. Aromatic rings can mediate π-π stacking interactions as well as act as hydrogen bond acceptor in aqueous environment (Levitt and Perutz, 1988). Resulting π-π stacking interactions developed between 4VBC-functionalized AC molecules are likely to be broken down at decreased rather than basic pH, supporting the observed complete dissolution of sample 4VBC25 in both HCl and AcOH solutions.

All photoactive solutions successfully yielded hydrogel networks when treated with UV light, irrespective of the type of monomer introduced on to AC (**Figures 1C,D**). To confirm the formation of a UV-cured hydrogel network and to explore the effect of methacrylamide and 4-vinylbenzyl residues on gelation kinetics, time sweep photorheometry was carried out prior to and during UV irradiation of AC photoactive solutions, and changes in viscosity (η) as well as storage (G') and loss (G'') modulus recorded. Prompt increase of G' and G'' was observed

following activation of the atelocollagen mixtures with UV light, in contrast to the case of the same sample being tested in the absence of UV light (**Figure 2**). Comparable values of G' and G'' were also measured in the latter case, providing indirect evidence of the absence of a crosslinked network at the molecular level (**Table 2**). Both the gelation, i.e., the time required for the storage and loss moduli to equate, and plateau in storage modulus were reached within 12 s and 180 s, respectively (**Table 2**). The photoinitiator concentration (1 wt.%) selected to prepare gel-forming AC solutions proved key to reduce gelation time and to generate hydrogels with increased elastic modulus with respect to gel-forming AC solutions supplemented with decreased (0.5 wt.%) photoinitiator concentration (**Figures 2B,C**).These results, together with the fact that the final values of G' were significantly higher compared to the values of G'' (**Table 2**), successfully indicate complete conversion of the photoactive solution into a UV-cured covalently-crosslinked network (McCall and Anseth, 2012). The obtained gelation kinetics curves are comparable to the ones described by thiol-ene collagen- poly(ethylene glycol) mixtures (Holmes et al., 2017), whereby gel points were recorded within ∼7 s of UV activation. This observation is interesting given that the orthogonality and oxygen-insensitivity of the UV-induced thiol-ene, with respect to the free-radical, crosslinking reaction, should be corelated with decreased gelation times (Van Hoorick et al., 2018).

Figure 3 and **Table 2** describe the gelation kinetic profiles of samples 4VBC25, MA0.3, and MA25 when dissolved in either 10 mM HCl, 17.4 mM AcOH or 10 mM PBS solutions supplemented with 1 wt.% I2959, whilst an atelocollagen control sample was also tested following solubilization in a 17.4 mM acetic acid solution supplemented with 1 wt.% I2959. Overall, sample MA25 was found to generate networks with the highest loss and storage modulus ($G' = 618 \pm 87 – 18897 \pm 4793$ Pa) and fastest gelation kinetics ($\tau \sim 6$ s), followed by samples 4VBC25 ($G' = 73 \pm 22 – 390 \pm 99$ Pa) and MA0.3 ($G' = 17 \pm 3 – 85 \pm 1$ Pa). In contrast, only a marginal increase of G' was observed following UV activation of the control atelocollagen solution, likely due to the much lower radical-induced crosslinking of amino acidic residues (Heo et al., 2016) with respect to the complete UV-induced network formation achieved with functionalized atelocollagen precursors. This result therefore demonstrates the importance of selected functionalization routes in ensuring the synthesis of full covalent
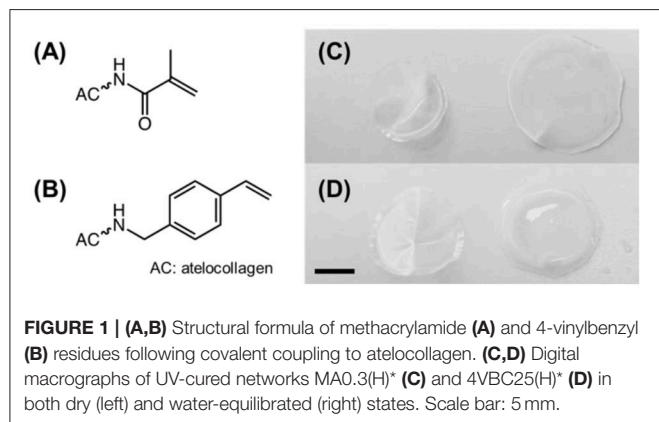
FIGURE 1 | (A,B) Structural formula of methacrylamide **(A)** and 4-vinylbenzyl **(B)** residues following covalent coupling to atelocollagen. **(C,D)** Digital macrographs of UV-cured networks MA0.3(H)* **(C)** and 4VBC25(H)* **(D)** in both dry (left) and water-equilibrated (right) states. Scale bar: 5 mm.
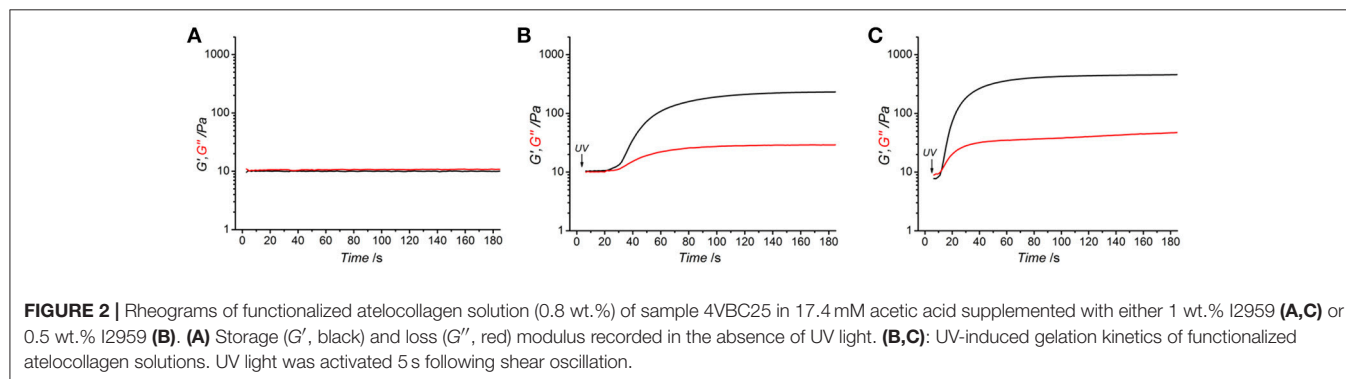
FIGURE 2 | Rheograms of functionalized atelocollagen solution (0.8 wt.%) of sample 4VBC25 in 17.4 mM acetic acid supplemented with either 1 wt.% I2959 **(A,C)** or 0.5 wt.% I2959 **(B)**. **(A)** Storage (G', black) and loss (G'', red) modulus recorded in the absence of UV light. **(B,C)**: UV-induced gelation kinetics of functionalized atelocollagen solutions. UV light was activated 5 s following shear oscillation.

TABLE 2 | Viscosity (η) and gelation time (τ) of hydrogel-forming solution as well as storage (G') and loss (G'') moduli of UV-cured hydrogel networks following complete gelation.

Sample ID	η /mPa·s [1]	G'_{max} /Pa	G''_{max} /Pa	τ /s
AC[2]	1777 ± 20	16 ± 1	13 ± 1	22 ± 5
*4VBC25(H)**	900 ± 70[a]	73 ± 22[b]	20 ± 3[b]	10 ± 0[a][d][c]
4VBC25(A)*	1820 ± 80	390 ± 99	42 ± 7	8 ± 0 [a]
MA0.3(H)*	390 ± 20[a][c]	17 ± 3[a]	8 ± 5[a]	12 ± 1[d][c]
MA0.3(A)*	240 ± 20[a]	58 ± 5[a]	17 ± 3[d]	11 ± 1
MA0.3(P)*	240 ± 20[c]	85 ± 1[a]	24 ± 2[a][d]	11 ± 1
MA25(H)*	1200 ± 130	12967 ± 265[a]	42 ± 4[a][b]	6 ±1[c]
MA25(A)*	920 ± 100[d]	618 ± 87[a][b]	8 ± 1[a][c]	n.a.
MA25(P)*	1400 ± 190	18897 ± 4793[b]	146 ± 366[b][c]	6 ± 0

Data are presented as mean ± SD (n = 3).
[1] Viscosity of hydrogel-forming AC solutions.
[2] Atelocollagen (0.8 wt.%) solution control prepared in 17.4 mM acetic acid supplemented with 1 wt.% I2959.
[a]&[c]$p < 0.001$; [b]$p < 0.01$; [d]$p < 0.05$.

FIGURE 3 | Kinetics of network formation studied via UV-equipped rheometry on samples 4VBC25 **(A)**, MA0.3 **(B)** and MA25 **(C)**, when dissolved (0.8 wt.%) in either 10 mM hydrochloric acid, 17.4 mM acetic acid or 10 mM PBS solution (each supplemented with 1 wt.% I2959). UV light was activated following 5 s shear oscillation. **(A)**: (···): 4VBC25(H)*; (—): 4VBC25(A)*. **(B)**: (···): MA0.3(H)*;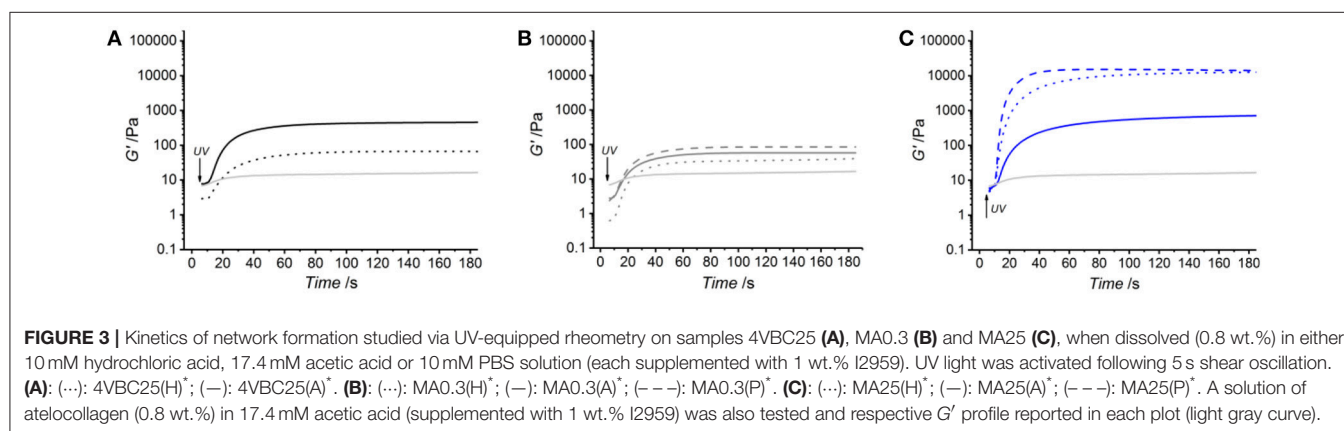 (—): MA0.3(A)*; (– – –): MA0.3(P)*. **(C)**: (···): MA25(H)*; (—): MA25(A)*; (– – –): MA25(P)*. A solution of atelocollagen (0.8 wt.%) in 17.4 mM acetic acid (supplemented with 1 wt.% I2959) was also tested and respective G' profile reported in each plot (light gray curve).

networks and provides additional evidence of the covalent coupling of selected monomers to atelocollagen. Other than the variation in elastic modulus, the viscosity of respective network-forming AC solutions was also recorded, whereby the sample MA25 proved to generate highly viscous solutions in all solutions investigated ($\eta = 920 \pm 100 – 1400 \pm 190$ mPa·s). The variations observed in loss and storage modulus and gelation kinetics support the trends in degree of functionalization recorded at the molecular scale of the atelocollagen precursors, whereby sample MA25 exhibited the highest molar content of photoactive residues with respect to the other two samples. Given that the covalently-coupled photoactive adducts mediate the UV-induced free-radical crosslinking reaction, the increased storage and loss moduli as well as decreased gelation time measured in these samples therefore provide indirect confirmation that changes in the degree of AC functionalization directly impact on the crosslink density, gelation kinetics and elastic properties of resulting UV-cured networks. The increased solution viscosity recorded with MA25 also correlates with respective degree of methacrylation, due to the increased molar content and molecular weight of derivatized lysine terminations.

Together with the effect of varied degrees of functionalization, equimolar functionalization of AC with distinct photoactive adducts, i.e., either methacrylamide or 4-vinylbenzyl residues, was also found to play a detectable effect on the macroscopic properties of resulting UV-cured hydrogels (**Table 2**). Both networks 4VBC25(H)* and 4VBC25(A)* displayed significantly increased storage and loss moduli with respect to the methacrylated equivalents (prepared in the same solvents). Also in this case, the trend in mechanical properties was supported by direct variations in respective network-forming solutions, whereby significantly-increased solution viscosity and decreased gelation times were measured with sample 4VBC25 ($\eta = 900 \pm 70 – 1820 \pm 80$ mPa·s; $\tau = 8 \pm 0 – 10 \pm 0$ s) compared to sample MA0.3 ($\eta = 240 \pm 20 – 390 \pm 20$ mPa·s; $\tau = 11 \pm 1 – 12 \pm 1$ s).

The significant difference in storage and loss modulus measured in UV-cured aromatized atelocollagen networks with respect to equivalent methacrylated variants gives evidence of the major role played by the monomer covalently-coupled to, and resulting photocrosslinked segment between, AC molecules. Aromatic interactions have been exploited for the formation of physically-crosslinked, self-assembled peptides (Birchall et al.,

2011), and for the controlled delivery of hydrophobic drugs (Li et al., 2010). The above-mentioned increased viscosity, storage modulus and loss modulus measured on 4VBC-functionalized atelocollagen solutions and corresponding UV-cured networks can mostly be attributed to π-π stacking interaction capability and increased molecular rigidity of aromatic 4VBC moieties and consequent UV-cured aromatized segment, respectively. Other than that, the decreased gelation time recorded in solutions of sample 4VBC25 with respect to solutions of sample MA0.3 seems to correlate with the increased segment length of the 4-vinylbenzyl, with respect to methacrylamide, moiety (**Figure 1A**), so that crosslinking-hindering steric effects are less likely in the former compared to the latter system. Rather than the typical variation of the molar content of photoactive groups, these results therefore demonstrate the possibility of adjusting the mechanical properties of atelocollagen hydrogels by simply varying the type of monomer covalently-coupled to the AC backbone.

Other than the degree and type of functionalization, the effect of the UV-curing aqueous solution was also explored as an additional parameter to control material behavior (**Figure 2**, **Table 2**). Hydrochloric acid solutions (10 mM, pH = 2.1) of AC precursors functionalized with equimolar content of either 4VBC or MA adducts yielded crosslinked hydrogels with the lowest storage ($G'_{4VBC25} = 73 \pm 22$ Pa; $G'_{MA0.3} = 17 \pm 3$ Pa) and loss ($G''_{4VBC25} = 20 \pm 3$ Pa; $G''_{MA0.3} = 8 \pm 5$ Pa) moduli, compared to hydrogels prepared from atelocollagen solutions in acetic acid (17.4 mM, pH 3.4) and PBS (10 mM, pH 7.5). Interestingly, similar trends were observed in the case of 4VBC-functionalized AC solutions, whereby significantly-increased viscosities were measured when the photoactive precursor was dissolved in hydrochloric acid ($\eta = 900 \pm 70$ mPa·s) compared to acetic acid ($\eta = 1820 \pm 80$ mPa·s) solutions (**Table 2**), whilst an opposite trend was observed in acidic solutions prepared with samples MA0.3 and MA25.

The solution-induced effect observed in AC products functionalized with equivalent molar content of methacrylamide and 4-vinylbenzyl residues is in agreement with the results reported by Ratanavaraporn et al. (2008), whereby increased solution viscosity and hydrogel compressive modulus were measured when native type I collagen was dissolved in aqueous solutions of decreased acidity. It is well known that the molecular organization of native collagen molecules can be altered depending on environmental factors, such as pH, ionic strength and salt concentration, given their effect on the ionization of amino acidic terminations and consequent secondary interactions (Salchert et al., 2004; Yunoki and Matsuda, 2008; Grant et al., 2009; Neel et al., 2013). The above-mentioned variations in network elastic properties suggest that a similar effect can still be observed in the case of functionalized atelocollagen with decreased F. Whilst fibrillogenesis was not expected during network formation ($T < 37°C$), the electrostatic repulsion of native atelocollagen molecules is expected to be increased in solutions of increased acidity (Ratanavaraporn et al., 2008; Li et al., 2009). Obviously, the degree and type of monomer adds further complexity to the solution-induced variability of protein organization, given that the atelocollagen functionalization is achieved by the consumption

of ionisable lysine terminations and that selected covalently-coupled adducts can mediate further secondary interactions, i.e., π-π stacking interactions and hydrogen bonds. The opposite pH-induced variation in solution viscosity measured with samples 4VBC25, on the one hand, and MA0.3 and MA25, on the other hand, reflects these considerations, given that aromatic interactions between 4-vinylbenzyl moieties are likely to be decreased at increased pH, whilst an opposite trend is expected with regards to the hydrogen bonding capability of methacrylamide residues. Whilst a solution pH-induced effect was clearly observed in hydrochloric and acetic acid solutions, the presence of salts in the PBS-based UV-curing system was likely to alter the capability of covalently-coupled moieties to mediate secondary interactions, explaining why no direct relationships between solution pH, on the one hand, and solution viscosity and hydrogel properties, on the other hand, could be observed.

Swelling, Gel Content and Compression Properties

Following the characterization of functionalized AC precursors and gelation kinetics, the gel content (G), swelling ratio (SR) and compressive properties were quantified to further elucidate the molecular architecture and assess the structure-property relationships of obtained UV-cured atelocollagen networks.

All UV-cured networks displayed an averaged gel content of at least 80 wt.%, with the exception of sample MA0.3(H)* ($G = 56 \pm 13$ wt.%) (**Figure 4**). Samples MA25* displayed the smallest variation in gel content when prepared in either HCl, AcOH, or PBS solutions, whilst the effect of the UV-curing solution was more visible in samples of MA0.3* and 4VBC25*. The high, and small solution-induced variation of, gel content measured in samples MA25* confirms that precursors with increased degree of functionalization generate highly crosslinked network, regardless of the type of UV-curing solution and solution-induced secondary interactions, as indicated previously (**Tables 1**, **2**).

In comparison to sample MA25*, networks 4VBC25(H)*, and MA0.3(H)* prepared in HCl solutions revealed the lowest gel content within the same sample group, whilst increased G values were measured in networks prepared in either AcOH, i.e., 4VBC25(A)* and MA0.3(A)*, or PBS, i.e., MA0.3(P)*. Given the comparable degree of functionalization in the network precursors (**Table 1**), these solution-induced variations in gel content seem to correlate with the above-mentioned results in UV-curing solution viscosity (**Table 2**), whereby an increase of solution pH from 2.1 (in 10 mM HCl) to 3.4 (in 17.4 mM AcOH) proved to generate hydrogels 4VBC25* with increased storage modulus (**Table 2**). An increase in solution viscosity is likely to be associated with an increased vicinity between atelocollagen molecules and respective crosslink-forming photoactive residues, so that increased chances of free-radical crosslinking reaction and minimized steric hindrance effects can be expected. Similar effects were also reported with collagen hydrogels prepared from solutions with decreased viscosity, whereby decreased

mechanical properties and increased pore size was observed (Ratanavaraporn et al., 2008).
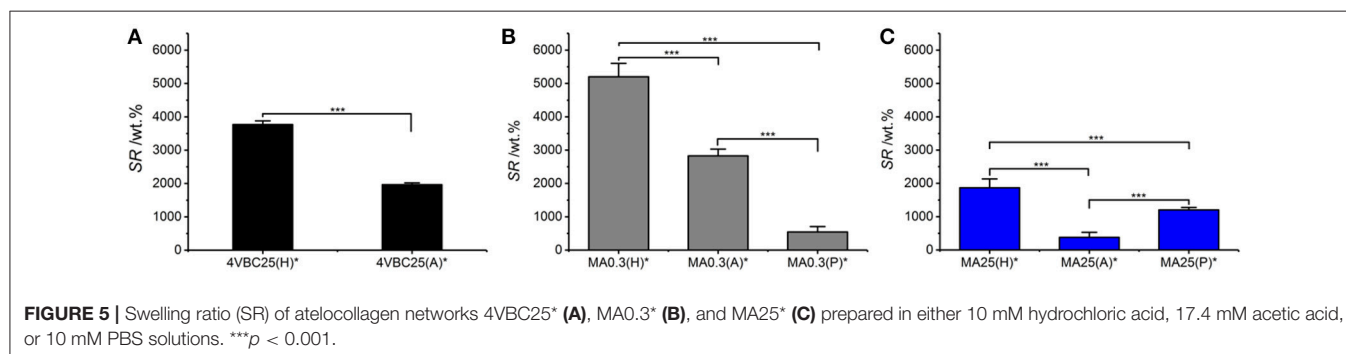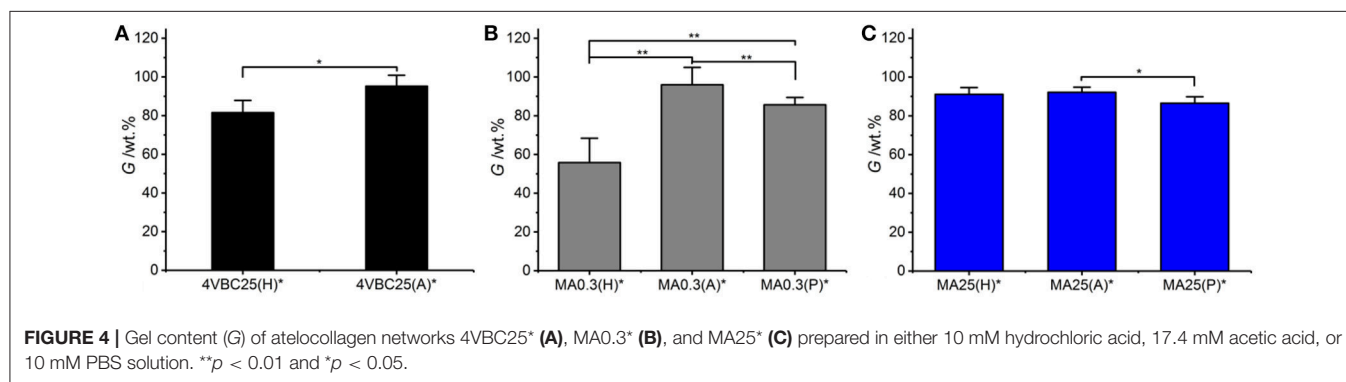
Previously-discussed results in gel content proved to support the trends in swelling ratio (**Figure 5**), whereby UV-cured networks described an inverse relationship between G and SR. For example, samples 4VBC25(H)* ($SR = 3769 \pm 111$ wt.%) and MA0.3(H)* ($SR = 5202 \pm 401$ wt.%) displayed the highest swelling ratio, confirming the higher water uptake capability of these materials with respect to sample variants prepared in AcOH solutions, reflecting above-discussed gel content trends.

Among the methacrylated groups, networks MA25* displayed the lowest value of SR (**Table 1**, **Figure 5**). Samples MA25* UV-cured in both AcOH and HCl solutions proved to display significantly decreased SR with respect to the ones of respective sample MA0.3*, in line with previous gel content data. On the other hand, an opposite trend was observed in networks synthesized in PBS, whereby sample MA25(P)* displayed higher SR with respect to sample MA0.3(P)*, despite the comparable gel content between the two samples (**Figure 4**) and the significantly higher degree of functionalization displayed by the former compared to the latter network precursor. Given that the swelling ratio was determined in PBS, the reason for this finding is likely explained by the fact that the increased molar content of methacrylamide moieties covalently-coupled to sample MA25 results in additional secondary interactions of the resulting network with PBS species, in line with the viscosity trends measured with the hydrogel-forming solutions (**Table 2**).

Overall, the water uptake capability of these atelocollagen networks was found to be comparable to the one of purely synthetic UV-cured PEG-based hydrogels (DiRamio et al., 2005)

and may be exploited for the design of multifunctional wound healing devices with enhanced exudate regulation capability (Bulman et al., 2015; Tronci et al., 2016b). The possibility to adjust the swelling properties of this atelocollagen system by simply varying the UV-curing solution rather than by the synthesis of new photoactive precursors is appealing aiming to expand material applicability yet minimizing additional time-consuming reactions.

Following characterization of the swelling behavior, the compressive properties of resulting UV-cured hydrogels were investigated. Typical stress-compression curves are reported in **Figure 6**, depending on the network architecture and type of UV-curing solvent employed. All samples revealed a J-shaped curve during compression, similarly to the case of previously-reported collagen hydrogels (Yunoki and Matsuda, 2008). Networks MA25* proved to display lower values of compression at break compared to both networks 4VBC25* and MA0.3* (**Figure 7**), in line with the increased degree of functionalization ($F = 88 \pm 1$ mol.%) of the former network precursors, yielding highly crosslinked networks ($G = 86 \pm 3 - 92 \pm 3$ wt.%). When comparing systems with comparable degrees of functionalization, samples 4VBC25* displayed a detectable increase in compression modulus ($E_c = 69 \pm 8 - 126 \pm 46$ kPa) when compared to samples MA0.3* ($E_c = 9 \pm 1 - 62 \pm 13$ kPa), in all environmental conditions investigated. Among the different aqueous media, UV-curing in HCl solutions was confirmed to yield networks with the lowest compression modulus (**Figure 7**), supporting previous rheological (**Table 2**), and gel content (**Figure 4**) measurements.

FIGURE 4 | Gel content (G) of atelocollagen networks 4VBC25* **(A)**, MA0.3* **(B)**, and MA25* **(C)** prepared in either 10 mM hydrochloric acid, 17.4 mM acetic acid, or 10 mM PBS solution. **$^{**}p < 0.01$ and $^{*}p < 0.05$.

FIGURE 5 | Swelling ratio (SR) of atelocollagen networks 4VBC25* **(A)**, MA0.3* **(B)**, and MA25* **(C)** prepared in either 10 mM hydrochloric acid, 17.4 mM acetic acid, or 10 mM PBS solutions. **$^{***}p < 0.001$.
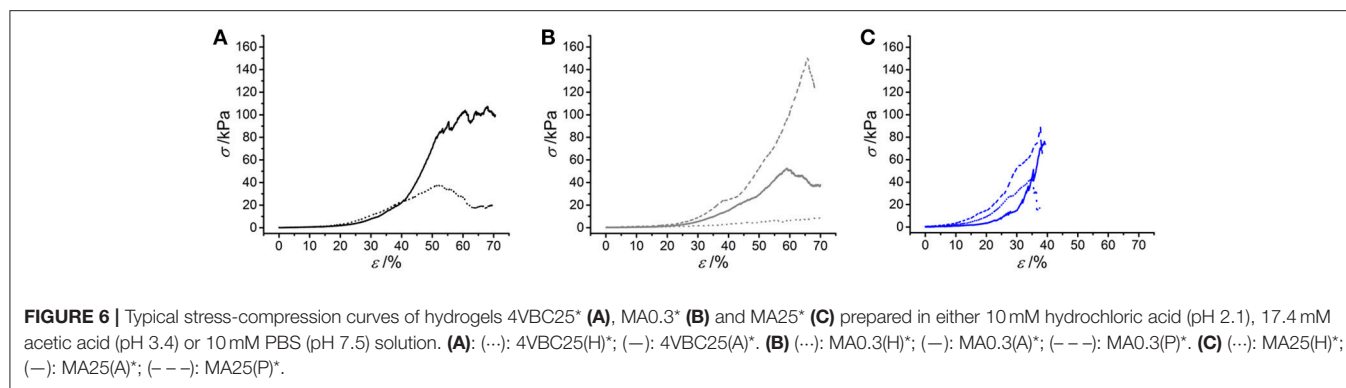
FIGURE 6 | Typical stress-compression curves of hydrogels 4VBC25* **(A)**, MA0.3* **(B)** and MA25* **(C)** prepared in either 10 mM hydrochloric acid (pH 2.1), 17.4 mM acetic acid (pH 3.4) or 10 mM PBS (pH 7.5) solution. **(A)**: (⋯): 4VBC25(H)*; (—): 4VBC25(A)*. **(B)**: (⋯): MA0.3(H)*; (—): MA0.3(A)*; (– – –): MA0.3(P)*. **(C)**: (⋯): MA25(H)*; (—): MA25(A)*; (– – –): MA25(P)*.
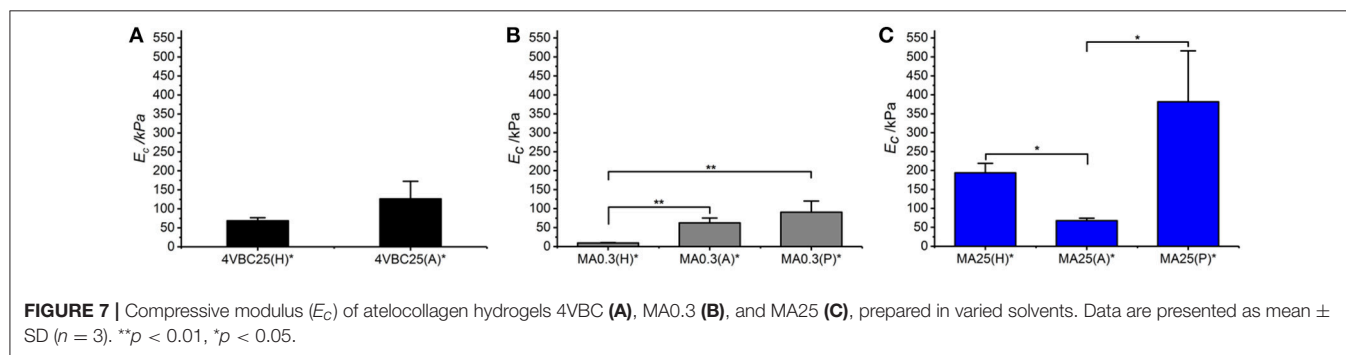

FIGURE 7 | Compressive modulus (E_c) of atelocollagen hydrogels 4VBC **(A)**, MA0.3 **(B)**, and MA25 **(C)**, prepared in varied solvents. Data are presented as mean ± SD ($n = 3$). **$p < 0.01$, *$p < 0.05$.
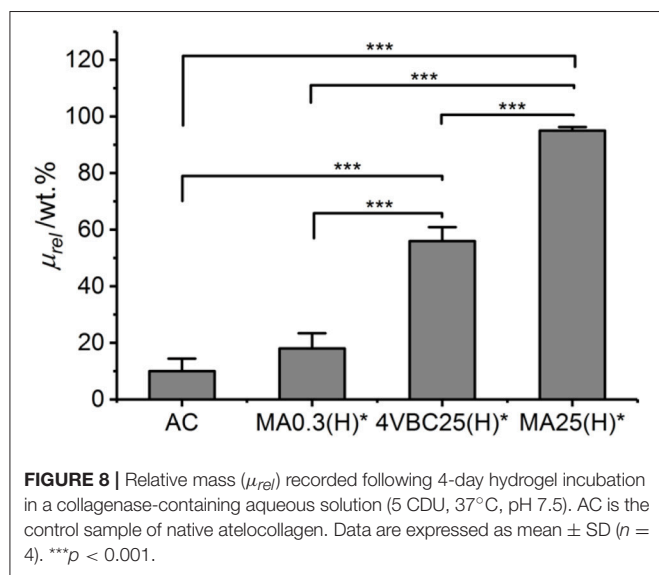

FIGURE 8 | Relative mass (μ_{rel}) recorded following 4-day hydrogel incubation in a collagenase-containing aqueous solution (5 CDU, 37°C, pH 7.5). AC is the control sample of native atelocollagen. Data are expressed as mean ± SD ($n = 4$). ***$p < 0.001$.
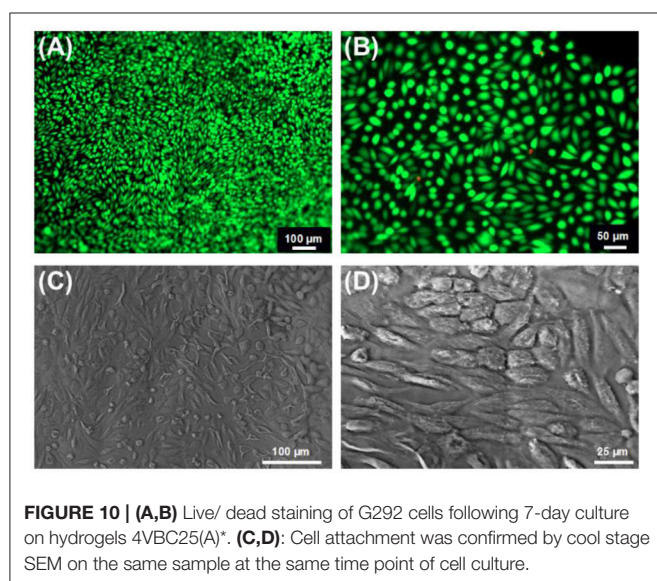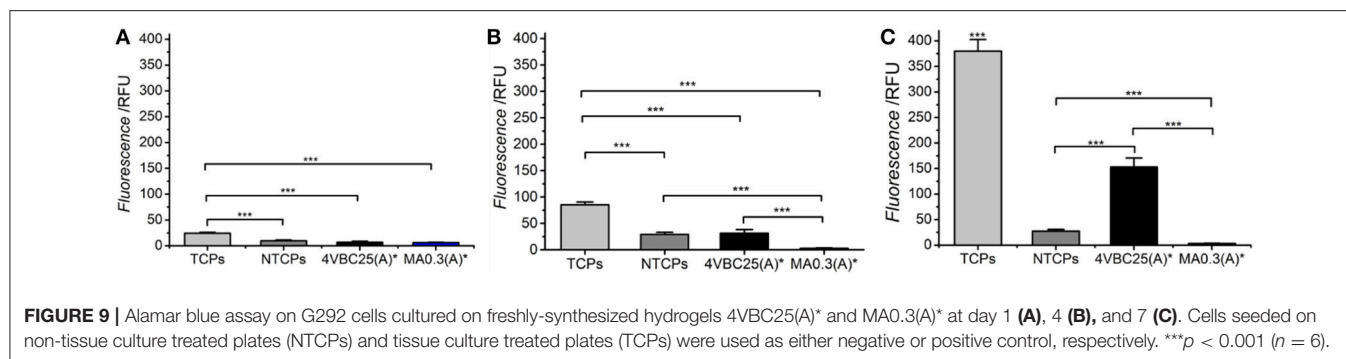
Remarkably, sample 4VBC25(H)* proved to display an averaged compressive modulus of about 70 kPa, despite an averaged swelling ratio of more than 3700 wt.%. In comparison, an equivalent methacrylated network exhibited a much lower averaged compressive modulus of less than 9 kPa, supporting the low gel content ($G = 56 \pm 13$ wt.%) and high swelling ratio ($SR = 5202 \pm 401$ wt.%). The uniquely high compressive modulus *and* swelling ratio of networks 4VBC25* provides additional evidence of the key role played by the molecular stiffness of the

4VBC-based crosslinking segment, in comparison to equivalent methacrylated atelocollagen networks obtained from precursors with comparable degree of functionalization.

When comparing systems with varied degree of functionalization, samples MA25* proved to display significantly increased compressive modulus with respect to samples MA0.3* (and 4VBC25*), confirming the previous trends in storage modulus (**Table 2**). The effect of the solvent in samples MA25* proved to be less obvious, as indicated by the variation of gel content and swelling ratio. On the one hand, the significant increase in molar content of methacrylamide residues is likely to generate UV-cured networks with increased crosslink density. On the other hand, significant atelocollagen methacrylation is expected to alter the protein capability to mediate secondary interactions, potentially resulting in altered structure-function relationships. Therefore, rather than aiming at increased degree of methacrylation, these results suggest that the introduction of a limited amount of stiff 4-vinylbenzyl moieties is preferable in order to achieve defined mechanically-competent atelocollagen hydrogels.

Enzymatic Degradability

A degradation study was carried out in enzymatic conditions in order to investigate how variations in network architecture were linked to the temporal stability of the hydrogel in near-physiologic conditions. Atelocollagen networks UV-cured in HCl solutions were selected for this investigation, due to the significant differences observed between samples 4VBC25(H)* and MA0.3(H)*. **Figure 8** describes the relative mass results

FIGURE 9 | Alamar blue assay on G292 cells cultured on freshly-synthesized hydrogels 4VBC25(A)* and MA0.3(A)* at day 1 **(A)**, 4 **(B)**, and 7 **(C)**. Cells seeded on non-tissue culture treated plates (NTCPs) and tissue culture treated plates (TCPs) were used as either negative or positive control, respectively. ***$p < 0.001$ ($n = 6$).

FIGURE 10 | (A,B) Live/ dead staining of G292 cells following 7-day culture on hydrogels 4VBC25(A)*. **(C,D)**: Cell attachment was confirmed by cool stage SEM on the same sample at the same time point of cell culture.

recorded following 4-day network incubation in an aqueous medium containing collagenase. As expected, samples of native atelocollagen revealed the highest enzymatic degradation with less than 10 wt.% remaining mass, followed by networks MA0.3H* ($\mu_{rel} = 18 \pm 5$ wt.%) and 4VBC25H* ($\mu_{rel} = 56 \pm 5$ wt.%), whilst the highest proteolytic stability was displayed by sample MA25H* ($\mu_{rel} = 95 \pm 1$ wt.%).

Chemical crosslinking of collagen has been described as a promising strategy to increase the enzymatic stability of collagen, since the covalent crosslinks between protein molecules can be insensitive to collagenases and affect the availability of tripe helical segments recognizable by enzymes (Olde Damink et al., 1995a; Haugh et al., 2011; Van Vlierberghe et al., 2011; Lee et al., 2013; Duan et al., 2014; Tronci et al., 2016b; Calciolari et al., 2018). Therefore, aforementioned degradation data successfully support the effect played by the network architecture on the enzymatic stability of the hydrogel, both in terms of type of covalently-coupled monomer as well as consequent degree of atelocollagen functionalization. Samples MA25(H)* displayed the highest enzymatic stability given the high degree of functionalization and gel content measured in network precursor and resulting crosslinked network, respectively. Other than that,

controlled enzymatic degradation can still be achieved by simply varying the type of monomer introduced, i.e., 4-vinylbenzyl with respect to methacrylamide residue, whilst keeping the degree of functionalization constant, in resulting photoactive precursors. The introduction of 4VBC moieties is likely to mediate secondary interactions with the exposed zinc site of active collagenases (Tronci et al., 2016b), so that consequent proteolytic inactivation explains the prolonged stability of sample 4VBC(H)* with respect to the equivalent variant MA0.3(H)*.

Similarly to the case of linear biopolymers (Lee et al., 2013), the manipulation of the atelocollagen network architecture is therefore proven to generate customizable hydrogels, whose degradation profiles can be combined with specific mechanical and swelling properties, depending on specific environmental (e.g., pH) and molecular parameters selected during UV-curing.

Cytotoxicity Evaluation

Following evaluation of the enzymatic degradability, the cellular tolerability of freshly-synthesized networks 4VBC25(A)* and MA0.3(A)* was exemplarily evaluated by culturing osteosarcoma G292 cells in direct contact with the hydrated material. Cellular metabolism was measured by Alamar blue assay at day 1, 4, and 7 (**Figure 9**).

Over the period of 7 days, G292 cells seeded on TCPs displayed significantly increased proliferation at all time points investigated. Between the group of 4VBC25(A)* and MA0.3(A)*, no significant difference was found at day 1; however, the proliferation rate of cells cultured on hydrogel 4VBC25(A)* was much higher than the one of cells cultured on hydrogel MA0.3(A)* at both day 4 and day 7. The dramatic turnover of cells on sample MA0.3(A)* was mainly due to the shrinkage of the hydrogel microstructure observed already following 1-day cell culture, in line with the fast enzymatic sample degradability measured following 4-day incubation in collagenase medium (**Figure 8**). Unsurprisingly, TCPs showed the highest rate of proliferation compared to 4VBC25(A)*; this observation is mainly due to the fact that the porous 3D structure of the 4VBC25(A)* hydrogel network induced low cell seeding efficiency and cellular penetration in comparison to 2D surfaces (Vunjak et al., 1998).

We also confirmed the cytotoxicity of the hydrogels via Live/Dead staining of G292 cells following 7-day culture

(**Figures 10A,B**). Almost no dead cell was found on hydrogel 4VBC(25)A*, indicating cellular tolerability in agreement with previously-discussed metabolic activity data. Besides Live/Dead staining, cool-stage SEM was also carried out on 7-day cultured hydrogel 4VBC25(A)*, as reported in **Figures 10C,D**, whereby full cellular attachment and complete surface cell coverage were observed, supporting previous findings. When the same SEM investigations were carried out on 7-day cultured hydrogel MA0.3(A)*, no cell attachment was observed (**Figure S3**), in line with Alamar blue results (**Figure 9**) and the fast enzymatic sample degradability (**Figure 8**).

Overall, these results prove that selected functionalization and network formation strategies did not affect atelocollagen biocompatibility, whilst proved successful in enabling systematic customization of the pristine building block.

CONCLUSION

The introduction of either 4-vinylbenzyl or methacrylamide adducts onto type I atelocollagen proved successful to enable the synthesis of customizable UV-cured hydrogel networks, depending on the type of monomer, degree of atelocollagen functionalization, and UV-curing solution. Reaction with MA led to highly tunable degree of atelocollagen functionalization (F_{MA}: $4 \pm 1 - 88 \pm 1$ mol.%), in contrast to the reaction carried out with 4VBC (F_{4VBC}: 18 ± 1 mol.%), although rapid gelation ($\tau = 6-12$ s) was still achieved with both precursors as confirmed by photorheometry. Introduction of 4-vinylbenzyl groups proved to yield atelocollagen networks with significantly increased compression modulus ($E_c = 69 \pm 8 - 126 \pm 46$ kPa), storage modulus ($G' = 73 \pm 22 - 390 \pm 99$ Pa) and 4-day enzymatic stability ($\mu_{rel} = 56 \pm 5$ wt.%), with respect to methacrylated equivalents, due to the increased molecular stiffness of, and secondary interactions mediated by, the aromatized UV-cured crosslinking segments. Comparable variations in material properties were also observed when UV-curing atelocollagen precursors functionalized with varied content of methacrylamide functions ($F = 19 \pm 2 - 88 \pm 1$ mol.%), supporting the direct relationships

between the degree of functionalization of network precursors and resulting network crosslink density. The solution pH proved to affect the viscosity of respective atelocollagen solutions, whereby the monomer capability to mediate secondary interactions was found to play a role. UV-curing solutions with decreased acidity proved to generate networks with increased compression and storage modulus, as well as decreased swelling ratio, whilst no toxic cellular response was observed. These findings demonstrate the monomer-induced customizability of presented UV-cured atelocollagen hydrogel networks, whereby structure-property relationships can be controlled to enable applicability in personalized medicine and to fulfill the requirements of complex and unmet clinical needs.

AUTHOR CONTRIBUTIONS

HL and GT conceived and designed the experiments; HL performed the experiments. DW and SR assisted in the preparation of the manuscript. GT and HL wrote the paper. All authors analyzed the data.

SUPPLEMENTARY MATERIAL

The Supplementary Material for this article can be found online at: https://www.frontiersin.org/articles/10.3389/fchem.2018.00626/full#supplementary-material

REFERENCES

Aggeli, A., Bell, M., Boden, N., Carrick, L. M., and Strong, A. E. (2003). Self-assembling peptide polyelectrolyte β-sheet complexes form nematic hydrogels. *Angew. Chemie. Int. Ed.* 42, 5603–5606. doi: 10.1002/anie.200352207

Billiet, T., Van Gasse, B., Gevaert, E., Cornelissen, M., Martins, J. C., and Dubruel, P. (2013). Quantitative contrasts in the photopolymerisation of acrylamide and methacrylamide-functionalised gelatin hydrogel building blocks. *Macromol. Biosci.* 13, 1531–1545. doi: 10.1002/mabi.201300143

Birchall, L. S., Roy, S., Jayawarna, V., Hughes, M., Irvine, E., Okorogheye, G. T., et al. (2011). Exploiting CH-p interactions in supramolecular hydrogels of aromatic carbohyrate amphiphiles. *Chem. Sci.* 2, 1349–1355. doi: 10.1039/c0sc00621a

Brinkman, W. T., Nagapudi, K., Thomas, B. S., and Chaikof, E. L. (2003). Photo-cross-linking of type i collagen gels in the presence of smooth muscle cells: mechanical properties, cell viability, and function. *Biomacromolecules* 4, 890–895. doi: 10.1021/bm0257412

Bubnis, W. A., and Ofner, C. M. III. (1992). The determination of ε-amino groups in soluble and poorly soluble proteinaceous materials by a spectrophotometrie method using trinitrobenzenesulfonic acid. *Anal. Biochem.* 207, 129–133. doi: 10.1016/0003-2697(92)90513-7

Bulman, S. E., Goswami, P., Tronci, G., Russell, S. J., and Carr, C. (2015). Investigation into the potential use of poly(vinyl alcohol)/methylglyoxal fibres as antibacterial wound dressing components. *J. Biomater. Appl.* 29, 1193–1200. doi: 10.1177/0885328214556159

Burdick, J. A., and Prestwich, G. D. (2011). Hyaluronic acid hydrogels for biomedical applications. *Adv. Mater.* 23, H41–H56. doi: 10.1002/adma.201003963

Calciolari, E., Ravanetti, F., Strange, A., Mardas, N., Bozec, L., Cacchioli, A., et al. (2018). Degradation pattern of a porcine collagen membrane in an in vivo model of guided bone regeneration. *J. Periodont. Res.* 53, 430–439. doi: 10.1111/jre.12530

Chen, L., Yao, X., Gu, Z., Zheng, K., Zhao, C., Lei, W., et al. (2017). Covalent tethering of photo-responsive superficial layers on hydrogel surfaces

for photo-controlled release. *Chem. Sci.* 8, 2010–2016. doi: 10.1039/C6SC0 4634G

DiRamio, J. A., Kisaalita, W. S., Majetich, G. F., and Shimkus, J. M. (2005). Poly(ethylene glycol) methacrylate/dimethacrylate hydrogels for controlled release of hydrophobic drugs. *Biotechnol. Progr.* 21, 1281–1288. doi: 10.1021/bp0495670

Duan, L., Liu, W., Tian, Z., Li, C., and Li, G. (2014). Properties of collagen gels cross-linked by N-hydroxysuccinimide activated adipic acid deriviate. *Int. J. Biol. Macromol.* 69, 482–488. doi: 10.1016/j.ijbiomac.2014.06.005

Everaerts, F., Torrianni, M., Hendriks, M., and Feijen, J. (2008). Biomechanical properties of carbodiimide crosslinked collagen: Influence of the formation of ester crosslinks. *J. Biomed. Mater. Res.* 85A, 547–555. doi: 10.1002/jbm.a.31524

Fairbanks, B. D., Schwartz, M. P., Halevi, A. E., Nuttelman, C. R., Bowman, C. N., and Anseth, K. S. (2009). A versatile synthetic extracellular matrix mimic via thiol-norbornene photopolymerization. *Adv. Mater.* 21, 5005–5010. doi: 10.1002/adma.200901808

Gaudet, I. D., and Shreiber, D. I. (2012). Characterization of methacrylated type-I collagen as a dynamic, photoactive hydrogel. *Biointerphases* 7:25. doi: 10.1007/s13758-012-0025-y

Gharaei, R., Tronci, G., Davies, R. P., Gough, C., Alazragi, R., Goswami, P., et al. (2016). A structurally self-assembled peptide nano-architecture by one-step electrospinning. *J. Mater. Chem. B* 4, 5475–5485. doi: 10.1039/C6TB01164K

Grant, C. A., Brockwell, D. J., Radford, S. E., and Thomson, N. H. (2009). Tuning the elastic modulus of hydrated collagen fibrils. *Biophys. J.* 97, 2985–2992. doi: 10.1016/j.bpj.2009.09.010

Haugh, M. G., Murphy, C. M., McKiernan, R. C., Altenbuchner, C., and O'Brien, F. J. (2011). Crosslinking and mechanical properties significantly influence cell attachment, proliferation, and migration within collagen glycosaminoglycan scaffolds. *Tissue Eng. Part A.* 17, 1201–1218. doi: 10.1089/ten.TEA.2010.0590

Head, D. A., Tronci, G., Russell, S. J., and Wood, D. J. (2016). *In silico* modeling of the rheological properties of covalently cross-linked collagen triple helices. *ACS Biomater. Sci. Eng.* 2, 1224–1233. doi: 10.1021/acsbiomaterials.6b00115

Heller, D. A., Levi, Y., Pelet, J. M., Doloff, J. C., Wallas, J., Pratt, G. W., et al. (2013). Modular 'click-in-emulsion' bone-targeted nanogels. *Adv. Mater.* 25, 1449–1454. doi: 10.1002/adma.201202881

Heo, J., Koh, R. H., Shim, W., Kim, H. D., Yim, H.-G., and Hwang, N. S. (2016). Riboflavin-induced photo-crosslinking of collagen hydrogel and its application in meniscus tissue engineering. *Drug Deliv. Transl. Res.* 6, 148–158. doi: 10.1007/s13346-015-0224-4

Holmes, R., Yang, X.-B., Dunne, A., Florea, L., Wood, D., and Tronci, G. (2017). Thiol-ene photo-click collagen-PEG hydrogels: impact of water-soluble photoinitiators on cell viability, gelation kinetics and rheological properties. *Polymers* 9:226. doi: 10.3390/polym9060226

Jia, Y., Wang, H., Wang, H., Li, Y., Wang, M., and Zhou, J. (2012). Biochemical properties of skin collagens isolated from black carp (*Mylopharyngodon piceus*). *Food Sci. Biotechnol.* 21, 1585–1592. doi: 10.1007/s10068-012-0211-1

Kishan, A. P., Nezarati, R. M., Radzicki, C. M., Renfro, A. L., Robinson, J. L., Whitely, M., et al. (2015). *In situ* crosslinking of electrospun gelatin for improved fiber morphology retention and tunable degradation. *J. Mater. Chem. B* 3, 7930–7938. doi: 10.1039/C5TB00937E

Koch, F., Müller, M., König, F., Meyer, N., Gattlen, J., Pieles, U., et al. (2018). Mechanical characteristics of beta sheet-forming peptide hydrogels are dependent on peptide sequence, concentration and buffer composition. *R. Soc. Open Sci.* 5:171562. doi: 10.1098/rsos.171562

Konieczynska, M. D., Villa-Camacho, J. C., Ghobril, C., Perez-Viloria, M., Tevis, K. M., Blessing, W. A., et al. (2016). On-demand dissolution of a dendritic hydrogel-based dressing for second-degree burn wounds through thiol–thioester exchange reaction. *Angew. Chem. Int. Ed.* 55, 9984–9987. doi: 10.1002/anie.201604827

Lee, Y., Woo Bae, J., Oh, D. H., Park, K. M., Chun, Y. W., and Park, K. D. (2013). *In situ* forming gelatin-based tissue adhesives and their phenolic content-driven properties. *J. Mater. Chem. B* 1, 2407–2414. doi: 10.1039/c3tb 00578j

Levitt, M., and Perutz, M. F. (1988). Aromatic rings act as hydrogen bond acceptors. *J. Mol. Biol.* 201, 751–754. doi: 10.1016/0022-2836(88)90471-8

Li, F., Zhu, Y., You, B., Zhao, D., Ruan, Q., Zeng, Y., et al. (2010). Smart hydrogels co-switched by hydrogen bonds and π-π stacking for

continuously regulated controlled-release system. *Adv. Funct. Mater.* 20, 669–676. doi: 10.1002/adfm.200901245

Li, Y., Asadi, A., Monroe, M. R., and Douglas, E. P. (2009). pH effects on collagen fibrillogenesis *in vitro*: electrostatic interactions and phosphate binding. *Mater. Sci. Eng. C* 29, 1643–1649. doi: 10.1016/j.msec.2009.01.001

Liang, H., Russell, S. J., Wood, D. J., and Tronci, G. (2018). A hydroxamic acid–methacrylated collagen conjugate for the modulation of inflammation-related MMP upregulation. *J. Mater. Chem. B* 6, 3703–3715. doi: 10.1039/C7TB0 3035E

Lynn, A. K., Yannas, I. V., and Bonfield, W. (2004). Antigenicity and immunogenicity of collagen. *J. Biomed. Mater. Res. B Appl. Biomater.* 71, 343–354. doi: 10.1002/jbm.b.30096

McCall, J. D., and Anseth, K. S. (2012). Thiol–Ene photopolymerizations provide a facile method to encapsulate proteins and maintain their bioactivity. *Biomacromolecules* 13, 2410–2417. doi: 10.1021/bm300671s

Neel, E., Bozec, L., Knowles, J. C., Syed, O., Mudera, V., Day, R., et al. (2013). Collagen—emerging collagen based therapies hit the patient. *Adv. Drug Deliv. Rev.* 65, 429–456. doi: 10.1016/j.addr.2012.08.010

Nimmo, C. M., and Shoichet, M. S. (2011). Regenerative biomaterials that "click": simple, aqueous-based protocols for hydrogel synthesis, surface immobilization, and 3d patterning. *Bioconjugate Chem.* 22, 2199–2209. doi: 10.1021/bc200281k

Olde Damink, L. H. H., Dijkstra, P. J., Van Luyn M., Van Wachem, P. B., Nieuwenhuis, P., and Feijen, J. (1995b). Glutaraldehyde as a crosslinking agent for collagen-based biomaterials. *J. Mater. Sci. Mater. Med.* 6, 460–472. doi: 10.1007/BF00123371

Olde Damink, L. H. H., Dijkstra, P. J. M.,Van Luyn, J. A., Van Wachem, P. B., Nieuwenhuis, P., and Feijen, J. (1995a). Crosslinking of dermal sheep collagen using hexamethylene diisocyanate. *J. Mater. Sci. Mater. Med.* 6, 429–434. doi: 10.1007/BF00120286

Qin, X.-H., Labuda, K., Chen, J., Hruschka, V., Khadem, A., Slezak, P., et al. (2015). Development of synthetic platelet-activating hydrogel matrices to induce local hemostasis. *Adv. Funct. Mater.* 25, 6606–6617. doi: 10.1002/adfm.2015 01637

Qin, X.-H., Wang, X., Rottmar, M., Nelson, B., and Maniura-Webe J. K. R. (2018). Near-infrared light-sensitive polyvinyl alcohol hydrogel photoresist for spatiotemporal control of cell-instructive 3D microenvironments. *Adv. Mater.* 30:1705564. doi: 10.1002/adma.201705564

Ratanavaraporn, J., Kanokpanont, S., Tabata, Y., and Damrongsakkul, S. (2008). Effects of acid type on physical and biological properties of collagen scaffolds. *J. Biomater. Sci. Polym. Ed.* 19, 945–952. doi: 10.1163/156856208784 613505

Ravichandran, R., Islam, M. M., Alarcon, E. I., Samanta, A., Wang, S., Lundström, P., et al. (2016). Functionalised type-I collagen as hydrogel building block for bio-orthogonal tissue engineering applications. *J. Mater. Chem. B* 4, 318-326. doi: 10.1039/C5TB02035B

Salchert, K., Streller, U., Pompe, T., Herold, N., Grimmer, M., and Werner, C. (2004). *In vitro* reconstitution of fibrillar collagen Type I assemblies at reactive polymer surfaces. *Biomacromolecules* 5, 1340–1350. doi: 10.1021/bm04 99031

Sridhar, B. V., Brock, J. L., Silver, J. S., Leight, J. L., Randolph, M. A., and Anseth, K. S. (2015). Development of a cellularly degradable PEG hydrogel to promote articular cartilage extracellular matrix deposition. *Adv. Healthc. Mater.* 4, 702–713. doi: 10.1002/adhm.201400695

Starcher, B. (2001). A ninhydrin-based assay to quantitate the total protein content of tissue samples. *Anal. Biochem.* 292, 125–129. doi: 10.1006/abio.2001.5050

Tronci, G., Grant, C. A., Thomson, N. H., Russell, S. J., and Wood, D. J. (2015a). Multi-scale mechanical characterization of highly swollen photo-activated collagen hydrogels. *J. R. Soc. Interface* 12:20141079. doi: 10.1098/rsif.2014.1079

Tronci, G., Grant, C. A., Thomson, N. H., Russell, S. J., and Wood, D. J. (2016a). Influence of 4-vinylbenzylation on the rheological and swelling properties of photo-activated collagen hydrogels. *MRS Advances* 1, 533–538. doi: 10.1557/adv.2015.11

Tronci, G., Kanuparti, R. S., Arafat, M. T., Yin, J., Wood, D. J., and Russell, S. J. (2015b). Wet-spinnability and crosslinked fibre properties of two collagen polypeptides with varied molecular weight. *Int. J. Biol. Macromol.* 81, 112–120. doi: 10.1016/j.ijbiomac.2015.07.053

Tronci, G., Neffe, A. T., Pierce, B. F., and Lendlein, A. (2010). An entropy–elastic gelatin-based hydrogel system. *J. Mater. Chem.* 20, 8875–8884. doi: 10.1039/c0jm00883d

Tronci, G., Yin, J., Holmes, R. A., Liang, H., Russell, S. J., and Wood, D. J. (2016b). Protease-sensitive atelocollagen hydrogels promote healing in a diabetic wound model. *J. Mater. Chem. B,* 4, 7249–7258. doi: 10.1039/C6TB02268E

Van Hoorick, J., Gruber, P., , Markovic, M., Geert-Jan, M. R., Vagenende, G. M., Tromayer, M., et al. (2018). Highly reactive thiol-norbornene photo-click hydrogels: toward improved processability. *Macromol. Rapid Comm.* 39:1800181. doi: 10.1002/marc.201800181

Van Vlierberghe, S., Dubruel, P., and Schacht, E. (2011). Biopolymer-based hydrogels as scaffolds for tissue engineering applications: a review. *Biomacromolecules* 12, 1387–1408. doi: 10.1021/bm200083n

Vunjak, G., Obradovic, N. B., Martin, I., Bursac, P. M., Langer, R., and Freed, L. E. (1998). Dynamic cell seeding of polymer scaffolds for cartilage tissue engineering. *Biotech Progr.* 14, 193–202. doi: 10.1021/bp970120j

Yang, Z., Hemar, Y., Hilliou, L., Gilbert, E. P., McGillivray, D. J., Chaieb, S. M., et al. (2016). Nonlinear behavior of gelatin networks reveals a hierarchical structure. *Biomacromolecules* 17, 590–600. doi: 10.1021/acs.biomac.5b01538

Younesi, M., Islam, A., Kishore, V., Anderson, J. M., and Akkus, O. (2014). Tenogenic induction of human MSCs by anisotropically aligned collagen biotextiles. *Adv. Funct. Mater.* 24, 5762–5770. doi: 10.1002/adfm.201400828

Yunoki, S., and Matsuda, T. (2008). Simultaneous processing of fibril formation and cross-linking improves mechanical properties of collagen. *Biomacromolecules* 9, 879–885. doi: 10.1021/bm7012058

Zhang, Y. S., and Khademhosseini, A. (2017). Advances in engineering hydrogels. *Science* 356:eaaf3627. doi: 10.1126/science.aaf3627

Conflict of Interest Statement: The authors declare that the research was conducted in the absence of any commercial or financial relationships that could be construed as a potential conflict of interest.

Functional Dynamics Inside Nano- or Microscale Bio-Hybrid Systems

Zhuojun Dai* and Shuqiang Huang

Institute for Synthetic Biology, Shenzhen Institutes of Advanced Technology, Chinese Academy of Sciences, Shenzhen, China

Soft nano- or microgels made by natural or synthetic polymers have been investigated intensively because of their board applications. Due to their porosity and biocompatibility, nano- or microgels can be integrated with various biologics to form a bio-hybrid system. They can support living cells as a scaffold; entrap bioactive molecules as a drug carrier or encapsulate microorganisms as a semi-permeable membrane. Especially, researchers have created various modes of functional dynamics into these bio-hybrid systems. From one side, the encapsulating materials can respond to the external stimulus and release the cargo. From the other side, cells can respond to physical, or chemical properties of the matrix and differentiate into a specific cell type. With recent advancements of synthetic biology, cells can be further programed to respond to certain signals, and express therapeutics or other functional proteins for various purposes. Thus, the integration of nano- or microgels and programed cells becomes a potential candidate in applications spanning from biotechnology to new medicines. This brief review will first talk about several nano- or microgels systems fabricated by natural or synthetic polymers, and further discuss their applications when integrated with various types of biologics. In particular, we will concentrate on the dynamics embedded in these bio-hybrid systems, to dissect their designs and sophisticated functions.

Keywords: nano/microgels, synthetic biology, fabrication technology, bio-hybrid system, dynamics

INTRODUCTION

Hydrogels are polymeric materials that consist of crosslinked three-dimensional (3D) networks. Due to their porosity and high water content, they can serve as ideal matrices for controlled release of biomolecules, cells encapsulation and delivery, as well as scaffolds in tissue engineering (Minh and Lee, 2010; Naderi et al., 2011; Smeets and Hoare, 2013; Suo et al., 2018). Stimulus-sensitive hydrogels, in particular, can swell or shrink in response to multiple modes of external stimulus such as temperature, pH, ionic strength, and light (Gorelikov et al., 2004; Gu et al., 2013; Trongsatitkul and Budhlall, 2013). Compared with macrogels (millimeters to a few centimeters), nano- or microgels (several nanometers to hundreds of microns) can respond more quickly to environmentally-triggered changes, enabling their uses in controlled and regulated applications (Dai and Ngai, 2013; Smeets and Hoare, 2013; Headen et al., 2014). Additionally, their small size allows administration by various routes (e.g., injection) (Liu and Garcia, 2016). These features provide numerous opportunities for versatile applications.

On the other hand, synthetic biology has emerged as a powerful approach for engineering systems with predicted applications (de Lorenzo, 2008; Ye and Fussenegger, 2014; Din et al., 2016). Advances in programming single cell or cell populations with well-characterized functions have demonstrated their potentials in broad areas spanning from biotechnology to new medicines

(Bacchus et al., 2013; Cao et al., 2017; Karig, 2017; Tay et al., 2017; Villarreal et al., 2018). A key focus for synthetic biology is engineering bacteria for medical and environmental related applications (Ye and Fussenegger, 2014; Slomovic et al., 2015; Higashikuni et al., 2017; Karig, 2017). However, these engineered cells need to be trapped and separated from the surrounding tissues and environment to avoid side effects (Chang, 2005; Auslander et al., 2012). Microgels mediated encapsulation provides a solution since the porous structure allows permeability of small molecules, such as oxygen, nutrients, growth factors, and signaling molecules. At the same time, it prevents large molecules, such as immunoglobulins and immune cells (high molecular weight complexes) from reaching the encapsulated cells, and encapsulated cells from reaching tissues and environment (Auslander et al., 2012; Ye and Fussenegger, 2014).

By far, the researchers have successfully integrated the nano- or microgels and biologics to demonstrate a broad range of applications. Nano- or microgels are integrated with therapeutics to treat diabetes and cancer (Das et al., 2006; Sung et al., 2012; Gu et al., 2013; Kanamala et al., 2016), or assembled with stem cells in the tissue engineering (Das et al., 2014; Caldwell et al., 2017). Recently, the integration of nano- or microgels with engineered cells has proven their superiority in diseases detection and treatment (Shao et al., 2017; Xue et al., 2017; Wang et al., 2018). We will start from the basic characteristics, crosslinking strategies, and synthesis scheme of several nano- or microgels systems, and later discuss their applications when integrated with various biologics. In particular, we will focus on the functional dynamics inside the bio-hybrid systems, from either materials or cells side.

NANO- OR MICROGELS SYSTEMS

Both natural and synthetic polymers have been used to synthesize the nano- or microgels (Silva et al., 2004; Oh et al., 2008; Kim et al., 2014). Although the source and batch variations provide limitations, natural polymers are generally bio-compatible, biodegradable, and have been successfully used in clinical applications (Dhandayuthapani et al., 2011). In comparison, nano- or microgels made by synthetic polymers normally have predictable and reproducible physical and chemical properties. The systems made by either natural or synthetic polymers can be further tailored for special purposes, such as sensing and targeting (Gan et al., 2005; Pich and Richtering, 2010). In this section, we will review several well-known and widely used natural and synthetic polymer systems, including their physical and chemical properties, as well as crosslinking strategies.

Natural Polymer Systems
Natural polymers include proteins (silk, collagen, etc.), polysaccharides (alginate, chitosan, cellulose, etc.), and polynucleotides (DNA and RNA). Especially, two natural polysaccharides: alginate and chitosan, are widely utilized in biomedical and bioengineering fields.

Alginate
Alginate is an anionic polysaccharide (α-D-mannuronic acid and β-L-guluronic acid) derived from seaweed, and has been broadly used due to its biocompatibility, flexibility in modifications, and mild crosslinking conditions (Lee and Mooney, 2012; Szekalska et al., 2016). Divalent cations are the most frequently used crosslinking agents to prepare alginate nano- or microgels. The gel structure forms when the divalent cations bind to guluronate blocks of one alginate chain and the other adjacent chain (Lee and Mooney, 2012). Calcium chloride is commonly used as a divalent cation related crosslinking agent. However, its high solubility and fast diffusion in aqueous solution typically lead to rapid but poorly controlled gelation. To control the gelation rate in order to attain a more uniform gel structure and better mechanical integrity, one approach is to use a buffer system containing phosphates. The phosphate groups will compete with carboxyl groups from alginate for calcium ions and slow down the overall gelation rate. Calcium sulfate and calcium carbonate, because of their lower solubility, can also be used to control the gelation rate and derive a more uniform crosslinking structure (Augst et al., 2006; Lee and Mooney, 2012).

The major concern about the ionically crosslinked alginate nano- or microgels is their limitation in long-term stability, since monovalent cations will gradually replace divalent cations and dissociate the network in the physiological condition. Therefore, cationic polymers such as poly (L-lysine) (PLL), have been utilized to coat the surface of alginate nano- or microgels based on their electrostatic interactions (polyanions and polycations) to enhance the overall stability. In another approach, chemical crosslinking (covalent bonding) can be applied parallelly with ionic crosslinking. For example, a photo crosslinked alginate-methacrylate microgel was prepared by integrating the ionic and chemical crosslinking strategies (Li et al., 2017). Ionic crosslinking was used in extrusion process for beads formation due to its fast gelation speed. Photo-crosslinking, which proceeds much slower, was used to increase the stability of beads due to the irreversibility of covalent bonding.

Chitosan
The positively charged polysaccharide chitosan is essentially composed of β-(1,4)-linked glucosamine units (2-amino-2-deoxy-β-d-glucopyranose) together with some proportion of N-acetylglucosamine units (2-acetamino-2-deoxy-β-d-glucopyranose), and prepared by partial deacetylation of the natural polymer chitin (Anitha et al., 2014). Chitosan is biocompatible, degradable and has been tested for biomedical applications ranging from wound dressing, drug delivery to tissue engineering (Lopez-Leon et al., 2005; Anitha et al., 2014). It is typically dissolved in acidic media (e.g., acetic acid) due to the existence of amine groups and high crystallinity.

Chitosan can form hydrogels by either chemical or ionic crosslinking. The most frequently used chemical crosslinkers for chitosan are dialdehydes, such as glutaraldehyde (Suh and Matthew, 2000; Berger et al., 2004). The reaction between amine groups (chitosan) and aldehyde groups (dialdehydes) forms covalent imine bonds. Although the reaction can proceed in gentle conditions (aqueous media, room temperature), there are

concerns due to the toxicity of dialdehydes (Berger et al., 2004). Alternatively, other chemical crosslinkers, such as genipin, which possesses similar crosslinking properties with glutaraldehyde, but without corrosiveness, cytotoxic and carcinogenic side effects, are preferably developed and applied in recent studies (Skop et al., 2013).

Compared with chemical crosslinking, ionic crosslinking of chitosan is much simpler and milder, and therefore applied widely in medical or pharmaceutical applications. The networks form due to the electrostatic interactions between positively charged amine groups from chitosan backbones and the negatively charged crosslinkers. Both polyanions, such as heparin, or anionic molecules, such as tripolyphosphate (TPP) or phytic acid (PA) can be applied as ionic crosslinkers (Gan et al., 2005; Lee et al., 2011). To reinforce the stability and mechanical property of the chitosan network, the chemical and ionic crosslinking strategies can also be integrated. For example, Skop et al. has demonstrated the fabrication of genipin covalently crosslinked chitosan–heparin complex microspheres (Skop et al., 2013). These microspheres were shown to be a more stable system. Fine tuning in the size, surface charge or other characteristics of nano- or microgels can be obtained by varying compositions and preparation conditions (Gan et al., 2005).

Synthetic Polymer Systems

Multiple synthetic polymers have been used to construct nano- or microgels. Especially, we discussed two synthetic polymers: poly(N-isopropylacrylamide) and poly (ethylene glycol), due to their stimulus responsiveness and bio-compatibility.

poly(N-isopropylacrylamide)

Poly(N-isopropylacrylamide) (pNIPAM) nano- or microgels systems have been one of the most widely studied systems due to its unique thermal sensitivity. Nano- or microgels made of pNIPAM have a lower critical solution temperature (LCST) at approximately 32°C (Wu and Zhou, 1996; Dai and Wu, 2010). The nano- or microgels swell or shrink when temperature is below or above the LCST, with their size changing by more than an order of magnitude (Dai and Wu, 2010). The incorporation of other monomers, such as acrylic acid (AA) or methacrylic acid (MAA) further equips the system with pH and ionic strength responsiveness (Gan et al., 2009; Dai et al., 2015).

pNIPAM nano- or microgels are usually prepared by precipitation polymerization (Acciaro et al., 2011; Li et al., 2012; Dai and Ngai, 2013). The NIPAM monomers, *N, N'*-methylenebis-acrylamide (MBA) crosslinkers, and free radical initiators (e.g., potassium persulfate) are all dissolved in water, and the polymerization is initiated by heating the system to 60–70°C. Besides pNIPMA, various comonomers (such as acrylic acid) can be co-polymerized into the nano- or microgels networks during the synthesis process, and the nano- or microgels size can be controlled from tens of nanometers to microns (Karg and Hellweg, 2009; Dai and Ngai, 2013).

Poly (Ethylene Glycol)

As another typical synthetic polymer, poly (ethylene glycol) (PEG) nano- or microgels are also widely studied and used. Especially, its utilization has been approved by FDA (The U.S. Food and Drug Administration) due to its biocompatibility, low protein adhesion, and non-immunogenicity (Chang et al., 2017). The end hydroxyl groups of PEG molecules can be readily modified with organic functional groups, such as carboxyl, thiol and acrylate, which greatly facilitates the nano, or microgels assembly, as well as the bioactive agents conjugation (Chang et al., 2017). PEG nano- or microgels can be fabricated by either batch or continuous fashions. For example, Tan et al. fabricated a PEG-protein nanogels by mixing PEG (modified with benzaldehyde end groups) and protein molecules (lysine residues) in a batch manner (Tan et al., 2012). In another work, Guerzoni et al. used a microfluidic device to generate PEG microgel capsules in a continuous way (Guerzoni et al., 2017). The resultant PEG microgels had a hollow core facilitating the bioactive molecules loading, while the shells were assembled by photo-crosslinking six-armed acrylated star-shaped PEG.

NANO- OR MICROGELS FABRICATION

Various synthesis routes are available to generate nano- or microgels (**Figure 1**; Liu and Garcia, 2016). Emulsion or precipitation polymerization techniques involving polymerization in bulk solution are the most frequently used methods, especially for synthetic polymers (Saunders and Vincent, 1999; Pich and Richtering, 2010). Lithographic technique utilizes a master template or mask to control the size and morphology of nano- or microgels (Helgeson et al., 2011). Microfluidic polymerization by a microfluidic device is a continuous synthesis route, which offers precise control over nano- or microgels size, morphology, and polydispersity (Wheeldon et al., 2010; Eydelnant et al., 2014). Electrospray technique can also be utilized to fabricate microgels, and the technique is convenient to encapsulate the living cells (Tapia-Hernandez et al., 2015).

Emulsion Polymerization and Precipitation Polymerization

Emulsion polymerization generally involves an aqueous phase containing surfactants, an oil phase containing monomers and crosslinkers, and initiators to start the radical polymerization process (**Figure 1A**; Tobita et al., 2000). The system is then homogenized to generate droplets of monomer in oil phase, surrounded by the water phase. The surfactants stabilize the droplets and prevent them from aggregation. By initiating the reaction (e.g., heating the system for a thermal initiator), the initiators react to form free radicals that start the polymerization process. In a variant of this technique (inverse emulsion polymerization), the aqueous phase contains the monomers and crosslinkers while the initiators can be in either of two phases. The particle size can be tuned by adjusting parameters such as the homogenization speed and the reaction temperature (Tobita et al., 2000). Biologics, such as functional proteins or drugs can be loaded by incubation with collected nano- or microgels after synthesis (Liu and Garcia, 2016). The system
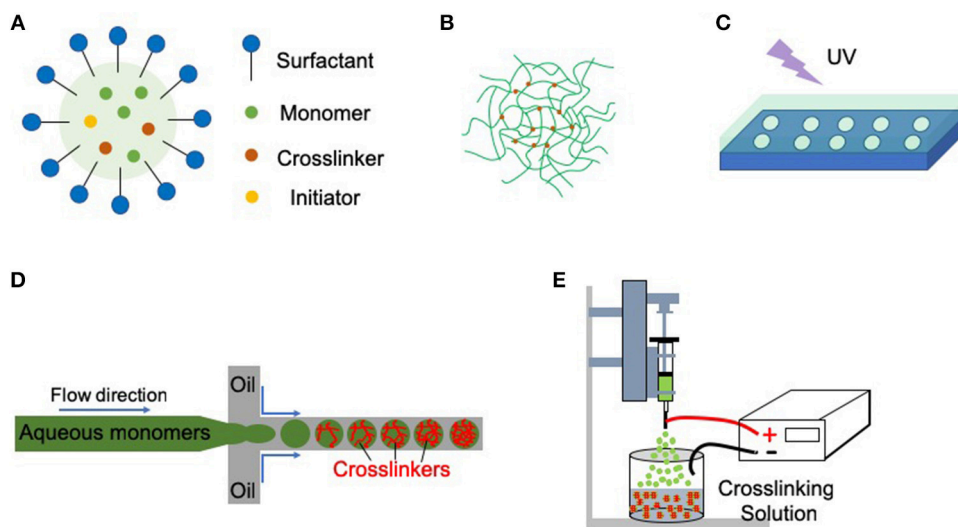
FIGURE 1 | Nano- or microgels can be fabricated by multiple methods. **(A)** Emulsion polymerization (oil-in-water). Droplets of monomers (the oil) are emulsified (with surfactants) in a continuous phase of water. The initiators (often thermally-activated) start the radical polymerization process and form the nano- or microgels. **(B)** Precipitation polymerization. Precipitation polymerization begins initially as a homogeneous system in a continuous phase, where the monomers and initiators are completely soluble. Upon initiation, polymer networks precipitate, and growth of microgel particles proceeds with the absorption of monomers and initiators. No surfactants or stabilizing agents are needed for precipitation polymerization. **(C)** Imprint lithography. Hydrogel precursors are filled into a template that acts as a mold. UV light is then used to photo-polymerize the precursors inside the mold. **(D)** Microfluidic polymerization. Multiple phases (e.g., monomers in the aqueous phase, crosslinkers in the oil phase) meet in a junction geometry (e.g., T-junction) where droplets form. Crosslinking occurs after the formation of these droplets. **(E)** Electrospray. The polymer solution is pushed through a syringe pump. An electrostatic potential is applied between the nozzle or syringe needle and the crosslinking solution. The formed nano- or microdroplets further crosslink in the crosslinking solution.

for emulsion polymerization may also be adjusted to remove the heating step, or the surfactants, to facilitate the biologics loading.

Resembling emulsion polymerization, precipitation polymerization also proceeds in a batch process. However, precipitation polymerization starts in a continuous phase, where the monomers and initiators are completely soluble, and no stabilizing agents are needed (**Figure 1B**). After initiating the reaction (e.g., increasing the system temperature), a spontaneous nucleation process occurs and polymerization proceeds.

Lithographic Processes

Lithographic technique fabricates nano- or microgels by templating hydrogels at nano- or micro-scale level. This method needs a template to control both the size and morphology of the product (Helgeson et al., 2011). For example, imprint lithography utilizes a template that acts as a mold for the hydrogel precursors, and UV light is then applied to polymerize the precursors inside the mold (**Figure 1C**). Nano- or microgels are recovered from the mold, typically by mechanical delamination post-synthesis. Biologics are often loaded by incubation with collected nano- or microgels after polymerization to avoid the UV light exposure. Alternatively, biologics can also be mixed with the hydrogel precursors if the crosslinking condition is mild. Lithographic technique provides a precise control over particle size, morphology, and monodispersity by tuning the template characteristics.

Microfluidic Polymerization

Microfluidic synthesis technique requires a lithographically fabricated microfluidic device (typically manufactured by polydimethylsiloxane), and generates nano-, or microgels droplets one at a time in a continuous manner. Taking emulsion-based microfluidic system as an example, multiple phases (monomers in aqueous, crosslinkers in oil, etc.) meet in a junction geometry and droplets form. Crosslinking will occur right after the formation of these droplets (**Figure 1D**). The biologics are often loaded by mixing with the monomers in the aqueous phase. Characteristics of nano- or microgels, including size, morphology, and size distribution can be precisely controlled by several parameters, such as the nozzle diameter and flow rate (Headen et al., 2014).

Electrospray Fabrication

In the electrospray, the liquid flows from a capillary nozzle through an electric field that disrupts a large droplet into nano- or microdroplets. The nano- or microdroplets are then collected and homogenized in the crosslinking solution (**Figure 1E**). When an electric field is applied to a droplet, the electric charge generates an electrostatic force into the droplet. Nano- or microdroplets will form when the electrostatic force overcomes the cohesive force of the droplet. The particle size and the size distribution can be tuned by adjusting parameters, such as the flow rate of the solution and the applied electric potential (Tapia-Hernandez et al., 2015). Electrospray has been developed into a mature technology with encapsulation systems (e.g.,

alginate/Ca^{2+}), and is particularly convenient to encapsulate medicines, foods, and microorganisms.

DYNAMICS INSIDE BIO-HYBRID SYSTEMS

Nano- or microgels systems have been widely used in diverse fields. When integrated with drugs, proteins and living cells, these bio-hybrid systems are endowed with various desired functions. Especially, researchers have created multiple modes of functions related dynamics inside these bio-hybrid systems, either from the side of materials or cells.

Controlled Release Systems—Response From Materials

Besides the general requirements for a drug delivery system, such as optimum loading capacity and biocompatibility, effective delivery of drugs at correct time and location is always considered a big challenge. It requires the system to sense the signals (environmental sensitivity) and actively respond to them (controlled release). Nano- or microgels are potential candidates since the materials can be engineered to sense the environmental cues, while the release of the drugs can be triggered by the volume change of materials (**Figure 2A**), or the pH induced hydrolysis (Liu et al., 2014; Yu et al., 2016).

Responsive nano or micro-drug delivery systems have been extensively studied in cancer therapy. Due to the weak acidic micro-environment of tumors, pH-responsive nano, or microgels carriers with acid-cleavable bond are usually designed to ensure the controlled drug release. Xiong et al. reported a drug carrier, poly(N-isopropylacrylamide-co-acrylic acid) nanogel with dual temperature and pH sensitivity (Xiong et al., 2011). The system precipitated on the heated cancer tissues (~42°C, local hyperthermia) due to the hydrophilic to hydrophobic transition when temperature was higher than its LCST. The anti-cancer drug doxorubicin (DOX) was covalent linked to the nanogel via an acid-cleavable bond, which could be released efficiently in the acidic microenvironment of tumor tissues. The system utilized both the temperature and pH sensitivity of the materials, as well as acid-cleavable design to ensure the controlled release missions.

In another work, Song et al. developed a responsive nanogel system to deliver both a chemotherapeutic drug (paclitaxel) and a cytokine (interleukin-2) to combat tumors (Song et al., 2017). They first modified the chitosan into two oppositely charged chitosan derivatives. The nanogels were then assembled by mixing these two chitosan derivatives, and further photo-crosslinked with addition of hydroxypropyl-β-cyclodextrin acrylate. The pH responsiveness of nanogel to a weak acidic tumor microenvironment could be fine-tuned by adjusting the formulation, while incorporation of hydroxypropyl-β-cyclodextrin acrylate increased the encapsulation efficiency of paclitaxel (very low solubility in aqueous phase). This responsive bio-hybrid nanogel system integrated chemotherapy and immunotherapy, and significantly enhanced the antitumor activity with improved calreticulin exposure and antitumor immunity.

These responsive nano- or microscale biohybrid system are also widely used in controlled diabetic therapeutic delivery. For example, Sung et al. developed a pH-responsive system consisting of chitosan and poly(γ-glutamic acid) for oral insulin delivery (Sung et al., 2012). Poly(γ-glutamic acid) was incorporated since it could conjugate with insulin via Zn^{2+} to enhance the loading efficiency. The acidic environment of gastric medium in the stomach stabilized the system due to the ionization of chitosan backbones. At intestine (pH ~ 7.0–8.0), the chitosan chains were deprotonated and collapsed. The swollen to shrunk transition of the encapsulating materials enabled the insulin release.
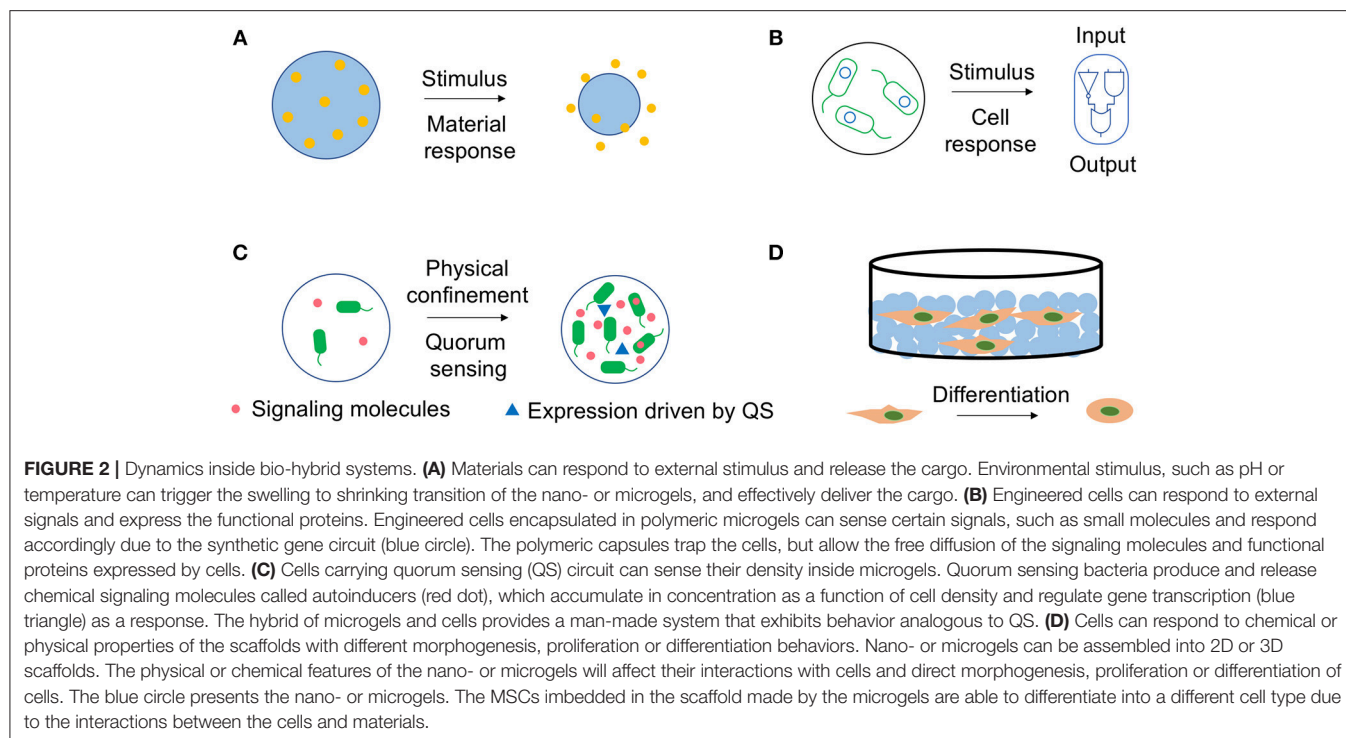
The stimulus-responsive features of nano- or microgels can be further coupled with other biologics, such as an enzyme, to achieve a more sophisticated signal-sensing capability. Gu et al. reported an injectable microgels for controlled glucose-responsive release of insulin by integrating a pH-responsive chitosan matrix, enzyme nanocapsules and insulins (Gu et al., 2013). The enzyme converted the glucose into the gluconic acid at the hyperglycemic condition, and therefore swelled the chitosan matrix due to the protonation of the chitosan networks. Consequently, these microgels were self-regulating and able to release insulins at the basal or higher rate based on normal or hyperglycemic conditions.

Controlled Release Systems—Response From Cells

Not only materials, engineered cells can also respond to the external signals accordingly (**Figure 2B**). Indeed, cell-based therapies are considered as one of the most promising next generation medicines. Various synthetic gene circuits have been assembled to treat diverse diseases, including metabolic disorders, cancer and immune diseases (Bulter et al., 2004; Higashikuni et al., 2017; Xue et al., 2017).

Wang et al. reported a pain management strategy based on microencapsulated cell-engineering principles (Wang et al., 2018). The engineered cells can respond to volatile spearmint aroma and produce an analgesic peptide (huwentoxin-IV) that selectively inhibits the pain-triggering voltage-gated sodium channel. Engineered cells were encapsulated in alginate capsules (400 μm). Their results showed that mice (chronic inflammatory and neuropathic pain model) implanted with the capsules demonstrated reduced pain-associated behaviors on oral or inhalation-based intake of spearmint essential oil, with negligible cardiovascular, immunogenic, and behavioral side effects.

In another example, Shao et al. demonstrated a smartphone-assisted treatment of diabetes in mice by microgel encapsulated cells (Shao et al., 2017). In their design, the implanted capsules carried both optogenetically engineered cells and wirelessly powered far-red light (FRL) LEDs (light-emitting diodes). The far-red light LEDs were remotely controlled by smartphone programs or bluetooth-active glucometer in a glucose-dependent manner. Optogenetically engineered cells could respond to FRL based on the bacterial light-activated cyclic diguanylate monophosphate (c-di-GMP) synthase, and activate the expression of mouse insulin. The mouse insulin would then diffuse out from the capsules to control the glucose level in blood.

FIGURE 2 | Dynamics inside bio-hybrid systems. **(A)** Materials can respond to external stimulus and release the cargo. Environmental stimulus, such as pH or temperature can trigger the swelling to shrinking transition of the nano- or microgels, and effectively deliver the cargo. **(B)** Engineered cells can respond to external signals and express the functional proteins. Engineered cells encapsulated in polymeric microgels can sense certain signals, such as small molecules and respond accordingly due to the synthetic gene circuit (blue circle). The polymeric capsules trap the cells, but allow the free diffusion of the signaling molecules and functional proteins expressed by cells. **(C)** Cells carrying quorum sensing (QS) circuit can sense their density inside microgels. Quorum sensing bacteria produce and release chemical signaling molecules called autoinducers (red dot), which accumulate in concentration as a function of cell density and regulate gene transcription (blue triangle) as a response. The hybrid of microgels and cells provides a man-made system that exhibits behavior analogous to QS. **(D)** Cells can respond to chemical or physical properties of the scaffolds with different morphogenesis, proliferation or differentiation behaviors. Nano- or microgels can be assembled into 2D or 3D scaffolds. The physical or chemical features of the nano- or microgels will affect their interactions with cells and direct morphogenesis, proliferation or differentiation of cells. The blue circle presents the nano- or microgels. The MSCs imbedded in the scaffold made by the microgels are able to differentiate into a different cell type due to the interactions between the cells and materials.

Physical Confinement—Response From Engineered Bacterium by Quorum Sensing

Quorum sensing (QS) refers to the ability of organisms to detect and respond to the population density with a specific behavior (**Figure 2C**; Scott et al., 2017; Shuma and Balazs, 2017). QS plays an essential role in the life cycle of bacteria, yeast, as well as social insects. Designing a man-made system mimicking QS behavior, that is sensing and responding to the system size and density is important but challenging (Ford and Silver, 2015; Li et al., 2017; Shuma and Balazs, 2017). In this notion, polymeric microgels can be integrated with QS cells, since the microgels provide a natural spatial segregation in differentiating the interior and exterior environments. Therefore, the cell populations in individual microgel are effectively insulated from the surrounding environment and other microgels. The porous structure traps the cells, but allows the free diffusion of nutrients and signaling molecules.

In this notion, Huang and Lee demonstrated an engineering safeguard to prevent unintended proliferation by coupling collective survival and environment sensing of bacteria (Lopatkin et al., 2016). Programmed by an engineered circuit, the cells can produce beta-lactamase (BlaM), which is able to degrade beta-lactam antibiotics, such as carbenicillin (Cb) only at a sufficiently high density regulated by QS. At the same time, sufficient cells were required to produce and secrete enough BlaM for population survival. Consequently, the cells inside the microgel can sense the physical confinement, produce BlaM and get rescued due to their high densities. Those escaping from microgel, instead, will be eliminated.

Interactions With Cells as Scaffold—Response From Cells

Nano- or microgels have been used as building blocks for scaffolds due to its several advantages including ease of fabrication and rapid response to stimulus (Gan et al., 2009; Dhandayuthapani et al., 2011). Cell adhesion on two-dimensional surface or three-dimensional scaffold has been a focus of biophysical research (Dai and Ngai, 2013). Multiple physical or chemical features of the nano- or microgels can dictate their interactions with cells, including the composition, physical properties (porosity, stiffness, etc.) and topography (Leach and Whitehead, 2018). These interactions will direct cells morphogenesis, proliferation, or even differentiation.

Mesenchymal stem cells (MSCs) have been a focus in cell-based therapies for tissue repair and regeneration because of their multilineage differentiation potentials (Augello et al., 2010; Boeuf and Richter, 2010). Growth factors and other chemical inductive cues can effectively induce MSCs differentiation. However, this approach suffers from its own restrictions including the potential off-target effects when treated in large dosages, and long-term maintenance of phenotype after the removal of these cues (Leach and Whitehead, 2018). It has been proven that extracellular matrix (ECM) can direct the MSCs fate through the physical interactions (Engler et al., 2006). Multiple studies have used nano- or microgels as building blocks to assemble the extracellular matrix (ECM) and investigate their effects on the MSCs differentiation (**Figure 2D**).

From composition perspective, Dai et al. demonstrated that the interactions between MSCs and pNIPAM-AA (poly-N-isopropylacrylamide-acrylic acid) microgels can have a direct

effect on osteogenesis of MSCs. Due to the existence of carboxyl groups in the microgels, supplementing microgels could either absorb the free calcium ions and prevent the osteogenesis (supplementing during early osteogenesis), or bind the calcium deposited cells (supplementing during the late osteogenesis) to further promote the osteogenesis through its interactions with cells.

In another work, Caldwell et al. assembled the PEG (polyethylene glycol) microgels into a microporous, covalently linked material, and seeded the human mesenchymal stem cells (hMSCs) into the porous scaffold (Caldwell et al., 2017). To assemble the scaffold, two PEG microgels functionalized with DBCO (dibenzocylcooctyne) or azide groups were separately prepared, and then mixed for crosslinking. Especially, they used two conditions (low shear and high shear) to generate microgels with different sizes. Microgels formed using low shear (votex) had a mean particle diameter of $120 \mu m$ (PEG microgels with DBCO) and $130 \mu m$ (PEG microgels with azide). Microgels formed using high shear (sonication) were an order of magnitude smaller, with average particle sizes of $16 \mu m$ (PEG microgels with DBCO), and $15 \mu m$ (PEG microgels with azide). While cells showed high survival rate in both cases, their morphology differed significantly in two scaffolds made by small or large microgels. The cells seeded in the networks made of small microgels had only small protrusions into the matrix, with only diffuse actin fibers present. Comparatively, in the networks made by the big microgels, hMSCs spread and exhibited visible actin fibers.

CONCLUSIONS

Nano- or microgels with tunable properties and sensitivities to external stimulus, have served not only as ideal model systems to explore fundamental questions in physical science, but also as suitable matrixes for diverse applications. With the fast growth in the area of synthetic biology, the integration of engineered microorganisms and polymeric carriers open another door to address both the fundamental problems in population dynamics and evolution, and the real challenges in biotechnology and medicines. This brief review covers several commonly used natural and synthetic nano- or microgels systems, and some of their applications when integrated with diverse biologics spanning from protein drugs, microbiome to mammalian cells. Especially, the dynamics inside the integrated systems to realize the desired function, either from the side of materials or the living organisms, are highlighted.

It is noteworthy that for each nano- or microgels system we are discussing here, it still bears some intrinsic limitations. For example, the typical method for alginate polymerization is introducing divalent cations, such as Ca^{2+} or Ba^{2+}, normally at a relatively high concentration comparing to the intracellular conditions. That means, the introduced ions may shift the physiological status of living organisms, complicating the biological processes. For many synthetic polymer system (e.g., pNIPAM), polymerization and crosslinking are mostly initiated by the radical ions. However, either chemical or light-induced method is detrimental to living organisms due to the strong oxidizing ability. Therefore, it is difficult to encapsulate the living cells inside these systems.

Although we have discussed various modes of dynamics inside the bio-hybrid systems, it is noted that all these dynamics remain in one-direction, from the side of either materials, or cells. We hardly find two-directional communications between the materials and biologics in a published bio-hybrid system, which may possess enormous potentials in both fundamental studies and real applications. For example, the cells can respond to physical confinement from the materials, while the materials can probe the dynamics of the cells. In this notion, we are expecting to design and discover bio-hybrid nano- or microgels systems with more delicate and sophisticated functional dynamics in the future.

AUTHOR CONTRIBUTIONS

ZD conceived and wrote the manuscript. SH wrote the manuscript. All authors listed have made a substantial, direct and intellectual contribution to the work, and approved it for publication.

ACKNOWLEDGMENTS

REFERENCES

Acciaro, R., Gilanyi, T., and Varga, I. (2011). Preparation of Monodisperse Poly(N-isopropylacrylamide). Microgel particles with homogenous cross-link density distribution. *Langmuir* 27, 7917–7925. doi: 10.1021/la2010387

Anitha, A., Sowmya, S., P.,Kumar, T. S., Deepthi, S., Chennazhi, K. P., et al. and Jayakumar, R. (2014). Chitin and chitosan in selected biomedical applications. *Prog. Polym. Sci.* 39, 1644–1667. doi: 10.1016/j.progpolymsci.2014.02.008

Augello, A., Kurth, T., and De Bari, C. (2010). Mesenchymal stem cells: a perspective from *in vitro* cultures to *in vivo* migration and niches. *Eur. Cells Mater.* 20, 121–133. doi: 10.22203/eCM.v020a11

Augst, A. D., Kong, H. J., and Mooney, D. J. (2006). Alginate hydrogels as biomaterials. *Macromol. Biosci.* 6, 623–633. doi: 10.1002/mabi.200600069

Auslander, S., Wieland, M., and Fussenegger, M. (2012). Smart medication through combination of synthetic biology and cell microencapsulation. *Metab. Eng.* 14, 252–260. doi: 10.1016/j.ymben.2011.06.003

Bacchus, W., Aubel, D., and Fussenegger, M. (2013). Biomedically relevant circuit-design strategies in mammalian synthetic biology. *Mol. Syst. Biol.* 9:691. doi: 10.1038/msb.2013.48

Berger, J., Reist, M., Mayer, J. M., Felt, O., Peppas, N. A., and Gurny, R. (2004). Structure and interactions in covalently and ionically crosslinked chitosan hydrogels for biomedical applications. *Eur. J. Pharmaceut. Biopharmaceut.* 57, 19–34. doi: 10.1016/S0939-6411(03)00161-9

Boeuf, S., and Richter, W. (2010). Chondrogenesis of mesenchymal stem cells: role of tissue source and inducing factors. *Stem Cell Res. Therapy* 1:31. doi: 10.1186/scrt31

Bulter, T., Lee, S. G., Wong, W. W., Fung, E., Connor, M. R., and Liao, J. C. (2004). Design of artificial cell-cell communication using gene and metabolic networks. *Proc. Natl. Acad. Sci. U.S.A.* 101, 2299–2304. doi: 10.1073/pnas.0306484101

Caldwell, A. S., Campbell, G. T., K.,Shekiro, M. T., and Anseth, K. S. (2017). Clickable microgel scaffolds as platforms for 3D cell encapsulation. *Adv. Healthc. Mater.* 6:1700254. doi: 10.1002/adhm.201700254

Cao, Y. X. L., Feng, Y. Y., Ryser, M. D., Zhu, K., Herschlag, G., Cao, C.Y., et al. (2017). Programmable assembly of pressure sensors using pattern-forming bacteria. *Nat. Biotechnol.* 35, 1087–193. doi: 10.1038/nbt.3978

Chang, B., Ahuja, N., Ma, C., and Liu, X. H. (2017). Injectable scaffolds: Preparation and application in dental and craniofacial regeneration. *Mat. Sci. Eng. R* 111, 1–26. doi: 10.1016/j.mser.2016.11.001

Chang, T. M. (2005). Therapeutic applications of polymeric artificial cells. *Nat. Rev. Drug Discov.* 4, 221–235. doi: 10.1038/nrd1659

Dai, Z., and Ngai, T. (2013). Microgel particles: the structure-property relationships and their biomedical applications. *J. Polymer Sci. Chem.* 51, 2995–3003. doi: 10.1002/pola.26698

Dai, Z., Shu, Y., Wan, C., and Wu, C. (2015). Effects of pH and thermally sensitive hybrid gels on osteogenic differentiation of mesenchymal stem cells. *J. Biomater. Appl.* 29, 1272–1283. doi: 10.1177/0885328214557904

Dai, Z., and Wu, C. (2010). Internal motions of linear chains and spherical microgels in theta and poor solvents. *Macromolecules* 43, 10064–10070. doi: 10.1021/ma1017814

Das, A., Barker, D. A., Wang, T., Lau, C. M., Lin, Y., and Botchwey, E. A. (2014). Delivery of bioactive lipids from composite microgel-microsphere injectable scaffolds enhances stem cell recruitment and skeletal repair. *Plos ONE* 9:e0101276. doi: 10.1371/journal.pone.0101276

Das, M., Mardyani, S., Chan, W., and Kumacheva, E. (2006). Biofunctionalized pH-responsive microgels for cancer cell targeting: rational design. *Adv. Mater.* 18, 80–83. doi: 10.1002/adma.200501043

de Lorenzo, V. (2008). Systems biology approaches to bioremediation. *Curr. Opin. Biotechnol.* 19, 579–589. doi: 10.1016/j.copbio.2008.10.004

Dhandayuthapani, B., Yoshida, Y., Maekawa, T., and Kumar, D. S. (2011). Polymeric scaffolds in tissue engineering application: a review. *Int. J. Polym. Sci.* 2011: 290602. doi: 10.1155/2011/290602

Din, M. O., Danino, T., Prindle, A., Skalak, M., Selimkhanov, J., Allen, K., et al. (2016). Synchronized cycles of bacterial lysis for *in vivo* delivery. *Nature* 536, 81–85. doi: 10.1038/nature18930

Engler, A., Sen, S., Sweeney, H., and Discher, D. (2006). Matrix elasticity directs stem cell lineage specification. *Cell* 126, 677–689. doi: 10.1016/j.cell.2006.06.044

Eydelnant, I. A., Betty Li, B., and Wheeler, A. R. (2014). Microgels on-demand. *Nat. Commun.* 5:3355. doi: 10.1038/ncomms4355

Ford, T. J., and Silver, P. A. (2015). Synthetic biology expands chemical control of microorganisms. *Curr. Opin. Chem. Biol.* 28, 20–28. doi: 10.1016/j.cbpa.2015.05.012

Gan, Q., Wang, T., Cochrane, C., and McCarron, P. (2005). Modulation of surface charge, particle size and morphological properties of chitosan-TPP nanoparticles intended for gene delivery. *Colloids Surf. B Biointerf.* 44, 65–73. doi: 10.1016/j.colsurfb.2005.06.001

Gan, T., Zhang, Y., and Guan, Y. (2009). *In Situ* Gelation of P(NIPAM-HEMA). Microgel dispersion and its applications as injectable 3D cell scaffold. *Biomacromolecules* 10, 1410–1415. doi: 10.1021/bm900022m

Gorelikov, I., Field, L., and Kumacheva, E. (2004). Hybrid microgels photoresponsive in the near-infrared spectral range. *J. Am. Chem. Soc.* 126, 15938–15939. doi: 10.1021/ja0448869

Gu, Z., Dang, T., Ma, M., Tang, B., Cheng, H., Jiang, S., et al. (2013). Glucose-responsive microgels integrated with enzyme nanocapsules for closed-loop insulin delivery. *ACS Nano* 7, 6758–6766. doi: 10.1021/nn401617u

Guerzoni, L. P. B., Bohl, J., Jans, A., Rose, J. C., Koehler, J., Kuehne, A. J. C., et al. (2017). Microfluidic fabrication of polyethylene glycol microgel capsules with tailored properties for the delivery of biomolecules. *Biomater. Sci.* 5, 1549–1557. doi: 10.1039/C7BM00322F

Headen, D. M., Aubry, G., Lu, H., and Garcia, A. J. (2014). Microfluidic-based generation of size-controlled, biofunctionalized synthetic polymer microgels for cell encapsulation. *Adv. Mater. Weinheim.* 26, 3003–3008. doi: 10.1002/adma.201304880

Helgeson, M. E., Chapin, S. C., and Doyle, P. S. (2011). Hydrogel microparticles from lithographic processes: novel materials for fundamental and applied colloid science. *Curr. Opin. Colloid Interface Sci.* 16, 106–117. doi: 10.1016/j.cocis.2011.01.005

Higashikuni, Y., Chen, W. C., and Lu, T. K. (2017). Advancing therapeutic applications of synthetic gene circuits. *Curr. Opin. Biotechnol.* 47, 133–141. doi: 10.1016/j.copbio.2017.06.011

Kanamala, M., Wilson, W. R., Yang, M. M., Palmer, B. D., and Wu, Z. M. (2016). Mechanisms and biomaterials in pH-responsive tumour targeted drug delivery: a review. *Biomaterials* 85, 152–167. doi: 10.1016/j.biomaterials.2016.01.061

Karg, M., and Hellweg, T. (2009). New "smart" poly(NIPAM). microgels and nanoparticle microgel hybrids: properties and advances in characterisation. *Curr. Opin. Colloid Interface Sci.* 14, 438–450. doi: 10.1016/j.cocis.2009.08.002

Karig, D. (2017). Cell-free synthetic biology for environmental sensing and remediation. *Curr. Opin. Biotechnol.* 45, 69–75. doi: 10.1016/j.copbio.2017.01.010

Kim, J. K., Kim, H. J., Chung, J. Y., Lee, J. H., Young, S. B., and Kim, Y. H. (2014). Natural and synthetic biomaterials for controlled drug delivery. *Arch. Pharm. Res.* 37, 60–68. doi: 10.1007/s12272-013-0280-6

Leach, J. K., and Whitehead, J. (2018). Materials-directed differentiation of mesenchymal stem cells for tissue engineering and regeneration. *ACS Biomater. Sci. Eng.* 4, 1115–1127. doi: 10.1021/acsbiomaterials.6b00741

Lee, H., Jeong, C., Ghafoor, K., Cho, S., and Park, J. (2011). Oral delivery of insulin using chitosan capsules cross-linked with phytic acid. *Bio Med. Mater. Eng.* 21, 25–36. doi: 10.3233/BME-2011-0654

Lee, K. Y., and Mooney, D. J. (2012). Alginate: properties and biomedical applications. *Prog. Polym. Sci.* 37, 106–126. doi: 10.1016/j.progpolymsci.2011.06.003

Li, P., Muller, M., Chang, M. W., Frettloh, M., and Schonherr, H. (2017). Encapsulation of autoinducer sensing reporter bacteria in reinforced alginate-based microbeads. *ACS Appl. Mater. Interfaces* 9, 22321–22331. doi: 10.1021/acsami.7b07166

Li, Z., Kwok, M., and Ngai, T. (2012). Preparation of responsive micrometer-sized microgel particles with a highly functionalized shell. *Macromol. Rapid Commun.* 33, 419–425. doi: 10.1002/marc.201100747

Liu, A. L., and Garcia, A. J. (2016). Methods for generating hydrogel particles for protein delivery. *Ann. Biomed. Eng.* 44, 1946–1958. doi: 10.1007/s10439-016-1637-z

Liu, J., Huang, Y. R., Kumar, A., Tan, A., Jin, S. B., Mozhi, A., et al. (2014). pH-Sensitive nano-systems for drug delivery in cancer therapy. *Biotechnol. Adv.* 32, 693–710. doi: 10.1016/j.biotechadv.2013.11.009

Lopatkin, A. J., Huang, S., Smith, R. P., Srimani, J. K., Sysoeva, T. A., Bewick, S., et al. (2016). Antibiotics as a selective driver for conjugation dynamics. *Nat. Microbiol.* 1:16044. doi: 10.1038/nmicrobiol.2016.44

Lopez-Leon, T., Carvalho, E., Seijo, B., Ortega-Vinuesa, J., and Bastos-Gonzalez, D. (2005). Physicochemical characterization of chitosan nanoparticles: electrokinetic and stability behavior. *J. Colloid Interface Sci.* 283, 344–351. doi: 10.1016/j.jcis.2004.08.186

Minh, K., and Lee, D. (2010). Injectable Biodegradable Hydrogels. *Macromol. Biosci.* 10, 563–579. doi: 10.1002/mabi.200900402

Naderi, H., Matin, M., and Bahrami, A. (2011). Review paper: critical issues in tissue engineering: biomaterials, cell sources, angiogenesis, and drug delivery systems. *J. Biomater. Appl.* 26, 383–417. doi: 10.1177/0885328211408946

Oh, J., Drumright, R., Siegwart, D., and Matyjaszewski, K. (2008). The development of microgels/nanogels for drug delivery applications. *Prog. Polym. Sci.* 33, 448–477. doi: 10.1016/j.progpolymsci.2008.01.002

Pich, A., and Richtering, W. (2010). Microgels by precipitation polymerization: synthesis, characterization, and functionalization. *Chem. Design Respons. Microg.* 234, 1–37. doi: 10.1007/12_2010_70

Saunders, B., and Vincent, B. (1999). Microgel particles as model colloids: theory, properties and applications. *Adv. Colloid Interface Sci.* 80, 1–25. doi: 10.1016/S0001-8686(98)00071-2

Scott, S. R., Din, M. O., Bittihn, P., Xiong, L. Y., Tsimring, L. S., and Hasty, J. (2017). A stabilized microbial ecosystem of self-limiting bacteria using synthetic quorum-regulated. *Nat. Microbiol.* 2:17083. doi: 10.1038/nmicrobiol.2017.83

Shao, J. W., Xue, S., Yu, G. L., Yu, Y. H., Yang, X. P., Bai, Y., et al. (2017). Smartphone-controlled optogenetically engineered cells enable semiautomatic glucose homeostasis in diabetic mice. *Sci. Transl. Med.* 9:aal2298. doi: 10.1126/scitranslmed.aal2298

Shuma, H., and Balazs, A. C. (2017). Synthetic quorum sensing in model microcapsule colonies. *Proc. Natl. Acad. Sci. U.S.A.* 114, 8475–8480. doi: 10.1073/pnas.1702288114

Silva, G., Costa, F., Neves, N., Reis, R., Hasirci, N., and Hasirci, V. (2004). Microparticulate release systems based on natural origin materials. *Biomaterials* 553, 283–300. doi: 10.1007/978-0-306-48584-8_22

Skop, N. B., Calderon, F., Levison, S. W., Gandhi, C. D., and Cho, C. H. (2013). Heparin crosslinked chitosan microspheres for the delivery of neural stem cells and growth factors for central nervous system repair. *Acta Biomater.* 9, 6834–6843. doi: 10.1016/j.actbio.2013.02.043

Slomovic, S., Pardee, K., and Collins, J. J. (2015). Synthetic biology devices for *in vitro* and *in vivo* diagnostics. *Proc. Natl. Acad. Sci. U.S.A.* 112, 14429–14435. doi: 10.1073/pnas.1508521112

Smeets, N. M. B., and Hoare, T. (2013). Designing responsive microgels for drug delivery applications. *J Polymer Sci. Chem.* 51, 3027–3043. doi: 10.1002/pola.26707

Song, Q. L., Yin, Y. J., Shang, L. H., Wu, T. T., Zhang, D., Kong, M., et al. (2017). Tumor microenvironment responsive nanogel for the combinatorial antitumor effect of chemotherapy and immunotherapy. *Nano Lett.* 17, 6366–6375. doi: 10.1021/acs.nanolett.7b03186

Suh, J. K., and Matthew, H. W. (2000). Application of chitosan-based polysaccharide biomaterials in cartilage tissue engineering: a review. *Biomaterials* 21, 2589–2598. doi: 10.1016/S0142-9612(00)00126-5

Sung, H. W., Sonaje, K., Liao, Z. X., Hsu, L. W., and Chuang, E. Y. (2012). pH-responsive nanoparticles shelled with chitosan for oral delivery of insulin: from mechanism to therapeutic applications. *Acc. Chem. Res.* 45, 619–629. doi: 10.1021/ar200234q

Suo, H., Zhang, D., Yin, J., Qian, J., Wu, Z. L., and Fu, J. (2018). Interpenetrating polymer network hydrogels composed of chitosan and photocrosslinkable gelatin with enhanced mechanical properties for tissue engineering. *Mater. Sci. Eng. C Mater. Biol. Appl.* 92, 612–620. doi: 10.1016/j.msec.2018.07.016

Szekalska, M., Pucilowska, A., Szymanska, E., Ciosek, P., and Winnicka, K. (2016). Alginate: current use and future perspectives in pharmaceutical and biomedical applications. *Int. J. Polym. Sci.* 2016:7697031. doi: 10.1155/2016/7697031

Tan, H., Jin, H. Q., Mei, H. C., Zhu, L. J., Wei, W., Wang, Q., et al. (2012). PEG-urokinase nanogels with enhanced stability and controllable bioactivity. *Soft Matter* 8, 2644–2650. doi: 10.1039/c2sm07072c

Tapia-Hernandez, J. A., Torres-Chavez, P. I., Ramirez-Wong, B., Rascon-Chu, A., Plascencia-Jatomea, M., Barreras-Urbina, C. G., et al. (2015). Micro- and

nanoparticles by electrospray: advances and applications in foods. *J. Agr. Food Chem.* 63, 4699–4707. doi: 10.1021/acs.jafc.5b01403

Tay, P. K. R., Nguyen, P. Q., and Joshi, N. S. (2017). A synthetic circuit for mercury bioremediation using self-assembling functional amyloids. *ACS Synth. Biol.* 6, 1841–1850. doi: 10.1021/acssynbio.7b,00137

Tobita, H., Kumagai, M., and Aoyagi, N. (2000). Microgel formation in emulsion polymerization. *Polymer* 41, 481–487. doi: 10.1016/S0032-3861(99)00183-4

Trongsatitkul, T., and Budhlall, B. (2013). Microgels or microcapsules? Role of morphology on the release kinetics of thermoresponsive PNIPAm-co-PEGMa hydrogels. *Polymer Chem.* 4, 1502–1516. doi: 10.1039/C2PY20889J

Villarreal, F., Contreras-Llano, L., Chavez, M., Ding, Y., Fan, J., Pan, T., et al. (2018). Synthetic microbial consortia enable rapid assembly of pure translation machinery. *Nat. Chem. Biol.* 14, 29–35. doi: 10.1038/nchembio.2514

Wang, H., Xie, M. Q., G., Charpin-El Hamri, Ye, H. F., and Fussenegger, M. (2018). Treatment of chronic pain by designer cells controlled by spearmint aromatherapy. *Nat. Biomed. Eng.* 2, 114–123. doi: 10.1038/s41551-018-0192-3

Wheeldon, I., Ahari, A., and Khademhosseini, A. (2010). Microengineering hydrogels for stem cell bioengineering and tissue regeneration. *Jala* 15, 440–448. doi: 10.1016/j.jala.2010.05.003

Wu, C., and Zhou, S. (1996). First observation of the molten globule state of a single homopolymer chain. *Phys. Rev. Lett.* 3053–3055. doi: 10.1103/PhysRevLett.77.3053

Xiong, W., Wang, W., Wang, Y., Zhao, Y. B., Chen, H. B., Xu, H. B., et al. (2011). Dual temperature/pH-sensitive drug delivery of poly(N-isopropylacrylamide-co-acrylic acid). nanogels conjugated with doxorubicin for potential application in tumor hyperthermia therapy. *Colloid Surface B* 84, 447–453. doi: 10.1016/j.colsurfb.2011.01.040

Xue, S., Yin, J. L., Shao, J. W., Yu, Y. H., Yang, L. F., Wang, Y. D., et al. (2017). A synthetic-biology-inspired therapeutic strategy for targeting and treating hepatogenous diabetes. *Mol. Therapy* 25, 443–455. doi: 10.1016/j.ymthe.2016.11.008

Ye, H. F., and Fussenegger, M. (2014). Synthetic therapeutic gene circuits in mammalian cells. *FEBS Lett.* 588, 2537–2544. doi: 10.1016/j.febslet.2014.05.003

Yu, J., Zhang, Y., Bomba, H., and Gu, Z. (2016). Stimuli-responsive delivery of therapeutics for diabetes treatment. *Bioeng. Transl. Med.* 1, 323–337. doi: 10.1002/btm2.10036

Conflict of Interest Statement: The authors declare that the research was conducted in the absence of any commercial or financial relationships that could be construed as a potential conflict of interest.

Micro-Patterning of PEG-Based Hydrogels With Gold Nanoparticles Using a Reactive Micro-Contact-Printing Approach

Cigdem Yesildag, Zhaofei Ouyang, Zhenfang Zhang* and Marga C. Lensen*

Nanopatterned Biomaterials, Department of Chemistry, Technische Universität Berlin, Berlin, Germany

In this work a novel, relatively simple, and fast method for patterning of gold nanoparticles (Au NPs) on poly(ethylene glycol) (PEG)-based hydrogels is presented. In the hereby exploited reactive micro-contact printing (reactive-μ-CP) process, the surface of a micro-relief patterned PDMS-stamp is first functionalized with an amino-silane self-assembled monolayer (SAM), which is then inked with Au NPs. The stamp is subsequently brought into conformal contact with thiol-functionalized PEG-based hydrogel films. Due to the strong gold-thiol interactions the Au NPs are adequately and easily transferred onto the surfaces of these soft, multifunctional PEG hydrogels. In this way, defined μ-patterns of Au NPs on PEG hydrogels are achieved. These Au NPs patterns allow specific biomolecular interactions on PEG surfaces, and cell adhesion has been studied. Cells were found to effectively adhere only on Au NPs micro-patterns and to avoid the anti-adhesive PEG background. Besides the cell adhesion studies, these Au NPs μ-patterns can be potentially applied as biosensors in plasmon-based spectroscopic devices or in medicine, e.g., for drug delivery systems or photothermal therapies.

Keywords: PEG hydrogel, Au NPs, micropatteming, cell adhension, multifunctional

INTRODUCTION

Hydrogels are three-dimensional networks of hydrophilic polymers, which can imbibe high amounts of water relative to their own weight and are widely used in industry as care products, agriculture, biology, and medicine (Drury and Mooney, 2003; Peppas and Hoffman, 2013). Recent research fields are focused on applying specific functionality to the hydrogel (Haraguchi and Takehisa, 2002; Schexnailder and Schmidt, 2009; Gaharwar et al., 2015; Motalleh and Kehr, 2017; Ren et al., 2017a; Yesildag et al., 2018a). Notably multi-functional hydrogels are highly desired as biomaterials that simultaneously exhibit various beneficial properties (Tkachenko et al., 2003; Sukhorukov et al., 2007; Chen et al., 2013; Li et al., 2017).

Biomaterials are natural or synthetic materials that are designed to augment or replace tissues, organs, or functions of the body, in order to maintain or improve the quality of life of the individual (Boretos and Eden, 1984; Williams, 1987). Examples for biomaterials are implants (Davis, 2003; Saini et al., 2015), prosthesis (Davis, 2003), wound healing or tissue regeneration (Lee and Mooney, 2001; El-sherbiny and Yacoub, 2013), repairing or supporting materials (Seal et al., 2001; Davis, 2003), and also biochips (Ferrari et al., 2007; Vo-Dinh and Cullum, 2008; Veitinger et al., 2014)

which can be used for example as biosensors (Ferrari et al., 2007; Lee, 2008; Vo-Dinh and Cullum, 2008; Shruthi et al., 2014; Sabr, 2016). For the successful design of biomaterials and the (micro- or nano-)fabrication of biointerfaces, fundamental understanding of interactions of the biomaterials with the biological system (e.g., organic tissue or bodily fluid) is required.

Precursors for hydrogels can have natural or synthetic origins. Whereas, hydrogels from natural origin are intrinsically cytocompatible, cytotoxicity can be an issue in the case of hydrogels from synthetic precursors. On the other hand, synthetic hydrogels may exhibit better mechanical integrity (bio)chemical stability, defined pore sizes, while the physical and chemical reactivity are easier to control. Among others, especially poly(ethylene glycol) (PEG) based hydrogels are highly desired in biological applications, due to the non-toxicity, non-immunogenicity, and bio-inert characteristics (Zalipsky and Harris, 1997). In our group, particularly PEG macro-monomers with acrylate or vinyl sulfone end-groups have been studied to have the ability to be cross-linked by UV-photo-polymerization process to achieve PEG hydrogels (see **Table 1**).

The mechanical properties of PEG hydrogels can be varied, depending on the molecular weight, crosslinking density, and synthetic procedure. Besides the tunable elastic property, multiple functionalities to PEG-based hydrogels can be also applied. In addition, star shaped or branched 6- or 8-arm PEG derivatives with the appropriate end groups could be polymerized by photo-polymerization and also by using Michael type addition reactions (Zhang et al., 2014). Using the latter approach, an ability for multifunctional PEG hydrogels is achieved, where certain amounts of acrylate groups are crosslinked and the others are left non-crosslinked for different types of additional multiple functionalities. Thus, various charged or non-charged functional chemical groups can be anchored (**Figure 1**). Not only molecules but also inorganic nanoparticles provide assorted amounts of functions. Especially gold nanoparticles (Au NPs), which have unique size- and shape -dependent optical properties via surface plasmons, little toxicity, easy synthesis procedures, are desired materials not only for industry, and catalysis but also for biology and medicine (Ren et al., 2017a,b; Yesildag et al., 2017a, 2018a,b).
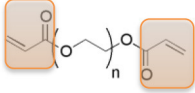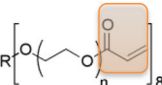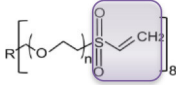
For providing cell adhesion on the bio-inert PEG surfaces, several micro-fabrication techniques have been developed to modify the surface properties and to promote cellular adhesion; for example, applying patterns of surface nano- or micro-topographies, patterns of elasticities, or chemical modifications. Micro-fabrication techniques can be basically categorized into two classes; the "top-down" and the "bottom-up" approaches. Top-down approaches made by miniaturization of bigger elements, such as photo-lithography, micro-contact printing, micro-molding in capillaries (Kim et al., 1996), fill-molding in capillaries (Kelleher et al., 2012), micro-contact deprinting (Chen et al., 2009), and also electron-beam lithography (van Dorp et al., 2000) are some examples. Examples for bottom-up approaches are self-assembled monolayers (SAM); spin-coating, dip-coating, dip-pen lithography (Piner et al., 1999),
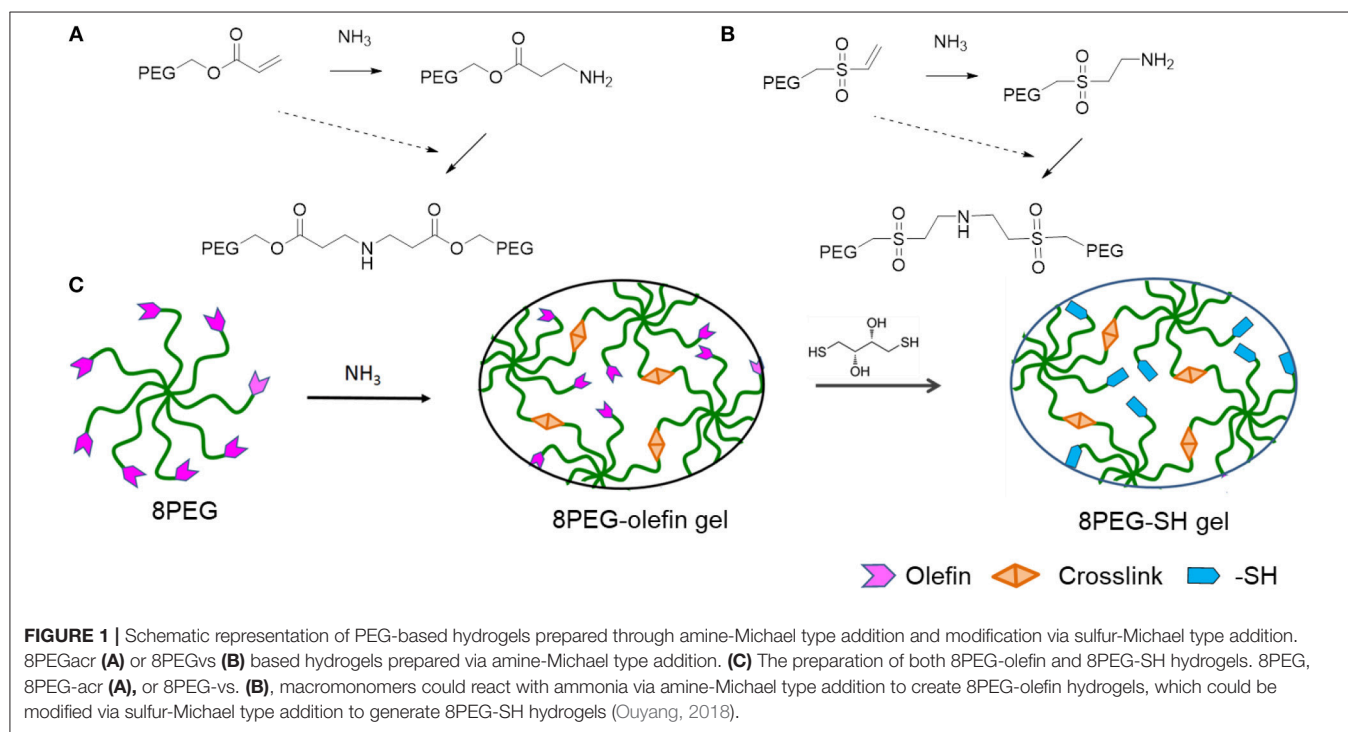
block copolymer micelle nanolithography (Glass et al., 2003) or supramolecular self-assembly (House et al., 2009). Reactive micro-contact printing (reactive-μ-CP) is a combination of top-down and bottom-up approaches and is a fast and relatively simple process for patterning of large area on a surface in a short period of time. Hereby the well-known micro-contact printing process (μ-CP) which was developed by Whitesides (Tien et al., 1998) group and the affinity contact printing (α-CP) by Delamarche et al. (Renault et al., 2002) were used as a basis. For the conventional μ-CP process usually a PDMS-stamp, an ink solution and a substrate are required; first of all the stamp is inked and after contacting of the hydrogel with the stamp the ink is transferred onto the surface of the substrate. Whitesides et al. further developed this process and introduced the reactive μ-CP process, where the substrate was made reactive toward the ink molecules, so that a covalent binding among the substrate and ink-molecules could be formed (Yan et al., 1998). In the procedure of Delamarche et al. proteins were printed on surfaces via specific functionalization of stamps with protein-anchoring groups (Renault et al., 2002).

In this work we introduce a novel reactive-μCP process where the reactivity of the surface of the stamp is additionally tuned toward the Au NPs. For this process, first of all, a PDMS-stamp was molded a micro- relief-patterned silicon master as template. As shown in our previous publications, amino-silanized surfaces can be effectively covered with citrate capped Au NPs with high density (Ren et al., 2017a,b; Yesildag et al., 2018b). Hereby the Au NPs were interacting electrostatically with the amino-silane surface and they could be effectively transferred onto PEG hydrogel surfaces by various methods, which we recently published (Ren et al., 2017a,b; Yesildag et al., 2017a,b, 2018a,b).

In this work a novel reactive micro-contact printing approach for patterning of gold nanoparticles (Au NPs) on poly(ethylene glycol) (PEG)-based hydrogels is presented. In this reactive μ-CP method the surface of the micro-relief patterned PDMS-stamp is first functionalized with a self-assembled monolayer (SAM) of amino-silane, exhibiting amino groups at the surface that have affinity for Au NPs, and subsequently decorated with citrate-capped Au NPs via relatively weak, yet collective, electrostatic interactions. The stamp is afterwards brought in conformal contact with flat, functionalized PEG- hydrogels, and the Au NPs are transferred onto the surfaces of these hydrogels. PEG-based hydrogels are on the one hand made of short linear chained PEG-precursors which result in relativelyrigid hydrogels and on the other hand of 8-arm star shaped PEG-precursors which yield softer and multi-functional hydrogels. On these micro-patterned Au NPs—PEG-hydrogel—composites, mouse fibroblast L929 cell adhesion was investigated. Our recent studies have shown effective cell adhesion on Au NPs layered surfaces even without prior bio-functionalization of the Au NPs with specific proteins; proteins included in the cell culture media were sufficient for aiding cells to guide and adhere on the Au NPs patterns. Cells adhere only on Au NPs micro-patterns and avoid the anti-fouling PEG material.

Material	PEG Diacrylate (PEG)	8-arm PEG Acrylate (8PEG)	8-arm PEG Vinyl Sulfone (8PEG-VS)
Structure			
M_W [Da]	575	15k	15k
Chain length	n ~ 72	n ~ 40	n ~ 40
State at r.t.	Liquid	Solid	Solid
Gel formation	UV	UV or Michael type addition (degradable)	UV or Michael type addition (non-degradable)

FIGURE 1 | Schematic representation of PEG-based hydrogels prepared through amine-Michael type addition and modification via sulfur-Michael type addition. 8PEGacr **(A)** or 8PEGvs **(B)** based hydrogels prepared via amine-Michael type addition. **(C)** The preparation of both 8PEG-olefin and 8PEG-SH hydrogels. 8PEG, 8PEG-acr **(A)**, or 8PEG-vs. **(B)**, macromonomers could react with ammonia via amine-Michael type addition to create 8PEG-olefin hydrogels, which could be modified via sulfur-Michael type addition to generate 8PEG-SH hydrogels (Ouyang, 2018).

MATERIALS AND METHODS

## Preparation of PEG Hydrogels

Photo-Polymerization

For the UV-photo-polymerization process acrylated PEG macromonomers were used. Linear PEG-diacrylate was purchased from Sigma Aldrich and used without further modification and the purchased 8-arm PEG macromonomer had hydroxyl-end groups and was acrylated which is briefly described in reference (Zhang, 2015). These PEG macromonomers with acrylate end-groups (PEG diacrylate (Mw = 575 g/mol) or 8-arm PEG acrylate) were crosslinked using the UV-photo-crosslinking process. For the UV-photo-crosslinking process the liquid PEG diacrylate or the at 60°C molten 8PEG acrylate was mixed with 1% of photo-initiator (Irgacure 2959). For having a good

distribution of the photo-initiator the mixture was sonicated for around 5 min. Then the mixture was dispensed on a glass slide and covered with a thin glass cover slip to achieve a flat hydrogel sample. This liquid mixture was put under UV-light source for 8 min and the glass cover slip was peeled off. The result was a thin, flat hydrogel sample, as a stand-alone films.

Crosslinking Via Michael-Type Addition Reaction

20 wt% of ammonium solution (30% NH_3 in H_2O) were added to the precursor solution of 8-arm poly(ethylene glycol) vinyl sulfone (8PEG-VS) with 50 wt% water content at room-temperature under vigorous magnetic stirring until the solution
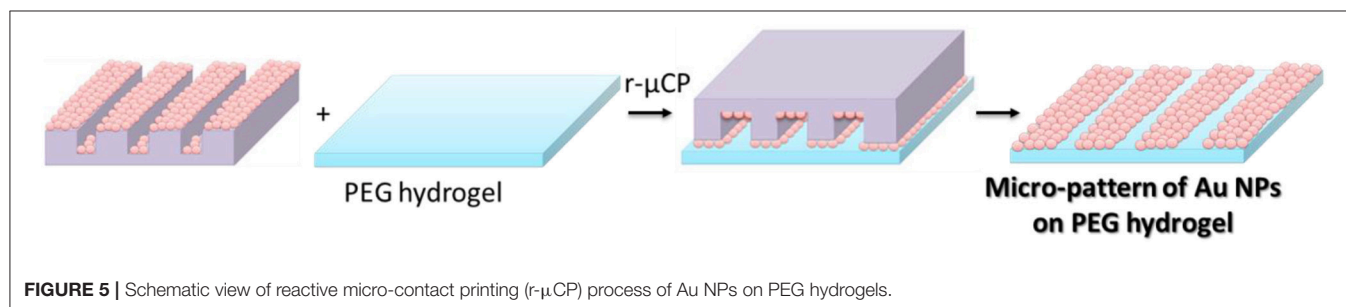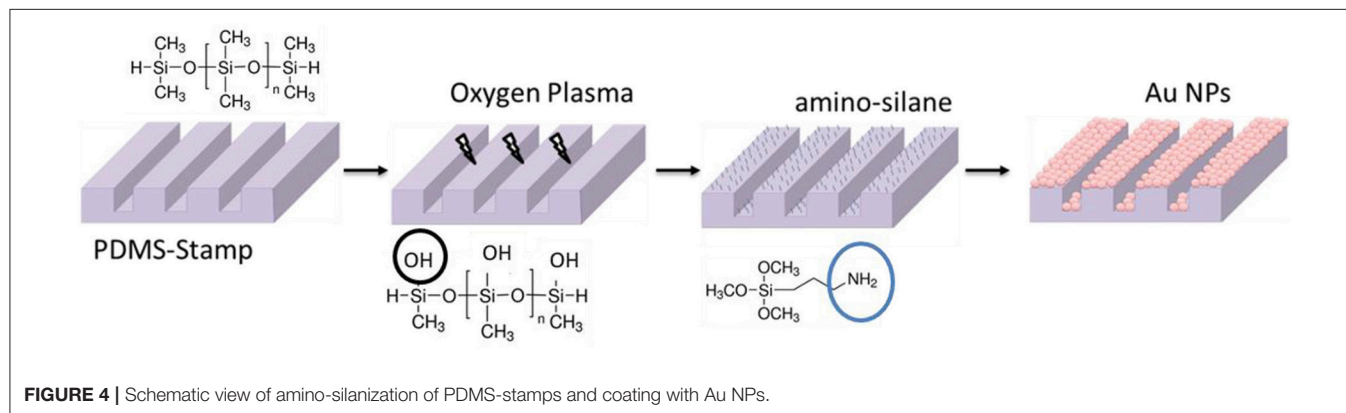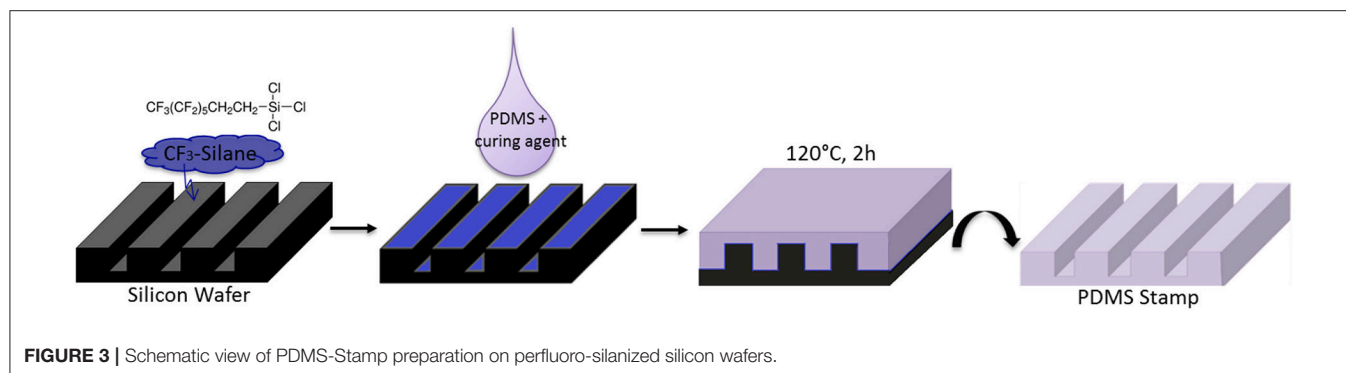
turned to a viscous liquid. The resulting liquids were deposited on a glass slide and covered with a glass cover slip. After 30 min,

FIGURE 2 | Structure of a silicon master.
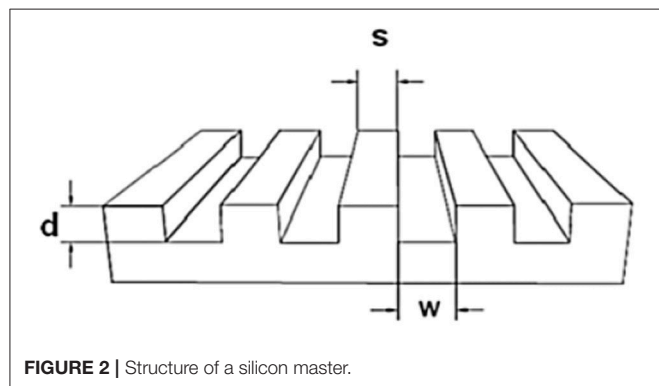
the 8PEG-VS hydrogels were formed. After gel formation, the transparent polymeric films formed with 5% NH_3 were peeled off mechanically. The stand-alone films (250–300 μm in thickness) were immersed in DTT solution (5 mg/mL) for 60 min. Afterwards, these hydrogels were washed thoroughly with water for several times and stored in water before use (Ren et al., 2017b).

Synthesis of Gold Nanoparticles (Au NPs)

The Au NPs were synthesized following the protocol of Bastús et al. (2011) First of all, Au NPs seeds were synthesized. In the next step the seeds were continuously grown to bigger particles; in this work Au NPs with 25 nm sizes are used. For the seed synthesis 150 ml aqueous solution of trisodium citrate ($Na_3C_6H_5O_7$) (2.2 mM) (Sigma Aldrich, Germany) was boiled for 15 min. Then 1 ml of $HAuCl_4$-solution (25 mM) (Sigma

FIGURE 3 | Schematic view of PDMS-Stamp preparation on perfluoro-silanized silicon wafers.

FIGURE 4 | Schematic view of amino-silanization of PDMS-stamps and coating with Au NPs.

FIGURE 5 | Schematic view of reactive micro-contact printing (r-μCP) process of Au NPs on PEG hydrogels.

Aldrich, Germany) is injected at once. The color of the solution was changed from yellow to bluish-gray and then finally to soft pink within 10 min. For growing of bigger sized particles the solution was cooled down to a temperature of 90°C. Into that solution 1 ml sodium citrate (60 mM) and 1 ml of a HAuCl$_4$-solution (25 mM) was injected. After 30 min the reaction was completed and again 1 ml of a HAuCl$_4$-solution (25 mM) was added. Thirty minutes later the solution was diluted by taking out 27.7 ml of the Au NP solution and adding 27.6 ml of water.

Preparation of Silicon Masters

For the preparation of the stamps a micro relief patterned silicon master was necessary. The sizes of the masters are described with a three-numeric code: w-s-d = width of the grooves—spacing between the grooves—depth of the grooves, as shown in **Figure 2**.

The surfaces of the silicon masters were made inert by applying trichloro(1H, 1H, 2H, 2H-perfluorooctyl)silane (Sigma Aldrich) molecules on its surface. For that the silicon masters were cleaned with water, acetone, and isopropanol and dried with a stream of nitrogen. For the activation of the surface, the cleaned silicon masters were oxidized via immersion in a piranha

FIGURE 6 | Reactive micro-contact printing (r-μCP) on Non-functional vs. SH-functional PEG.

solution (H$_2$SO$_4$: H$_2$O$_2$; 7: 3; v/v) for 30 min. Then the master was washed with deionized water and isopropanol and dried with a stream of nitrogen. After the activation of the surfaces, the silicon masters were placed in a clean petridish and then placed into a desiccator. Incidentally, in a small vial containing 1–2 drops of the silanizing agent perfluoro-silane agent was placed into the desiccator together with the silicon masters. Then, the desiccator was kept under vacuum for 2 h. After that, the silanized silicon wafers were washed with toluene and isopropanol and then dried under a flow of nitrogen.

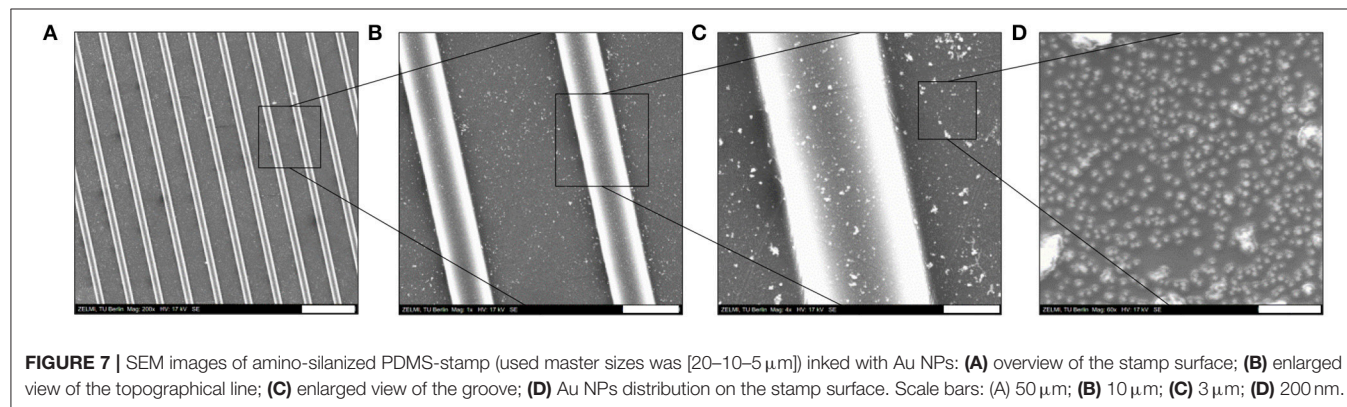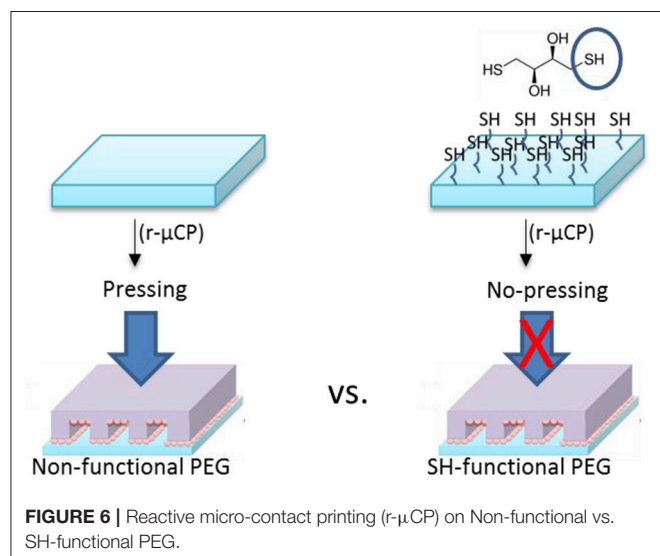## Preparation of Au NPs Decorated PDMS-Stamps

The inert silicon master was cleaned with water, acetone and isopropanol and dried with a stream of nitrogen and is used as tamplate for the PDMS-stamp.

The PDMS-stamp was prepared by using a mixture of Sylgard 184 silicone elastomer and curing agent (10:1; v/v). Then the mixture was degassed in a desiccator and casted on the inert silicon master using the micromolding process, cured for 2 h at 120°C and finally was peeled off from the silicon master (see **Figure 3**).

The as-prepared PDMS-stamps were oxidized in oxygen plasma for around 10 min. Thereafter the oxidized PDMS-stamps were silanized with aminopropyltrimethoxysilane (Sigma Aldrich) in a desiccator using the vapor method; for that the PDMS-stamps were placed in a desiccator containing two drops of amino-silane agent and vacuum was kept for 2 h. After the amino-silanization of the PDMS-stamps they were immersed in Au NPs solutions for around 1 h (see **Figure 4**). Thereafter the stamps containing the Au NPs on their surfaces were washed with water and dried under a stream of nitrogen gas.

Reactive Micro-Contact Printing on PEG Hydrogels

For the reactive micro-contact printing process, the free standing PEG hydrogels were prepared following the procedures described above. These hydrogels were then contacted with the Au NPs coated PDMS-stamps (see **Figure 5**). Depending on the reactivity of the PEG hydrogel the contact force is was varied: on the hard and rigid PEG hydrogel the stamp was firmly contacted

FIGURE 7 | SEM images of amino-silanized PDMS-stamp (used master sizes was [20–10–5 μm]) inked with Au NPs: **(A)** overview of the stamp surface; **(B)** enlarged view of the topographical line; **(C)** enlarged view of the groove; **(D)** Au NPs distribution on the stamp surface. Scale bars: (A) 50 μm; (B) 10 μm; (C) 3 μm; (D) 200 nm.

with the PEG hydrogel in order to transfer the Au NPs from the stamp onto the surface of hydrogels. For multifunctional hydrogels from 8PEG precursors with thiol surface functions the hydrogel was contacted only with a mere contact and the Au NPs were readily transferred onto the surface of the hydrogel through aided by strong and collective chemical interactions (see **Figure 6**).

Cell Adhesion

Mouse fibroblasts L929 cells were cultured in the tissue culture plate in RPMI 1,640 medium with addition of 10% Fetal Bovine Serum (FBS) and 1% Penicillin/Streptomycin (PS) in a cell culture plate in an incubator at controlled temperature (37°C) and CO_2 atmosphere (5%).

First of all a confluency of at least 75% should be reached. Thereafter the cells were washed with PBS, detached by using trypsin and after the centrifugation process a new medium is added on the cells and mixed properly. Ten microliter of this cell medium solution is put on a cell counter chamber in order to count the cell number by using an optical microscope and achieve a concentration of 40,000 cells/ml. Depending on the counted cell number the cell solution was mixed with a defined amount of new

medium. The samples were placed in a TCPS plate; two drops of Au NPs solution or the washed and precut hydrogel. The samples were then cultured within these cells for 24 h, at 37°C in a 5% CO_2 atmosphere.

Critical Point Drying

Critical point drying is an established method of dehydrating biological tissues before the scanning electron microscopic (SEM) imaging (Rostgaard and Christensen, 1975)[1]. In the course of this work murine fibroblasts, which adhered on specifically designed surfaces were inter alia measured by SEM. For that after 24 h of incubation the cells were prior fixed on the sample on the sample using 4% formaldehyde for 30 min. Then the medium is removed and replaced by PBS, which was later stepwise exchanged by ethanol or acetone (30–100% v/v) and the samples were placed in a critical point drying apparatus, where ethanol or acetone was exchanged by CO_2. The final dried samples were sputtered with carbon.

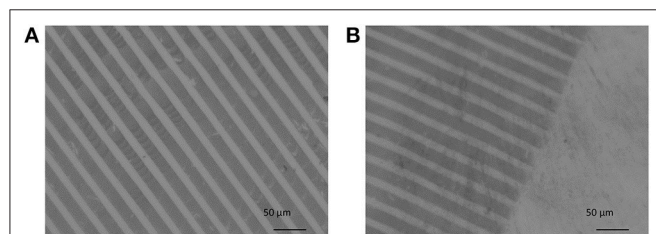[1]https://www.emsdiasum.com/microscopy/technical/datasheet/critical_drying.aspx

FIGURE 8 | (A,B) Optical micrograph of Au NPs on PEG-hydrogel fabricated by the reactive μ-CP process. Scale bars: (A,B) 50 μm.
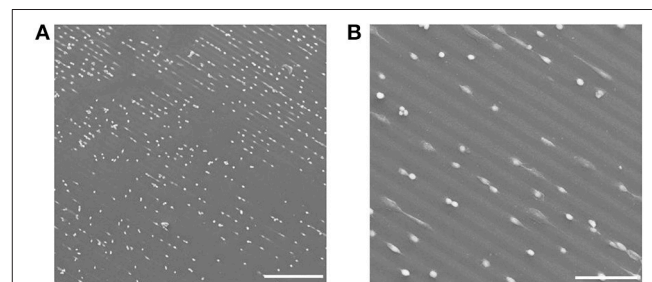

FIGURE 10 | (A,B) SEM images of cell adhesion on mico-patterned Au NPs lines on PEG-hydrogel. Scale bars: (A) 300 μm; (B) 100 μm.
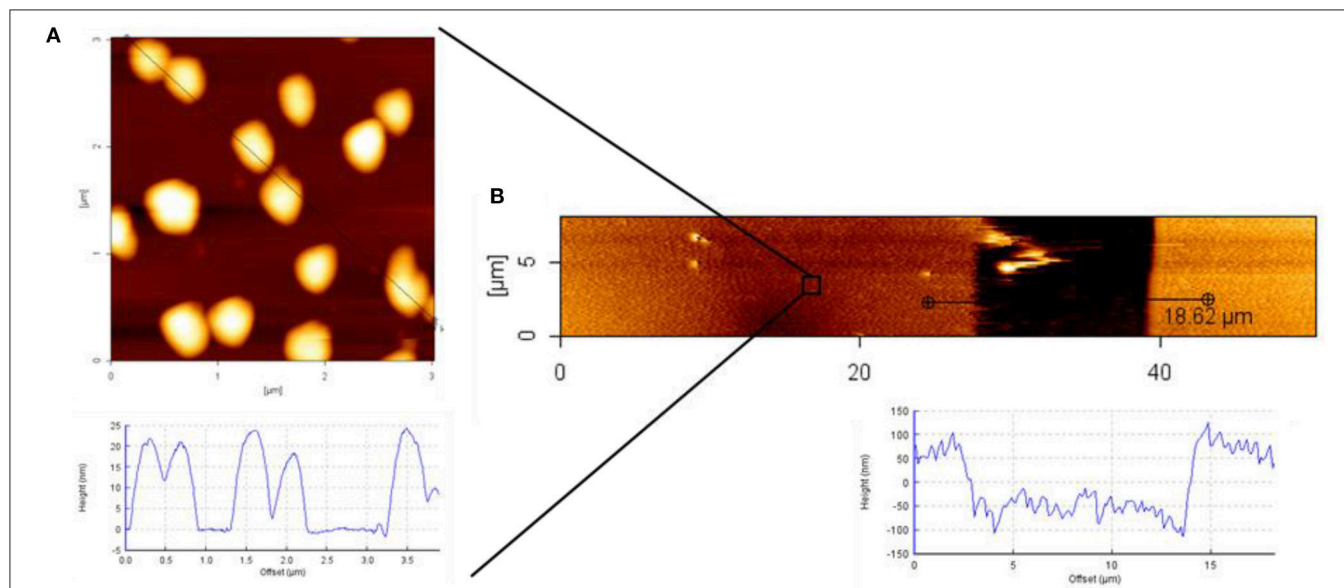

FIGURE 9 | AFM height image and cross section profile of: (A) Au NPs on silicon wafer; (B) Au NPs pattern on PEG hydrogel; used stamp size [15-50-15].

Characterization Instruments

Optical images were taken with the Axio Oberserver.Z1 (Carl Zeiss) and analyzed using the Axio Vision software (V4.8.2 Carl Zeiss). Scanning electron images were taken with a Hitachi S-520 using an acceleration voltage of 20 kV and a working distance of 10 mm. Pictures were taken using the Digital Image Processing System(2.6.20.1, Point Electronic).

RESULTS AND DISCUSSION

First of all PDMS-stamps were prepared by using a perfluorinated silicon master that had topographical sizes of [w-s-d] = width of the grooves—spacing between the grooves—depth of the grooves of a relief pattern: [20–10–5 μm] (see **Figure 3**).

Thereafter, as schematically shown in **Figure 4**, the surface of the PDMS-stamp was activated by oxidation in oxygen plasma for around 10 min and silanized with amino-silane using the vapor silanization method. Thereafter, the PDMS-stamp was inked with Au NPs solution for 1 h and washed with water and dried with a stream of nitrogen. The Au NPs-coated PDMS-stamp is shown in the SEM images in **Figures 7A–D**.

In **Figures 7B,C** it can be observed that the Au NPs were located on the topographical lines and also on the grooves and **Figure 7D** shows the distribution of the Au NPs on the stamp surface in an enlarged view; there it can be seen that the surface coverage of the Au NPs was relatively high which was also expected due to the electrostatic attractive interactions between the citrate-capped Au NPs and the amino-silane layer. Besides the well-resolved Au NPs there were also larger (around 100–500 nm) white features observables, which might be agglomerated Au NPs and/or uneven PDMS features where the electrons couldn't be conducted and caused a brighter image. The thus Au NPs-inked PDMS-stamps were contacted with PEG
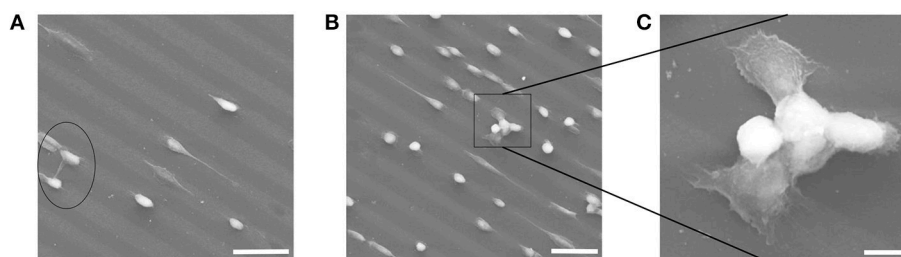

FIGURE 11 | (A–C) SEM images of cell adhesion on Au NPs micro-patterns exhibiting line-bridging cells. Scale bars: (A) 50 μm; **(B)** 50 μm; **(C)** 10 μm.
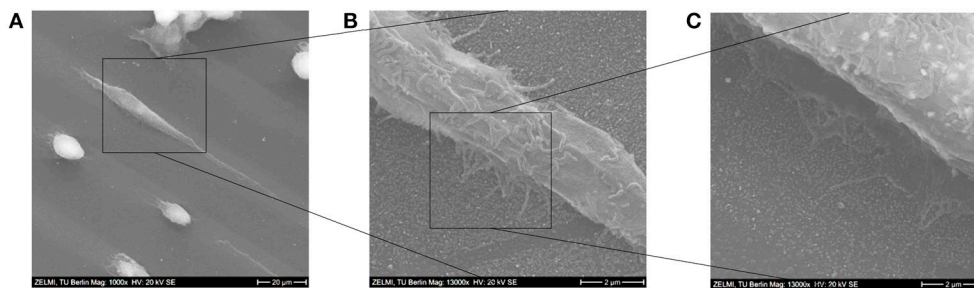

FIGURE 12 | (A–C) SEM images of a stretched cell on the Au NPs micro-pattern. Scale bars: **(A)** 20 μm; **(B)** 2 μm; **(C)** 2 μm.
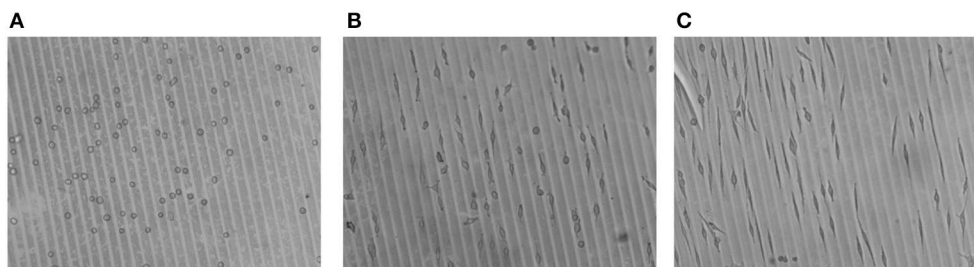

FIGURE 13 | Optical micrographs of cell adhesion on Au NPs patterned 8PEG hydrogel : **(A)** directly after seeding (0 min); **(B)** after 24 h, and **(C)** after 48h of cell culture.
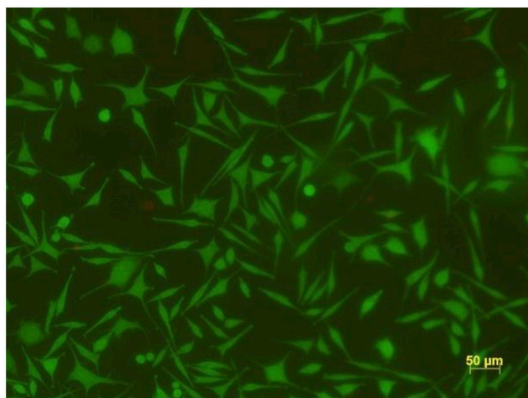
FIGURE 14 | Live/dead assay on Au NPs decorated 8PEG hydrogel surface.

hydrogel surfaces; the process was schematically depicted in **Figure 5**.

The Au NPs were then successfully transferred onto the surface of the PEG hydrogels, which can be recognized by optical microscopy, as evident from the micrographs in **Figure 8**.

Depending on the type of PEG-precursors (linear or 8PEG), and availability of reactive functional groups on PEG-based hydrogel surfaces, the transfer efficiency could be optimized, which we have shown in our previous publications (Ren et al., 2017a,b). The highest transfer yield was achieved on thiol-functionalized PEG hydrogel derivatives. The interaction of amino-silane surface among the PDMS-stamp and the Au NPs were relatively weak electrostatic interactions which can be quite easily released; also onto non-functional PEG hydrogels, Au NPs could be transferred with applying certain forces. On the other hand, the interaction of the Au NPs with the mercapto/thiol-functionalised PEG hydrogels is strong; in that case, even without applying any forces, i.e., just by slight contact, transfer of the Au NPs pattern was effective. For this process, the interactions or reactivity of all surfaces—stamp and PEG hydrogel—with the Au NPs was precisely tuned.

In **Figure 8** the darker lines represent the Au NPs micro-pattern and the brighter area the non-contacted, pure PEG hydrogel. As shown in **Figure 7**, the contact line pattern area of the stamp had widths of $20 \mu m$ and distances of $10 \mu m$. That can be also seen in **Figures 8A,B**. Taking a closer look into the micrograph in **Figure 8**, some white spots are visible. In **Figure 8B** the edge of the contact area of the stamp with the PEG hydrogel is seen. Nearly the original pattern size of the PDMS-stamp was clearly printed on PEG hydrogel without showing notable defect structures.

For an even more detailed characterization of the transferred patterns of Au NPs, atomic force microscopy (AFM) measurements were conducted. In Figure, the AFM characterization of the Au NPs pattern on 8PEG hydrogel is shown. The size of the particles can be recognized from **Figure 9A**; the sizes of the particles were around 20 nm. In **Figure 9B** the pattern is shown, hereby the stamp had sizes

of [15-50-15], thus the stamped area was $50 \mu m$ and the gap between the contacts were $15 \mu m$, which is clearly observable in the AFM image.

After having achieved a clear and documented micro-pattern of Au NPs on PEG hydrogel surfaces, cell adhesion study was investigated. Hereby murine fibroblast L929 cells were cultured on the Au NPs patterned PEG hydrogels in a cell culture medium, which contained 1% PS and 10% FBS, in a 5% CO_2 atmosphere at 37°C for 24 h.

In **Figures 10A,B** SEM images of the cell adhesion results are shown. In order to be able to image cells with SEM without losing the original structure, the cells were fixed with formaldehyde on the hydrogel for 30 min and dried via critical point drying procedure. After sputtering the hydrogels with carbon the SEM measurement was performed. In **Figures 10A,B** it can be seen that the cells were adhering on the Au NPs patterned PEG hydrogel surface; following the patterned Au NPs lines.

PEG materials are known to be inert to biomolecular interactions. That was also observable on the micro-patterned PEG Au NPs surfaces; the cells effectively avoided the pure PEG hydrogel and only adhered on Au NPs layers. The hereby chosen pattern sizes of $20 \mu m$ for the Au NPs lines and $10 \mu m$ for the distances between the Au NPs lines allowed cells bridging over the PEG lines and to have contacts with two parallel Au NPs lines. This was observable in a few cases, such as in **Figure 11**. In **Figure 11A** the bridge-over of one whole cell happened via stretching of protrusions, while in **Figures 11B,C** the bridging occurred via joining of a few cells. **Figure 11C** is an enlarged view of the joined bridging cells; on this SEM image it can be obviously seen that the cells that had contacts with the Au NPs lines were spread and show adherent protrusions, while on the bridging area over the PEG hydrogel line no protrusions were visible; that means that they didn't have any adhesive contacts with this line.

In the SEM images in **Figure 12A** the morphologies of some adhered cells are shown; while some cells were adherent, yet only stretched to around 110–150% of their original sizes, other ones were elongated, and had lengths of around 300% of their original sizes. After the cells were settled down they started forming focal adhesions with their lamellipodia and show also some finger-like protrusions, which is more clearly visible in the SEM images in **Figures 12B,C**.

In **Figure 13**, a larger area of cell culture on the micro-patterned hydrogels is shown, to give the overall impression of selective cell adhesion to the micro-lines of Au NPs and adaptation of the cell morphology, i.e., elongation.

As a subconclusion, it can be said that micro-patterning with Au NPs on PEG based hydrogels was an effective way in order to guide the cells to follow specific paths and have adhesions only on these areas while avoiding unwanted areas; hence the cell behavior could be effectively controlled.

Finally, and not less importantly, the viability of the cells on these novel nanocomposite materials was investigated. In **Figure 14** the result of the live/dead assay is shown, manifesting that at least 99% of the cells were alive.

CONCLUSIONS

In this work a novel reactive micro-contact printing approach for patterning of gold nanoparticles (Au NPs) on poly(ethylene glycol) (PEG)-based hydrogels was presented. For this patterning method, the surface of the micro-relief patterned PDMS-stamp was functionalized with an amino-silane self-assembled monolayer (SAM) and was subsequently decorated with citrate capped Au NPs via electrostatic interactions. The stamp was afterwards brought in conformal contact with flat PEG-based hydrogels and the Au NPs were transferred onto the surfaces of these functional hydrogels. Depending on the chemical functionality on PEG hydrogel surfaces the transfer could be facilitated. Stamping on non-functional PEG hydrogel surfaces required certain force in order to transfer the Au NPs onto its surface, while on specifically functionalized PEG hydrogel surface with thiol-functions only a slight contact was sufficient to transfer the Au NPs efficiently onto the surface of PEG hydrogels. On these micro-patterned Au NPs—PEG-hydrogel—composite biointerfaces, murine fibroblast L929 cell adhesion was investigated. Cells adhered only on Au NPs micro-patterns and effectively avoided the anti-adhesive PEG background. With this method, a platform to control the cell adhesion has been established. Furthermore, owing to the unique optical characteristics of the Au NPs, these nanocomposite materials are potentially useful probes for SERS or LSPR applications.

AUTHOR CONTRIBUTIONS

CY and ZZ conceived and performed the experiments and analyzed the data. ZO synthesized the macromonomers and CY wrote the paper. ML monitored and guided the process of designing the experiments, contributing the methods and infrastructure, interpreting and discussing the data, and improving the manuscript.

REFERENCES

Bastús, N. G., Comenge, J., and Puntes, V. (2011). Kinetically controlled seeded growth synthesis of citrate-stabilized gold nanoparticles of up to 200 nm: size focusing versus ostwald ripening. *Langmuir* 27, 11098–11105. doi: 10.1021/la201938u

Boretos, J. W., and Eden, M. (1984). *Contemporary Biomaterials: Material and Host Response, Clinical Applications, New Technology, and Legal Aspects.* California, CA: Noyes Publications. doi: 10.1016/S0376-7388(00)81555-0

Chen, J., Arafeh, M., Guiet, A., Felkel, D., Loebus, A., Kelleher, S. M., et al. (2013). Hybrid hierarchical patterns of gold nanoparticles and poly(ethylene glycol) microstructures. *J. Mater. Chem. C.* 1, 7709–7715. doi: 10.1039/c3tc30811a

Chen, J., Mela, P., Möller, M., and Lensen, M. C. (2009). Microcontact deprinting: a technique to pattern gold nanoparticles. *ACS Nano.* 3, 1451–1456. doi: 10.1021/nn9002924

Davis, J. R. (ed.). (2003). "Overview of biomaterials and their use in medical devices," in *Handbook of Materials for Medical Devices* (Ohio: ASM International), 1–12.

Drury, J. L., and Mooney, D. J. (2003). Hydrogels for tissue engineering: scaffold design variables and applications. *Biomaterials* 24, 4337–4351. doi: 10.1016/S0142-9612(03)00340-5

El-sherbiny, I. M., and Yacoub, M. H. (2013). Hydrogel scaffolds for tissue engineering: progress and challenges. *Glob. Cardiol. Sci. Pract.* 38, 316–342. doi: 10.5339/gcsp.2013.38

Ferrari, M., Bashir, R., and Wereley, S. (eds.). (2007). "Volume IV: biomolecular sensing, processing and analysis," in *BioMEMS and Biomedical Nanotechnology* (New York, NY: Springer), XXII, 410.

Gaharwar, A. K., Peppas, N. A., and Khademhosseini, A. (2015). Nanocomposite hydrogels for biomedical applications. *Biotechnol. Bioeng.* 111, 441–453. doi: 10.1002/bit.25160

Glass, R., Möller, M., and Spatz, J. P. (2003). Block copolymer micelle nanolithography. *Nanotechnology* 14, 1153–1160. doi: 10.1088/0957-4484/14/10/314

Haraguchi, K., and Takehisa, T. (2002). Nanocomposite hydrogels: a unique organic - inorganic network structure with extraordinary mechanical, optical, and swelling/de-swelling properties. *Adv. Mater.* 14, 1120–1124. doi: 10.1002/1521-4095(20020816)14:16<1120::AID-ADMA1120>3.0.CO;2-9

House, D., Walker, M. L., Wu, Z., Wong, J. Y., and Betke, M. (2009). "Tracking of cell populations to understand their spatio-temporal behavior in response to physical stimuli," in *2012 IEEE Computer Society Conference on Computer Vision and Pattern Recognition Workshops* (Miami, FL), 186–193.

Kelleher, S., Jongerius, A., Loebus, A., Strehmel, C., Zhang, Z., and Lensen, M. C. (2012). AFM characterization of elastically micropatterned surfaces fabricated by fill-molding in capillaries (FIMIC) and investigation of the topographical influence on cell adhesion to the patterns. *Adv. Eng. Mater.* 14, 56–66. doi: 10.1002/adem.201180087

Kim, E., Xia, Y., and Whitesides, G. M. (1996). Micromolding in capillaries: applications in materials science. *J. Am. Chem. Soc.* 118, 5722–5731. doi: 10.1021/ja960151v

Lee, K. Y., and Mooney, D. J. (2001). Hydrogels for tissue engineering. *Chem. Rev.* 101, 1869–1880. doi: 10.1021/cr000108x

Lee, T. M. (2008). Over-the-counter biosensors: past, present, and future. *Sensors* 8, 5535–5559. doi: 10.3390/s8095535

Li, Y., Han, Y., Wang, X., Peng, J., Xu, Y., and Chang, J. (2017). Multifunctional hydrogels prepared by dual ion cross-linking for chronic wound healing. *ACS Appl. Mater. Interfaces* 9, 16054–16062. doi: 10.1021/acsami.7b04801

Motealleh, A., and Kehr, N. S. (2017). Nanocomposite hydrogels, and their applications in tissue engineering. *Adv. Healthc. Mater.* 6:1600938. doi: 10.1002/adhm.201600938

Ouyang, Z. (2018). *Preparation, and Pattern of Bioactive Poly(ethylene glycol)-Based Hydrogels for Biomineralization and Protein Immobilization.* TU Berlin.

Peppas, N. A., and Hoffman, A. S. (2013). *Chapter I.2.5 - Hydrogels BT - Biomaterials Science, 3rd Edn.* Amsterdam; Boston, MA; Heidelberg; London; New York, NY; Oxford; Paris; San Diego, CA; San Francisco, CA Singapore; Sydney, NSW; Tokyo: Academic Press. 166–179. doi: 10.1016/B978-0-08-087780-8.00020-6

Piner, R. D., Zhu, J., Xu, F., Hong, S., and Mirkin, C. A. (1999). 'Dip-pen' nanolithography. *Science* 283, 661–663. doi: 10.1126/science.283.5402.661

Ren, F., Yesildag, C., Zhang, Z., and Lensen, M., (2017b). Surface patterning of gold nanoparticles on PEG-based hydrogels to control cell adhesion. *Polymers.* 9, 154. doi: 10.3390/polym9050154

Ren, F., Yesildag, C., Zhang, Z., and Lensen, M. C. (2017a). Functional PEG-hydrogels convey gold nanoparticles from silicon and aid cell adhesion onto the nanocomposites. *Chem. Mater.* 29, 2008–2015. doi: 10.1021/acs.chemmater.6b03548

Renault, J. P., Bernard, A., Juncker, D., Michel, B., Bosshard, H. R., and Delamarche, E., (2002). Fabricating microarrays of functional proteins using affinity contact printing. *Angew. Chem. Int. Ed. Engl.* 41, 2320–2323. doi: 10.1002/1521-3757(20020703)114:13<2426::AID-ANGE2426>3.0.CO;2-Y

Rostgaard, J., and Christensen, P. A. (1975). Multipurpose specimen-carrier for handling small biological objects through critical point drying. *J. Microsc.* 105, 107–113. doi: 10.1111/j.1365-2818.1975.tb04041.x

Sabr, A. K. (2016). Biosensors. *Am. J. Biomed. Eng.* 6, 170–179. doi: 10.5923/j.ajbe.20160606.03

Saini, M., Singh, Y., Arora, P., Arora, V., and Jain, K. (2015). Implant biomaterials: a comprehensive review. *World J. Clin. Cases* 3, 52–57. doi: 10.12998/wjcc.v3.i1.52

Schexnailder, P., and Schmidt, G. (2009). Nanocomposite polymer hydrogels. *Colloid Polym. Sci.* 287, 1–11. doi: 10.1007/s00396-008-1949-0

Seal, B. L., Otero, T. C., and Panitch, A. (2001). Polymeric biomaterials for tissue and organ regeneration. *Mater. Sci. Eng. R* 34, 147–230. doi: 10.1016/S0927-796X(01)00035-3

Shruthi, G. S., Amitha, C. V., and Mathew, B. B. (2014). Biosensors: a modern day achievement. *J. Instrum. Technol.* 2, 26–39. doi: 10.12691/jit-2-1-5

Sukhorukov, G. B., Rogach, A. L., Garstka, M., Springer, S., Parak, W. J., Muñoz-Javier, A., et al. (2007). Multifunctionalized polymer microcapsules: novel tools for biological and pharmacological applications. *Small* 3, 944–955. doi: 10.1002/smll.200600622

Tien, J., Xia, Y., and Whitesides, G. M. (1998). Microcontact Printing of SAMs. *Thin Film* 24, 227–250.

Tkachenko, A. G., Xie, H., Coleman, D., Glomm, W. R., Ryan, J. A., Anderson, M. F., et al. (2003). Multifunctional gold nanoparticle-peptide complexes for nuclear targeting. *J. Am. Chem. Soc.* 215, 4700–4701. doi: 10.1021/ja0296935

van Dorp, W. F., Zhang, X., Feringa, B. L., Hansen, T. W., Wagner, J. B., and De Hosson, J. T. (2000). Electron beam lithography : resolution limits and applications. *Appl. Surf. Sci.* 164, 111–117. doi: 10.1016/S0169-4332(00)00352-4

Veitinger, M., Oehler, R., Umlauf, E., Baumgartner, R., Schmidt, G., Gerner, G., et al. (2014). A platelet protein biochip rapidly detects an Alzheimer's disease - specific phenotype. *Acta Neuropathol.* 128, 665–677. doi: 10.1007/s00401-014-1341-8

Vo-Dinh, T., and Cullum, B. (2008). Biosensors and biochips: advances in biological and medical diagnostics. *Fresenius. J. Anal. Chem.* 366, 540–551. doi: 10.1007/s002160051549

Williams, D. F. (1987). "Definitions in biomaterials," in *Proceedings of a Consensus Conference of the European Society for Biomaterials* (Amsterdam: Elsevier).

Yan, L., Zhao, X., and Whitesides, G. M. (1998). Patterning a preformed, reactive SAM using microcontact printing. *J. Am. Chem. Soc.* 120, 6179–6180. doi: 10.1021/ja980770z

Yesildag, C., Bartsch, C., De Vicente, G., Dwelete and Lensen, M. C., (2017a). Novel wet micro-contact deprinting method for patterning gold nanoparticles on PEG-hydrogels and thereby scontrolling cell adhesion. *Polymers* 9:176. doi: 10.3390/polym9050176

Yesildag, C., Bartsch, C., and Lensen, M. C. (2018b). Micropatterning of Au NPs on PEG hydrogels using different silanes to control cell adhesion on the nanocomposites. *ACS Omega* 3, 7214–7223. doi: 10.1021/acsomega.8b00863

Yesildag, C., Tyushina, A., and Lensen, M. (2017b). Nano-contact transfer with gold nanoparticles on PEG hydrogels and using wrinkled PDMS-stamps. *Polymers* 9:199. doi: 10.3390/polym9060199

Yesildag, C., Zhang, Z., Ren, F., De Vicente, G., and Lensen, M. C., (2018a). "Nano- and micro-patterning of gold nanoparticles on PEG-based hydrogels for controlling cell adhesion," in *Noble and Precious Metals, Properties, Nanoscale Effects and Applications,* ed M. Seehra (London, UK: IntechOpen), 139–160.

Zalipsky, S., and Harris, J. M. (1997). Introduction to Chemistry and Biological Applications of Poly (ethylene glycol). *ACS Symposium Series* 680, 1–13. doi: 10.1021/bk-1997-0680.ch001

Zhang, Z. (2015). *Synthesis, and Characterization of 8 Arm-Poly(ethylene glycol) Based Hydrogels via Michael Addition or Click Chemistry for Biomedical Applications.* Technische Universität Berlin.

Zhang, Z., Loebus, A., de Vicente Lucas, G., Ren, F., Arafeh, M., Ouyang, Z., et al. (2014). Synthesis of Poly(ethylene glycol)-based hydrogels via amine- michael type addition with tunable sti ff ness and postgelation chemical functionality. *Chem. Mater.* 26, 3624–3630. doi: 10.1021/cm500203j

Advantages of publishing in Frontiers

OPEN ACCESS
Articles are free to read
for greatest visibility
and readership

FAST PUBLICATION
Around 90 days
from submission
to decision

HIGH QUALITY PEER-REVIEW
Rigorous, collaborative,
and constructive
peer-review

TRANSPARENT PEER-REVIEW
Editors and reviewers
acknowledged by name
on published articles

Frontiers
Avenue du Tribunal-Fédéral 34
1005 Lausanne | Switzerland

Visit us: www.frontiersin.org
Contact us: info@frontiersin.org | +41 21 510 17 00

REPRODUCIBILITY OF RESEARCH
Support open data
and methods to enhance
research reproducibility

DIGITAL PUBLISHING
Articles designed
for optimal readership
across devices

FOLLOW US
@frontiersin

IMPACT METRICS
Advanced article metrics
track visibility across
digital media

EXTENSIVE PROMOTION
Marketing
and promotion
of impactful research

LOOP RESEARCH NETWORK
Our network
increases your
article's readership